

VANDERBILT UNIVERSITY
2301 Vanderbilt Place, Nashville, TN 37235

SOIL COLLECTION AND TESTING MECHANISM FOR EXTRATERRESTRIAL MISSIONS

PRELIMINARY DESIGN REVIEW

NASA STUDENT LAUNCH COMPETITION

2025 - 2026

NOVEMBER 3, 2025

VANDERBILT AEROSPACE DESIGN LABORATORY





0 Contents

Table of Contents	1
List of Figures	6
List of Tables	12
1 Summary	13
1.1 Team Summary	13
Team Summary	13
1.2 Launch Vehicle Summary	13
1.2 Launch Vehicle Summary	13
1.3 Payload Summary	13
1.3 Payload Summary	13
2 Changes Since Proposal	14
2.1 Vehicle Changes	14
2.2 Payload Changes	14
2.3 Project Plan Changes	15
3 Vehicle Design	16
3.1 Selection, Design and Rationale of Launch Vehicle	16
3.1.1 Mission Statement and Success Criteria	16
3.2 Alternative Vehicle Designs	17
3.2.1 Vehicle Trade Studies Overview	17
3.2.2 Nosecone and Nosecone Bulkplate Retention	17
3.2.3 Joints at Separation Points	19
3.2.4 Airframe	20
3.2.5 Avionics Bulkplates	21
3.2.6 Parachute Detachment System	23
3.2.7 Leg Deployment System	26
3.2.8 Tension Members	27
3.2.9 Rotating Bulkplate System	29
3.2.10 Rail Buttons	30
3.2.11 Motor Retention/Fin Can	32
3.2.12 Alternative Motors	33
3.2.13 Fins	35
3.2.14 Boat Tail	36



3.3	Leading Launch Vehicle Designs	37
3.3.1	Launch Vehicle Overview.....	37
3.3.2	Vehicle Massing	38
3.3.3	Airframe Material and Dimensions	40
3.3.4	Nosecone and Nosecone Bulkplate Retention.....	42
3.3.5	Ballast Integration	44
3.3.6	Main Parachute Bay.....	45
3.3.7	Avionics Bay.....	45
3.3.8	Drogue Bay.....	46
3.3.9	Parachute Detachment Bay	47
3.3.10	Leg Deployment Bay.....	49
3.3.11	Rotating Bulkplate System.....	50
3.3.12	Payload Bay	55
3.3.13	ACS Bay.....	57
3.3.14	Tail Section: Fin Can and Motor Retention Bay	57
3.3.15	Fin Material and Design	62
3.3.16	Boat Tail.....	62
3.3.17	Motor Selection	63
3.4	Alternative Recovery Subsystems	64
3.4.1	Recovery and Avionics Overview.....	64
3.4.2	Alternative Avionics and Altimeters	64
3.4.3	Avionics Housing Materials.....	65
3.4.4	Avionics Switches and Wire Strain Relief.....	66
3.4.5	Battery Trade Study	67
3.4.6	GPS Analysis	67
3.4.7	Dual Deployment Overview	68
3.4.8	Analysis of Alternative Drogue Parachutes.....	69
3.4.9	Analysis of Alternative Main Parachutes.....	70
3.4.10	Parachute Ejection and Retainment	71
3.4.11	Shock Cord Selection	73
3.5	Leading Recovery Design	74
3.5.1	Recovery Events Overview	74
3.5.2	Avionics Bay Design	74
3.5.3	GPS Tracking Device.....	77
3.5.4	Shear Pins	77
3.5.5	Energetics Sizing	77
3.5.6	Leading Parachutes	78
3.5.7	Leading Shock Cord Analysis/Design	79
3.5.8	Anchor Point Hardware	83
3.5.9	Recovery System Redundancy	84



3.6 Mission Performance Predictions	84
3.6.1 Overview of Flight Simulation Framework	85
3.6.2 Target Apogee for Competition	86
3.6.3 Thrust-to-Weight Ratio	88
3.6.4 Launch Rail Exit Velocity	89
3.6.5 Aerodynamics Analysis	89
3.6.6 Static Stability Margin	93
3.6.7 ACS, Ballast and Wind Effects on Apogee Prediction	94
3.6.8 Flight Profile - OpenRocket	97
3.6.9 Flight Profile - MATLAB	98
3.6.10 Flight Profile - RockSim	100
3.6.11 Landing Sections Kinetic Energy	100
3.6.12 Descent Time Predictions	101
3.6.13 Drift Predictions	102
4 Payload Design	104
4.1 Payload Mission Objectives	104
4.1.1 Payload Mission Sequence	104
4.1.2 Success Criteria	104
4.2 Alternative Payload Designs	105
4.2.1 Soil Extraction Methods — Feasibility Study	105
4.2.2 Shovel Extraction Designs	106
4.2.3 Soil Housing Designs	109
4.2.4 Water Injection Justification	110
4.2.5 Water Injection Designs	111
4.2.6 Computing Unit	112
4.2.7 Inertial Measurement Units	112
4.2.8 Motor and Motor Controller	113
4.2.9 Power Delivery Trade Study	114
4.2.10 Sensor Selection Overview	114
4.2.11 Sensor Selection: pH	115
4.2.12 Sensor Selection: Electrical Conductivity	116
4.2.13 Electronic Board and Housing	116
4.3 Leading Payload Design	117
4.3.1 Mechanical Subsystem Overview	117
4.3.2 Rotating Shovel Opening Mechanism	118
4.3.3 Tipping Calculation	123
4.3.4 Soil Housing Chamber	125
4.3.5 Water Injection System	126
4.3.6 STEMNaut Selection and Housing	128
4.3.7 Electrical Systems Overview	130
4.3.8 Electrical Schematic	131



4.3.9	Chosen Electrical Components	131
4.3.10	Payload Battery Sizing and Life Calculations	131
4.3.11	Chosen Soil Sensors and Integration	133
4.3.12	Electrical Mounting	133
4.3.13	PCB Manufacturing	133
4.3.14	Payload Mass Breakdown	134
4.3.15	Payload Verification Plan	134
4.3.16	Mock Tail Section Design and Manufacturing	135
4.3.17	Tip-Over Test	137
4.3.18	Drop Test	137
4.4	Apogee Control System (ACS)	138
4.4.1	ACS Objective	139
4.4.2	Success Criteria	139
4.4.3	ACS Alternative Designs Overview	140
4.4.4	Fin Design	140
4.4.5	Fin Deployment Mechanism	143
4.4.6	Electronics Design	145
4.4.7	Software and State Machine (CONOPS)	146
4.4.8	Apogee Prediction Model	147
4.4.9	Manufacturing Methods and Estimated Massing	147
4.4.10	System Verification	147
4.4.11	ACS Fin Design	147
5	Safety	148
5.1	Safety Overview and Processes	148
5.1.1	Project Components	148
5.1.2	Safety Personnel	148
5.1.3	Safety Practices Overview	149
5.1.4	Compliance with Laws and Regulations	150
5.1.5	Documentation Processes	151
5.1.6	Safety Matrices	152
5.2	Personnel Hazard Analysis	153
5.3	Failure Modes and Effect Analysis	157
5.4	Environmental Concerns	164
5.5	Project Management Risks	167
6	Project Plan	169
6.1	VADL Internal Requirements Derivation and Verification	169
6.2	Testing Plan	182
6.2.1	Vehicle	182
6.3	Budgeting	182
6.4	Project Timelines	191
6.5	Program Management	194
6.6	Outreach Overview and Update	194



Appendices	196
A References	196
B Federal Aviation Regulations	197
B.1 Subpart C—Amateur Rockets	197
B.1.1 § 101.21 Applicability	197
B.1.2 § 101.22 Definitions	197
B.1.3 § 101.23 General Operating Limitations	198
B.1.4 § 101.25 Operating Limitations for Class 2—High-Power Rockets and Class 3—Advanced High-Power Rockets	198
B.1.5 § 101.27 ATC Notification for All Launches	198
B.1.6 § 101.29 Information Requirements	199
C NAR High Power Rocket Safety Code	201
D Written Safety Statement	203



0 List of Figures

1	Vehicle breakdown of trade studies	17
2	Considered Nosecone Geometries	18
3	Parachute Detachment System Methods PoC	24
4	Leg Deployment Prototype	27
5	Comparison of Rail Linked and Cup Linked configurations	30
6	Giant Leap Rocketry Delrin Rail Button	31
7	Vehicle Subsystem Layout	36
8	Full-scale launch vehicle, showing subsystem breakdown	38
9	Locations of separation points and energetics	38
10	Massing Breakdown of Landed Vehicle Sections	39
11	Wet Mass Breakdown by System	39
12	Mechanical Test Setup and Integration	41
13	Stress-strain diagram of specimen under axial compression	41
14	Stress-strain diagram of specimen under axial tension	42
15	Elliptical nosecone with nosecone bulk plate	42
16	Molded subscale elliptical nose cone	43
17	Nosecone bulkplate drawing	44
18	Main parachute bay	45
19	Avionics bay assembled and exploded views	46
20	Drogue Parachute Bay	47
21	Parachute Detachment System CAD model	48
22	PDS prototype 2 inside Payload Drop Testing Platform aft section	48
23	Parachute Detachment System Schematic	49
24	Passive deployment of legs after drogue deployment	50
25	RBS Prototype	51
26	RBS prototype snatch-force tensile pull	51
27	Experimental schematic of tip test	52
28	Results of Tip Test	52
29	RBS Active and Passive side drawings	53
30	Passive side load bearing cup meshing parameters.	55



31	Passive side load bearing cup Von Mises stress map. The resulting safety factor during shock loading is 6.50.	55
32	Active side load bearing cup meshing parameters.	55
33	Active side load bearing cup Von Mises stress map	55
34	Assembly drawing of payload bay structural components	55
35	Locating the ACS Bay in the assembly	57
36	Exploded view of tail assembly	57
37	Exploded view of Fin Can and Motor Retention assembly.	58
38	Drawing of the slotted tail section airframe	60
39	Subscale Tail Section Fabrication Jig	60
40	Assembled Tail Section and Failure Points	61
41	Drawing of main fin geometry	62
42	Boat Tail 3D view and drawing	63
43	MissileWorks 6-32 PCB Screw Switch	66
44	DaFuRui Screw Terminal Blocks	67
45	Recovery packing/protection options.	72
46	Giant Leap Rocketry looped ½" shock chord	73
47	Avionics Bay with Callouts	74
48	3D Model of Avionics Housing	75
49	Avionics Wiring Schematic	76
50	MissileWorks 6-32 PCB Screw Switch	76
51	Leading parachutes used for dual-deployment recovery.	79
52	Pflanz Chart	80
53	Descent Under Drogue and Main Parachutes	82
54	Anchor Point Eye Bolt	83
55	E-Trailer Forged Steel U-Bolt (P.N APUBR-8)	84
56	Overview of the flight simulation framework	85
57	Thrust-to-Weight Ratio for L1940	88
58	Chosen Motor Burn Velocity Profile	89
59	Ansys Fluent mesh for full-scale vehicle. 0 degree ACS deflection.	90
60	CD vs. Freestream Velocity, 0 deg ACS deflection. Average CD is 0.42	91
61	CP vs. Freestream Velocity, 0 deg ACS deflection. Average CP is 72.4 in.	92
62	Velocity streamlines around ACS fins at 90 degree deflection	92
63	CD vs. Freestream Velocity, varying ACS deflection angles	93
64	ACS Achieved v. Target Apogee	95



65	Apogee (ft) vs. Time (s) with varying ballast mass (lbm)	96
66	Apogee (ft) vs Time (s) for varying wind conditions	97
67	VADL launch vehicle representation in OpenRocket	97
68	Nominal Altitude, Acceleration, and Velocity	98
69	Nominal Flight Profile Predicted by MATLAB	99
70	MATLAB-simulated flight profile	99
71	Nominal RockSim-simulated ascent profile	100
72	Initial Payload CAD Exploded Assembly.	108
73	Second Soil Design with Pointed Tip	108
74	Second shovel redesign, modified AoA	108
75	Current Shovel Design	108
76	EC/Nitrate Values vs. Moisture Graph	110
77	Proposed payload bay and ballooned list of subassemblies.	117
78	Shovel Extension Gearbox CAD.	118
79	Shovel Extension Calculation Diagram.	119
80	Forces on Shovel	120
81	Shovel Excavation Diagram.	123
82	Soil Housing Chamber with Sensors	125
83	Exploded View Soil Chamber	126
84	Exploded View Water Integration	127
85	STEMNaut housing in Payload Bay	129
86	STEMNaut housing assembly engineering drawing	129
87	Flowchart of payload states and primary component operations	130
88	Payload Electronics Schematic	131
89	Drop-Test Assembly of the Rocket Aft Section	136
90	Manufacturing Process of the Payload Test Platform	136
91	Fully Assembled Tail Section	136
92	Subassembly Drop Test of the Payload Platform.	136
93	Fully Assembled Payload	136
94	Preliminary ACS CAD	139
95	Predicted apogee vs. time for prior full-scale flight data.	141
96	3 Different Fin Transition Orientations and Effects	144
97	(left) Miter and spur gear train for the ACS and (right) fin deployment demo.	144
98	ACS software flow diagram.	146



99	Safety Documentation Excerpts	151
100	Risk assessment scoring matrix	152
101	Risk Key	153
102	Personnel hazard analysis matrix	157
103	Failure modes and effect analysis matrix	164
104	Environmental concerns analysis matrix	166
105	Project management risks matrix	168
106	Breakdown of current funds raised	183
107	Breakdown of current expenses	183
108	Breakdown of remaining expenses	188
109	NASA milestones gantt chart	192
110	VADL milestones gantt chart	194
111	National Association of Rocketry - High Power Rocket Safety Code	202
112	Written Safety Agreement	203



0 List of Tables

Team Summary Information	13
Launch Vehicle Summary Information	13
1 Mission Success Criteria	16
2 Nosecone Shape Trade Study	18
3 Airframe Interior Diameter Trade Study	20
4 Airframe Material Trade Study	20
5 Bulkhead Geometry Trade Study	22
6 Bulkhead Material Trade Study	22
7 Latch Design Trade Study	24
8 PDM Actuation Trigger Method Trade Study	25
9 Actuation Type Trade Study	26
10 Leg Deployment Material Trade Study	27
11 Fastener Component Trade Study	28
12 Rod Pattern Factor of Safety Comparison	29
13 Design Evaluation Comparison for Bulkplate Concepts	30
14 Rail Guide Design Trade Study	31
15 Fin Mounting Design Trade Study	33
16 Propulsion data and dimensions of potential motors	34
17 Primary Motor Trade Study	34
18 Fin Geometry Trade Study	35
19 Fin Material Options Trade Study	36
20 Boat Tail Design Trade Study	37
21 Fiberglass airframe specimen geometry	40
22 Motor Performance Comparison (3 lb Ballast, No ACS)	64
23 Avionics System Analysis Trade Study	65
24 Avionics Housing Material Trade Study	66
25 Avionics Battery Trade Study	67
26 GPS Transmitter Trade Study	68
27 Drogue Parachute Trade Study	69
28 Main Parachute Trade Study	70



29	Parachute Deployment Retainment Systems Trade Study	73
30	Parachute Deployment Retainment Systems Trade Study	73
31	Deployment charge sizes	78
32	Key parameters for leading parachutes.	79
33	Shock Cord Key Values	81
34	Leading shock cord lengths.	83
35	Current Target Apogee for Competition Day	86
36	Predicted Apogee with no ACS deployment	86
37	Apogee Prediction Comparison	86
38	Thrust-to-Weight Summary	88
39	Launch Rail Exit (LRE) and Maximum Velocity Summary	89
40	Aerodynamic Summary (Ascent C_d and Vehicle CP)	90
41	Mesh element quality for varying ACS deployment angles	91
42	SSM at critical points in flight	94
43	Landing kinetic energy of each independent section	101
44	Recovery drift as a function of wind speed based on OpenRocket simulations	103
45	Payload Success Criteria	104
46	Payload Sampling Method Trade Study	106
47	Shovel Extraction Design Trade Study	107
48	Soil Entry Mechanism Trade Study	110
49	Water Integration Design Trade Study	112
50	Evaluation of final computing unit options	112
51	IMU Trade Study	113
52	Motor and Controller Trade Study	113
53	Power Delivery Trade Study	114
54	Soil pH Sensor Trade Study	115
55	Soil Nitrate Sensor Trade Study	115
56	Soil Electrical Conductivity Sensor Trade Study	116
57	Electronics Boards Trade Study Trade Study	116
58	Variables used to solve shovel torque and mass requirement calculations. .	122
59	Shovel Opening Mechanism Trade Study	125
60	Soil Chamber Material Trade Study	126
61	Payload Mass Breakdown	134
62	Payload Verification Plan	135



63	Tip-Over Test — Expected Results	137
64	Drop Test — Expected Results	138
65	Flight Control System Verification Criteria	139
66	Apogee Control System (ACS) General Design Trade Study	140
67	Fin Design Trade Study	142
68	NACA Fin Design Trade Study	143
69	VADL General Requirements	169
70	Airframe (Spiral Wound Epoxy Glass Tubing (Fiber Glass)) Load Testing . .	182
71	3D Printed Filaments (PLA, PETG, ONYX) Load Testing	182
72	Avionics (EasyMini V2) Pressure Tests	182
73	VADL Expenses Breakdown	183
74	VADL Remaining Expenses Budget	189

1 Summary

1.1 Team Summary

Team Information	
Team Name	Vanderbilt Aerospace Design Laboratory
Mailing Address	Amrutur Anilkumar, Prof. of the Practice, Dept. of Mechanical Eng., #351592, 2301 Vanderbilt Pl., Nashville, TN 37235-1592
Launch Location	Huntsville, Alabama (Competition Week)
Mentor (NAR Certified)	
Mentor	Chris Dondanville, Safety Officer and Rocketry Mentor
NAR/TRA Number	NAR #92729
Certification Level	Level 3
Contact	chris.dondanville@gmail.com, 931-446-4370
Social Media	
Instagram	@VADL
LinkedIn	Vanderbilt Aerospace Design Laboratory (VADL)
YouTube	Vanderbilt Aerospace

1.2 Launch Vehicle Summary

The launch vehicle houses the R.O.L.L. payload, ascends to 4,200 ft (s.t. NASA 2.1), and recovers via a dual-deploy parachute system. It has a total length of 100 in and a ballasted wet mass of 51.1 lbm. The AeroTech L1940 is the primary motor, with the Cesaroni L2375 as backup.

Motor Selection	
Primary	AeroTech L1940 (973 lbf·s)
Backup	Cesaroni L2375 (1093 lbf·s)
Vehicle Size and Mass	
Total Length	100"
Section Lengths	Nosecone: 13.2", Recovery: 34.6", Tail: 52.2"
Dry / Wet / Ballasted	44.1 / 47.1 / 51.1 lbm
Burnout Mass	47.1 lbm
Landing Mass (N/R/T)	5.3 / 13.6 / 28.1 lbm
Recovery System	
Drogue	Fruity Chutes 24", 92.1 ft/s
Main	Fruity Chutes 144", 12.6 ft/s
Altimeter	Altus Metrum EasyMini (Apogee / 550')
Energetic Material	Black powder — Drogue 3/3.6 g, Main 4.4/5.3 g

1.3 Payload Summary

Payload Title: Rotating Omnidirectional Land Laboratory (R.O.L.L.)

The R.O.L.L. collects and retains soil using an extending rotating shovel (s.t. NASA 4.1). The soil is analyzed for pH, conductivity, and nitrate content (s.t. NASA 4.2). A secondary payload adjusts apogee by fin deflection to increase drag (s.t. VADL 3.6.2).

2 Changes Since Proposal

2.1 Vehicle Changes

Coefficient of Drag: A refined C_d value (0.42) was determined during the PDR design period (see Section 3.6.5), permitting motor down-sizing. The nosecone was also changed from ogive to elliptical, with negligible drag effects.

Motor Selection: Due to the above refinements, a lower-impulse motor was selected to reach the targeted apogee. The primary motor was switched to a L1940, with the previous primary, a L2375, now the backup. This is subject to VADL Requirement 2.1.7.

Overall Length: Due to increases in the payload, nosecone, and tail section length for clearance, the total length of the launch vehicle increased from 93 in to 100 in.

Overall Mass: As each vehicle and payload subsystem matured in design, the total wet mass of the launch vehicle increased from approximately 47 lb during the Proposal phase to 51 lb during the PDR phase. Even with the changes, the launch vehicle maintains a thrust-to-weight ratio of 8.53:1 (see Section 3.6.3, s.t. NASA 2.12).

Predicted Apogee: Using a more accurate predictive model (see Section 3.6.2) and accounting for the changes in thrust, mass, and drag coefficient, the team refined the expected altitude performance. During the Proposal period, a no-ACS-deployment apogee of ~5000 ft and a goal apogee of 4800 ft with ACS deployment were reported. Following the above design changes, a no-deployment apogee of ~4400 ft and a goal apogee of 4200 ft have been established.

2.2 Payload Changes

Shovel Extension. During experiments (see Section 4.3.2), the pulley system's digging force was limited by retaining springs and could not be rotated in the opposite direction. Maintaining this opening mechanism would reduce reliability, as the shovel could not tip itself over to avoid ground debris and continue digging. The system was redesigned as a gear train to deliver higher reliability, as it can be back-driven by reversing the payload's electric motor. This configuration also provides greater allowable torque, since gear-to-gear mating is mechanically stronger than the pulley's support system.

Soil Housing Chamber. The overall structure remains largely unchanged, except for new mounting points added to accommodate the conductivity, pH, and nitrate sensors.

Data Capture and Sensor Integration. Three dedicated sensor probes are now used for more accurate readings. The previous 7-in-1 sensor was only reliable for conductivity measurements; interpolated pH and nitrogen-nitrate content values were inaccurate during testing (see Section 4.3.9).



Water Injection System. Replacing the complex syringe-based design, a rubber bladder now holds the water (see Section 4.3.5). As the payload spins around the stationary rod that drives the gear train, it pulls a Kevlar cord tied with three (two redundant) highwayman's hitch knots. After approximately six rotations, the knots untie, releasing water into the soil housing.

Landing Legs. The landing legs have been shortened to extend 2.89 in beyond the outer diameter of the airframe. This change reduces mass, lowers the payload closer to the surface, and improves the containment of water within the soil collection chamber.

2.3 Project Plan Changes

Timeline: The team continues to follow the NASA-specific schedule while also maintaining a VADL-specific project timeline as outlined in Section 6. The VADL timeline provides greater specificity and is divided into phases covering the development, integration, and testing of the subscale vehicle, payload, and full-scale vehicle. Specific dates are established for subscale flight (11/22) and vehicle demonstration flight (2/20). Additionally, the team has moved away from using Jira as project management software due to challenges with implementation and usability. Instead, more frequent progress meetings are held, and Excel sheets are now used to track tasks and deliverable status across subteams.

Budget and Fundraising: The team remains on track to stay under budget by approximately \$1,400, based on current and projected expenses. Fundraising efforts have exceeded expectations, raising \$800 beyond the initial goal of \$5,000, largely due to the generosity of VADL alumni. Detailed financial information and projections are provided in Section 6.3.

3 Vehicle Design

3.1 Selection, Design and Rationale of Launch Vehicle

3.1.1 Mission Statement and Success Criteria

The objective of the launch vehicle is to deliver the payload to the altitude specified in NASA USLI Requirement 2.1 and safely recover it. To accomplish the HAUS payload mission objectives, the full-scale launch vehicle integrates multiple subsystems within a modular airframe architecture. The vehicle is segmented into the following primary sections: **nosecone, main and drogue parachute bays, avionics bay, leg deployment system (LDS), payload bay, apogee control system (ACS) bay, and motor-fin assembly (Tail) bay**. Mission success for the vehicle is defined by the successful execution of the following:

Table 1: Mission Success Requirement

Criterion #	Description	NASA Requirement #	VADL Requirement #
1	The vehicle launches successfully and maintains a stable ascent.	Vehicle Requirement 2.11	N/A
2	The vehicle achieves a target apogee altitude of 4,200 ft.	Vehicle Requirement 2.1	N/A
3	The drogue parachute deploys successfully to initiate deceleration within 2 seconds.	Recovery Requirement 3.1.2	N/A
4	The main parachute deploys successfully for controlled descent.	Recovery Requirement 3.1.1	N/A
5	The vehicle is recovered under parachute without damage.	Vehicle Requirement 2.4	N/A
6	The Parachute Detachment System (PDS) activates successfully post-landing.	N/A	HAUS Payload Requirement 3.2.1
7	The vehicle initiates apogee control system (ACS) as planned.	N/A	ACS Requirement 2.2.3



3.2 Alternative Vehicle Designs

3.2.1 Vehicle Trade Studies Overview

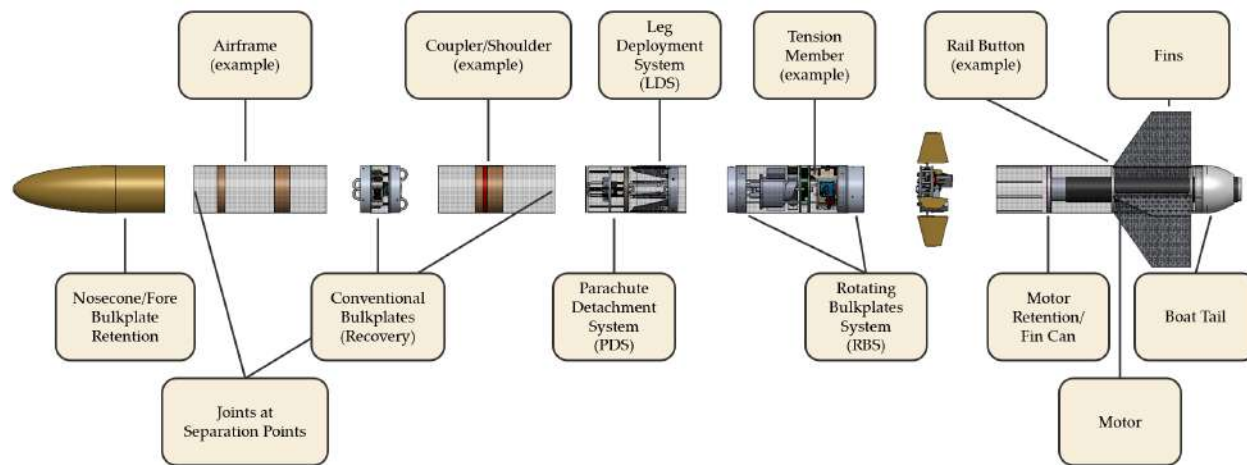
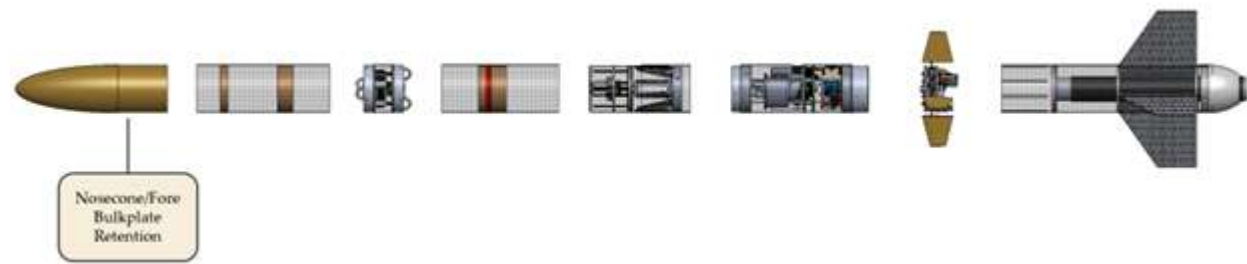


Figure 1: Vehicle breakdown of trade studies

To determine the optimal configuration for the integrated launch vehicle and associated subsystems, a structured series of trade studies was performed during the preliminary design phase. Each evaluation criterion was assigned a normalized weighting factor such that the total weighting sum equaled 1.0. Candidate design options were subsequently scored on a numerical scale from 1 to 10 for each criterion. The weighted scores were then computed and compared, and the design achieving the highest overall weighted score was selected for further development.

3.2.2 Nosecone and Nosecone Bulkplate Retention



The nosecone profile governs the vehicle's aerodynamic performance, drag characteristics, and structural efficiency. Profile selection directly affects axial and pressure drag, normal-force behavior, and the aerothermal environment (VADL Requirement 2.1.6), and must be balanced with manufacturability (VADL Requirement 2.1.5) and structural integration (VADL Requirement 2.1.2) to ensure a safe, predictable flight trajectory.



Figure 2: Considered Nosecone Geometries

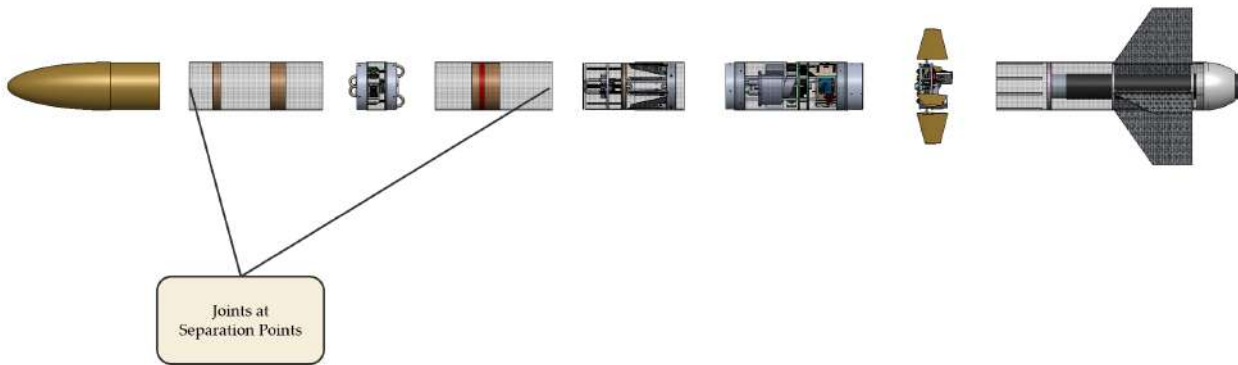
Table 2: Nosecone Shape Trade Study

Design	Drag / Aerodynamics	Manufacturability / Cost	Strength / Tip Durability	Availability	Structural / CG Impact	Total Weighted Score
	30%	35%	15%	10%	10%	
Elliptical L/D=1	7	8	9	9	8	8.05
Elliptical L/D=2	8	9	8	8	6	8.25
Elliptical L/D=3	9	7	7	7	4	7.30
Ogive L/D=1	8	7	7	7	8	7.50
Ogive L/D=2	9	6	6	6	6	6.90
Ogive L/D=3	9.5	5	5	5	4	5.95
Haack L/D=1	9	6	6	7	8	7.25
Haack L/D=2	9.5	5	5	6	6	6.70
Haack L/D=3	10	4	3	5	4	5.45

For nosecone profile, Elliptical L/D=2 was selected for having the highest rating of drag, manufacturability, tip durability, and structural/CG impact. It avoids excessive rocket length while maintaining aerodynamic efficiency.



3.2.3 Joints at Separation Points



Separation points present challenges to vehicle fabrication in two primary ways. Slight manufacturing defects in these regions can lead to significant bending in the rocket body and negatively affect flight stability. However, because separation points are also utilized in recovery deployment, these sections must detach smoothly to avoid interfering with parachute operation.

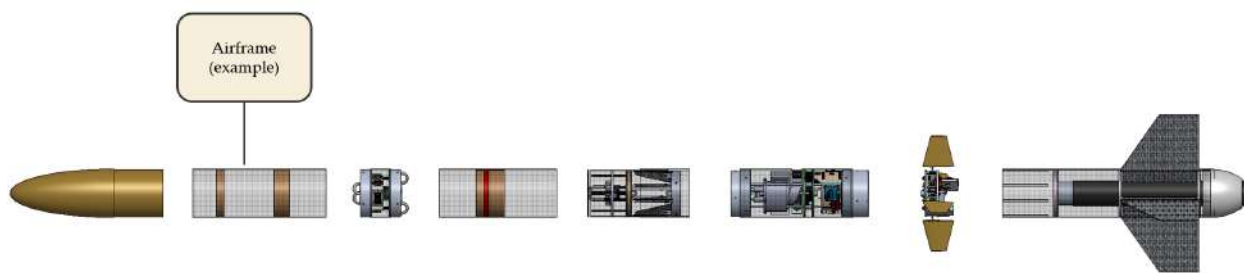
These two needs act in opposition — a tight coupler improves vehicle rigidity, but it can hinder reliable separation. For this reason, NASA USLI Requirement 2.5.1 mandates a minimum shoulder length of one caliber, and NASA USLI Requirement 2.5.3 specifies a minimum nosecone shoulder length of half a caliber. The team has chosen to adhere strictly to these standards for both parachute compartments, as larger shoulders increase mass and require greater ejection charge energy to achieve the same internal pressure on the bulkheads during deployment.

Shear pins are used to ensure that rocket sections remain connected until deployment charges are ignited. They must shear easily during ejection but withstand all flight loads beforehand. The team evaluated two nylon shear pin sizes: #2-56 and #4-40.

Static testing on a load frame determined that a **2-56** pin requires **31 lbf** to shear, while a **4-40** pin requires **42 lbf**. A higher shear strength offers greater resistance to premature separation (for example, main separation occurring at drogue deployment), but it also demands a larger ejection charge to achieve separation. We selected the **2-56** pins because lower shear strength improves separation reliability despite reducing resistance to premature loading. To ensure that the **2-56** pins can still withstand drogue deployment loads, we studied the main parachute compartment located between the nosecone and avionics sections. The mass supported by its shear pins corresponds to the 5.33 lbm nosecone. During drogue deployment, an acceleration of 10 g induces a shear force of 53.3 lbf on the pins. Since static testing determined that 31 lbf is required to shear a 2-56 pin, the team selected 4 shear pins for all recovery separation points to provide an adequate safety margin of 2.3.



3.2.4 Airframe



When designing the airframe, two critical factors must be considered: airframe dimensions and material selection. Dimensions impact structural integrity, weight, and the functionality of payload mechanisms, while material choice influences strength, manufacturability, cost, and performance under varying environmental conditions.

Table 3: Airframe Interior Diameter Trade Study

Interior Diameter	Advantages	Disadvantages	Notes	Total Weighted Score
5.0 in	Smaller overall size	Less space for payload and mechanisms.	May constrain shovel pivot and soil capsule placement	6.4
5.5 in	Balanced size and payload accommodation	Less space for payload and mechanisms.	Provides acceptable space for payload while maintaining structural integrity	7.3
6.0 in	More room for payload and mechanisms; larger diameter decreases the likelihood of buckling failure	Potentially more material cost	Provides maximum payload flexibility	8.1

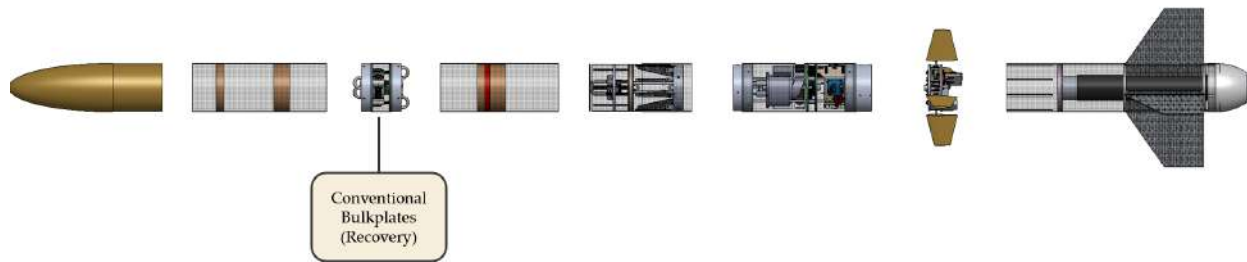
Table 4: Airframe Material Trade Study

Material	Advantages	Disadvantages	Notes	Total Weighted Score
Solid Carbon Fiber	Extremely strong and stiff	Very expensive; time-consuming to fabricate (requires wrapping around aluminum mandrels and demolding)	Best performance but impractical for this project timeline	7
Blue Tube Carbon Fiber	Slightly easier to manufacture; almost as strong as solid carbon fiber	High expansion/contraction with temperature/humidity changes	Could compromise dimensional stability in outdoor environments	7.5
Blue Tube Alone	Cheapest and easiest to manufacture	Not strong enough; highly variable under environmental conditions	Not viable for structural needs	6.2
Team-Performed Fiberglass Layups	Very cheap; good hands-on practice	Weak; will not improve rocket strength	Useful for practice but not recommended for airframe structure	5
Commercially Available Fiberglass Tubes	Medium expense; very consistent tolerances; easy to work with	Less strong than carbon fiber; slightly heavier	Good balance between strength, cost, and manufacturability	8.8



Based on the trade studies above, the 6-inch diameter airframe was chosen buying commercially available fiberglass tubes. This configuration provides sufficient internal space for the payload and shovels mechanism while maintaining a balance between weight, structural integrity, and ease of fabrication as covered in VADL Requirement 2.1.5. Commercially available fiberglass tubes offer consistent tolerances and reasonable strength, making this the most practical choice for our rocket's design.

3.2.5 Avionics Bulkplates



The avionics bulkplates are critical structural components of the launch vehicle, as they house the avionics hardware and must withstand parachute shock loads and blast-charge pressure. These plates must ensure proper load transfer and maintain an airtight seal to protect internal systems. Additionally, VADL Requirement 4.1.7 specifies that the bulkplates must support modular bolted assembly, enabling repeated disassembly and re-use of the rocket.

Key selection criteria include:

- **Structural Strength (VADL Requirement 2.1.1):** Must withstand parachute shock loads and internal pressure forces.
- **Manufacturability (VADL Requirement 2.1.6):** Feasible to produce with tight tolerances and machining repeatability.
- **Weight:** Must minimize mass while maintaining structural integrity.
- **Assembly & Sealing:** Must enable modular bolting and provide a reliable pressure seal.
- **Material Adaptability & Cost:** Material selection must balance manufacturability, reusability, and cost efficiency.



Table 5: Bulkhead Geometry Trade Study

Geometry	Strength	Manufacturability	Weight	Assembly & Sealing	Total Score
	30%	30%	20%	20%	100%
Flat Plate	3	8	7	3	5.3
Plate with Shoulder	7	6	6	7	6.5
Plate with Two Shoulders	9	4	5	9	6.7

Table 6: Bulkhead Material Trade Study

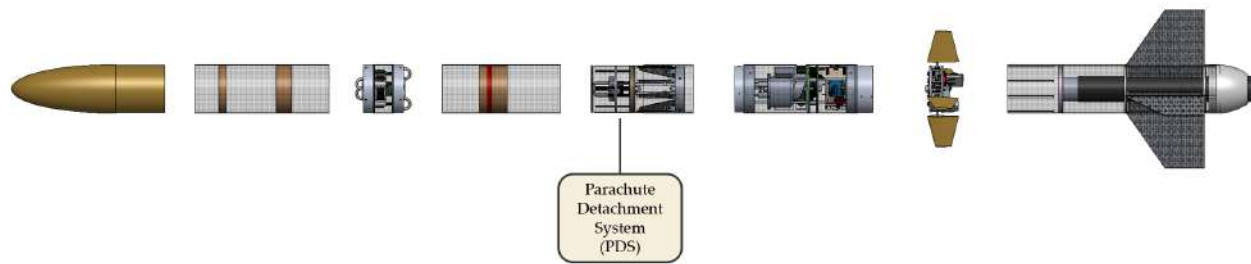
Material	Strength to Weight	Manufacturability	Reusability / Adaptability	Low Cost & Sealing	Total Score
	30%	30%	20%	20%	100%
MDF	1	9	2	10	5.4
Plywood	2	9	2	9	5.5
Onyx (Nylon Print Filament)	4	8	2	8	5.6
Aluminum	7	6	9	7	8.1
Carbon Fiber	10	3	4	4	5.5
Fiberglass	9	3	4	5	5.4

Based on the trade studies above, the selected design is a **6061-T6 aluminum bulkhead with a lip and two shoulders** selected for the following reasons:

- **Strength & Alignment:** The shoulder and dual lips ensure proper alignment, increase structural strength, and allow the airframe to be held tightly to the bulkhead.
- **Material:** Aluminum provides a strong, lightweight, and machinable option.
- **Manufacturing:** CNC machining allows tight tolerances, ensuring a reliable seal for avionics protection.
- **Modularity & Reuse:** Design meets VADL requirements for bolted assembly, enabling disassembly and reuse of the rocket.



3.2.6 Parachute Detachment System



When the vehicle lands, the Parachute Detachment System actuates, allowing the payload to begin digging without being pulled by a wind-filled parachute. So, it needs an electrical system to initiate detachment and a load-bearing structure to withstand the parachute snatch force. Multiple designs were considered to create a system that reliably serves these two functions. The maximum tensile load the PDS will experience is 731 lbf from parachute shock exerted over a fraction of a second. The PDS must withstand high dynamic loads and actuate to detach the parachute, as required by VADL Requirement 2.3.1.

The team considered the overall design of the PDS, as well as its control. The two trade studies below outline that design process, which included team leads from both the mechanical and electrical subteams for this critical component. The designs using EM latches utilized SouthCo R4-EM-05D00-150, which offer the highest strength in a commercially available, appropriately sized, and weighted EM latch.

The SouthCo latch in the selected design has an ultimate tensile strength of 1061 lbf before failure. However, loading up to this maximum can cause yielding, significantly affecting functionality and the ambient temperature cycle life of 40,000. SouthCo does not list the maximum load before impacting cycle life, and in-lab testing would require excessive time and financial resources. Assuming the failure point is steel-steel contact, an endurance limit (infinite life region) of 50% of its maximum load was used. Therefore, the latch's maximum allowable load is 530.5 lbf.



Table 7: Latch Design Trade Study

Design	Low Weight	Resilience to Off-Angle Shock Loading	Ease of Manufacturing	Protection of Decision-Making Mechanism	Max Load	Total Weighted Score
	10%	20%	20%	30%	20%	100%
Multiple EM latches in parallel (5–6 for 3.0+ FoS)	4	2	9	2	5	4.2
In-house mechanically advantaged latch design	6	9	3	8	6	6.6
U-bolt, EM latch shock-cord wrap method	6	7	6	7	9	7.1
Ball in dimple, actuated by mag-lock payload rotation	3	6	2	8	5	5.3

The chosen design is the U-bolt EM latch shock cord wrap for its versatility and weight-efficiency. This method follows the Capstan Equation (cord wrapped around a solid body) to transfer the majority of parachute shock cord load away from the EM latch and apply it to the U-bolt, bulkplates, and the remainder of the designed load path. Mechanically, this occurs due to the friction between the Kevlar shock cord and the steel U-bolt.

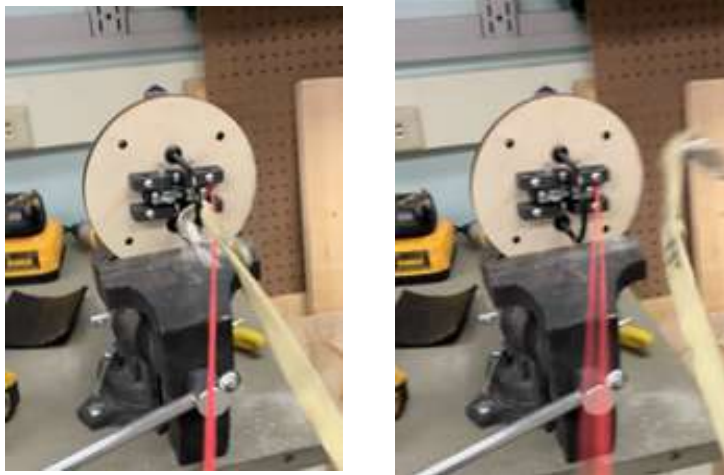


Figure 3: Initial proof-of-concept demonstration of the preferred Parachute Detachment System (PDS) method; left is before and right is after release is actuated.

The system achieves low tension in the holding chord while maintaining high load tension, enabling consistent and rapid quick-link release upon latch actuation. Further details are provided in Section 3.3.9.

The selected latch concept uses the Capstan Equation to achieve passive load-holding. The maximum expected load at the foremost portion of the aft section (location of PDS) during parachute snatch is calculated as $T_{load,max} = 731 \text{ lbf}$, corresponding to 28.13 lbm under 26 Gs of acceleration.



$$T_{\text{load}} = T_{\text{hold}} e^{\mu\phi}, \quad \mu = 0.25 \text{ (Kevlar–steel friction coefficient)}, \quad \phi = 360^\circ = 2\pi \text{ rad}$$

Thus, the load ratio is

$$\frac{T_{\text{load}}}{T_{\text{hold}}} = e^{\mu\phi} = e^{0.25 \cdot 2\pi} \approx 4.81$$

and the required holding tension is

$$T_{\text{hold}} = \frac{T_{\text{load,max}}}{4.81} = \frac{731}{4.81} \approx 151.98 \text{ lbf.}$$

Given the latch allowable capacity of 530.5 lbf, the factor of safety is

$$\text{FoS} = \frac{530.5}{151.98} \approx 3.49.$$

According to the calculations, the single-wrap U-bolt PDS design provides a safety factor of 3.49 (coupled with an estimated latch endurance limit of 50% of the reported UTS), which complies with VADL Requirement 2.1.1. Further testing will be conducted, and if a larger safety factor is required, more wraps or a higher-friction U-bolt can easily be employed to further decrease the load on the latch.

In addition to the mechanical system, the electrical controls system for the PDS was decided using the trade study below. To compensate for the rotational payload, various detachment actuation methods were evaluated to simplify the vehicle's electrical system and prevent wire or component damage. An in-air parachute detachment presents a significantly higher safety hazard than a failure to detach upon landing. Thus, the latter category is weighted lower.

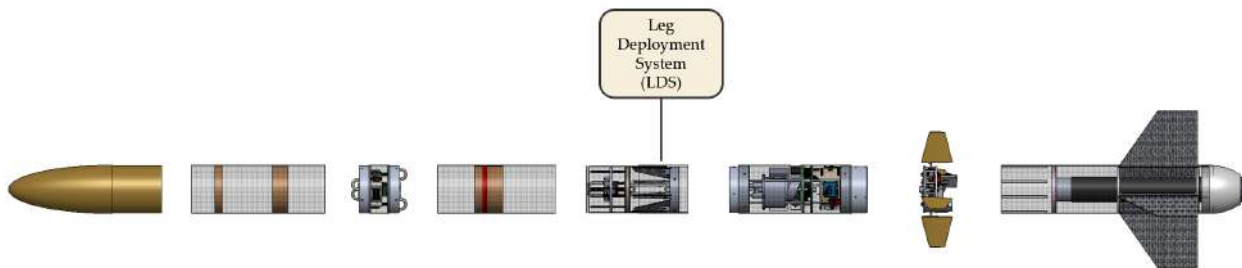
Table 8: PDM Actuation Trigger Method Trade Study

Design	Likelihood of Actuating On-Ground	Low Likelihood of Actuating In-Air	Weight	Ease of In-Field Assembly	Total Weighted Score
	20%	50%			
Controlled from payload: Break-wires on outside airframe	9	2	9	4	4.5
Controlled from payload: Hardwired link	4	6	9	2	5.1
Controlled from payload: Bluetooth	3	3	9	9	4.8
Controlled independently (separate IMU + MCU in PDS bay)	7	8	2	5	6.6



Our chosen design for controls includes an independent IMU and microcontroller in the PDS bay, increasing reliability against in-air latch actuation, which is a greater risk in inter-bay communication mechanisms like Bluetooth or a breakwire. It will also simplify assembly prior to launch and increase overall vehicle modularity, which streamlines troubleshooting.

3.2.7 Leg Deployment System



Key considerations in designing the leg deployment system include the actuation type, which determines the number of steps required for the legs to reach their desired position, and the leg material, which influences impact energy absorption and resistance to fracturing at landing in accordance with VADL Requirement 2.4.4. The design must balance reliability, manufacturability, and impact performance to ensure safe deployment and landing.

Table 9: Actuation Type Trade Study

Deployment Design	Reliability 60%	Reliability Notes	Manufacturability 40%	Manufacturability Notes	Total Weighted Score 100%
Translating plate with spring	8	No electromechanical actuator; low possibility of spring failure	7	Most components can be 3D printed; components must be precisely positioned	7.6
Translating plate with actuator	6	Electromechanical failure; actuators add failure points and complexity	6	Most components can be 3D printed; extra joint assembly required; increases weight	6.0
Motor controlled legs	6	Electromechanical failure; actuators add failure points and complexity	5	Mounted directly to leg joint; less mass and fewer components	5.6



Table 10: Leg Deployment Material Trade Study

Material	Shear Strength 40%	Notes	Bending / Impact	Manufacturability	Total Weighted Score
			30%	30%	100%
Plywood	2	600–1000 psi	2	10	4.4
Carbon Fiber	10	30,500 psi	8	3	7.3
Fiberglass Plate	6	8,000 psi	8	6	6.6

After considering reliability, manufacturability, and impact performance, the team selected a passively deployed carbon fiber leg mechanism that deploys a drogue chamber decoupling. This combination maximizes deployment reliability, landing safety, and manufacturability within the design constraints of VADL Requirements 2.4.5.

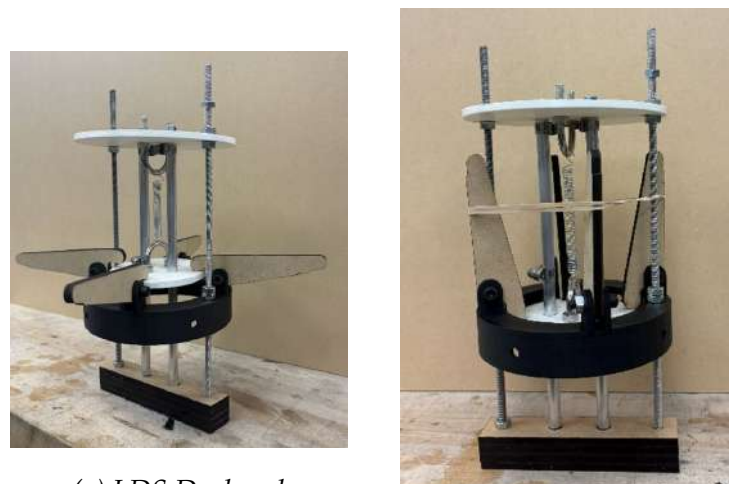
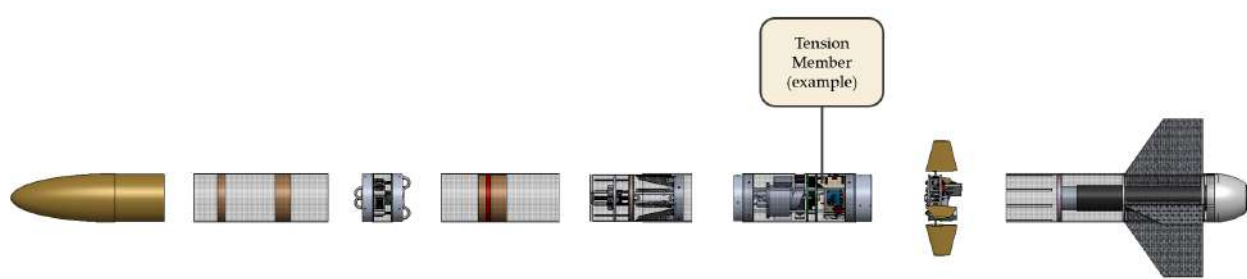


Figure 4: Prototype of the leg deployment system. (a) shows the deployed configuration, and (b) shows the stowed configuration without the coupler installed (a rubber band is temporarily holding the legs in place).

3.2.8 Tension Members





When selecting load-bearing materials, it's essential to understand expected failure modes. Space-faring and high-power model rockets in NASA's USLI competition are no exception. High-strength airframe materials—fiberglass, BlueTube, and carbon fiber—with inner diameters of 5", 5.5", and 6" were considered. Stiff, hollow tubing provides optimal buckling resistance under unpredictable flight loads, so bulky internal components with high moments of inertia were omitted for their unnecessary weight and space claim. The compressive-load grading column is minimally weighted in the trade study, and threaded rods are used only in the Avionics and Payload bays, where weight is considered but secondary to tensile strength.

Table 11: Fastener Component Trade Study

Component	Strength (Tension)	Strength (Compression)	Weight 20%	Cost 10%	Manufacturability / Ease of Use 20%	Total Weighted Score
	30%	20%				100%
Break-line, 0.035" wall, 1/2"	5	8	8	7	Easy to handle; moderate assembly	6.0
Aluminum Threaded Rod (1/4")	4	2	9	8	Easy to machine	5.6
Mild Steel Threaded Rod (1/4-20)	7	5	7	7	Moderate machinability	6.6
316 Stainless Threaded Rod (1/4-20)	8	6	6	6	Moderate machinability; corrosion resistant	6.8

Using the above trade study, the design team selected **316 Stainless Steel** threaded rods for major tension members throughout the rocket, trading the added weight for the added strength, especially in the tail section where parachute snatch force is considerable. In the following calculation, 2, 3, and 4 tension rod patterns are qualified for use in the full-scale rocket with their factors of safety calculated below.

Known parameters:

$$m_{\text{recovery}} = 13.58 \text{ lbm}, \quad m_{\text{tail}} = 28.12 \text{ lbm}, \quad P_{u,316} = 75 \text{ ksi}, \quad A_{\text{eff,rod}} = 0.032 \text{ in}^2.$$

Peak landing shock load:

$$F_{\max} = (m_{\text{recovery}} + m_{\text{tail}}) a_{\text{shock}} = (13.58 + 28.12) \times 26 g \approx 1,084 \text{ lbf.}$$

Per-rod capacity:

$$P_{y,\text{rod}} = \sigma_y A_t = 25,000 \text{ psi} \times 0.032 \text{ in}^2 = 795 \text{ lbf}, \quad P_{u,\text{rod}} = \sigma_u A_t = 75,000 \text{ psi} \times 0.032 \text{ in}^2 = 2,385 \text{ lbf.}$$

For $n = 4$ rods:

$$P_{y,\text{total}} = 4P_{y,\text{rod}} = 3,180 \text{ lbf}, \quad P_{u,\text{total}} = 4P_{u,\text{rod}} = 9,540 \text{ lbf.}$$



Factors of Safety:

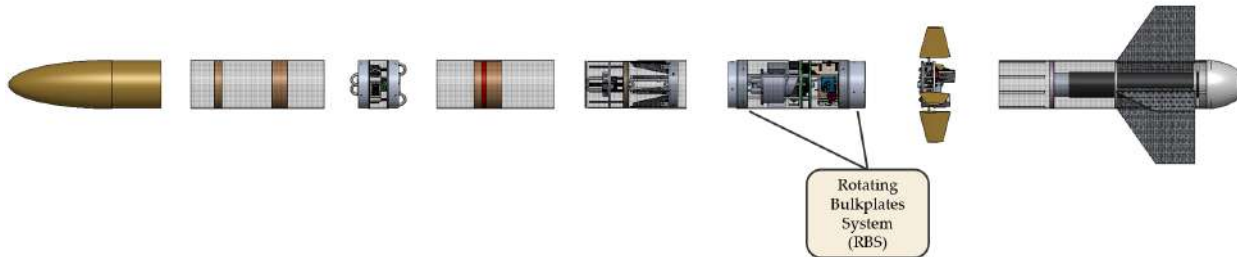
$$\text{FoS}_{\text{yield}} = \frac{3180}{1084} \approx 2.94, \quad \text{FoS}_{\text{ultimate}} = \frac{9540}{1084} \approx 8.81.$$

Table 12: Rod Pattern Factor of Safety Comparison

N (Rod Pattern)	FoS Yield	FoS Ultimate
4 (Abs. Max)	2.93	8.80
3 (Abs. Max)	2.20	6.60

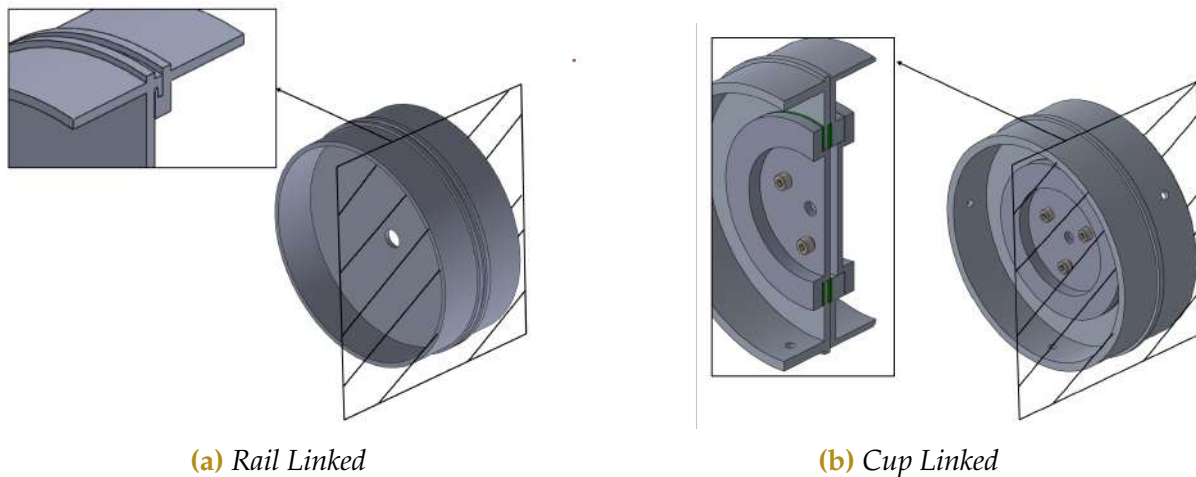
These are conservative design estimates, as the airframe fiberglass will be involved in the parachute snatch force load patch. This assumption with a 2.0+ FoS allows for unpredictable loading throughout flight and leaves a healthy margin for the main load path components, while allowing for further iteration to meet VADL Requirement 2.1.1.

3.2.9 Rotating Bulkplate System



The Rotating Bulkplate System (RBS) is a structural subsystem that transmits torque to the fins during payload operation. The assembly must permit the free rotation of the bulkplates while simultaneously resisting axial loading during flight in accordance with VADL Requirements 2.1.1-2 and 2.1.4. Core design constraints consider mass, manufacturability, and reliability of torque transfer during payload actuation.

To reduce risk and retain redundant capabilities, the RBS is divided into an *active* side containing the powered drive interface, and a *passive* side without a motor. Two competing designs were evaluated: the Rail-Linked Bulkplate System and the Cup-Linked Bulkplate System. The Rail-Linked Bulkplate System uses a concentric rail to transmit axial loading while allowing rotation between bulkplates. In contrast, the Cup-Linked Bulkplate System connects bulkplates through removable “cups” that are secured with bolts.



(a) Rail Linked

(b) Cup Linked

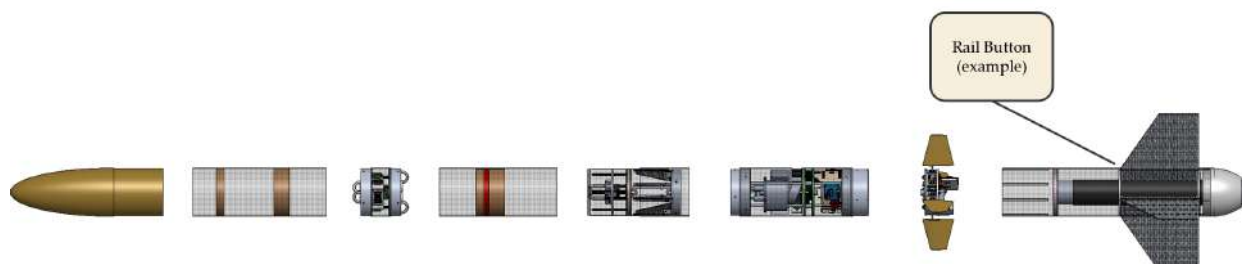
Figure 5: Comparison of Rail Linked and Cup Linked configurations

Table 13: Design Evaluation Comparison for Bulkplate Concepts

Design / Constraint	Predicted Mass	Predicted Strength	Predicted Rotational Resistance	Predicted Space-Claim	Ease of Manufacturing	Ease of Assembly	Weighted Total
	15%	25%	20%	10%	15%	15%	100%
Rail-Linked Bulkplates	10	6	4	8	6	4	6.10
Cup-Linked Bulkplates	6	10	10	8	10	10	8.90

Comparative evaluation metrics include predicted mass, overall strength, rotational resistance, volume, manufacturability, and ease of total subsystem assembly. While the rail-linked design may offer lower mass, the cup-linked design provides significantly higher structural reliability and a lower risk of falling out of specification during manufacturing or rocket flight. The cup-linked design benefits from increased load-bearing surface area and machined interfaces secured with mechanical fasteners, eliminating weld-induced material distortion that could compromise structural integrity and assembly concentricity. Therefore, the cup-linked system has been selected for further design as it offers superior safety margins, better manufacturing procedures, and lower operational risk, aligning more effectively with NASA and VADL requirements.

3.2.10 Rail Buttons





The rail buttons are the primary launch guide interface, ensuring controlled ascent during initial flight off of the launch rail. Key criteria in selecting appropriate rail buttons include minimizing friction against the launch rail, maintaining sufficient hardness and wear resistance for repeated use, and ensuring dimensional compatibility with the vehicle's outer diameter and rail size. Additional considerations include the availability of off-the-shelf (OTS) parts to ensure reliable sourcing and consistent surface finish, as well as mass and drag minimization to prevent unnecessary aerodynamic losses.

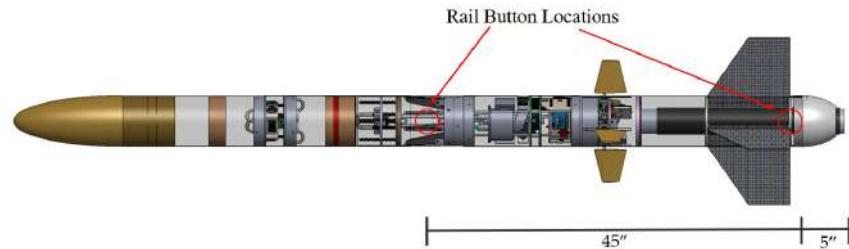
Table 14: Rail Guide Design Trade Study

Design	Low Friction	Durability / Hardness	Ease of Installation	Proven Flight Record	Cost / Availability	Total Weighted Score
Giant Leap Rocketry – Small Airfoil	9	8	9	7	8	8.4
Giant Leap Rocketry – Large Airfoil	8	9	8	9	8	8.5
Circular Rail Buttons	6	7	9	6	9	7.2
Custom Machined (In-House)	7	9	4	4	3	6.0

The selected rail button is the Giant Leap Rocketry Large Airfoil model. This option balances low drag and friction while maintaining high durability and contact surface area due to its Delrin construction and flight-proven reliability. The team plans to purchase new components instead of reusing old ones to ensure a clean, unblemished surface finish on the Delrin contact face, minimizing rail wear and launch friction. These OTS components also simplify replacement and reduce integration risk compared to custom fabrication.

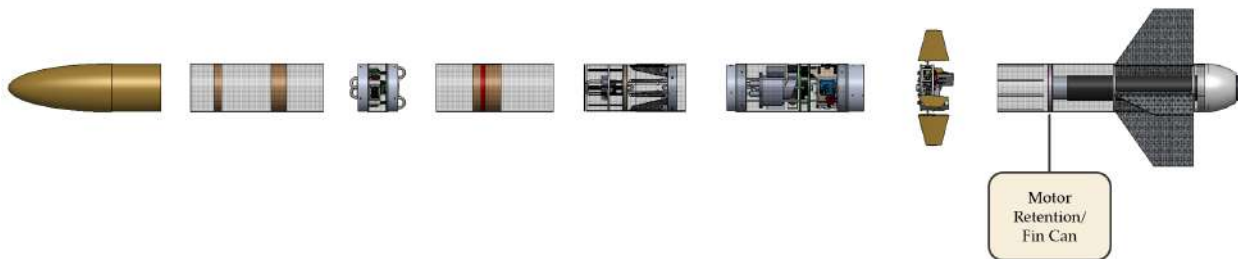


Figure 6: Giant Leap Rocketry Delrin Rail Button



The rail buttons will be placed 5" and 50" from the aftmost end of the rocket to provide an effective rail length of 94" off of the 144" rail.

3.2.11 Motor Retention/Fin Can



When considering fin can and motor retention designs, particular emphasis must be placed on ease of manufacturing. The fin can is at the aft end of the rocket, and its loading is typically not governed by tension during parachute snatch. Instead, it directly distributes the compressive load of the burning motor to the rest of the rocket, and so it should be designed primarily for this application. An effective way to achieve this is to increase the moment of inertia of the motor can assembly as much as possible, with rigid connections between each member. However, this rigid connection can make it difficult to swap out parts if they break. For that reason, it's important to consider both modular and rigid motor can assembly structures.

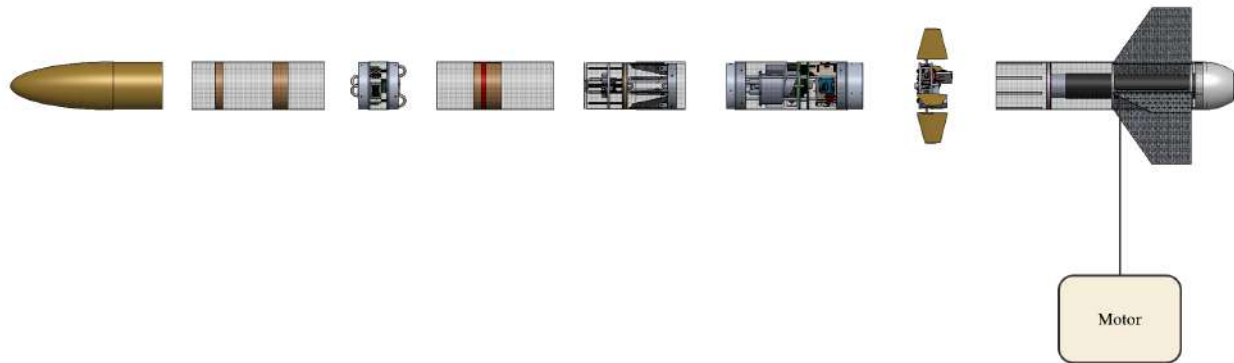


Table 15: Fin Mounting Design Trade Study

Design	Overall Strength	Replaceability / Modularity	Low Weight	Low Likelihood of Fluttering	Total Weighted Score
	30%	30%	20%	20%	100%
Two-level filleted motor tube, airframe fin structure	9	3	7	8	6.6
Modular structure: fins bolted to plate on motor tube	6	9	3	3	5.7

The trade study above formalized and verified the design team's early consensus that a modular fin structure—though easy to repair—would impart significant flexural shear loads on the bolted joints at the motor tube plate attachment. Since our design this year uses the fins as landing legs, it is of mission-critical importance that we eliminate stress concentrations and potential failure points by employing a double-filletted fin motor can assembly. In this configuration, the carbon fiber DragonPlate fins are epoxied and composite-filletted to both the motor tube and the outer airframe.

3.2.12 Alternative Motors



Motor selection is first constrained by the following Student Launch requirements: the flight apogee must be between 4,000 and 6,000 ft AGL (NASA 2.1); propulsion must be a commercially available APCP solid motor certified by NAR/TRA/CAR and limited to a single-motor system (NASA 2.7-8); total impulse may not exceed 5,120 N·s (NASA 2.9); the vehicle must have a minimum liftoff thrust-to-weight ratio $\geq 5:1$ (NASA 2.11-12); rail-exit velocity must be at least 52 ft/s (NASA 2.14); the vehicle shall remain subsonic throughout flight (NASA 2.20.6); and any ballast is limited to 10% of the unballasted pad weight (NASA 2.20.7).

Based on these requirements, the team identified four leading options for this year's project:



- AeroTech L1940
- Cesaroni (CTI) L2375
- Cesaroni (CTI) L1720
- Cesaroni (CTI) L1350

Key propulsion data and dimensions for each option are listed in Table 16.

Table 16: Propulsion data and dimensions of potential motors

Parameter	L1940	L2375	L1720	L1350
Diameter (in)	2.95	2.95	2.95	2.95
Length (in)	22.0	24.4	19.1	19.1
Total Impulse (lbf·s)	973	1093	823	958
Burn Time (s)	2.2	1.9	2.0	3.16
Peak Thrust (lbf)	521	629	437	376
Average Thrust (lbf)	436	551	398	303
Delay Time	Plugged with smoke	No delay (ejection)	Plugged with smoke	Plugged with smoke
Propellant Mass (lb)	4.02	5.12	3.87	4.20
Loaded Mass (lb)	8.50	9.17	7.36	7.87

To select the appropriate leading and backup motor, the team used the following design criteria:

- Ballast required to reach a no-ACS apogee of approximately 4,500 ft
- Launch rail exit velocity and burn time. Motors with higher early-time thrust increase rail-exit velocity for a given rail length. Higher exit speed improves aerodynamic stability and reduces wind-cocking risk.
- Availability and lead time

Table 17: Motor ballast, lead time, and launch rail exit (LRE) velocity trade study

Motor	Ballast Added to Achieve 4500 ft with No ACS	Expected Lead Time	LRE Velocity	Total Weighted Score
	60%	20%	20%	100%
L1940	2 lb ballast added to reach an apogee of 4514 ft. (Score: 7/10).	Four motors on order, arrival expected soon. (Score: 5/10).	83.1 ft/s (Score: 8.3/10).	8.1
L1720	No ballast added; apogee is 3873 ft (below minimum requirement). (Score: 0/10).	Moderate lead time; 2 in stock. (Score: 7.5/10).	74.3 ft/s (Score: 4.0/10).	2.3
L2375	9.5 lb ballast added to reach 4531 ft; near ballast limit. (Score: 3/10).	Four motors in stock. (Score: 10/10).	86.5 ft/s (Score: 10/10).	5.8
L1350	1 lb ballast added to reach an apogee of 4537 ft. (Score: 9/10).	Long lead time expected. None in stock (Score: 0/10).	66.1 ft/s (Score: 0/10).	5.4

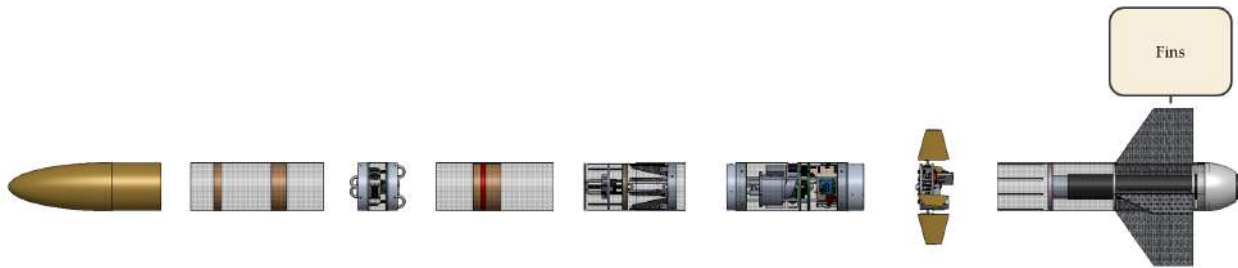
Based on the trade study in Table 17, the team selected the **Aerotech L1940** as the primary motor. It satisfies all NASA requirements, meets the target flight profile, and



provides approximately 3 lbm of ballast capacity. We will use this ballast as a design margin to accommodate potential mass creep as the vehicle matures.

As a backup, the team chose the **Cesaroni L2375**. It is readily available in the lab and delivers higher thrust and rail-exit performance, making it a suitable hedge against unexpected mass growth.

3.2.13 Fins



Due to the design of this mission's payload, a 4-fin configuration was necessary to provide the required initial vertical clearance between the airframe and the payload shovel as it begins rotation. A 3-fin pattern would have required prohibitively long and large fins to achieve this height. With that in mind, the following trade study was conducted to determine the specific characteristics of our launch vehicle. Fin geometry and material selection are critical to the rocket's aerodynamic stability and structural performance. Key considerations include the center of pressure (C_p), overall weight, manufacturability, and aerodynamic efficiency. For this year's vehicle, bending strength and flexural rigidity are the primary drivers, because the fins also function as structural legs supporting the spinning payload bay and shovel assembly after landing.

Table 18: Fin Geometry Trade Study

Geometry	Cp Location (Aft Bias)	Manufacturability	Structural Integration as Legs	Aerodynamic Efficiency	Total Weighted Score
					100%
Box	6	9	7	6	7.2
Clipped Delta	8	8	9	8	8.3
Swept	9	5	8	9	7.8
Inset Tab	7	6	6	8	6.9
Elliptical	8	7	6	9	7.5



Table 19: Fin Material Options Trade Study

Material	Strength / Bending Rigidity	Weight 20%	Manufactura- bility 20%	Cost 10%	Proven Performance 20%	Total Weighted Score
	30%					100%
DragonPlate Carbon Fiber	10	8	7	4	9	8.3
G10 Fiberglass	8	7	9	7	9	8.0
Fiberglass / Plywood Layup	7	6	8	8	8	7.4
Hardwood Plywood	6	7	9	9	7	7.3
Softwood Plywood	4	8	9	10	6	6.9
MDF	3	5	9	10	5	6.0
Plastic	2	9	8	9	4	5.9

The selected fin configuration is a clipped delta geometry made from DragonPlate carbon fiber. This combination provides exceptional flexural rigidity, which is crucial as the fins double as landing legs for the payload section during soil collection. The clipped delta shape offers an ideal tradeoff between ease of manufacturing and an adequately aft Cp location for static stability. While a swept fin could achieve a slightly greater stability margin, its complex alignment during fabrication introduces unnecessary build risk. Since the fins must extend significantly from the airframe to achieve stable leg geometry (see Section 4.3.3), their surface area inherently provides sufficient aerodynamic stability. Although box and elliptical fins would be marginally easier to align, they would shift the Cp forward and reduce leg effectiveness, making the clipped delta geometry the optimal choice for this mission’s design team.

3.2.14 Boat Tail

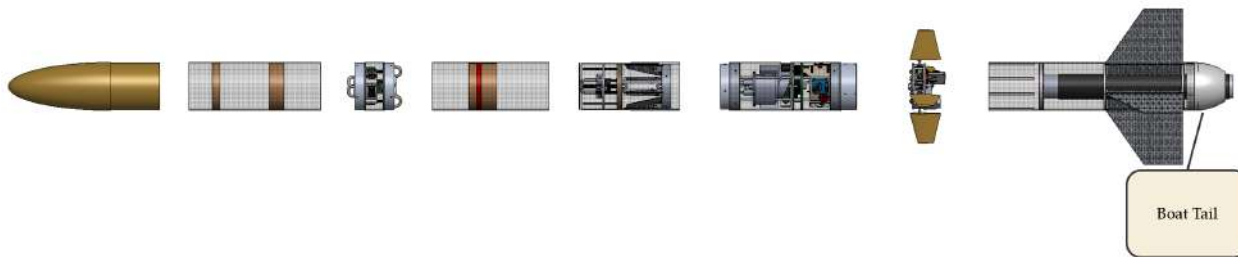


Figure 7: Vehicle subsystem layout used to guide trade study development.

In the trade study below, the design team compared mass, drag reduction, heat distortion resistance, and ease of manufacturing to optimize the aftmost section of the rocket. The



boat tail plays a critical role in reducing base drag and improving aerodynamic efficiency, but it must also remain structurally stable under thermal and mechanical loading during motor burn. The design should balance aerodynamic benefit with manufacturability and weight efficiency to ensure overall performance alignment with the NASA Requirement 2.1, reaching an apogee of 3,500 ft.

Table 20: Boat Tail Design Trade Study

Potential Design	Added Mass 10%	Effect on Reducing Drag 30%	Heat Distortion Resistance 40%	Ease of Manu- facturing 20%	Weighted Rating
					100%
Aluminum Boat Tail	3	7	6	6	6.0
3D-Printed Boat Tail	6	6	8	9	7.4
Elongated Boat Tail	2	9	7	4	6.5

Based on the trade study, the team selected the 3D-printed boat tail. This design balances drag reduction and ease of fabrication without introducing excessive weight. Designing our own boattail allows for tailored improvements in aerodynamics. Additionally, the simplicity of manufacturing a 3D-printed component ensures simple integration to vehicle CAD model to run flight simulations and tests.

3.3 Leading Launch Vehicle Designs

3.3.1 Launch Vehicle Overview

After conducting trade studies on each system in Section 3, we now thoroughly review the leading design. The full-scale launch vehicle has a total length of **100 in**, an outer diameter of **6.17 in**, and a wet mass of **51.1 lbm**. This corresponds to an overall aspect ratio of **AR = 16.2:1**. The airframe is organized into three primary sections: a nose cone / fore section, a recovery section, and a tail section containing the fin can and motor.

Our leading vehicle design is shown in Figure 8 below:

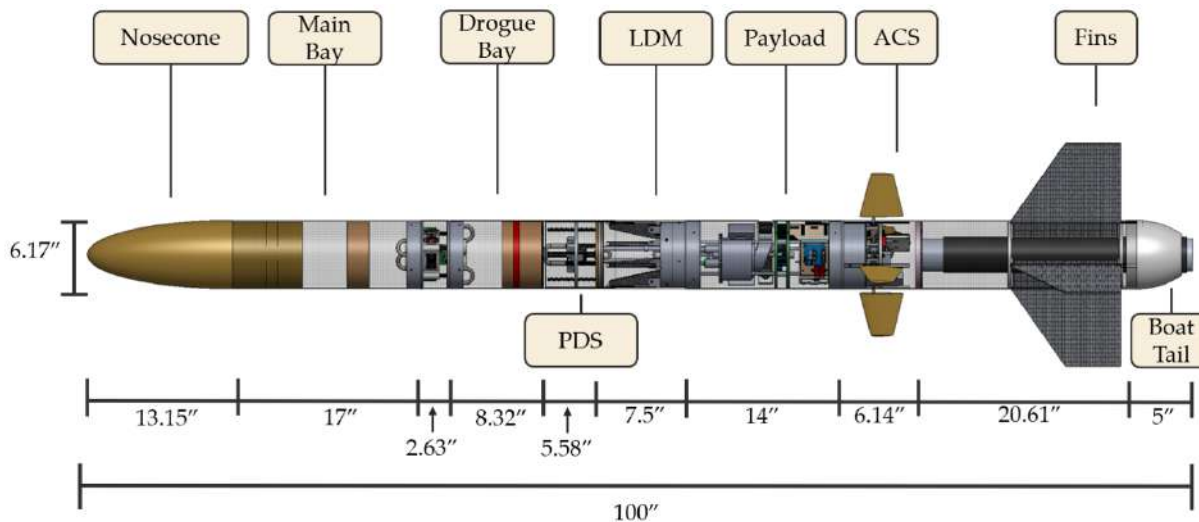


Figure 8: Full-scale launch vehicle, showing subsystem breakdown

The vehicle separates into three tethered sections across two separation points: one at the aft end of the recovery section (between the drogue bay and the parachute detachment system bay), and one at the forward end (between the nose cone and the main bay). At apogee, the tail section separates from the recovery and nose cone sections, deploying the drogue parachute. After descending to 550 ft AGL, the nose cone separates from the recovery section and deploys the main parachute, in accordance with NASA Requirement 3.1.1. The locations of these separation points as well as energetics materials, are shown in Figure 9.

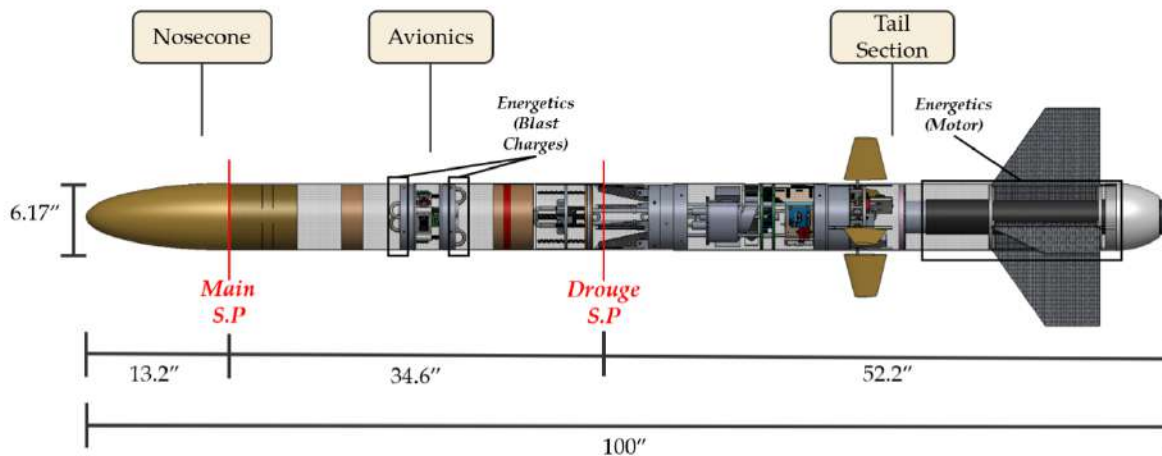


Figure 9: Locations of separation points and energetics

3.3.2 Vehicle Massing

An overview of the mass distribution across vehicle sections is shown in Figure 10. The total vehicle dry mass is 47.1 lbm. The tail section carries the majority of the mass and



weighs 28.1 lbm dry.

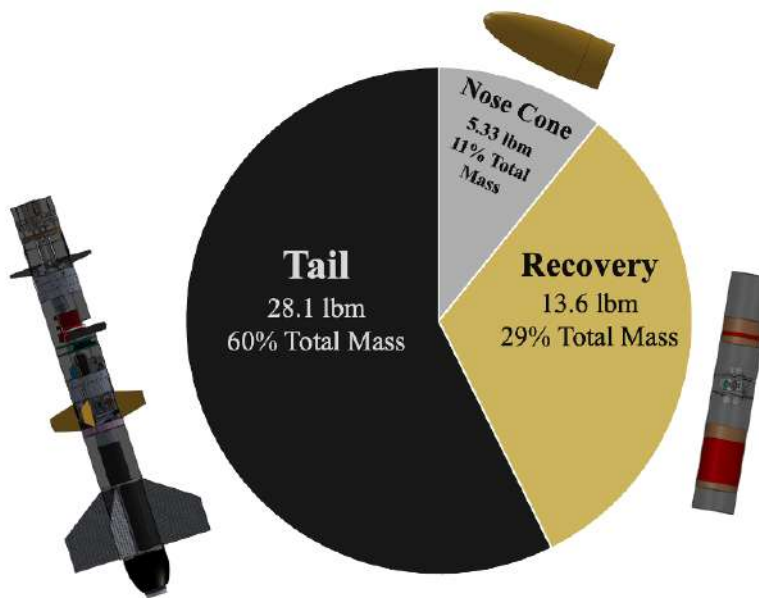


Figure 10: Massing Breakdown of Landed Vehicle Sections

Figure 11 shows wet mass broken down by system to highlight the primary drivers of total vehicle wet mass. The total vehicle wet mass is 51.1 lbm.

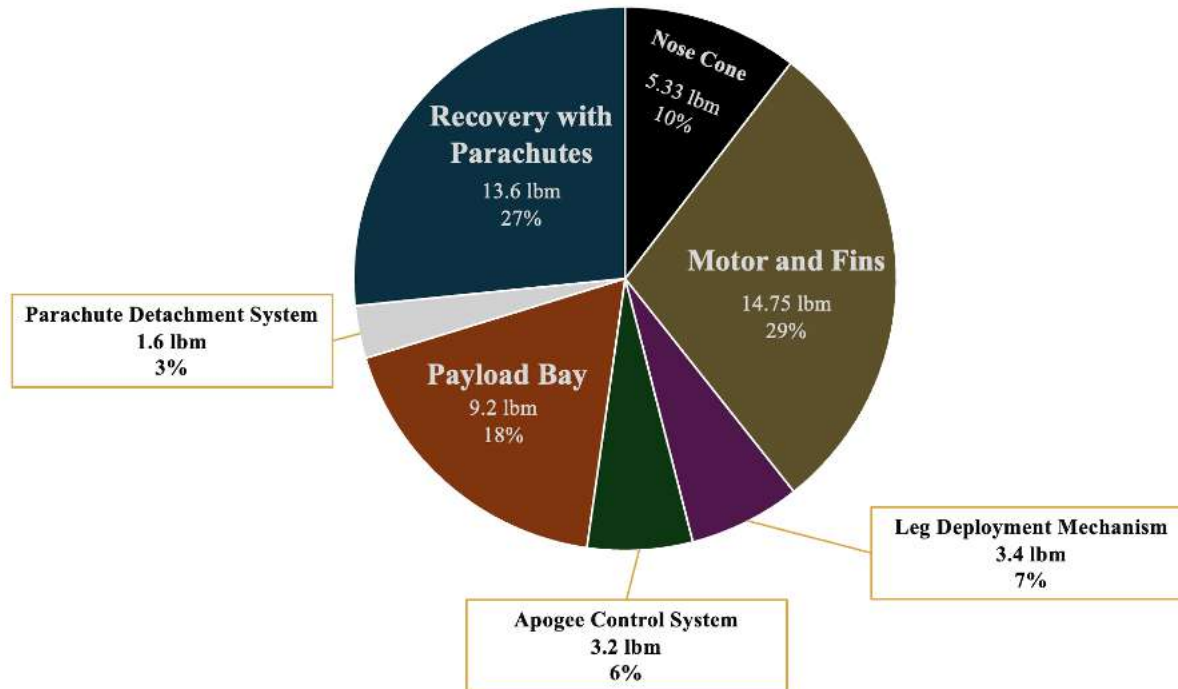


Figure 11: Wet Mass Breakdown by System

3.3.3 Airframe Material and Dimensions

The chosen material for the full-scale vehicle airframe is 6" G12 fiberglass composite tubing. Fiberglass tubing offers high axial strength, high impact toughness, high polar moment of inertia, manageable weight, while remaining cost effective.

To provide insight into the performance of this material and confirm its suitability for this years project, a 4" fiberglass section was used to approximate allowable forces for various expected failure modes, such as compressive strength and axial bolt tear-out. The summary of the methods and results of this test procedure is outlined below.

Procedure All tests were performed on a hydraulic load frame. A subscale (4 in) fiberglass airframe section was tested and material properties were extrapolated from the results. A single strain gauge was used in each test to record strain. Each test type was conducted once.

Specimen geometries are summarized below:

Table 21: *Fiberglass airframe specimen geometry*

Length, L (in)	OD (in)	ID (in)	Bolt hole edge distance, e (in)
7.75		4.02 3.90	0.50

Loading Protocol Two loading configurations were tested. In the first, *axial compression*, the tube was mounted vertically and loaded in compression up to 5 kN. In the second, *bolt tear-out*, a bolt plate was attached to the tube using four 10-32 screws (0.2 in diameter) and loaded in pure shear until complete tear-out occurred.

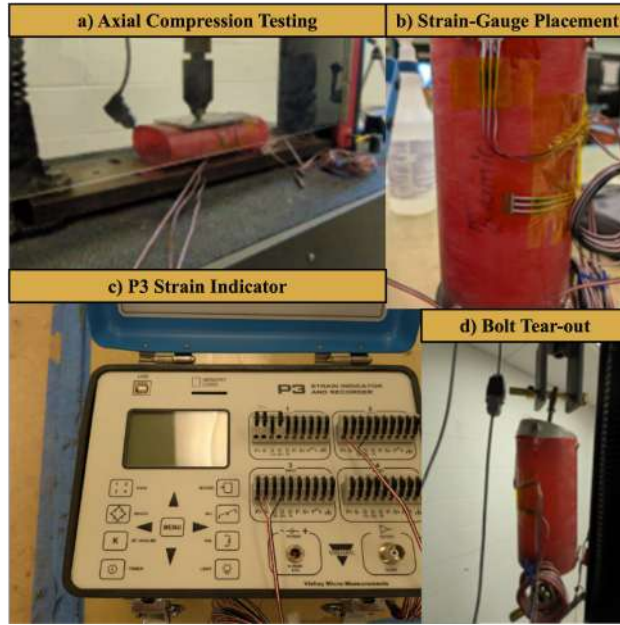


Figure 12: Composite of the mechanical test setup and instrumentation. Shown are (a) the specimen configured for axial-compression testing, (b) strain-gauge placement on the sub-scale fiberglass airframe specimen, (c) the strain indicator used for data acquisition, and (d) bolt tear-out (pure shear) testing.

Axial Compression The axial stress-strain response was roughly linear over the full load range used in the test. Stress was computed from the applied load using the tube cross-sectional area $A = \frac{\pi}{4}(OD^2 - ID^2)$ with $OD = 4.02$ in and $ID = 3.90$ in. A linear fit to the engineering stress versus engineering strain measured by the axial gauge yielded a Young's modulus of

$$E = 1278 \text{ MPa (1.28 GPa).}$$

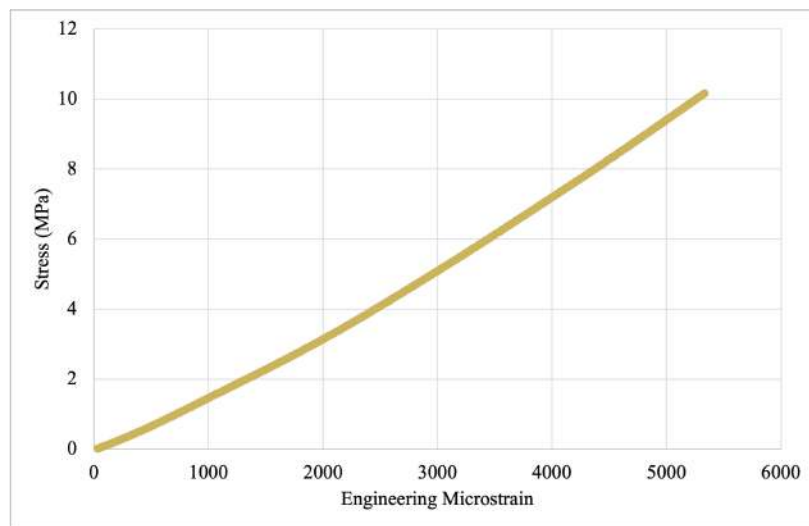


Figure 13: Stress-strain diagram of specimen under axial compression



Bolt Tear-Out An aluminum bulk plate was fixed to the fiberglass airframe using four 10–32 bolts and 0.2 in diameter holes. Under increasing shear load the fastener holes exhibited progressive bearing deformation (egging) in the laminate around the bolts until complete tear-out occurred.

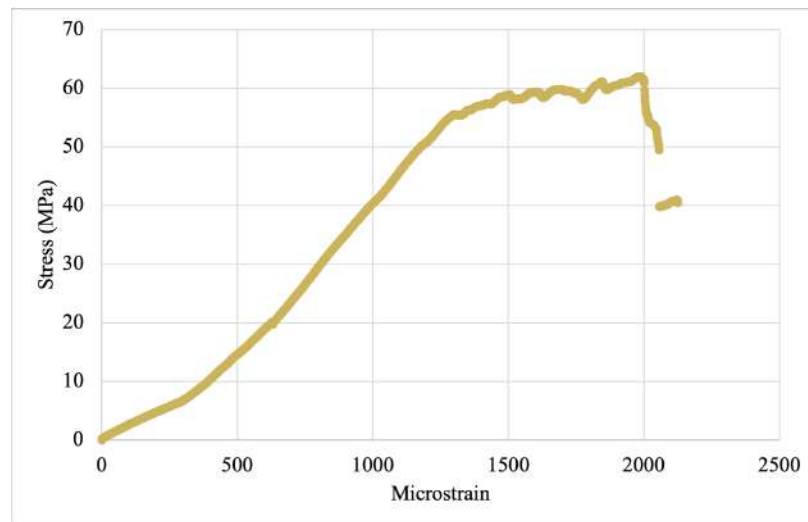


Figure 14: Stress-strain diagram of specimen under axial tension

The tests were performed on a 4 in diameter section with a gauge length of 7.75 in. The measured compressive modulus of elasticity (1.28 GPa) is taken as representative of the material and can be applied to the full-scale 6 in body tube to assess both axial compressive capacity. Likewise, the diameter-independent nature of the bolt tear-out stress was used to characterize the joint; this metric can be extrapolated to body tubes used within the full-scale provided the fastener details are comparable (four 10–32 bolts with holes located 0.50 in from the free edge).

3.3.4 Nosecone and Nosecone Bulkplate Retention

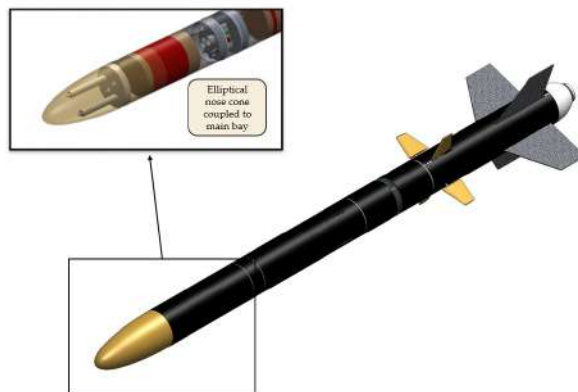


Figure 15: Elliptical nosecone with nosecone bulk plate



Based on a trade study conducted in Section 3.2.2, an elliptical nose cone was selected in order to remain in compliance with VADL Requirements 2.1.5-6.. The total length including the coupler is 19.45 in. A coupled section at the aft end has a 5.92 in diameter and is 6.375 in long, in accordance with NASA Requirement 2.5.1.

The team is planning on manufacturing the elliptical nose cone using 3D printed male-female molds. The team has already successfully molded an elliptical nose cone for our subscale rocket.

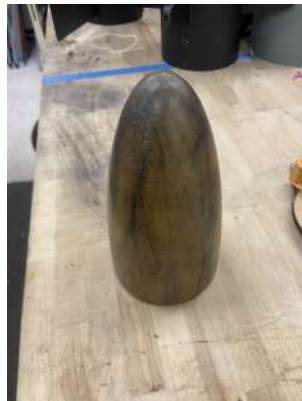


Figure 16: Molded subscale elliptical nose cone

The full-scale nose cone will incorporate a coupler that will be epoxied to the inside of the molded nose cone. The coupler will be inset into the nose cone 3" with the remaining 6.375" protruding. The 6.375" protruding male section sits inside the fore section (in compliance with NASA Requirement 2.5.1) of the main bay and is retained with 2-56 nylon shear pins (Section 3.2.3). A 0.3 in radially thick aluminum bulk plate will be inserted inside the coupler and will bolt through the coupler and molded nose cone into the airframe. The bulk plate mounts the 3/8"-16 steel U-bolt used to attach the 12 ft shock cord (Section 3.5.7). The bulk plate also includes mounting holes for 5/16-inch ballast screws so that mass can be added within the nose's available volume. A drawing of the nose cone bulk plate (Figure 17) below shows key dimensions.

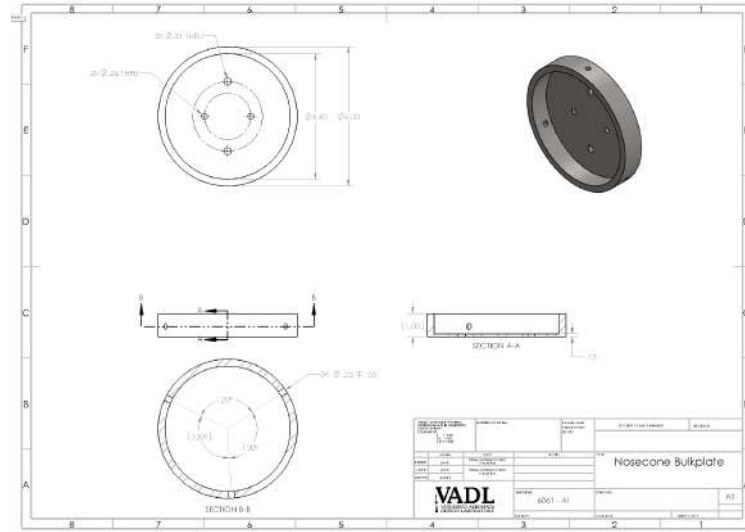


Figure 17: Nosecone bulkplate drawing

Deployment load on structure Maximum forces on the structure occur at main parachute deployment at an estimated acceleration of 26 gs. Because the bolt holes are far from the edge of the coupler, there is no risk of bolt tear-out. The other main structural concern for the nose cone assembly is tear out of the U-bolt that secures the Kevlar shock cord to the main parachute. Given the nose cone section is estimated to weigh only 5.33 lbm, the aluminum bulkplate and U-bolt retain a high factor of safety against stripping loads. All of these design decisions are made in accordance with VADL Requirement 2.1.5, weighing weight, structural integrity, and ease of fabrication.

3.3.5 Ballast Integration

Ballast is housed inside the hollow volume of the nose cone and attaches to the nose bulkplate. Based on current mass estimates, a nominal 3 lbm of ballast is planned to trim apogee so the ACS can meet the target altitude. The ballast hardware consists of 5/16-in steel threaded rods secured to the bulkplate with steel washers and nuts. Steel washers are then stacked on the rods to set the required mass and are locked in place with nuts (lock-nut pair). This arrangement provides coarse–fine adjustability by adding or removing washers. A ballast mass of 3 lbm complies with NASA Requirement 2.20.7 that ballast not exceed 10% of the vehicle’s unballasted wet mass.



3.3.6 Main Parachute Bay

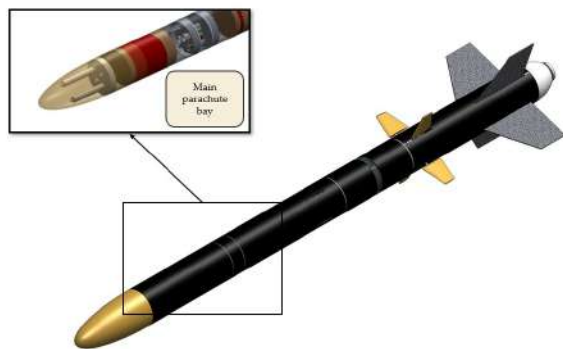


Figure 18: Main parachute bay

The main parachute bay houses the 12 ft main parachute, shock cords, and recovery hardware. It is comprised of a 6 in inner diameter G12 fiberglass body tube measuring 17.7 in. With a volume of roughly 500 in³, we expect it to comfortably house the main parachute, shock cords, and other recovery hardware, which we estimate to occupy about 250 in³, 80 in³, and 50 in³, respectively. These conservative estimates still leave ample free volume for clean deployment; any remaining space will be lightly filled with cellulose ("dog barf") to prevent shifting and protect the chute bundle.

The aft side of the main parachute bay will be coupled to the nose cone coupler using 4, 2-56 nylon shear pins. Shear pin calculations can be found in Section 3.2.3 and energetics calculations can be found in Section 3.5.5.

3.3.7 Avionics Bay

The avionics bay houses the 3D-printed avionics housing and all flight electronics (see Section 3.5.2). Structural tie-down is provided by lift-rated forged steel 3/8 in eye bolts, which serve as both shock-cord anchors and through-rods that clamp the bay together. A 3 in section of 6 in-ID G12 fiberglass airframe surrounds the bay and includes pressure ports and access for arming.

Key design details:

- **Pressure porting:** Four 1/4,in diameter holes are drilled through the airframe to provide clean static pressure to the barometric altimeters and to allow tool access to the screw terminal used to arm/disable the avionics prior to flight. Port hole sizing calculations can be found in Section 3.5.2.
- **Snatch-force sizing:** The governing load case is main-parachute deployment. The resulting factor of safety for the eye-bolts is 2.58, as computed from the main-deployment snatch force in Section 3.5.8.
- **Charge routing and sealing:** EM-match wiring from the avionics housing to the ejection charges is routed through each bulkplate via pass-throughs. Putty is applied on both



bulkplate faces to seal the avionics chamber so that deployment pressures do not affect the altimeters.

- **Charge hardware:** Blast-charge caps are rigidly mounted to each bulkplate.



Figure 19: Avionics bay assembled and exploded views

3.3.8 Drogue Bay

The drogue parachute bay houses the 24 in Fruity Chutes Classic Elliptical drogue, 38 ft of 1/2 in Kevlar shock cord, and associated recovery hardware (Nomex fire blanket, quick links, swivel link, and packing “dog barf”). It is comprised of a 6 in inner diameter G12 fiberglass body tube measuring 8.1 in. With a volume of roughly 229 in^3 , we expect it to comfortably house the drogue parachute, shock cord, and other recovery hardware, which we estimate to occupy about 40 in^3 , 90 in^3 , and 25 in^3 , respectively. These conservative estimates still leave ample free volume for clean deployment; any remaining space will be lightly filled with cellulose (“dog barf”) to prevent shifting and protect the drogue bundle.

The drogue parachute bay will be coupled to the parachute detachment bay coupler using 4, 2-56 nylon shear pins. Shear pin calculations can be found in Section 3.2.3 and energetics calculations can be found in Section 3.5.5.

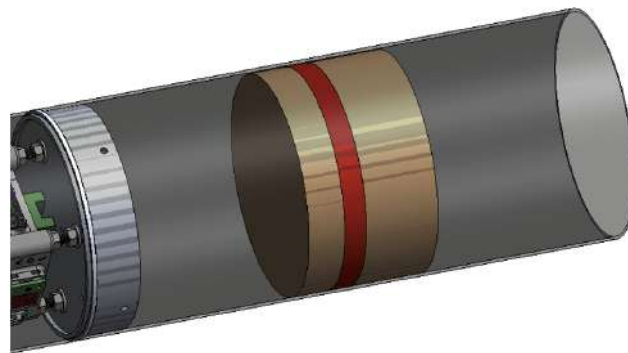
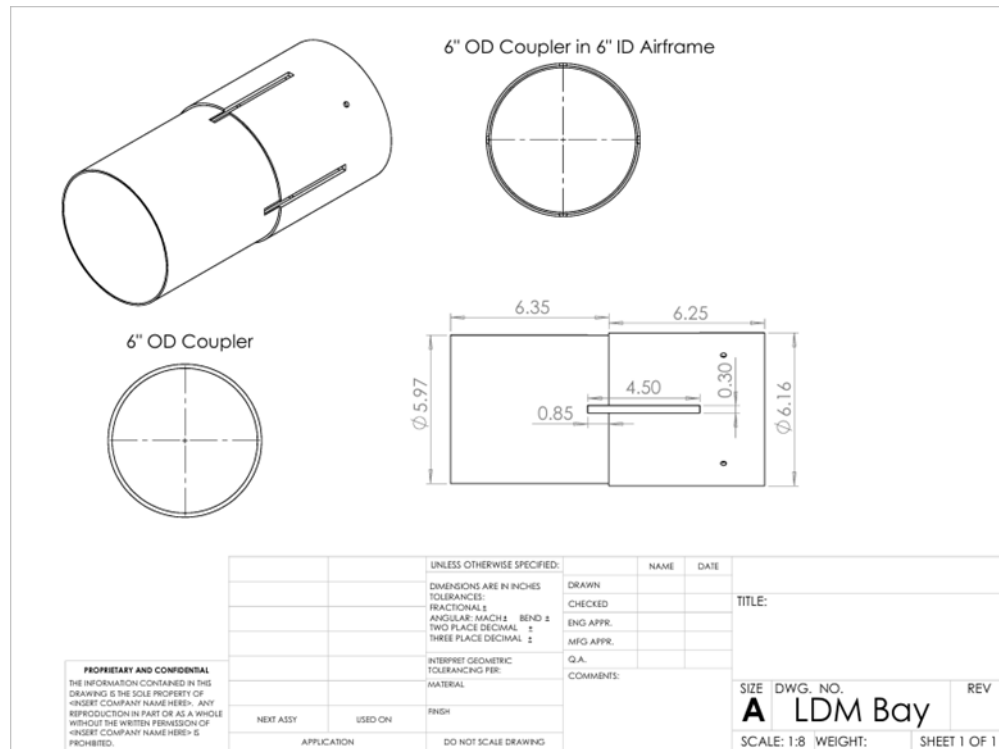


Figure 20: Drogue parachute bay, including packing volumes (left to right) for 12 ft shock chord, 24" drogue parachute, 26 ft shock chord

3.3.9 Parachute Detachment Bay

The Parachute Detachment Bay is an extension of the Leg Deployment Bay, as it is set inside the coupler rigidly attached to the LDS. This is the coupler that interfaces with the drogue bay. The PDS sits inside the drogue coupler, which itself is a component of the LDS bay. This combined airframe structure (with cutouts for leg deployment) is included below with dimensions called out. In accordance with NASA Requirement 2.5.1, the total length of this coupler is 12.6", greater than two airframe diameters in length, with greater than one body diameter of surface contact between each coupled section.



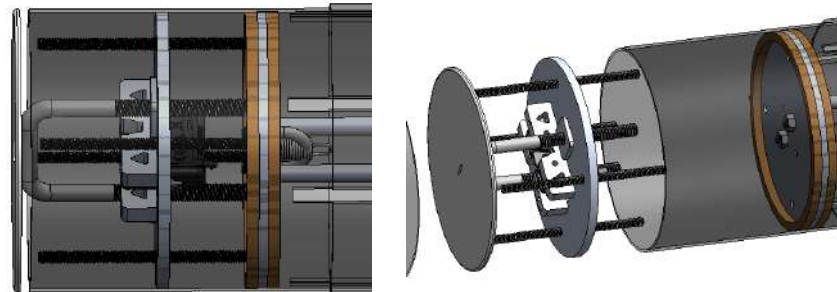


Figure 21: Parachute Detachment System CAD model

The structure of the PDS bay and the design-for-assembly methodology employed are outlined here. The entirety of the PDS (mechanical and electrical components) can be assembled outside of the PDS bay with ample space for troubleshooting and adjustment. This PDS assembly is then rigidly attached through threaded rods to the foremost LDS bulkplate. This bulkplate is epoxied to the airframe to ensure non-rotation and fixture of its axial location, but this epoxy joint does not take the majority of the load imparted on the PDS Bay from parachute shock, as described below.

Anticipated Load Path

The majority of shock load imparted on the PDS is transferred through the PDS mounting rods to the smooth guiding rods in the Leg Deployment Bay, then through the Rotating Bulkplates and Payload Bay.



Figure 22: PDS prototype 2 inside Payload Drop Testing Platform aft section

In addition to the initial testing completed in Section 3.2.6 when evaluating alternative designs, future testing will be done on this second prototype to test landing electronics/-



logic and the addition of a blast plate/tensioner plate. It will also be directly tested above our maximum expected dynamic load to validate the structural integrity of the design.

The Parachute Detachment System (PDS) electronics are responsible for detecting flight states and initiating parachute detachment upon vehicle landing. The PDS shares a nearly identical architecture with the Payload Electrical System 4.3, utilizing the same Teensy microcontroller, onboard IMU, battery, and voltage regulation circuitry. This shared design approach reduces system complexity and intends to maintain consistency between both the Payload Electrical System and PDS landing detection, allowing for the electrical reliability layed out in VADL Requirements 2.3.4-5

To meet the electromagnetic latch's voltage requirements, a compact LM358-N operational amplifier circuit is included to step up the Teensy's native 3.3 V control signal. The PDS firmware continuously monitors IMU acceleration and altitude data to determine touchdown conditions, triggering the detachment sequence only after vertical velocity and altitude have stabilized below predefined thresholds. The timely sequence of landing detection and latch activation is necessary to meet VADL Requirement 4.1.6.

A schematic of the Parachute Detachment System electronics, housed within the Parachute Detachment Bay, is provided below (Figure 23).

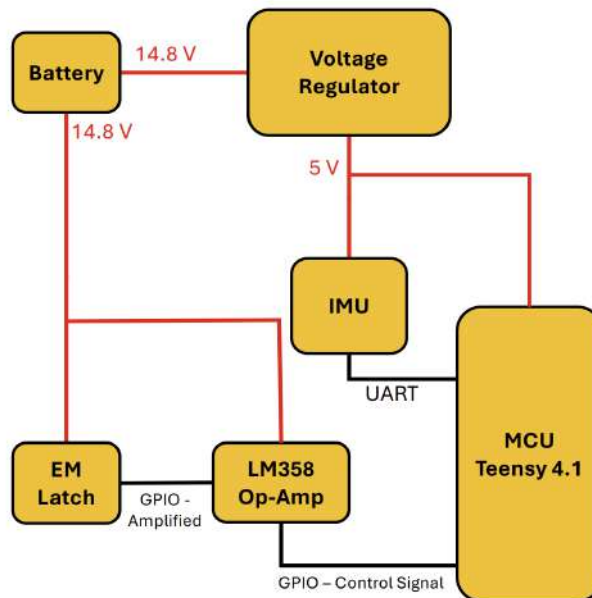


Figure 23: Parachute Detachment System Schematic

3.3.10 Leg Deployment Bay

The leg deployment bay houses the mechanism that deploys the tail section's landing legs. When deployed, the legs extend 3.25 in from the rocket body; the fixed tail fins extend 7.5 in. The legs provide the required stability at touchdown so the tail section can safely support the vehicle and complete the mission, in accordance with VADL Requirement 2.4.3.

The legs are sized to provide sufficient stability while keeping the landing vehicle slanted. After landing, the rocket is intended to rest on a slight uphill slope so the



shovel and soil capsule—mounted below the leg bay—operate correctly. The capsule's left "waterline" is intentionally lower, so soil shed from the shovel naturally falls into the capsule.

Leg deployment is passive and is triggered during main-parachute separation, in accordance with VADL Requirement 2.4.2. As the fore section airframe pulls away, a spring-driven translating plate moves upward and rotates the four legs outward. Collars limit travel, preventing the legs from rotating beyond 90°. The mechanism uses three primary joints: (1) a press-fit joint coupling the translating plate to each leg, (2) a bracket joint that provides a secondary tie to prevent any skew from the press-fit, and (3) a spring-to-U-bolt joint that anchors the springs between the two plates. The springs are preloaded during assembly when the drogue coupler is inserted into the drogue bay; upon aft-section separation from the recovery section, this stored energy lifts the plate and deploys the legs. The leg-bay airframe includes longitudinal slits that allow the legs to swing out from the body during deployment while keeping them contained during ascent and drogue descent.

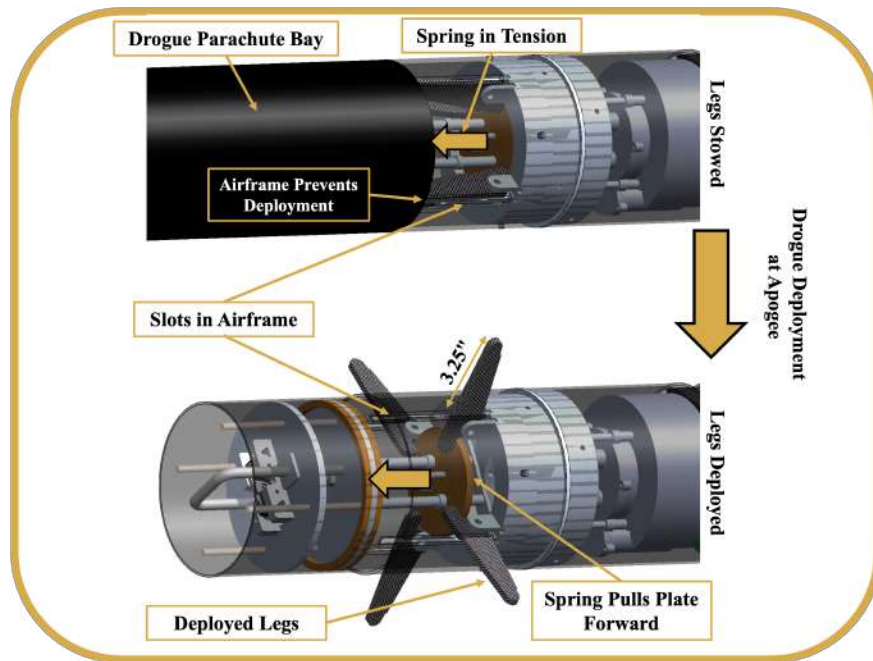


Figure 24: Passive deployment of legs after drogue deployment

3.3.11 Rotating Bulkplate System

The Rotating Bulkplate System (RBS) serves as the method by which the payload rotates enabling it to collect soil, while also resisting large axial and shear forces during parachute deployment and landing. The geometry of the selected design (cup-mounted bulkplates) has been developed throughout the semester, with multiple iterations. The final design is able to most efficiently balance constraints such as assembly mass, assembly strength, rotational resistance, ease of manufacturing, and ease of assembly.

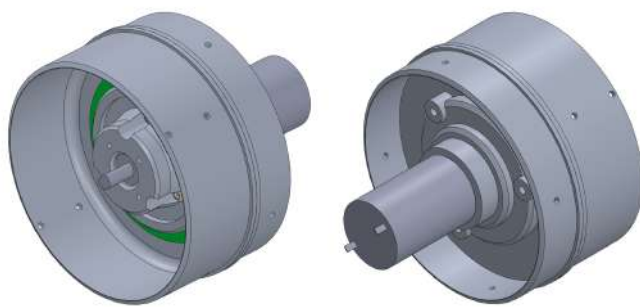


Figure 25: Current iteration of RBS prototype with improvements based on preliminary testing. The front and back of the active side are on the left and right respectively.

To quickly validate the mechanical architecture prior to final machining, a full-scale prototype was fabricated on a Prusa i3 MK3S using PLA at 25% infill. This enabled rapid iteration on small design features details such as cup lip thickness, chamfer sizes, and bolt-hole clearances, while also providing initial insight into assembly fit, rotational smoothness, and qualitative strength.

Two primary loading events — parachute shock and landing impact — were replicated to assess gross failure modes:

Snatch-force Tensile Pull: The printed RBS assembly was attached to an airframe section and pulled axially using #10-32 bolt anchors to simulate parachute loading. Failure occurred at approximately 45 lbf, with cracking concentrated at the outer bulkplate lip. This failure aligned with the PLA layer direction, reinforcing that while printed PLA was a beneficial step for iteration, its anisotropic strength did not represent the expected aluminum behavior.



Figure 26: The left image displays how the strings were mounted to the airframe bolts. The right image shows the loading procedure. The scale shows a tensile force of approximately 45 lbf. Eye protection was worn in the event that a small plastic piece would break off.



Tip Over Test: A tail-section mockup was rotated to the predicted impact orientation to simulate ground contact loads. The active-side cup lip fractured at the interface between printed layers, similar to the snatch-test behavior. Although driven by printed material limitations, the test confirmed areas of elevated stress concentration and highlighted the benefit of increasing lip cross-section and fillet/chamfer size.

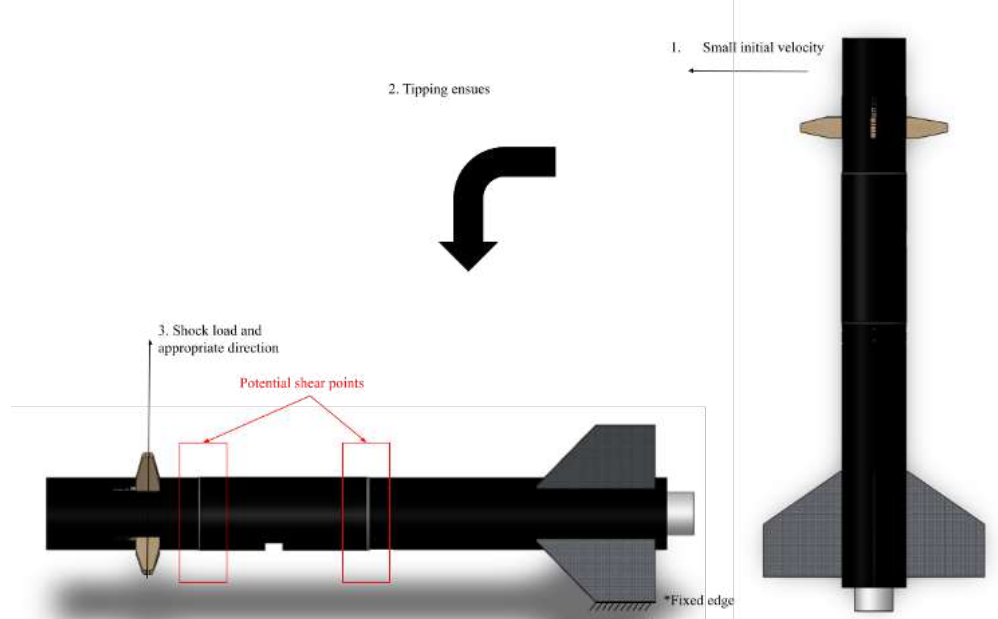


Figure 27: Experimental schematic of tip test. The rocket was held by a team member on its side and tipped over to replicate the landing condition on the full-scale rocket

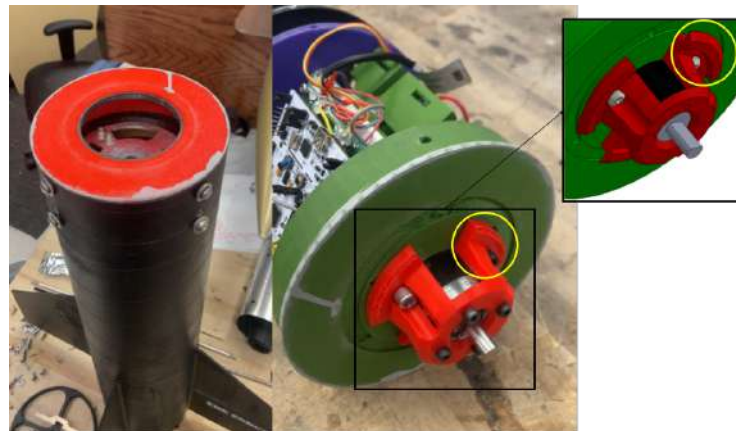


Figure 28: Results of tip test in which the active side lip is sheared off, as seen in the yellow circle compared to break-out view. The corresponding tail section is also shown (left).

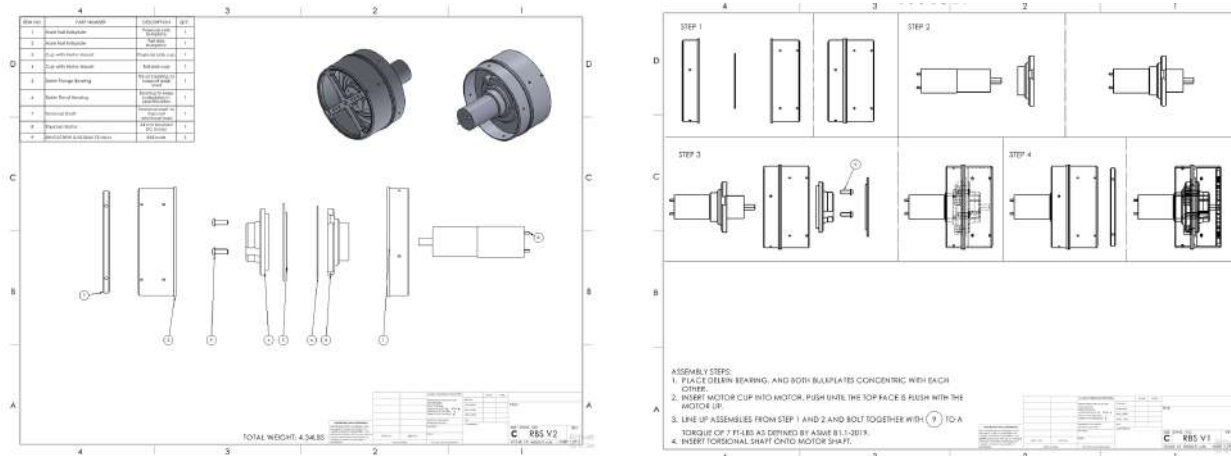
Based on prototype behavior, cup geometry was refined to improve strength and manufacturability:

Several design refinements were implemented to improve manufacturability and structural performance. The lip thickness was increased from $1/16$ in to $1/8$ in, fillets were replaced with chamfers to reduce machining time and minimize stress concentrations, and



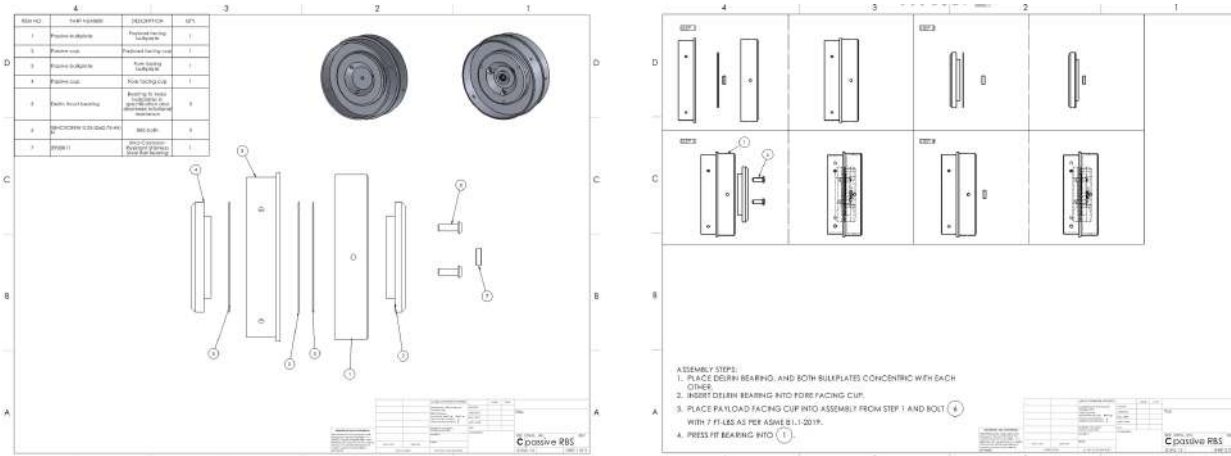
fastener fit tolerances were improved to ensure consistent shaft alignment.

These adjustments were made while maintaining compliance with VADL manufacturability requirements and minimizing mass growth.



Active side RBS bill of materials drawing

Active side RBS global assembly drawing



Passive side RBS bill of materials drawing

Passive side RBS global assembly drawing

Figure 29: RBS Active and Passive side drawings

RBS Bolt Tear Out Calculations To ensure that the bolts do not strip during main parachute deployment, the following calculation will determine the tensile resistance of the $\frac{1}{4}$ -20. Here, the aluminum tap in the bulkplate will be modeled for failure, as opposed to the steel bolt thread, as the former material is weaker in shear than the latter.

Generally, the bolt pull-out force can be defined as:

$$F_{\text{pullout}} = \pi d_{\text{avg}} L_E \tau_{\text{shear}}$$

Where:

$$d_{\text{avg}} = \frac{d_{\text{major}} + d_{\text{minor}}}{2} = \frac{0.25 + 0.201}{2} = 0.2255 \text{ in}$$

$$L_E = 0.375 \text{ in}$$

$$\tau_{\text{shear}, 6061} = 25000 \text{ psi}$$

$$F_{\text{pullout}} = [\pi \times 0.2255 \text{ in} \times 0.375 \text{ in}] 25000 \text{ psi} = 6638 \text{ lb}$$

As a conservative estimate, let's consider the maximum shock load in this assembly for the load case $F_{\text{shock}} \approx 1084 \text{ lb}$. The calculated safety factor for the three bolt assembly is 18.4, in accordance with VADL Requirements 2.1.1-2.

$$\text{SF} = \frac{3 \times 6638 \text{ lb}}{1084 \text{ lb}} = 18.4.$$

Although PLA prototypes allow for rapid validation of assembly fit, rotation behavior, and loading paths, the brittle nature of printed materials caused premature failure and did not accurately reflect expected performance in aluminum components. However, these tests informed critical refinements to lip thickness, chamfer design, and bolted interfaces. To quantify the structural margins of the final configuration and satisfy the VADL Requirements 2.1.1-2 and 2.1.5 for structural verification, finite-element analysis (FEA) was performed. The FEA examines the RBS cups and bulkplate under parachute shock, focusing on stress regions, deflection, and safety factor relative to the yield strength of 6061-T6 aluminum.

Load Bearing Member Finite Element Analysis

To ensure that the structure remains up to specification based on VADL requirements, FEA will be performed. Here, the cups will be the primary focus due to their complicated geometry and inaccuracy to hand calculations. Based on the load path of parachute shock (the largest load present during flight), the bottom facing cups will be analyzed.

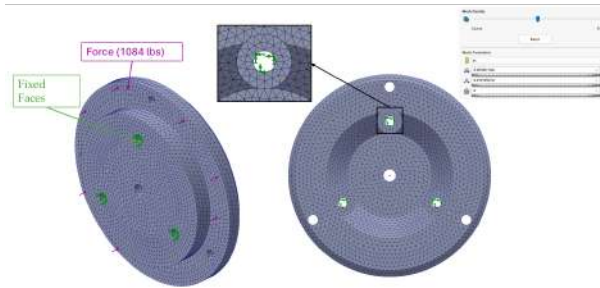


Figure 30: Passive side load bearing cup meshing parameters.

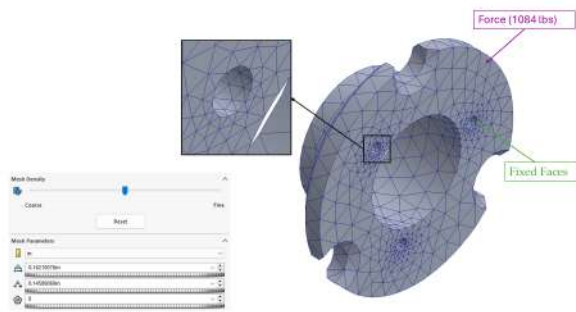


Figure 32: Active side load bearing cup meshing parameters.

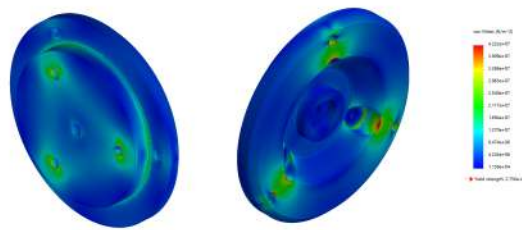


Figure 31: Passive side load bearing cup Von Mises stress map. The resulting safety factor during shock loading is 6.50.

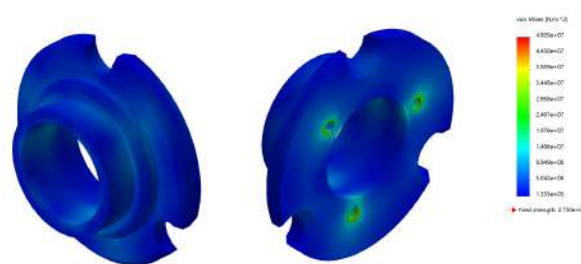


Figure 33: Active side load bearing cup Von Mises stress map. The resulting safety factor during shock loading is 5.59.

3.3.12 Payload Bay

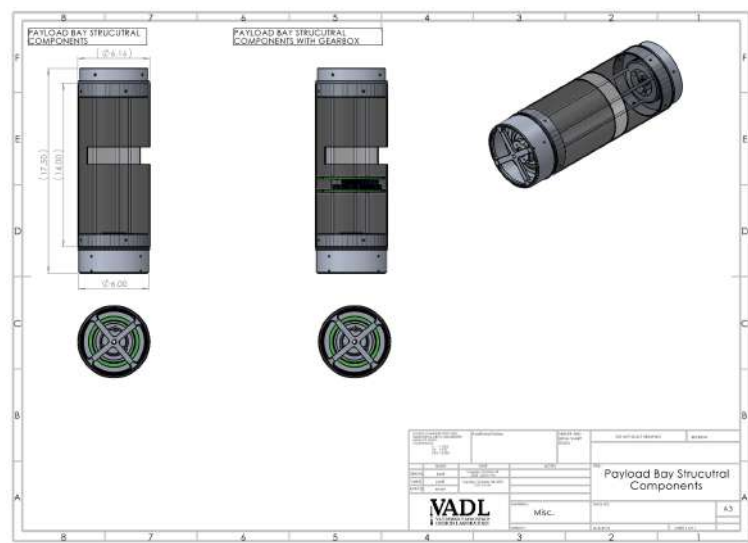


Figure 34: Assembly drawing of payload bay structural components

The payload bay houses the extension mechanism, payload electronics, and soil collection chamber. It sits between the two rotating bulkplates (RBS) and must be able to



withstand axial loadings experienced during takeoff and main parachute deployment.

Geometry, structure and retention The bay is housed within G12 fiberglass airframe with an internal length of $L = 14$ in. The airframe will be secured to the inner shoulders of the rotating bulkplates using four 10-32 bolts. To accomplish the mission, a section of the airframe will be cut out to allow the shovel to radially extend outwards. To prevent aerodynamic effects during flight, a sheet of Mylar will be taped over the cutout in the airframe. Upon landing, the shovel will pierce through the Mylar. In addition to being coupled to the shoulders of the rotating bulkplates, the airframe is bolted into the gear train bulkplates.

Internally, the bay is structurally held by three, 1/4-20 steel threaded rods (AISI 316) arranged 120° apart at a radius of ≈ 1.85 in from the tube centerline. The rods will be threaded into tapped holes within the inner RBS bulkplate. This “skeleton” of three-rods along with the airframe provides torsional stiffness and axial loading capacity and keeps the RBS gears concentric during high-load events.

Axial Rod Capacity To validate the payload bay’s three threaded tie rods in tension, we treat the airframe as non-load-bearing (worst case) and use the tensile stress area of fully threaded 1/4–20 316 stainless rods ($A_t = 0.0318$ in² each). The aft mass supported at main deployment is the tail mass plus payload mass plus ACS mass, $m = 23.5$ lbm. With a snatch acceleration of 26g,

$$F_{\text{total}} = 26m = 26 \times 23.5 \approx 611 \text{ lbf}, \quad F_{\text{rod}} = \frac{F_{\text{total}}}{3} \approx 203.7 \text{ lbf}.$$

The rod tensile stress and safety factor (against yield, $S_y \approx 30$ ksi for 316 SS) are

$$\sigma = \frac{F_{\text{rod}}}{A_t} = \frac{203.7}{0.0318} \approx 6.4 \text{ ksi}, \quad SF_y = \frac{S_y}{\sigma} \approx \frac{30}{6.4} \approx 4.7.$$

Thus, even under these conservative assumptions, the 1/4–20 316 stainless tie rods have ample margin in axial tension for the 26g main-parachute event, and comply with VADL Requirement 2.1.1.



3.3.13 ACS Bay

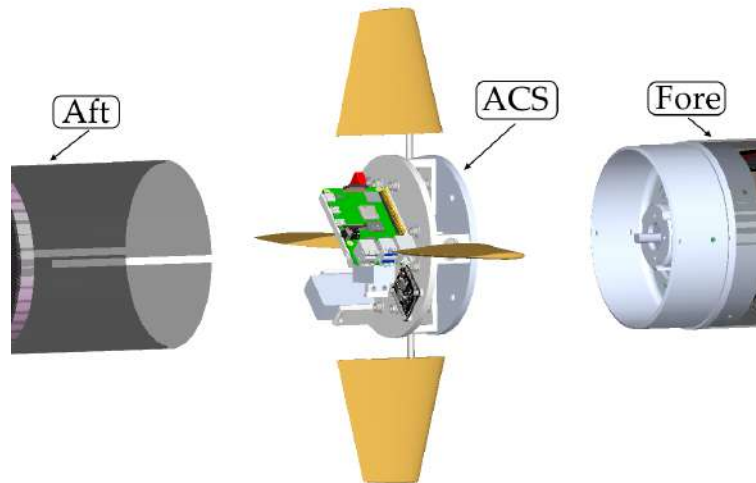


Figure 35: Locating the ACS Bay in the assembly

The Apogee Control System (ACS) bay is positioned immediately forward of the motor bay so the deployable fins sit well aft of the vehicle center of gravity. The ACS hardware mounts to a single aluminum bulkplate that fastens to the non-rotating side of the rotating bulkplate; by design, the ACS plate and electronics are non-load-bearing. Each fin is retained by Onyx 3D-printed brackets bolted to the ACS bulkplate, and the electronics mount to a 3D-printed avionics plate. Slots are cut in the local airframe to provide fin travel during deployment, with clearances set to prevent interference under expected bending. The team is also evaluating an aft shielding bulkplate (carbon fiber) epoxied into the airframe to protect ACS electronics and wiring from motor-induced heating and EMI. More information on the intricacies of the ACS system itself is found in Section 4.4.

3.3.14 Tail Section: Fin Can and Motor Retention Bay



Figure 36: Exploded view of tail assembly

The role of the fin can and motor retention bay is to properly transmit loading forces during burn, ensure that the motor is retained and center the motor during assembly. Shown above in Figure 36 is an exploded view of our tail section assembly including the following components (from left-to-right): (1) the carbon fiber insulating disk, (2) fiberglass airframe with cutouts for main fins and ACS, (3) motor retention and fin can assembly, (4) boat tail.

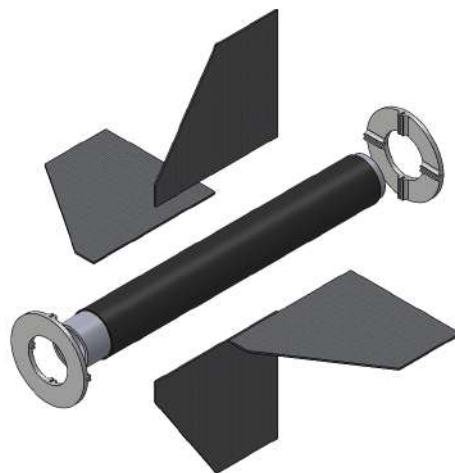


Figure 37: Exploded view of Fin Can and Motor Retention assembly.

Figure 37 above shows an exploded view of the fin can and motor retention subassembly. The motor casing is fit into a 3" inner diameter BlueTube section. 3D printed Onyx centering rings are epoxied to the BlueTube and provide concentricity between the airframe and motor casing during assembly; additionally, the centering rings contain slots to ensure fin alignment. Fins are rigidly adhered to the BlueTube using Fiberglass fillet reinforcements. 2000 Series Fiber Glast Epoxy Resin with 2160 Hardener will be used for all Fiberglass layups. Throughout assembly, adjustable fixturing will be used to ensure square, true and plum alignment of all components

Assembly Overview The tail assembly is constructed over several days of manufacturing and can be summarized by the following four steps:

1. Assemble the tail section alignment jig and line up all components.
2. Epoxy the fins to the motor tube, ensuring proper fit-up and aligning with the slots of the centering rings.
3. Add multi-layer fiberglass fillets on all eight fin-tube interfaces, with 45–90° rotational offsets to maximize omnidirectional strength and maintain compliance with VADL Requirement 2.1.3. (**Fin Can and Motor Retention Assembly is now finished.**)
4. Slide the Fin Can and Motor Retention Assembly into the slotted airframe, using centering rings for concentric alignment. Add multi-layer fiberglass epoxy fillets.

Excerpt from internal VADL tail section manufacturing procedure:

Fiberglass Layup Procedures

Required PPE: Nitrile gloves, respirator, eye protection

Materials:

- Fiberglass cloth (cut to size)
- Rice paper
- Cotton sheets
- Epoxy resin and hardener (Fibreglast 23:100 ratio)



- Mixing cups and sticks
- Masking tape
- Vacuum bag and pump

Day 1 — Fin and Centering Ring Bonding

1. Confirm location of centering rings on the motor tube and score bonding surfaces.
2. Assemble alignment rig, leaving the top plate uninstalled. Verify level on all sides.
3. Mix 24-hour epoxy (1:1 ratio by volume).
4. Apply epoxy to the bonding surfaces of fins and centering rings.
5. Install fins and centering rings using the rig for alignment.
6. Secure the top MDF plate above the top centering ring to maintain vertical alignment.
7. Allow epoxy to cure undisturbed for 24 hours.

Day 2 — Inner Fiberglass Fillet Layup

1. Cut 4 in × 4 in fiberglass cloth strips to span the motor tube and extend 1 in onto each fin.
2. Cut rice paper and cotton sheets matching the required dimensions (cotton sheets 1 in larger on each side).
3. Mix Fibreglast epoxy resin and hardener at a 23:100 ratio by weight.
4. Evenly wet out each fiberglass strip with mixed resin.
5. Apply each strip over the motor tube/fin interface.
6. Cover each with rice paper, then tape cotton sheets over the top.
7. Add additional cotton pieces along fin edges for even pressure.
8. Place the assembly in a vacuum bag, seal, and cure in the hot box at 140 °C overnight.

Day 3 — Outer Fiberglass Fillet Layup

1. Cut 4 in × 4 in fiberglass cloth strips (adjust dimensions per airframe/fin interface).
2. Cut rice paper and cotton sheets to match dimensions (cotton 1 in larger per side).
3. Mix Fibreglast epoxy resin and hardener at a 23:100 ratio by weight.
4. Wet out fiberglass strips completely and evenly.
5. Apply each strip over the airframe/fin interface.
6. Cover with rice paper and tape cotton layers on top.
7. Add cotton pieces along fin edges.
8. Seal assembly in a vacuum bag and cure in the hot box at 140 °C overnight.

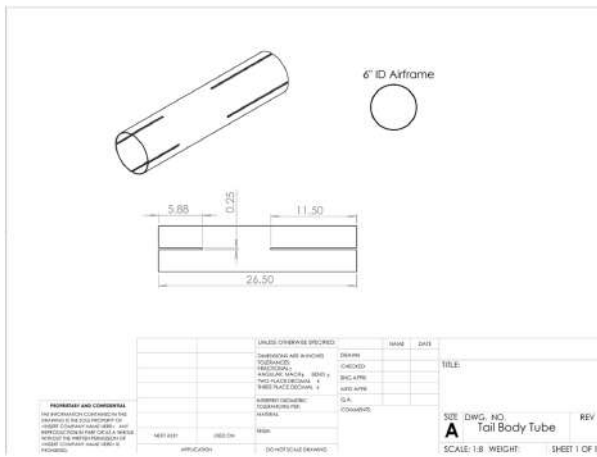


Figure 38: Drawing of the slotted tail section airframe



Figure 39: Subscale Tail Section Fabrication Jig

Slots within the G12 fiberglass airframe for the tail section will be cut out using a Dremel (Figure 38). Adjustable fixturing (jigs) is essential to ensure proper alignment during fabrication. The team has already begun qualifying this process with preliminary subscale manufacturing (Figure 39).

Motor Tube Adaptability Our leading motor, the Aerotech L1940 uses an RMS-75/3840 motor casing, while our backup the Cesaroni L2375 uses a Pro75-4G. Both have the same diameter and accommodate the same ring-retention mechanism. The entire tail section assembly is also designed to accommodate the length of both the L1940 and L2375 in case the backup motor is chosen.

Structural Integrity - Launch Loads The primary loads resisted by the fin can are experienced during launch, where the maximum thrust exerted by the motor is 521 lbf which is felt entirely by the fin can as it is at the aft of the rocket. Under this load case, two dominant failure modes are considered:

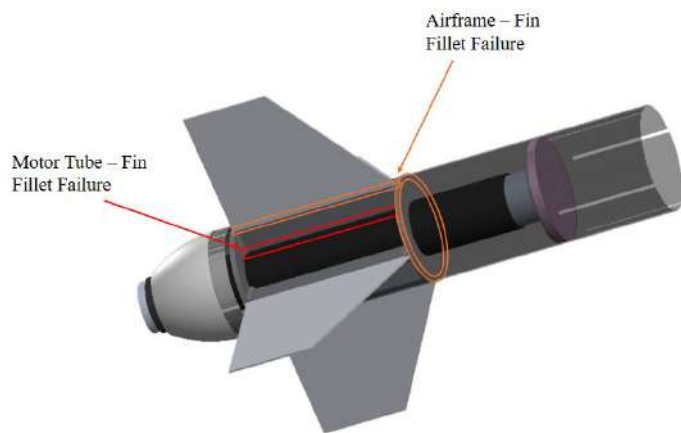


Figure 40: Assembled Tail Section with considered failure points called out considering the expected load patch from motor thrust.

- 1. Motor Tube - Fin Fillet Failure:** The motor retention tube rips free of its epoxy supports.
- 2. Airframe - Fin Fillet Failure:** The entire fin can assembly (centering rings, fillets, and fins) rips through its fiberglass supports and damages the airframe.

This load is transferred through the fiberglass fillets that attach the fins to the motor tube, the fins to the airframe, and the centering rings to the airframe. Because the bond length between the motor tube and fins is relatively short, the most likely failure mode is Mode 1: delamination at the fin/motor-tube interface due to adhesive shear failure. The following calculation evaluates that adhesive joint.

The effective bonded area for each fin–motor tube junction is based on a 10 in total fin length and a conservative effective fillet leg length of 1/16 in. Given there are eight bonded interfaces (two per fin for four fins), the total effective area can be calculated as:

$$A_{\text{effective, total}} = 8(10 \text{ in})(0.0625 \text{ in}) = 5.0 \text{ in}^2$$

Using a tensile strength of 9,828 psi (provided by the Fibre Glast System 2000 resin and 2160 hardener), and assuming a shear strength equal to 60% of the tensile strength, the total shear capacity of all epoxy fillets is then

$$F_{\text{capacity}} = \tau_{\text{shear}} \times A_{\text{effective, total}} = (0.6)(9,828 \text{ psi})(5.0 \text{ in}^2) = 29,484 \text{ lbf}$$

Finally, the factor of safety (FOS) under the 521 lbf launch load is

$$\text{FOS} = \frac{F_{\text{capacity}}}{F_{\text{applied}}} = \frac{29,484 \text{ lbf}}{521 \text{ lbf}} = 56.6$$

This high safety factor is necessary due to the unique geometry of this rigidly adhered connection. Namely the exact shear strength of the epoxied motor-fin connection will



deviate from the Fibreglast listed data as the geometry (thin fin cross section contacting curved airframe surface) deviates from their experimental test setup that generated the strength characteristic.

Despite this unique joint design, the team is confident that an epoxy fillet with sufficient contact area and the calculated FoS of 56.6 renders the tail section design able to withstand and effectively transfer the compressive loads of motor thrust throughout the vehicle airframe, and renders this joint design compliant with VADL Requirement 2.1.2.

3.3.15 Fin Material and Design

The chosen fin material (1/8" DragonPlate Carbon Fiber) can be easily water-jet cut to the specified clipped-delta fin geometry shown below.

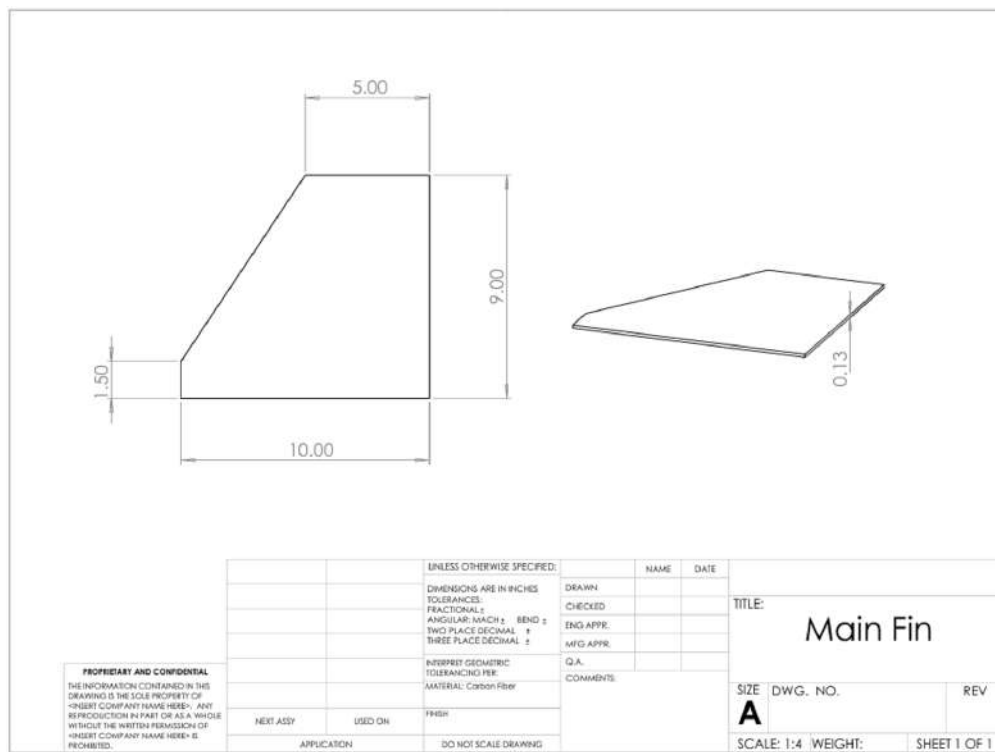


Figure 41: Drawing of main fin geometry

Upon fabrication, the flat-bottomed fins can be easily assembled using the jig described in Section 3.3.14.

3.3.16 Boat Tail

The goal of a boat tail is to reduce aerodynamic drag while only adding a relatively small amount of mass. This drag minimization effect puts the fullscale launch vehicle design in compliance with VADL Requirement 2.1.6. With this criterion in mind, the ideal boat tail would be one made of a lightweight material with a length long enough to have an impact on the drag while also avoiding unwanted heat distortion from the motor. To



achieve this, we chose to make our boat tail geometry taper from an outer radius of $R=3.02$ inches to an inner radius of $R=1.81$ inches over 5 inches with a wall thickness of 0.107 inches. This geometry, if constructed from a lightweight 3D printed material, only adds a mass of 0.36 lbm. Additionally, past CFD studies [2] have documented significant drag reductions for rockets that include a boat tail. In the study, a half-taper angle of 3.8 degrees was used, as opposed to our 13.7 degrees; however, since our boat tail accomplishes the same geometric smoothing, the main argument can still be applied to our case even if the values differ.

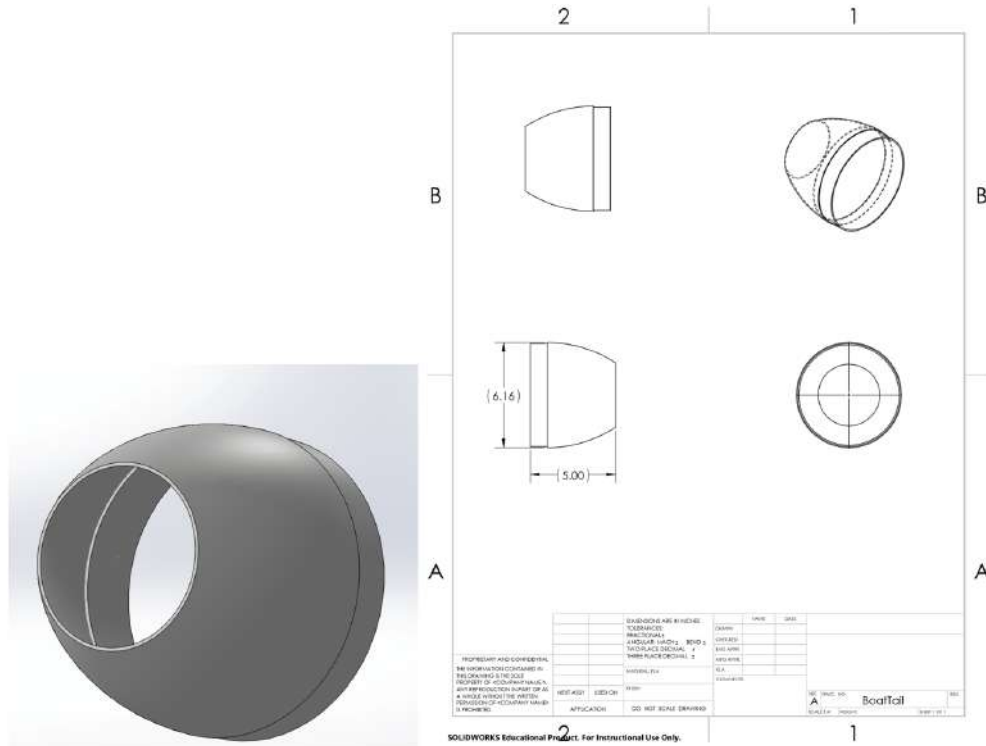


Figure 42: Boat Tail 3D view and drawing

3.3.17 Motor Selection

As seen in the motor trade study (Section 3.2.11), the most optimal motor configurations to use that yield results closest to the target apogee with ACS deployment above 3500 ft are the L1940 and the L1350. Because the L1350 has a longer burn time and lower average thrust compared to the L1940, it could be more susceptible to a higher amount of grain loss before launch rail exit. Additionally, the L1940 has no ACS and no ballast apogee of 4748 ft, which allows the ACS to operate over a larger altitude correction range than the L1350, with an apogee of 4675 ft, given VADL Requirement 3.2. These are the reasons the L1940 was chosen as our primary motor. The L2375 motor has been chosen as our backup motor in the event of a mass creep significant enough that the L1940 motor would not reach the target apogee of 4200 ft with ACS deployment. Seen below are full scale vehicle dynamics data given the primary and backup motor choices. Simulations used 5 degrees launch rail angle and 5 mph windspeeds.

Table 22: Motor Performance Comparison (3 lb Ballast, No ACS)

Motor	Apogee (ft)	Avg. T/W	Max Ascent Accel. (Gs)	Rail Exit Vel. (fps)	Landing KE (lb-ft)
L1940	4389	8.53	10.4	85.1	70.7
L2375	4591	10.64	11.7	90.9	69.1

3.4 Alternative Recovery Subsystems

3.4.1 Recovery and Avionics Overview

Competition rules necessitate that the launch vehicle lands safely and is reusable.

To meet NASA Requirement 2.4, our recovery system is designed with a dual-deployment framework: the drogue parachute deploys at apogee to slow descent and stabilize the rocket, and the main parachute deploys 550 feet above ground level to ensure a safe, controlled landing.

Altimeters, the core avionics component, provide real-time altitude data and initiate parachute deployment at the correct altitudes. In addition to altimeters, blast charges are used to separate the airframe and release the parachutes, while harnessing equipment ensures secure connections between the parachutes and the vehicle. Other necessary hardware includes power supplies, arming switches, and electrical circuits to ensure the recovery system is activated at the appropriate times.

To appropriately select the hardware for these subsystems, the team has conducted preliminary trade studies and calculations, carefully analyzing factors such as reliability, cost, size, and weight. Based on these studies, the team has chosen the leading hardware for all key subsystems and events.

3.4.2 Alternative Avionics and Altimeters

Avionics are a critical component of the recovery system and are responsible for ensuring that the rocket deploys its recovery parachutes at the correct points in flight. Altimeters monitor rocket altitude using barometric or IMU devices and trigger energetic parachute deployment events at precise moments.

Given the importance of the altimeter in safe recovery, varying off-the-shelf avionics systems have been reviewed to ensure the chosen system is reliable, accurate and efficient. This is in accordance with NASA Requirement 3.3, which states that only commercial altimeters shall be used. The team has also defined VADL Requirement 4.2.1 on sampling rate and VADL Requirement 4.2.2 on power consumption. A trade study was conducted to evaluate a variety of commercial avionics systems:

**Table 23:** Avionics System Analysis Trade Study

Design	Altitude Logging Resolution	Power Con- sumption	Available in Lab	Total Weighted Score	Total Weighted Score
	40%	20%	30%	10%	100%
PerfectFlite Stratologger CF	8	10	0	9	6.1
Entacore AIM	3	6	10	6	6.0
AltusMetrum EasyMini	10	3	10	10	8.6

PerfectFlite Stratologger CF

The **PerfectFlite Stratologger CF** is a highly efficient avionics system that offers a compact and easy-to-use design, making it an excellent choice for rocketry applications. It samples data at a rate of 20 Hz and operates with a very low current draw of only 1.4 mA, ensuring prolonged battery life with a standard 9 V battery. However, the team has decided not to use the Stratologger as we do not currently own one, have not used one in the past and the data logging frequency is low.

Entacore AIM USB

The **Entacore AIM USB** is a system the team has used in the past. Its mixed performance has deterred the team from selecting it for this year's mission. It offers a low 10 Hz sampling rate and a moderate 15 mA current draw. Additionally, the system's large profile makes integration more difficult.

Altus Metrum EasyMini

The **Altus Metrum EasyMini V2.1** has proven to be a reliable avionics system that we have successfully used in previous rocket launches and yielded dependable results. It logs data at 100 Hz on ascent, providing high-resolution data ideal for tracking rapid altitude changes during flight. The small and lightweight design make it an excellent fit. It uses a built-in micro-USB port to facilitate easy connection to a computer for configuration and data extraction. The biggest drawback is the current draw of 30 mA; however, a standard 9 V battery with 500 mAh of capacity will have a run time well over the 4 hour requirement specified by VADL Requirement 4.2.2. With these points to consider, the team is confident in selecting the Altus Metrum EasyMini for our avionics system.

3.4.3 Avionics Housing Materials

The avionics housing secures and retains all onboard flight computers and power systems. Although the sled is not a load-bearing component, it is essential that the housing safely retains all components and facilitates the secure installation of avionics. Several materials were considered for the housing, and a trade study was conducted to evaluate



their suitability based on key parameters. The materials considered for this trade study are ABS, PLA, and Fiberglass.

Table 24: Avionics Housing Material Trade Study

Design	Strength 40%	Ease of Manu-fac-turing 30%	Weight 30%	Total Weighted Score 100%
				8.00
ABS	8	10	0	8.00
PLA	3	6	10	6.0
Fiberglass	10	3	10	8.6

Based on the trade study, the housing will be manufactured out of ABS. This material offers the best balance of strength, ease of manufacturing, and weight. It will allow us to precisely design a 3D-printed structure with accurate mounting points for avionics components. The 3D printing process enables us to iteratively customize the housing to meet our specific needs and streamline production, while maintaining durability and a lightweight design for optimal performance.

3.4.4 Avionics Switches and Wire Strain Relief

Based on NASA Requirements 3.5-6, the avionics must be activated via a mechanical arming switch that is both accessible from the exterior of the rocket (allowing it to be armed on the pad) and capable of being locked into an on position. This ensures that, during flight, the avionics do not lose power. So, the team investigated several switching options, including the Featherweight Magnetic Switch, the Talon igniter switch (pull-pin), and the MissileWorks 6-32 PCB Screw Switch. After careful consideration, the team has chosen the MissileWorks 6-32 PCB Screw Switch due to its mechanical reliability and ease of use in high-power rocketry applications. The team has used the MissileWorks Screw Switch in past flights and had successful results, encouraging the team to reuse it.



Figure 43: MissileWorks 6-32 PCB Screw Switch

Wire Strain Relief

To connect the altimeter to the E-Matches which detonate the energetic charges, additional screw terminal blocks will be used to prevent overuse of the screw terminal blocks on the altimeter themselves. This is crucial to prevent the wires from loosening due to being repeatedly unscrewed, or damage due to vibrations or forces during launch and



flight. The screw terminals ensure that the connections remain tight and secure, even under mechanical stresses of rocket flight. The team chose screw terminals over other options such as snap connectors as they can easily be modified allowing for convenient rewiring while still providing a reliable mechanical connection.



Figure 44: DaFuRui Screw Terminal Blocks

3.4.5 Battery Trade Study

Ensuring the avionics are reliably powered is a crucial aspect. Considering our avionic altimeter takes a range of 4-12V, the following trade study was conducted on battery types:

Table 25: Avionics Battery Trade Study

Design	Weight 30%	Size 20%	Hazard 50%	Total Weighted Score 100%
				7.4
9 V Alkaline	6	8	8	7.4
7.4 V Lithium Ion	3	6	5	4.6
7.4 V Lithium Potassium	9	10	4	6.70

Based on the trade study, the Alkaline 9V battery is the most consistent and safest option. Being a cheap and non-rechargeable option means it won't sustain degradation as we will use a new battery for every test.

3.4.6 GPS Analysis

Maintaining a constant vehicle location during launch and recovery is crucial to ensuring a successful recovery. The team will install a standalone, independently powered GPS radio transmitter to achieve this, fulfilling NASA Requirements 3.12-13 and VADL Requirement 4.2.3. The GPS system selected is the *BigRedBee* GPS APRS transmitter. This module was chosen for its tested reliability in past missions. Since this year's entire airframe remains tethered for the duration of the flight, we require only one tracking system.

The GPS recovery system will be mounted on the same bulkplate as the Parachute Detachment System (PDS); however, the GPS module will be powered as a standalone system, completely electrically separate from the PDS, satisfying NASA Requirement 3.13.4.



The GPS module will be housed separately from the PDS electronics using a shielded enclosure, satisfying NASA Requirements 3.13.2-3.

Several other off-the-shelf systems were considered for the role of the GPS transmitter before we selected the *BigRedBee* GPS transmitter.

Table 26: *GPS Transmitter Trade Study*

Design	Availability	Ease of Integration	Transmissi and Perfor mance	Reliability & Features	System Cost	Total Weighted Score
						100%
BigRedBee APRS Tracker	10	8	7	9	4	7.9
Altus Metrum TeleMetrum v2.0	1	9	6	10	6	5.9
Missile Works WTX-T3	1	9	10	5	9	6.9
Featherweight GPS Tracker	1	10	10	10	4	7.15

In compliance with NASA Requirement 3.13, licensed amateur radio operators of the VADL ground team will operate a ground station to receive communications from the GPS recovery system. The data transmitted from the system will be stored on the ground station for post-flight analysis and reporting. The BigRedBee GPS transmitter operates in the 70 cm amateur radio band (420-450 MHz) and transmits AX.25 data packets at 100 mW. The system will be powered by a single-cell Li-Po battery, operating nominally at 3.7V. To satisfy VADL Requirement 4.2.3, which requires 4 hours of continuous runtime, the supplied 750 mAh battery, which is rated for 10 hours of use, will be verified with a drain test. The internal GPS module will log positional data at 1 Hz in the internal memory and transmit location data once every 5 seconds. Time slotting will be used to mitigate packet collisions with other transmitters on the same frequency.

3.4.7 Dual Deployment Overview

To satisfy NASA Student Launch requirements related to descent time, landing kinetic energy, and recovery safety, the team employs a dual-deployment recovery strategy. This system allows the vehicle to meet, descent time (NASA 3.11), and structural safety constraints while minimizing drift (NASA 3.10) and ensuring controlled descent throughout flight.

The dual-deployment approach uses two sequential parachute events: a drogue parachute deployed at apogee and a main parachute deployed at low altitude (550 ft AGL). The drogue slows and stabilizes the rocket after motor burnout, reducing tumbling and ensuring the airframe remains aligned for a clean main deployment. The main parachute then further reduces descent velocity for a safe touchdown, keeping the landing kinetic energy within NASA's prescribed limits.

Overall, the dual-deployment strategy enables the team to achieve all NASA recovery



performance criteria—balancing descent time, drift minimization, and impact safety—while maintaining a robust and redundant recovery system architecture.

3.4.8 Analysis of Alternative Drogue Parachutes

The drogue parachute is responsible for stabilizing the vehicle, reducing terminal velocity and limiting drift from apogee to 550 feet when the main parachute is deployed. The drogue parachute must generate enough drag to slow the vehicle from freefall without adding excessive descent time or drift.

To select the optimal drogue parachute, several commercial options were considered based on the following criteria:

1. **Descent time:** The drogue should provide a reasonable descent rate between apogee and main deployment, minimizing overall recovery duration
2. **Terminal Velocity:** The chosen parachute must reduce velocity sufficiently to ensure a safe main parachute deployment
3. **Availability in Lab:** Readily available equipment lowers cost and test time
4. **Reliability:** Proven performance in previous VADL flights

Table 27: Drogue Parachute Trade Study

Design	Descent Time 30%	Terminal Velocity 30%	Availability in Lab 20%	Reliability 20%	Total Weighted Score 100%
Fruity Chutes 18" Type: Elliptical Coefficient of Drag: 1.5	9	3	10	10	7.6
Fruity Chutes 24" Type: Elliptical Coefficient of Drag: 1.5	7	8	10	10	8.5
Top Flight X-Type 24" Type: Cross-Type Coefficient of Drag: 1.4	8	7	0	3	5.1

The team has chosen the Fruity Chutes 24" Classic Elliptical Parachute for our leading drogue parachute as it offers reasonable descent time, provides a good terminal velocity to keep main deployment snatch forces within safety factors, is available in lab, and has been previously used by the team reliably. The smaller 18" Classic Elliptical Parachute offers lower descent time but increases main deployment loads while the Top Flight X-Type has not been used by the team before and is currently not available in lab.

The 24-inch Fruity Chutes model, with a drag coefficient of approximately 1.5, has demonstrated reliable performance across VADL rockets and integrates cleanly with existing recovery hardware. This choice ensures stable drogue descent, controlled transition to main deployment, and compliance with NASA recovery safety requirements.



3.4.9 Analysis of Alternative Main Parachutes

The main parachute is responsible for reducing the rocket's terminal descent velocity to ensure a safe landing while minimizing landing kinetic energy in accordance with NASA 3.2. The parachute must generate sufficient drag to achieve a soft landing while also ensuring the overall descent time remains within mission constraints and that recovery occurs near the launch site.

To select the optimal main parachute, several commercial options were considered under the following criteria:

- Landing Kinetic Energy:** The parachute must limit the vehicle's terminal velocity such that landing kinetic energy remains under 75 ft-lbf as required by NASA 3.2.
- Descent Time:** The parachute should minimize descent time and drift.
- Availability in Lab:** Readily available equipment lowers cost and test time
- Reliability:** Proven flight heritage and consistent performance

Table 28: Main Parachute Trade Study

Design	Landing Energy	Descent Time	Availability in Lab	Reliability	Total Weighted Score
	30%	30%	20%	20%	100%
Fruity Chutes Iris Ultra 120" Type: Toroidal Coefficient of Drag: 2.2	3	9	10	10	7.6
Fruity Chutes Iris Ultra 144" Type: Toroidal Coefficient of Drag: 2.2	9	6	10	10	8.5
Top Flight X-Type 144" Type: Cross-Type Coefficient of Drag: 1.8	1	10	0	3	3.9

The Fruity Chutes Iris Ultra 144-inch parachute was selected as the primary main recovery system. It offers the lowest descent velocity and landing kinetic energy of the options considered. This is particularly important for this year's project as the large tail section mass necessitates that the main parachute provides a very slow landing. With a drag coefficient of approximately 2.2, this parachute enables a nominal descent rate of 12.6 ft/s, yielding a tail section landing kinetic energy of 69.6 ft-lbf which satisfies NASA requirement 3.2 which imposes a 75 ft-lbf limit.

The Fruity Chutes Toroidal 120-inch parachute, while compact and readily available, produces a higher terminal velocity that would increase landing kinetic energies beyond program limits. The Top Flight X-Type 144" similarly does not provide sufficient drag to provide a safe landing and has also not been used in past VADL rocket flights.



The Iris Ultra 144-inch chute provides an ideal balance between landing speeds and descent times. This selection ensures compliance with all NASA landing safety and descent time requirements while maintaining a reliable, and flight-proven recovery system.

3.4.10 Parachute Ejection and Retainment

Parachute ejection and retainment serve as a significant place of interest to ensure the safety and reliability of rocket recovery. There are a multitude of options available varying in both effectiveness and complexity. Choosing the best method requires an analysis of options, ranking them based on available external data and team experience.

Available options:

1. **Deployment bags:** Fabric bags which allow the parachute to come out during deployment. This can reduce opening shock and help prevent entanglement while protecting the parachute from residual blast charge heat.
2. **Dog Barf:** Traditional method using flame resistant cellulose. This material is packed between the black powder charge and the parachute to protect it and absorb residual heat.
3. **Piston System with Bulkplate:** A bulkplate sandwiched between the parachute and ejection charge which completely isolates the chute during deployment. When the charge fires, the pressure accelerates the face of the bulkplate, guiding the parachute out of the coupler. This bulkplate is usually made of plywood or composite material.
4. **Fire (Nomex) Blankets:** Typically made of Kevlar, Nomex, or fiberglass cloth, they wrap around the packed chute and protect it from heat, and particles.
5. **Combination of Fire Blanket and Dog Barf:** Attaching fire blankets in combination with dog barf would utilize the benefits of both methods while still ensuring clearance for both.



(a) Nomex deployment bag (*Valkyrie Recovery Systems*).



(b) Cellulose "dog barf" recovery wadding.



(c) Piston system with bulkplate (*LOC Precision*).



(d) Nomex fire blanket (*Fruity Chutes*).

Figure 45: Recovery packing/protection options.

Based on the above options, a trade study was conducted to evaluate the best option for this years project.



3.4.11 Shock Cord Selection

Table 29: Parachute Deployment Retainment Systems Trade Study

Design	Deployment Reliability	Low Weight	Ease of Assembly	Low Packing Volume	Total Weighted Score
	40%	20%	20%	20%	100%
Deployment Bags	7	7	5	8	6.8
Wadding/Dog Barf	8	8	8	6	7.6
Piston System	5	5	7	6	5.6
Fire (Nomex) Blankets	5	9	8	6	6.6
Fire (Nomex) Blankets and Dog Barf	9	7	9	5	8.0

When choosing shock chord material, it is important to consider strength, cost, and ease of packing. The team decided on rectangular cross-section Kevlar due to its superior strength and packability. However, whether $\frac{3}{4}$ " or $\frac{1}{2}$ " was used was depended on the expected maximum load in the shock chord. With this in mind, the following trade study was conducted:

Table 30: Parachute Deployment Retainment Systems Trade Study

Design	Strength [wt = 0.2]	Low Weight [wt = 0.2]	Availability [wt = 0.3]	Packability [0.3]	Total Weighted Score
	20%	20%	30%	30%	100%
3/4" Flat Kevlar	9	2	9	4	4.5
1/2" Flat Kevlar	7	8	2	5	6.6

Since both shock chords boasted sufficient safety factors, the strength addition of the $\frac{3}{4}$ " inch chord was not worth the additional cost, weight, and difficulty packing. The $\frac{1}{2}$ " Kevlar Chord from Giant Leap Rocketry is rated for 6000 lb, and the maximum expected load is 1084 lb, as calculated in 3.5.7, allowing a Safety Factor of 5.53 which is greater than the value of 4 required by VADL Requirement 4.1.4.



Figure 46: Giant Leap Rocketry looped $\frac{1}{2}$ " shock chord



3.5 Leading Recovery Design

3.5.1 Recovery Events Overview

The team employs a dual-deployment recovery system to ensure a safe and controlled descent in compliance with NASA Requirements 3.3 and 3.10. At apogee, the drogue parachute deploys to stabilize the rocket and initiate descent while maintaining a high descent rate to minimize drift. The main parachute deploys at 550 feet above ground level (AGL), significantly reducing descent velocity to meet the landing kinetic energy outlined in NASA Requirement 3.2.

Both events are triggered by redundant Altus Metrum EasyMini altimeters operating on independent circuits. The backup drogue charge is configured with a 1.0-second delay following apogee detection to prevent simultaneous charge activation. The backup main charge is programmed to deploy at 500 feet AGL, providing sufficient separation between the primary and backup events to mitigate premature deployment risk.

The recovery sequence utilizes Fruity Chutes parachutes, including a 24-inch Classic Elliptical drogue and a 144-inch Iris Ultra Compact main parachute. These parachutes were selected based on provided drag, proven reliability, and flight heritage within VADL rockets. Both parachutes are attached via Kevlar shock cords sized according to snatch-force analyses to ensure adequate factors of safety during deployment events.

3.5.2 Avionics Bay Design

The avionics bay forms the central element of the recovery system, housing the dual-deployment flight computers and associated power, switching, and wiring hardware that govern parachute ejection. The bay is mechanically located between the drogue and main parachute compartments and is isolated from payload electronics in accordance with NASA Requirements 3.13.1-4, ensuring no interference from transmitting or magnetic devices.

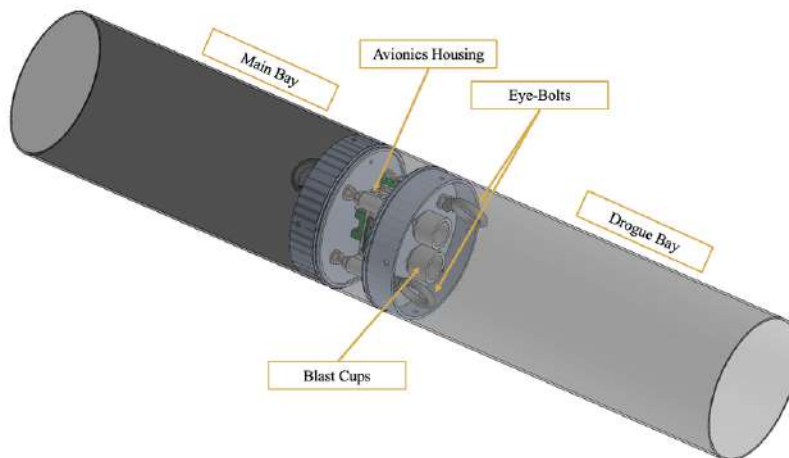


Figure 47: Avionics Bay with Callouts

As shown above, the bay assembly is secured between two CNC-machined aluminum



bulk plates, connected by threaded eyebolts that serve as both mechanical fasteners and recovery attachment points. Each end includes a $\frac{1}{2}$ -inch Kevlar strap linked to the drogue and main parachutes. The internal avionics housing, which retains all flight computers and batteries, is 3D-printed from ABS plastic as determined by the team's material trade study. ABS was selected for its dimensional precision, ease of fabrication, and sufficient mechanical strength under launch-induced vibration and acceleration loads.

Avionics Housing

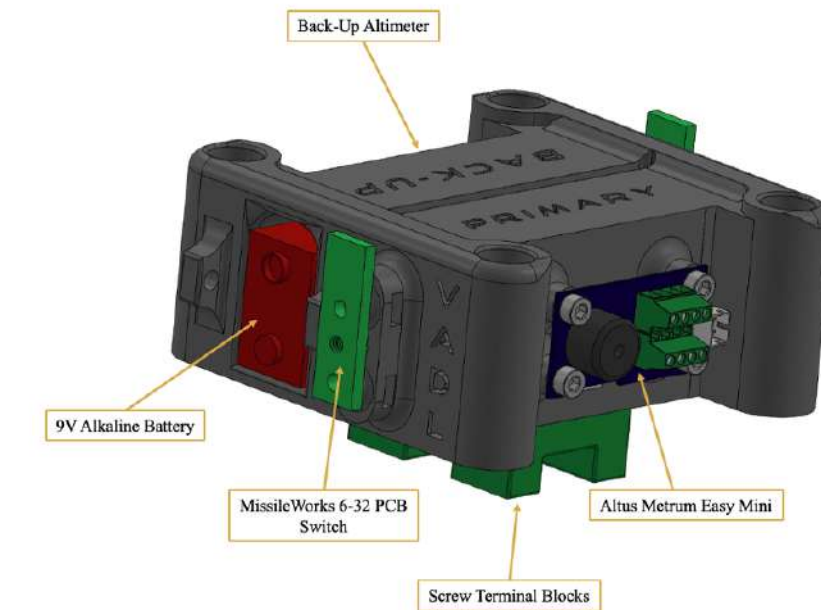


Figure 48: 3D Model of Avionics Housing

The bay design shown above accommodates two independent Altus Metrum EasyMini V2.1 altimeters (primary and backup), each with its own circuit and dedicated 9 V alkaline battery, which meets NASA USLI Requirements 3.3-4. Each battery is restrained within a printed compartment and secured with a zip tie to prevent disconnection during launch. Threaded brass heat inserts are used for M3 mounting hardware to rigidly fasten the altimeters to the housing.

The wiring architecture is duplicated across both circuits, including independent power and e-match outputs. Screw terminals are employed as strain-relief interfaces between the EasyMini outputs and ejection charge wiring, minimizing the risk of wire fatigue and disconnection under vibration. The full wiring schematic is shown below:

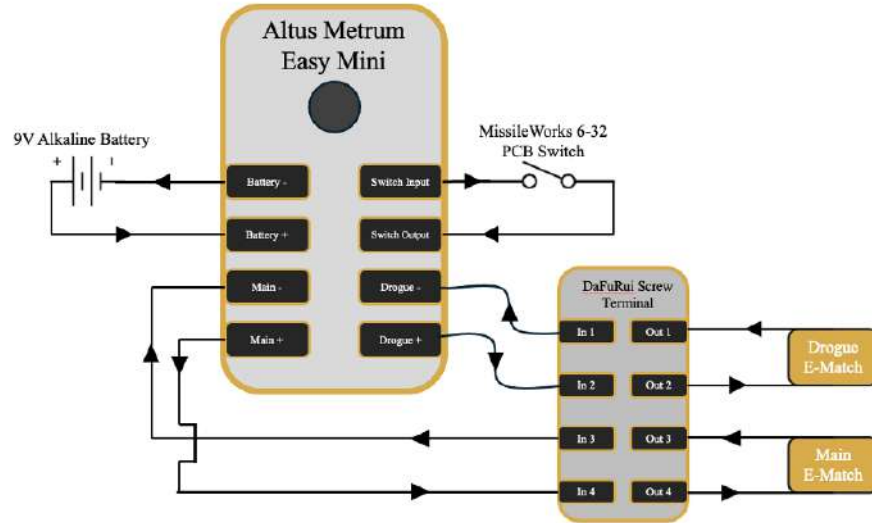


Figure 49: Avionics Wiring Schematic

For arming and disarming the avionics, the team selected the MissileWorks 6-32 PCB Screw Switch, which satisfies NASA Requirement 3.5 (each altimeter must have a dedicated mechanical arming switch accessible from the exterior of the airframe). The switch mounts directly to the housing using heat inserts and 4-40 bolts through plated holes, allowing secure fastening and repeatable engagement.



Figure 50: MissileWorks 6-32 PCB Screw Switch

Avionics Port Hole Sizing

The avionics bay includes four $\frac{1}{4}$ -inch pressure port holes spaced evenly around the circumference of the airframe. Proper sizing and placement of these holes are critical to ensure that the internal pressure tracks external atmospheric changes accurately at the EasyMini's 100 Hz sampling rate while minimizing aerodynamic effects. Using the relation

$$\dot{V} = V f_{\text{sample}} 0.5, \quad A_{\text{total}} = \frac{\dot{V}}{c}, \quad D_{\text{each}} = \sqrt{\frac{4A_{\text{total}}}{n\pi}}$$

with a bay volume $V = 74.7 \text{ in}^3$, altimeter sampling rate $f_{\text{sample}} = 100 \text{ Hz}$, speed of sound $c = 13,500 \text{ in/s}$ and $n = 4$ yields an individual hole diameter of approximately $D_{\text{each}} = 0.3 \text{ in}$ to exchange the internal volume of air every 2 samples. Based on this calculation, the four $\frac{1}{4}$ -inch ports provide sufficient air exchange without aerodynamic disturbance, ensuring accurate altitude sensing.



Compliance and Safety Considerations

All avionics components are electrically isolated from payload and GPS circuits, as required by 3.7 of the NASA handbook, and will be verified through continuity and ejection testing prior to every flight. The EasyMini altimeters are configured with independent firing logic and timing delays to prevent simultaneous charge activation, in accordance with redundancy best practices.

3.5.3 GPS Tracking Device

Based on a trade study conducted in 3.4.6, the team has chosen the BigRedBee GPS APRS Transmitter to track the vehicle during flight and recovery. The BigRedBee GPS requires 100 mW of power during use, operates on the 70 cm amateur radio band (420-450 MHz), and transmits at a frequency of 1 Hz. The team plans to use a single-cell Li-Po battery running nominally at 3.7V with 900 mAh to power the tracker; this energy capacity allows for sufficient hours of use and will be verified with drain testing. The team has chosen the transmission frequency of 433.92 MHz.

3.5.4 Shear Pins

We use #2-56 nylon shear pins at both recovery separations, per our shear-pin trade study. Four pins, spaced evenly around the circumference, secure (i) the drogue bay to the PDM coupler and (ii) the nosecone coupler to the main bay. During manufacturing, matched holes will be drilled through both the airframe and the couplers with the assemblies fixtured to ensure alignment; all holes are deburred and sized for a tight-fit of the nylon fasteners. New pins are installed for each flight.

3.5.5 Energetics Sizing

Black powder charges deploy parachutes by exerting enough force onto the bulk plates to separate the sections and allow the parachute to eject clear of the vehicle. The force exerted on the bulk plates is proportional to the internal pressure in the compartment. Using the ideal gas law, the black powder charge mass can be calculated as follows: Black powder charges deploy parachutes by exerting enough force onto the bulk plates to separate the sections and allow the parachute to eject clear of the vehicle. The force exerted on the bulk plates is proportional to the internal pressure in the compartment. Using the ideal gas law, the black powder charge mass can be calculated as follows:

$$m = \frac{PV}{RT}$$

Where P is burst pressure in psi, V is the internal volume of the compartment in in^3 , R is the gas constant for black powder in $lbf\cdot in/(lbm\cdot R)$, and T is the burning temperature of black powder in R. The burst pressure is calculated as follows:

$$P = \frac{nF}{A}$$



Where n is the number of shear pins, F is the force required to break a 2-56 shear pin, and A is the bulk plate area. Both bulk plates have 6 in diameters.

In accordance with VADL Requirement 4.3.1 black powder charges are given a safety factor of 4 to ensure deployment occurs. Using the above equations, charges for the drogue and main compartments can be calculated: **Drogue:**

$$P = \frac{4 * 31 \text{ lbf}}{\frac{\pi}{4} * 6^2 \text{ in}^2} = 4.4 \text{ psi}$$

$$m = 4 * \frac{4.4 \text{ psi} * (\frac{\pi}{4} * 6^2 * 8.1) \text{ in}^3}{265.92 \frac{\text{lbf} * \text{in}}{\text{lbf} * \text{in}^2} * 3307 \text{ R}} * 456.6 \frac{\text{g}}{\text{lbfm}} = 2.1 \text{ g}$$

Main:

$$p = \frac{4 * 31 \text{ lbf}}{\frac{\pi}{4} * 6^2 \text{ in}^2} = 4.4 \text{ psi}$$

$$m = 4 * \frac{4.4 \text{ psi} * (\frac{\pi}{4} * 6^2 * 17.7) \text{ in}^3}{265.92 \frac{\text{lbf} * \text{in}}{\text{lbf} * \text{in}^2} * 3307 \text{ R}} * 456.6 \frac{\text{g}}{\text{lbfm}} = 4.5 \text{ g}$$

VADL Requirement 4.3.2 requires back up charges to be 20% greater in mass, yielding 2.5 and 5.4 g for drogue and main respectively.

Table 31: Deployment charge sizes

Event	Safety Factor	Primary (g)	Backup (g)
Drogue	4	2.1	2.5
Main	4	4.5	5.4

3.5.6 Leading Parachutes

Based on the recovery trade study in Sec. 30, the team selected two Fruity Chutes canopies as the leading configuration: a Fruity Chutes 24" Classic Elliptical as the drogue and a Fruity Chutes Iris Ultra 144" as the main. The 24" elliptical provides stable, controlled descent between apogee and 550 ft, while the 144" Iris Ultra achieves the low terminal velocity needed to satisfy NASA landing-energy limits. These selections balance reliability, descent time, and landing energy and align with our trade-study results.



Fruity Chutes 24" Classic Elliptical
(Drogue)

Fruity Chutes Iris Ultra 144" (Main)

Figure 51: Leading parachutes used for dual-deployment recovery.

Table 32: Key parameters for leading parachutes.

Model	Type
Fruity Chutes 24 Classic Elliptical (Drogue)	Elliptical
Fruity Chutes Iris Ultra 144 (Main)	Toroidal

3.5.7 Leading Shock Cord Analysis/Design

Our recovery tethers use 1/2 " Kevlar flat webbing as the primary shock cord between all separated sections (nose cone, recovery section, tail section). 1/2 " Kevlar straps have an ultimate strength of 6000 lbf. During descent, the shock cord accomplishes the following:

1. Carry and transmit deployment loads without failure
2. Provide vertical separation so sections do not collide midair
3. Maintain the correct staging

Snatch-Force Calculations

When the main parachute deploys, the vehicle experiences a transient force spike known as the opening shock or snatch force. This occurs as the parachute inflates and decelerates the vehicle from its drogue descent rate to the steady-state main descent velocity. To estimate this peak force, the Pflanz finite-mass method was selected. This method, documented in the USAF Recovery Systems Design Guide (AFFDL-TR-78-151) [9] and Knacke's *Parachute Recovery Systems Design Manual* [4], balances physical realism with analytical simplicity by accounting for both aerodynamic overshoot and the finite-mass effects of the vehicle-canopy system.

The Pflanz method expresses the peak opening force as a function of the instantaneous



full-open drag, the aerodynamic overshoot and a finite-mass reduction:

$$F_{\max} = \underbrace{\frac{1}{2} \rho V_{\text{term}}^2 (C_D S)_0}_{\text{instantaneous full-open drag}} \times \underbrace{C_x}_{\text{aerodynamic overshoot}} \times \underbrace{X_1}_{\text{finite-mass reduction}}$$

- ρ : air density at deployment altitude (550 ft AGL, 1400 ft above sea level)
- V_{term} : vehicle terminal velocity under drogue
- $(C_D S)_0$: drag area at steady state post full inflation
- C_x : shock/overshoot factor. Depends on canopy type, typically 1.6–1.8 for solid elliptical parachutes. The leading parachute is a Fruity Chutes Iris Ultra 144" toroidal canopy for which a value of $C_x = 1.7$ was selected.
- X_1 : finite-mass reduction, obtained by ballistic parameter A and the Pflanz Chart

$$A = \frac{2m}{\rho V_{\text{term}} (C_D S)_0 t_{\text{infl}}}, \quad t_{\text{infl}} \approx \frac{n_d D_f}{V_{\text{term}}}$$

Here m is the launch vehicle dry mass, D_f is the main's final diameter. n_d is an empirical inflation-distance factor representing the number of diameters to fill the parachute. Based on the AFFDL and Knacke handbooks, we estimate $n \approx 1$ for a linear, quick opening. With these values, $t_{\text{infl}} \approx 0.13$ s and $A = 0.43$. We then use the opening-force reduction factor versus ballistic parameter Figure 52:

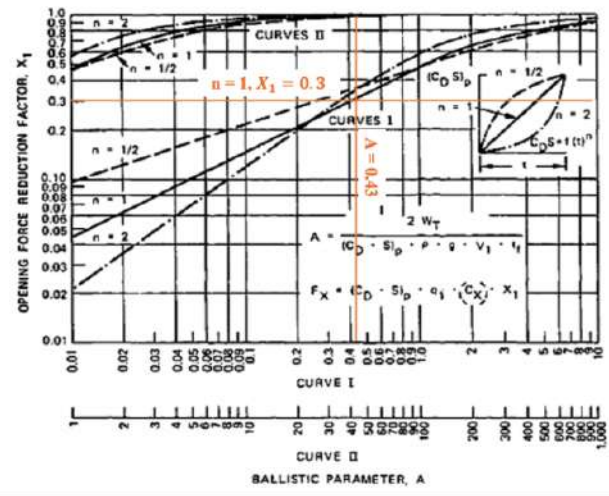


Figure 52: Pflanz Opening-Force Reduction Factor versus Ballistic Parameter

Using $X_1 = 0.3$ and $C_x = 1.7$, we calculate F_{\max} to be:

$$F_{\max} = \frac{1}{2} \rho V_{\text{term}}^2 (C_D S)_0 \cdot C_x \cdot X_1 = 1224.24 \text{ lb}$$

This force is distributed across both shock cords, so to calculate the force experienced by the shock cord attached to the recovery and tail sections, we can say:

$$F_{\max, \text{recovery+tail}} = F_{\max} \frac{m_{\text{recovery}} + m_{\text{tail}}}{m_{\text{tot}}} = 1224.24 \times \frac{13.58 \text{ lb} + 28.13 \text{ lb}}{47.1} = 1084 \text{ lb}$$



Additionally, we can calculate the acceleration felt by the launch vehicle as:

$$F_{\max} = ma \Rightarrow a = 836.9 \frac{\text{ft}}{\text{s}^2} = 26 g$$

We can compare the force on the shock cord to the tensile strength of $\frac{1}{2}$ in Kevlar (6000 lbf) to calculate the following factor of safety:

$$\text{FOS} = \frac{\text{Ultimate Strength}}{\text{Expected Load}} = \frac{6000}{1084} = 5.5$$

Calculated values are summarized in Table 33 below:

Table 33: Shock Cord Key Values

Variable	Calculated Value
Shock Cord Factor of Safety	5.5
Max Expected Force on Shock Cord	1084 lbf
Max Expected Acceleration	26 g

Shock Cord Lengths

Our shock cord lengths control geometric separation of independent sections; analytically choosing shock cord lengths reduces the risk of re-contact, entanglement, deployment forces and large snatch forces. To reduce shock loads and mass we choose the shortest lengths that still guarantee safe separation in both drogue and main configurations.

VADL has derived the following shock-cord length requirements:

- **VADL 4.1.1, 3x Section Backstop:** each cord length $\geq 3x$ the connecting section
- **VADL 4.1.2, 10 ft minimum separation:** when taut, connected sections must be ≥ 10 ft apart
- **VADL 4.1.3, Tail section first:** to ensure an ideal landing configuration, the tail section must land first
- **VADL 4.1.5, Minimum shock cord length:** each shock cord must be ≥ 5 ft to reduce deployment forces

Descent under Drogue

At apogee, the tail section will separate from the recovery and nosecone, releasing the drogue parachute from the drogue parachute bay. Figure ?? shows the descent configuration. We attach a quick-link connector to the swivel link attached to the drogue parachute, then attach the two Kevlar shock cords to the quick link. The recovery and nosecone section have a total length of 47.8 in while the tail section has a length of 52.2 in. First we calculate the shock cord length between the drogue and the fore sections (recovery and nosecone) as:

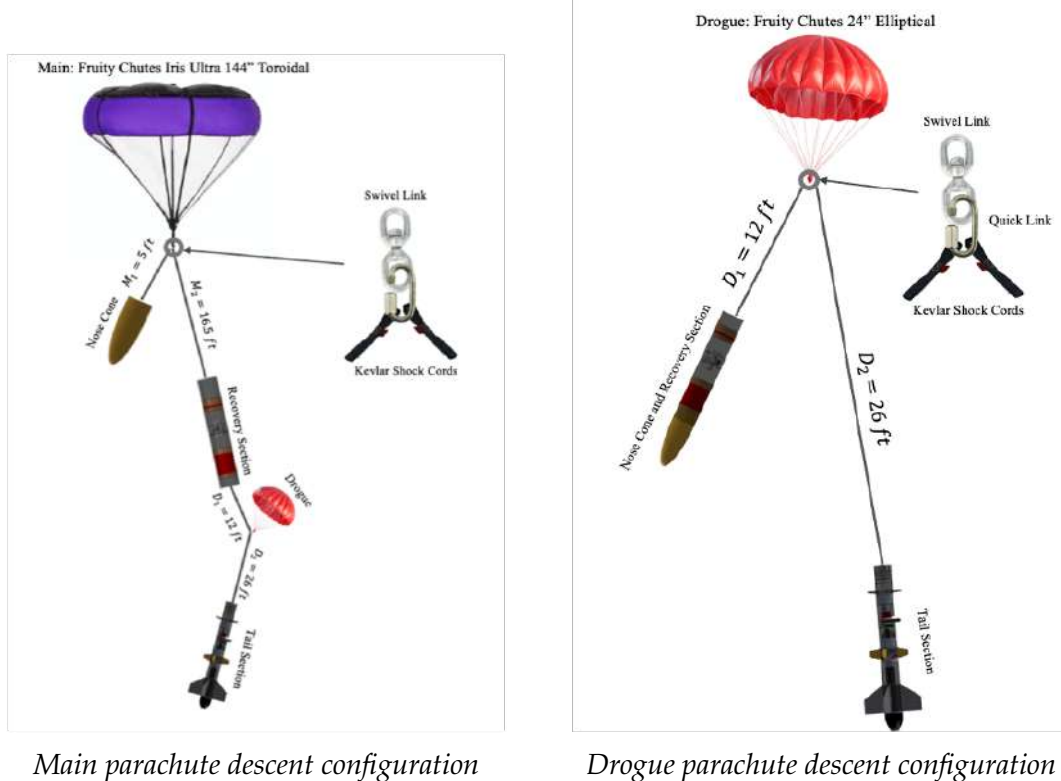
$$D_1 = 3 \times L_{\text{recovery+nose cone}} = 3 \times 47.6 \text{ in} \approx 12 \text{ ft.}$$

For the shock cord between the drogue parachute and the tail section, we follow VADL



Requirement 4.1.2 such that:

$$D_2 = D_1 + 10 \text{ ft} + L_{\text{recovery+nose cone}} = 26 \text{ ft.}$$



Main parachute descent configuration Drogue parachute descent configuration

Figure 53: Descent under main parachute (left) and drogue parachute (right).

Descent under Main

At 550 feet AGL, the nose cone section will separate from the recovery section, releasing the main parachute. Figure 53 shows the descent configuration. Once again, a quick link connector will be attached to the swivel link of the parachute, then both Kevlar shock cords will be fixed by the quick link. The shock cord length between the main parachute quick link and the nosecone can be calculated as:

$$M_1 = 3 * L_{\text{nose cone}} = 3 * (13 \text{ in} + 6 \text{ in}) \approx 5 \text{ ft}$$

Where $L_{\text{nose cone}}$ includes the coupler added onto the nosecone section.

Lastly, we calculate the length of the shock cord coupling the main parachute and the tail section to be:

$$M_2 = M_1 + 10 \text{ ft} + L_{\text{nose cone}} \approx 16.5 \text{ ft}$$

Leading shock cord lengths are shown in the Table 34:



Table 34: Leading shock cord lengths.

Shock Cord	Length (ft)
Drogue to nose cone and recovery section (D_1)	12
Drogue to tail section (D_2)	26
Main to nose cone (M_1)	5
Main to recovery section (M_2)	16.5

The team will order custom length 1/2 in Kevlar shock cords with pre-sewn ends from Fruity Chutes. Short extensions will be used to achieve

3.5.8 Anchor Point Hardware



Figure 54: McMaster (P.N. 3014T906) lifting eye (1400 lb listed static load capacity)

The above forged-steel Eye-bolt (Figure 54 will be used on the avionics bulkheads, serving both as an anchor point for the attached quick links and to tie the avionics bay together (as described in Section 3.3). Each eye bolt has a load capacity of 1,400 lb, and two are used for each parachute attachment point. Therefore, the absolute minimum safety factor for this anchor point is as follows:

$$\text{Safety Factor} = \frac{2800 \text{ lb}}{1084 \text{ lb}} \approx 2.58$$

Because the listed load of 1,400 lb is rated for constant static load and considering the safety factors imposed on the supplier when rating lift-critical hardware, it can be assumed that the actual ultimate tensile safety factor is significantly higher than this.

To further explore the load capability of this eye-bolt and ensure that this anchor point can withstand maximum flight loads on its threads with the fastener hardware supplied, a bolt tear-out calculation will be performed. Similar to the calculations performed for the RBS in Section 3.3.11, the maximum load can be taken as main deployment. However, the thread engagement will be deeper, the yielding material will be steel -as both the tap (in this case the nut) and the bolt are the same grade of steel- and the bolt diameter will be larger. Thus,

$$F_{\text{pullout}} = \pi d_{\text{avg}} L_c \tau_{\text{shear}}$$

Where:

$$d_{\text{avg}} = \frac{d_{\text{major}} + d_{\text{minor}}}{2} = \frac{0.375 + 0.302}{2} = 0.3385 \text{ in}$$

$$L_{E,\text{nut}} = 0.22 \text{ in}$$



$$\tau_{\text{shear},6061} = 90000 \text{ psi}$$

$$F_{\text{pullout}} = [\pi \times 0.3385 \text{ in} \times 0.22 \text{ in}] 90000 \text{ psi} = 21055 \text{ lbs}$$

The calculated safety factor for the threads two bolt assembly assuming full engagement with the nut is:

$$\text{SF} = \frac{2 \times 21055 \text{ lbs}}{1084 \text{ lbs}} = 38.8$$

PDS U-Bolt



Figure 55: E-Trailer Forged Steel U-Bolt (P.N APUBR-8)

The above forged-steel U-bolt will be used in the Parachute Detachment mechanism. It's load capacity of 7,000 lb provides an absolute minimum Factor of Safety of 7000 lb/1084 lb = 6.5. (Maximum parachute snatch force of 1084 lbf calculated in Section 3.5.7)

3.5.9 Recovery System Redundancy

To ensure that the recovery hardware deploys properly during deployment, back up charges are utilized. These charges ensure deployment if the primary charge fails to ignite due to an electronic disconnect with the altimeter but also ensures the recovery hardware is ejected properly in the event of a successful ignition but failed separation. Both altimeters utilize separate fresh 9V alkaline batteries to increase points of failure. Following all launches, 9V batteries used in altimeters are disposed of.

According to NASA Requirement 3.1.2, the backup apogee event may not have a delay of greater than 2 seconds. This prevents excessive loading on the drogue chute during opening as the rocket increases velocity as it starts to fall. Excessive drogue opening forces may also cause the main parachute to open prematurely by breaking the main compartment shear pins. VADL has decided to utilize a backup delay of 1 s for the drogue event.

The primary main deployment altitude is set to 550 ft, with a backup at 500 ft. These deployment altitudes satisfy NASA USLI Requirement 3.1.1 which imposes a main parachute deployment at no lower than 500 ft. These deployment altitudes were chosen to ensure compliance with NASA requirement 3.11 which states that the vehicle descent time shall be no greater than 90 s.

3.6 Mission Performance Predictions



3.6.1 Overview of Flight Simulation Framework

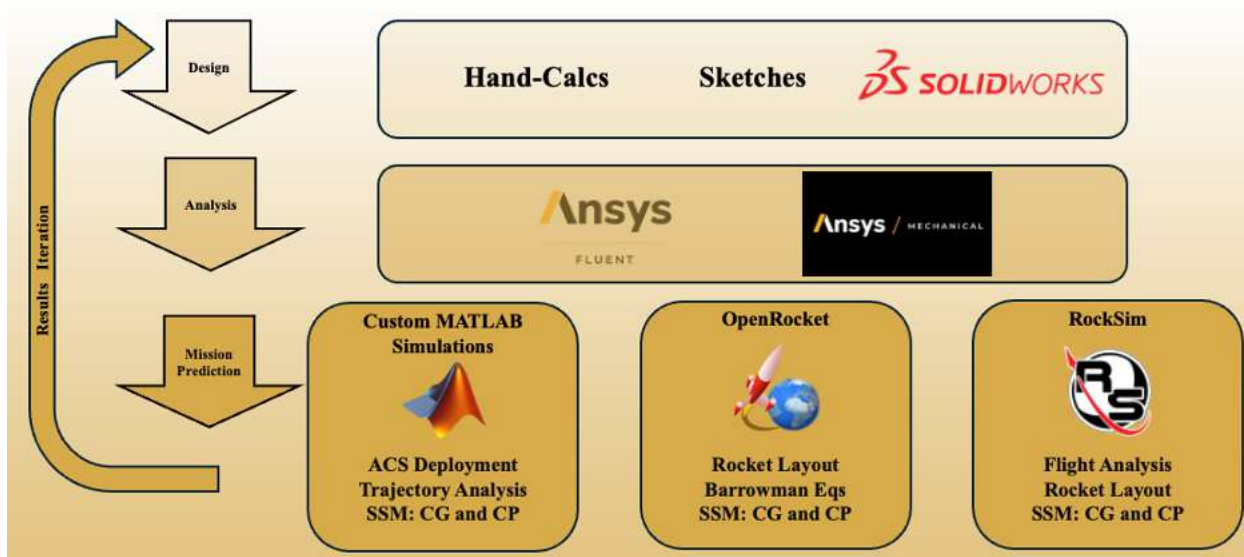


Figure 56: Integration between design, analysis, and mission prediction tools

To predict and validate the vehicle's flight behavior throughout ascent and descent, the team developed a multi-tiered simulation framework that integrates SolidWorks, ANSYS, OpenRocket, RockSim, and custom MATLAB simulations. Each tool supports a specific stage of the design and analysis pipeline, and their results are iteratively cross-checked through analytical hand calculations to ensure that all models remain physically consistent and traceable.

The process begins with simple hand-calcs and sketches where we draw out potential vehicle designs. Eventually, we converge onto a design then utilize SolidWorks, where the complete 3D vehicle geometry and mass properties are established. These CAD models serve as the foundation for both structural and aerodynamic analysis. ANSYS Mechanical is then used to assess structural response under thrust, aerodynamic, and recovery loads, while ANSYS Fluent provides computational fluid dynamics (CFD) simulations to estimate drag coefficients (C_d) and rocket center of pressure (C_P).

For mission simulation and trajectory modeling, the team employs OpenRocket and RockSim, both of which model the rocket's flight using the Barrowman equations to compute aerodynamic stability parameters such as the center of pressure (CP) and static stability margin (SSM). OpenRocket enables iterative testing of design modifications and mass distribution effects, while RockSim provides independent verification using an alternative solver and drag model, ensuring consistency between predictions. Key outputs include apogee altitude, maximum velocity, and recovery sequence timing.

To extend beyond these static models, custom MATLAB programs are used for advanced simulations. Our MATLAB simulation framework supports Monte Carlo analyses that incorporate uncertainty in launch conditions (mass tolerance, motor performance, and wind variation) to estimate apogee dispersion and landing footprints. It is also used to simulate dynamic events such as Attitude Control System (ACS) deployment, enabling time-resolved modeling of forces and vehicle orientation changes during flight.



Finally, all numerical predictions are validated through hand calculations based on first-principles physics. This process ensures that every result, whether from CFD, OpenRocket or MATLAB remains grounded.

Together, this integrated framework allows the team to progress systematically from design to validation. The convergence of these tools produces a comprehensive understanding of vehicle performance, ensuring confidence in both nominal and off-nominal flight predictions.

3.6.2 Target Apogee for Competition

The VADL launch vehicle is seeking to achieve a competition target apogee of 4,200 feet above ground level (AGL). This target altitude is informed by detailed flight simulations and accounts for multiple factors that affect apogee performance on flight day.

Table 35: Current Target Apogee for Competition Day

Metric	Value
Target Apogee for Competition Day	4,200 ft

Baseline Apogee Predictions

Using the L1940 primary motor with no apogee control system deployment, the vehicle's predicted apogee varies slightly across different simulation methods. OpenRocket simulations yield an apogee of 4,349 feet, RockSim simulations result in a predicted apogee of 4370 feet, while MATLAB-based analytical calculations predict 4,401 feet. These simulations assume standard atmospheric conditions at a launch elevation of 850 feet above sea level, zero wind, and baseline vehicle mass configuration (3 lbm ballast).

Table 36: , no wind, no cant, 3lbm balalst by Simulation Software

Analytical Tool	Predicted Apogee (ft)
OpenRocket	4,349
MATLAB	4,401
RockSim	4,370

Under more realistic launch day conditions including a 5 degree cant into the wind and 5 mph of wind the adjusted predicted apogees are as shown below:

Table 37: Apogee Prediction Comparison (Expected Conditions, 5 mph winds, 5 degree cant)

Analytical Tool	Predicted Apogee (ft)
OpenRocket	4,275
MATLAB	4,317
RockSim	4,301



The vehicle incorporates an Apogee Control System (ACS) to modulate apogee through controlled fin deflection. CFD analysis indicates that ACS deployment at the maximum deflection angle increases the total vehicle drag coefficient from 0.42 to 2.14, resulting in a maximum apogee reduction of approximately 150 feet when deployed at 3500 feet AGL. This predictable apogee modulation provides the team with precise control authority to meet the competition target; VADL Requirement 3.6.2 requires the ACS to modulate the competition apogee to within 5% of the target apogee.

Ascent Hand-Calculation Verification

To verify the results produced by MATLAB, OpenRocket and RockSim with a simplified analytical model, Nakka Rocketry's Simplified Method for Estimating the Flight Performance of a Hobby Rocket is used [6]. Nakka's methodology assumes vertical ascent, constant average thrust, constant ascent drag coefficient, and an empirical coast "drag-efficiency" factor. We first calculate burn time as:

$$t_b = \frac{I_{\text{tot}}}{T_{\text{avg}}} = \frac{973.6}{436} \approx 2.23 \text{ s} \quad (1)$$

Next, we calculate the ideal burnout altitude (no drag) as:

$$h_{\text{burnout}} = \frac{1}{2} \left(\frac{T_{\text{avg}}}{m} - g \right) t_b^2 = 631 \text{ ft} \quad (2)$$

We calculate the burnout velocity (no drag) as:

$$V_1 = \sqrt{\frac{2 h_{\text{burnout}}}{m} (T_{\text{avg}} - mg)} = 565.9 \text{ ft s}^{-1} \quad (3)$$

We also calculate the peak altitude with no drag as:

$$h_{\text{apogee,ideal}} = \frac{F h_{\text{burnout}}}{mg} = 5603.1 \text{ ft} \quad (4)$$

We then calculate the drag influence number as:

$$N = \frac{C_d D^2 V_1^2}{1000 m_{\text{dry}}} = 143.7 \quad (5)$$

Using Nakka's chart, the peak altitude factor f_z for $N = 143.7$ is ≈ 0.78 . Using this, we calculate predicted apogee with drag as:

$$h_{\text{apogee}} = h_{\text{apogee,ideal}} \times 0.78 = 4370 \text{ ft} \quad (6)$$

This result aligns well with our simulations results.



3.6.3 Thrust-to-Weight Ratio

Thrust-to-weight is an important metric to ensure that the motor will have appropriate thrust to lift the vehicle successfully. NASA Requirement 2.12 requires that the launch vehicle have a minimum thrust-to-weight ratio of 5.0:1.0. Thrust-to-weight can be calculated in many ways; to keep calculations simple and conservative, we use the manufacturer-reported average thrust and divide by our predicted vehicle wet mass. For our leading motor, the AeroTech L1940, the thrust-to-weight can be calculated as:

$$\frac{T_{\text{avg}}}{m_{\text{wet}} g} = \frac{435.9 \text{ lbf}}{51.1 \text{ lbm}} \rightarrow 8.53 : 1.0 \quad (7)$$

Additionally, we can use Open Rocket to plot the thrust-to-weight from ignition to burnout for the L1940:

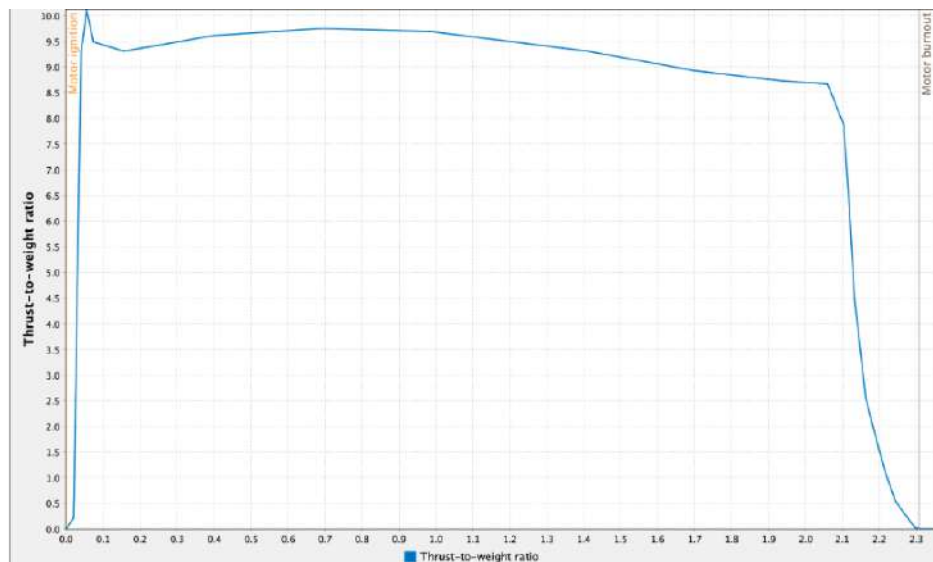


Figure 57: Thrust-to-Weight Ratio for L1940

Lastly we tabulate the thrust-to-weight for both the L1940 and our backup motor the L2375:

Table 38: Thrust-to-Weight Summary

Motor	Average Thrust (lbf)	Vehicle Wet Mass (lbm)	Thrust-to-Weight Ratio
Aerotech L1940 (Leading)	435.9	51.1	8.53
Cesaroni L2375 (Backup)	551.0	51.8	10.64

3.6.4 Launch Rail Exit Velocity

Launch rail exit (LRE) velocity is a key safety and performance metric: the vehicle must leave the rail with sufficient speed to ensure stable and weathercock-resistant flight. NASA Requirement 2.14 specifies a minimum 52 ft/s at rail exit. We verify LRE velocity using both OpenRocket and our MATLAB ascent model.

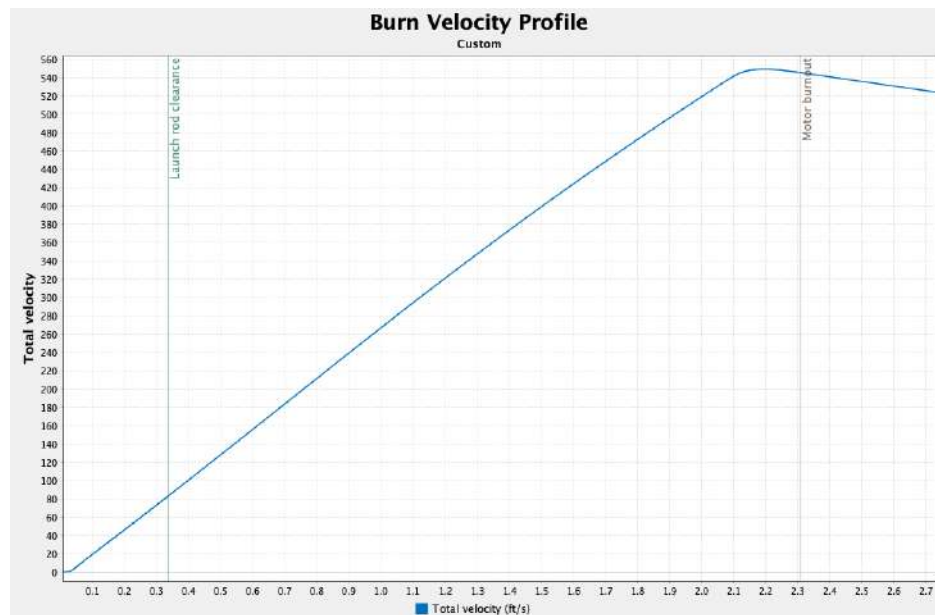


Figure 58: Burn velocity profile for the Aerotech L1940 (chosen motor). The curve shows total velocity from ignition through burnout; vertical markers indicate launch-rod clearance and motor burnout.

Table 39: Launch Rail Exit (LRE) and Maximum Velocity Summary

Motor	LRE Velocity (ft/s)	Max Velocity (ft/s)
Aerotech L1940 (Leading)	83.1	549
Cesaroni L2375 (Backup)	86.4	636

3.6.5 Aerodynamics Analysis

Aerodynamic factors such as Ascent Coefficient of Drag and center of pressure are extremely important to consider for ascent dynamics. In this section, we utilize varying methods (mainly ANSYS Fluent's CFD) to estimate these values to inform our ascent analysis. The final values generated from our analysis are tabulated below:

Table 40: Aerodynamic Summary (Ascent C_d and Vehicle CP)

Parameter	Value
Average Ascent Drag Coefficient, C_d	0.42
Vehicle Center of Pressure (inches from tip of nose cone)	72.4 in.

CFD Background

CFD allows the team to characterize important aerodynamic properties such as C_D at varying velocities and ACS deflection angles. Proper characterization of the vehicle allows for accurate flight simulations and ensures that the vehicle meets all VADL and NASA imposed standards for stability and safety during flight.

The two most common turbulence models in CFD are the $k-\epsilon$ model and the $k-\omega$. Both models approximate the Reynolds-averaged Navier-Stokes (RANS) equations for fluid motion. The $k-\epsilon$ model is well suited for solving free-stream conditions but is not as accurate in the boundary layer near walls and may underpredict flow separation. The $k-\omega$ model is more accurate, however may not converge in free-stream conditions. Combining the two allows for more robust predictions in models with flow separation in boundary layers and free-stream conditions [5]. This is called the $k-\omega$ SST (Shear Stress Transport) model where the free-stream is modeled with $k-\epsilon$ and the boundary layer close to walls is modeled with $k-\omega$. The team decided to utilize the $k-\omega$ SST model in Fluent.

Model Setup

To set up the simulations, a simplified vehicle geometry was imported into Ansys and a fluid domain was placed around the vehicle taking care to ensure that the domain walls are a large distance away. This prevents the boundary layers on the domain walls from interfering with the flow around the vehicle. The mesh was generated to maximize the element quality and minimize size close to the boundaries of the vehicle, while being relaxed further from the vehicle. Additional mesh refinement was added to the ACS fin edges to reduce element size even further. These steps were repeated for three ACS deflection angles: 22.5, 45, and 90 degrees.

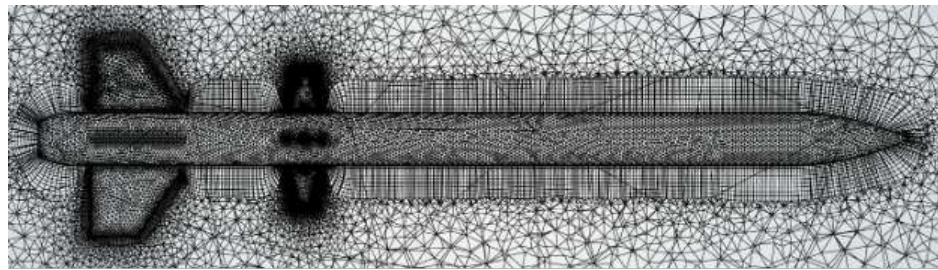


Figure 59: Ansys Fluent mesh for full-scale vehicle. 0 degree ACS deflection.

Numerical accuracy can vary greatly based on mesh quality. Therefore, the team paid special attention to ensure that the average mesh quality was as close to 1 (maximum element quality) as possible.

Table 41: Mesh element quality for varying ACS deployment angles

ACS Angle (deg)	# of Elements	Avg. Quality
0.0	3,027,578	0.74
22.5	3,112,524	0.75
45.0	3,157,014	0.74
90.0	3,227,264	0.74

The boundary conditions for the simulations are as follows: the inlet was given a free-stream velocity condition, the outlet given a gage pressure of 0, and the walls of the vehicle and remaining walls of the fluid domain were given a no-slip shear condition.

CFD Simulation Results

The simulations ranged from 50 to 600 feet per second for all four ACS deployment angles of 0, 22.5, 45, and 90 degrees.

The ascent CD results are shown in the following figure. The average CD across the various velocities yielded 0.42.

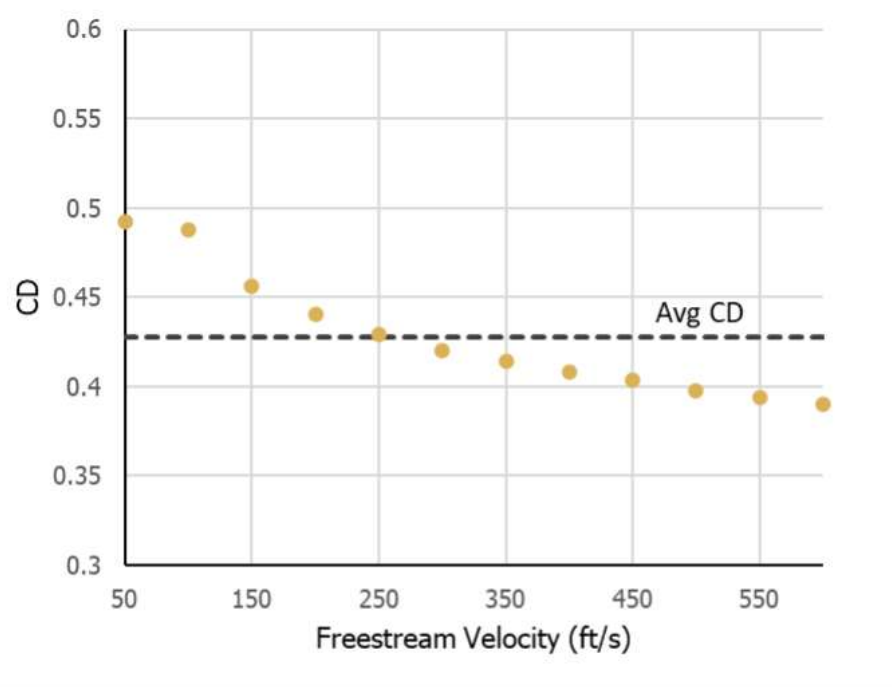


Figure 60: CD vs. Freestream Velocity, 0 deg ACS deflection. Average CD is 0.42

To validate the CP results generated in OpenRocket and RockSim, CFD was also used to calculate the CP of the full-scale vehicle. This was done using an expression in CFD-Post to divide the product of the pressure moment across the rocket by the total pressure. This yielded an average CP of 72.4 inches from the tip of the nose cone. OpenRocket uses the Barrowman equations for calculating CP and yields 72.1 inches. This difference of 0.6 percent provides a strong confidence in the vehicle's static stability margin.

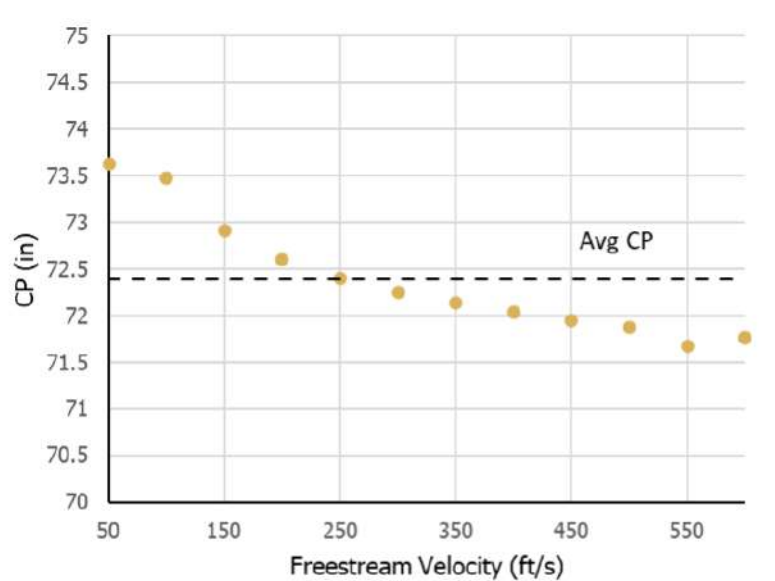


Figure 61: CP vs. Freestream Velocity, 0 deg ACS deflection. Average CP is 72.4 in.

As mentioned above, CFD simulations also covered different ACS deflection angles. The ACS fins were modeled as flat plates to simplify the geometry. This was done because at high AoA, the NACA 0012 airframe acts analogous to a flat plate where CD dominates CL.

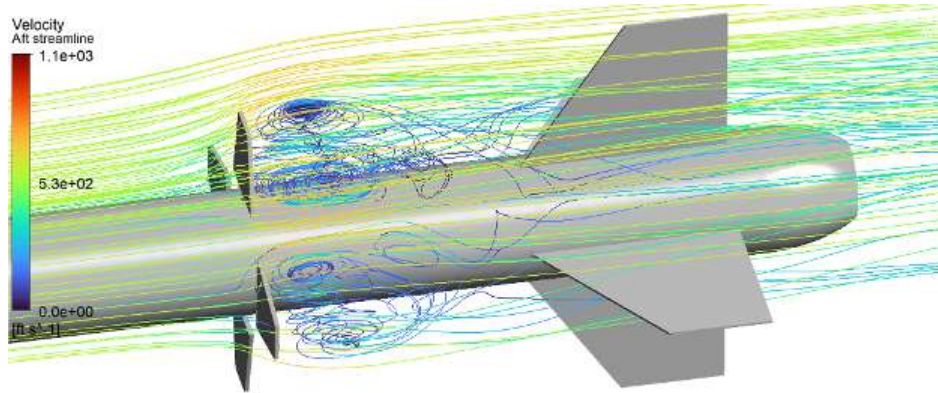


Figure 62: Velocity streamlines around ACS fins at 90 degree deflection

To meet VADL Requirement 3.6.1, the CD of the rocket must be at least 2 when the fins are deployed to 90 deg. The CD of the fins were also investigated at 22.5 and 45 deg to better characterize the increase in drag with angle and allow for greater flexibility in choosing deflection angle.

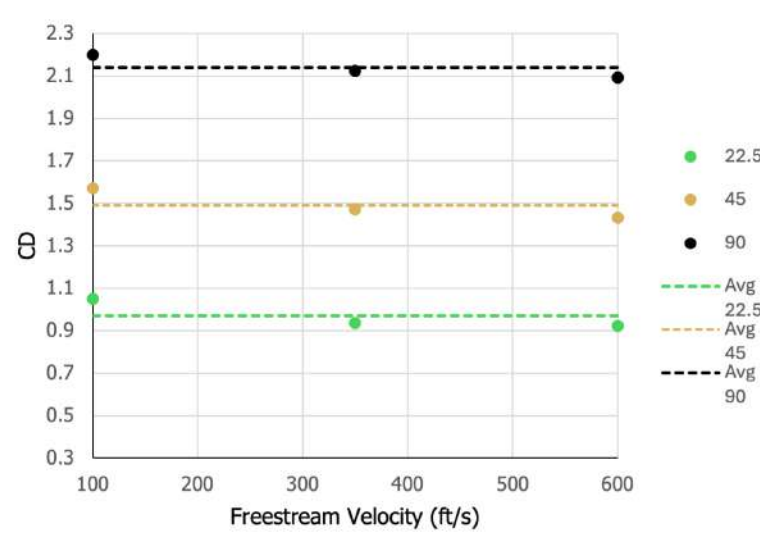


Figure 63: The average CDs are 0.97, 1.49, and 2.14 for 22.5, 45, and 90 deg respectively

3.6.6 Static Stability Margin

Static stability margin is a critical measure of vehicle stability that quantifies how far the center of pressure is located aft of the center of gravity. A healthy SSM ensures the rocket will passively recover from perturbations during flight and maintain stable flight throughout ascent and descent. NASA Requirement 2.14 mandates a minimum stability margin of 2.0 calibers at rail exit to guarantee safe flight operations.

Calculation Methodology

Static stability margin is calculated using the relationship:

$$SSM \text{ (cal)} = \frac{CP - CG}{\text{Airframe Diameter (in)}} \quad (8)$$

As stated earlier, the center of pressure (CP) is derived from ANSYS Fluent CFD analysis using k- ω SST turbulence modeling, yielding a value of 72.4 inches from the nose cone. This CFD-calculated CP was validated against Barrowman equations computed in OpenRocket and RockSim, which yielded 72.1 inches, confirming our aerodynamic analysis within 1% error. The center of gravity is determined through detailed mass accounting in OpenRocket, accounting for mass shifts during motor burnout due to propellant consumption.

Mission Stability Performance

The vehicle maintains robust stability throughout ascent, with SSM remaining well above the minimum requirement at all critical points:

Table 42: SSM at critical points in flight

Flight Phase	CG (in)	CP (in)	SSM (cal)
On Pad	58.4	72.4	2.27
Launch Rail Exit	58.1	72.4	2.32
Post MECO	55.8	72.4	2.70

3.6.7 ACS, Ballast and Wind Effects on Apogee Prediction

This section analyzes how vehicle apogee varies with active control system deployment, ballast configuration, and atmospheric wind conditions. Understanding these relationships enables more informed apogee targeting on competition day.

ACS Affect on Apogee

The VADL vehicle employs an Apogee Control System (ACS) consisting of mechanical fins, which increases drag through controlled fin deflection during ascent. The ACS modulates vehicle apogee by increasing the total drag coefficient as a function of deployment angle. Computational fluid dynamics analysis using ANSYS Fluent quantifies the drag penalty imposed by ACS deflection across the full velocity range. The drag on the entire launch vehicle increases substantially with ACS deflection angle: at a maximum deployment angle of 90 degrees, the entire launch vehicle drag coefficient increases from 0.42 to roughly 2.14 as shown in Figure 63. This increase in drag directly reduces ascent and vehicle apogee.

ACS Deployment Strategy and Safety Margin

The VADL ACS employs an on-flight predictive algorithm that continuously estimates vehicle apogee during ascent. The flight computer integrates real-time sensor data (velocity, altitude) and uses a fourth-order Runge-Kutta (RK4) numerical integration model to predict apogee in real-time. When the predicted apogee reaches the target value of 4,200 feet, the ACS deploys to 90 degrees, increasing drag and capping the vehicle's final apogee at the competition target.

To ensure compliance with NASA Requirement 2.1, VADL Requirement 2.2.3 is derived so that the ACS must deploy no earlier than 3,500 feet AGL. The team has also derived VADL Requirement 3.6.2, which requires the ACS to modulate the final apogee within 5 percent of the target.

Apogee Sensitivity to Deployment Apogee

The following figure illustrates how the final vehicle apogee varies with the ACS deployment apogee setpoint, demonstrating the algorithm's ability to regulate to different competition objectives. The MATLAB simulation assumes 5 mph wind, 5 degree cant, vehicle ballast of 3 lbm and an ACS deployment angle of 90 degrees.

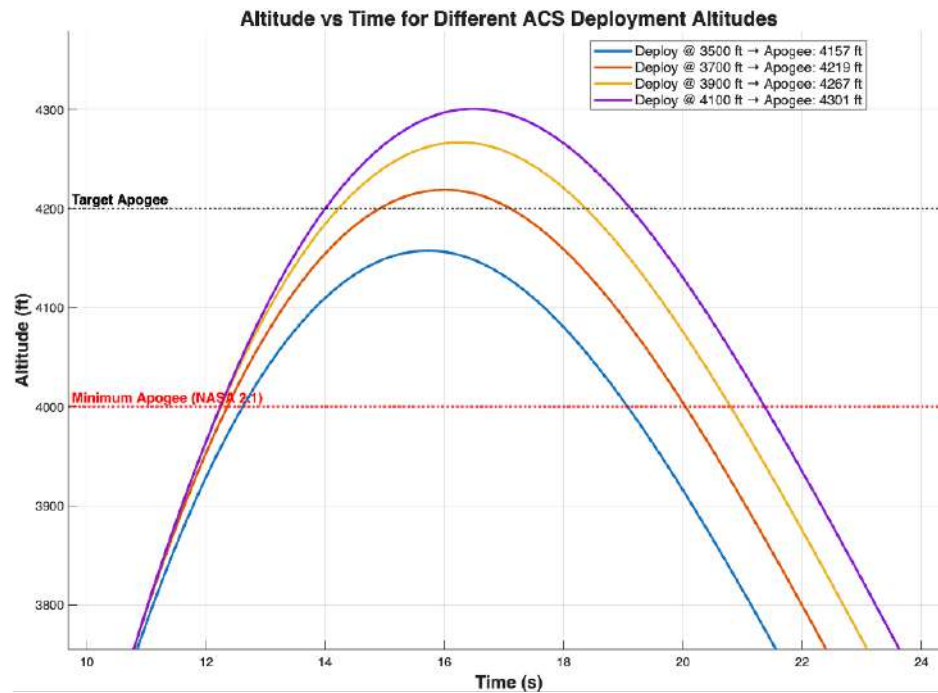


Figure 64: Plot of Achieved Apogee (ft) vs. ACS Target Apogee Setpoint (ft) with 90° deflection

Ballast Affects on Apogee

Vehicle ballast serves dual critical functions: it adjusts the center of gravity to achieve target static stability margin, and it modulates vehicle mass to control ascent performance and apogee without active control deployment. By strategically positioning ballast mass along the vehicle axis, the team can simultaneously optimize stability while tuning the baseline (no-ACS) apogee to nominal design specifications.

The following plot illustrates the inverse relationship between ballast loading and final vehicle apogee. All simulations assume nominal atmospheric conditions with no active control system deployment, steady 5 mph winds, and a 5 degree cant:

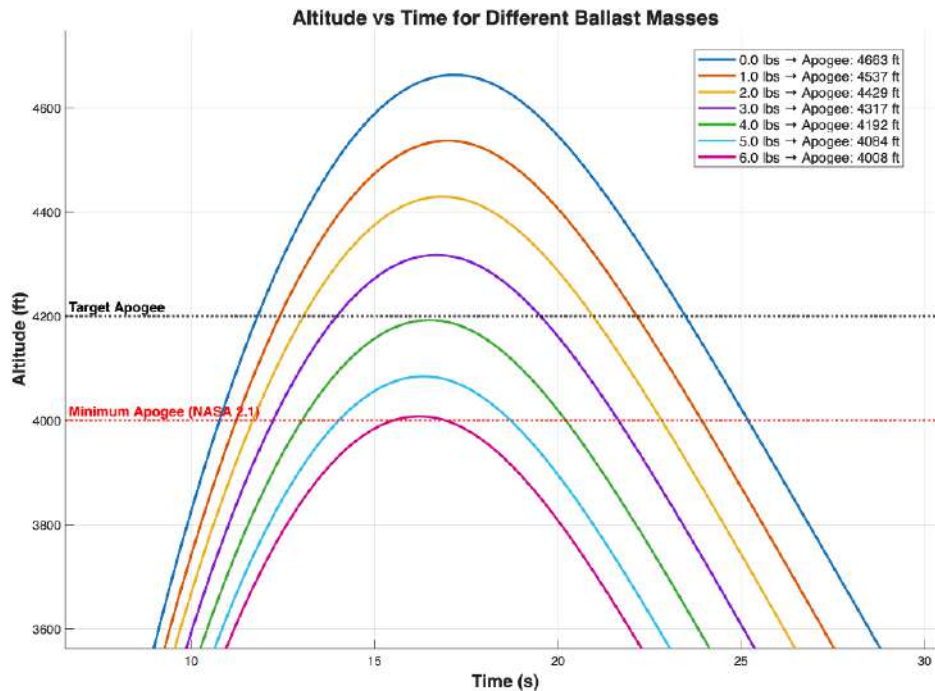


Figure 65: Apogee (ft) vs. Time (s) with varying ballast mass (lbm)

Based on this ballast sensitivity analysis, the VADL team has selected a nominal ballast mass of 3 lbm to achieve the baseline apogee (no-ACS deployment) of approximately 4,315 feet.

Wind Effects on Apogee

Atmospheric wind conditions during launch induce a weathercocking effect on the vehicle. As the rocket ascends through wind shear layers, transverse wind forces cause the vehicle to orient into the wind direction (weathercock), which lengthens the flight path. This extended trajectory reduces the maximum altitude achieved compared to calm conditions. The magnitude of apogee reduction is dependent on wind speed and the vehicle's stability margin, which governs how aggressively the vehicle weathercocks during ascent.

The following plot illustrates how vehicle apogee varies with constant wind speed due to weathercocking effects. All simulations assume no active control system deployment, 3 lbm nominal ballast, and a launch rail canted to 5 degrees with the wind, providing an assessment of wind effects under baseline flight configuration:



Figure 66: Apogee (ft) vs Time (s) for varying wind conditions

3.6.8 Flight Profile - OpenRocket

OpenRocket is a free, open-source flight simulation software that predicts rocket trajectories using Barrowman aerodynamic equations and integrates motor thrust curves with detailed vehicle mass properties. The VADL vehicle model in OpenRocket includes all structural components, avionics, payload, recovery system, and nominal ballast loading to accurately represent flight performance.

The OpenRocket representation of the vehicle is shown below:

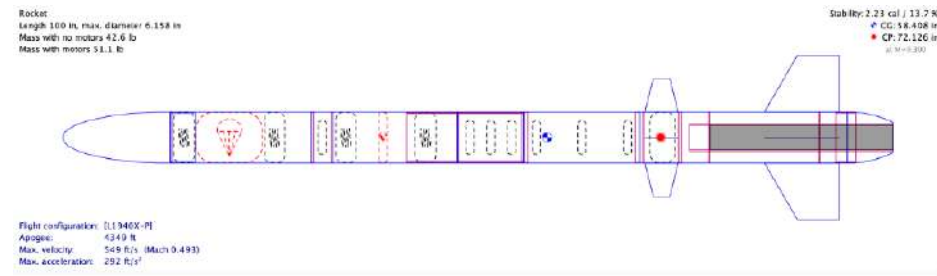


Figure 67: VADL launch vehicle representation in OpenRocket

The following plot shows the predicted flight profile at nominal launch conditions (3 lbm ballast, no ACS deployment, 0 mph wind):

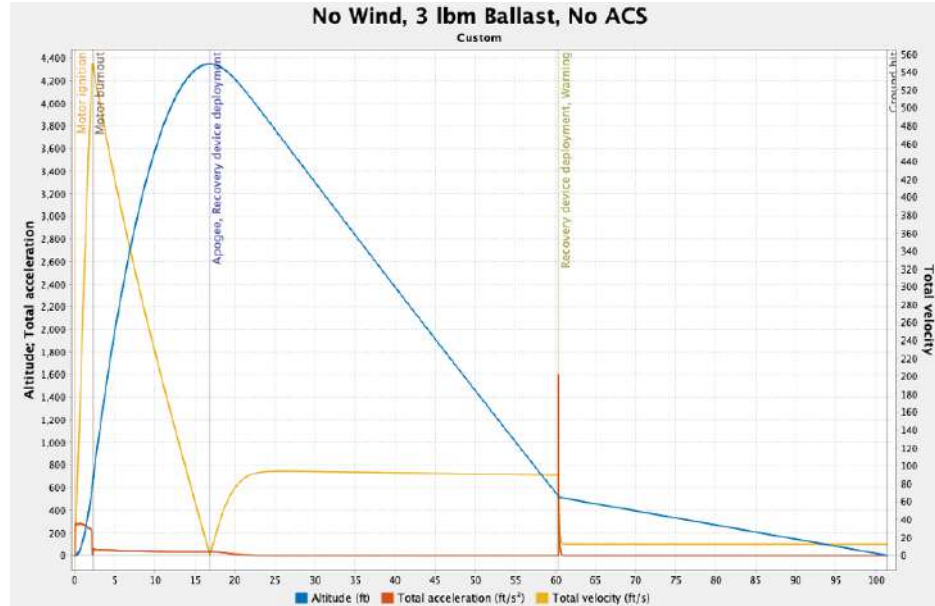
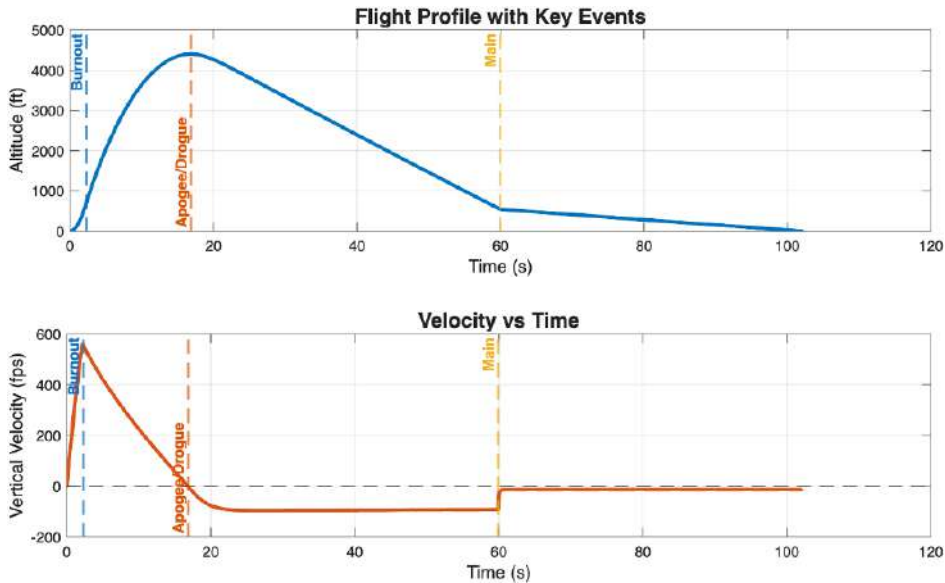


Figure 68: Altitude (ft), total acceleration (ft/s^2), total velocity (ft/s) vs time under nominal conditions

3.6.9 Flight Profile - MATLAB

Our MATLAB simulation framework is built on an object-oriented architecture that enables highly parameterized and configurable flight simulations. The framework allows users to rapidly iterate across vehicle configurations, environmental conditions and ACS deployment configurations. Its modular design allows the team to integrate in more complex modeling for dynamic events such as launch rail ascent, ACS deployment and parachute deployment.

Shown below is the nominal flight profile predicted by MATLAB with 3 lbm ballast, no wind, no cant and no ACS deployment:



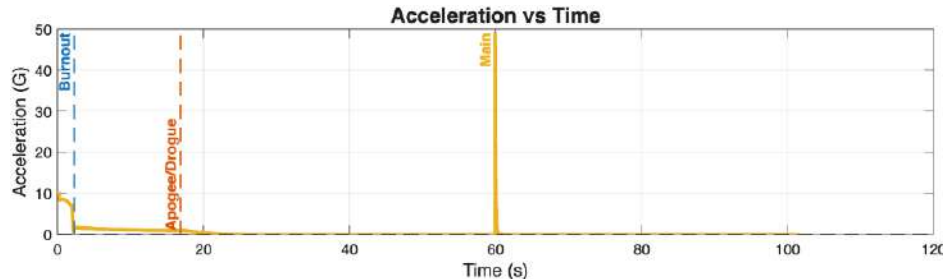


Figure 69: Nominal flight profile predicted by MATLAB; no wind, no cant, no ACS deployment, 3 lbm ballast

Note that in the final acceleration vs time plot, the model shows a high spike at 60 seconds. In the MATLAB simulations, parachute opening is modeled as instantaneous, generating an unrealistically high snatch force at main deployment.

MATLAB Flight Profile with ACS Deployment

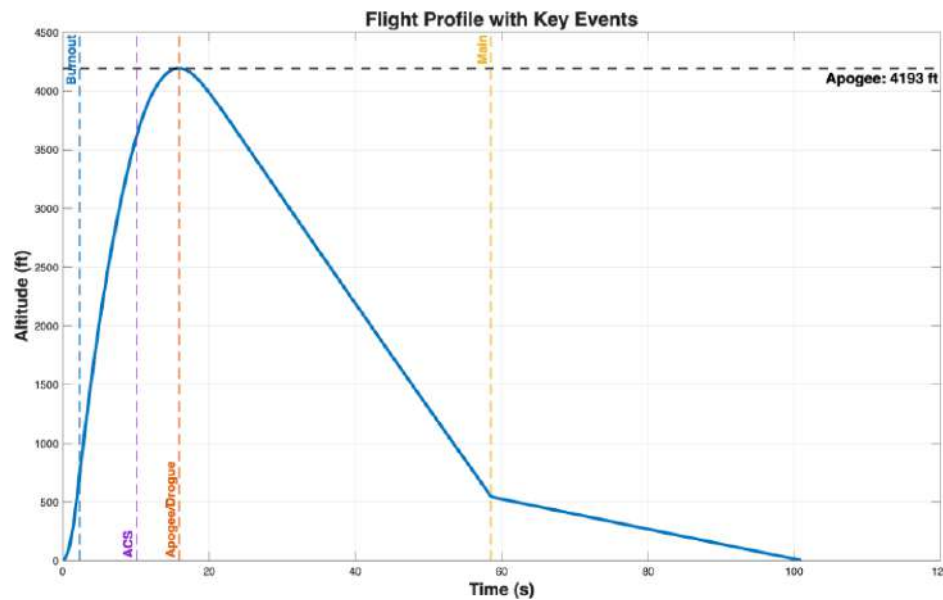


Figure 70: MATLAB-simulated flight profile with ACS deployment under expected launch conditions

To further illustrate the vehicle's predicted flight performance with active control, Figure 70 shows the MATLAB-simulated flight profile incorporating ACS deployment. This simulation was run with 3 lbm of ballast, 5 mph steady winds, and a 5° cant into the wind to emulate realistic launch-day conditions. The simulation utilizes the same predictive model that the apogee control system will utilize in flight to inform the ACS when to deploy. In the simulation, the ACS deploys at approximately 3,650 ft AGL, resulting in a final apogee of 4,193 ft, 7 feet below the competition target altitude of 4,200 ft. This simulation demonstrates the ACS's capability to precisely modulate apogee under expected field conditions while maintaining a stable ascent and nominal descent sequence.



3.6.10 Flight Profile - RockSim

RockSim is another flight simulation tool used to model and verify the vehicle's ascent performance. Like OpenRocket, it solves the Barrowman equations for aerodynamic stability and uses manufacturer-provided motor thrust curves, but with an independent solver and aerodynamic model. To cross-validate results, the VADL team modeled the full vehicle in RockSim using identical mass and geometry inputs.

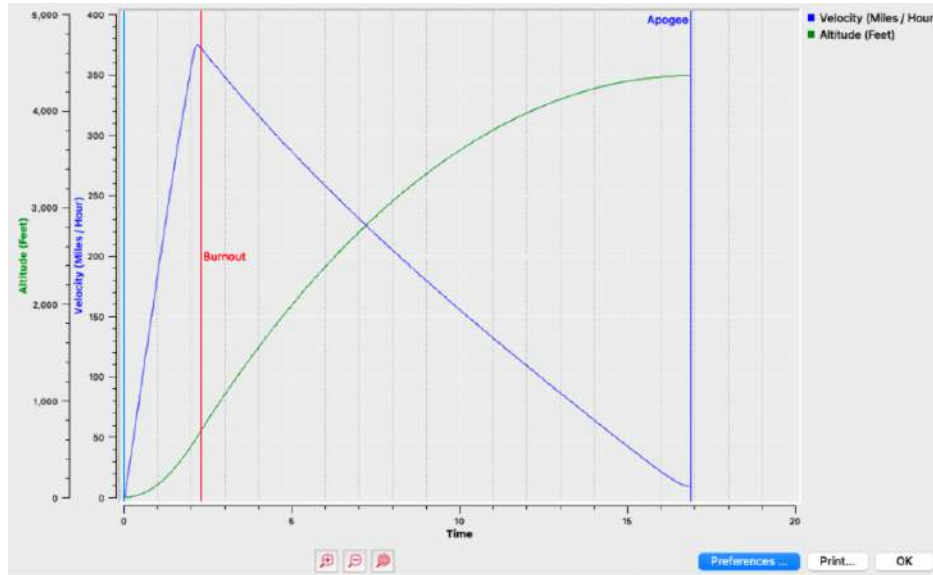


Figure 71: RockSim-simulated ascent profile of the VADL launch vehicle under nominal conditions (3 lbm ballast, no wind, no cant, no ACS deployment).

3.6.11 Landing Sections Kinetic Energy

To calculate the kinetic energy of each section, we first calculate the terminal velocity of the vehicle using:

$$v_{\text{term}} = \sqrt{\frac{2mg}{C_D A \rho}} \quad (9)$$

Where m is the dry mass of the vehicle in slugs, C_D is the coefficient of drag of the main parachute, A is the area of the main parachute and ρ is the density of the air at ground level. The values for C_D and A are for the Fruity Chutes Iris Ultra 144" Compact Parachute as discussed in Section 3.5.6. This calculation is conservative as it neglects the additional drag effects of the rocket body and the drogue parachute. Using this formula, we calculate $v_{\text{term}} = 12.6 \text{ ft s}^{-1}$.

Using this descent velocity, we can calculate the landing kinetic energy as:

$$KE = \frac{1}{2} m_{\text{section}} v_{\text{term}}^2 \quad (10)$$



Table 43: Landing kinetic energy of each independent section

Section	Mass (lbm)	Kinetic Energy (ft-lbf)
Nose Cone	5.33	13.1
Recovery Section	13.58	33.5
Tail Section	28.13	69.4

All sections fall under NASA Requirement 3.2 which specifies that each section of the launch vehicle shall have a maximum kinetic energy of 75 ft-lbf at landing. Additional efforts will be made to reduce the mass of the tail section to ensure that the team stays compliant with said requirement.

3.6.12 Descent Time Predictions

The vehicle's descent time can be calculated as:

$$t_{desc} = t_{drogue} + t_{main} \quad (11)$$

Where t_{desc} is the total descent time, t_{drogue} is the descent time under the drogue parachute ($z_m > z(t) > \text{apogee}$) and t_{main} is the descent time under the main parachute ($0 > z(t) > z_m$).

Descent time under drogue parachute :

To calculate the descent time under drogue, we consider Newtons II law as follows:

$$F_{\text{drag,drogue}} + F_{\text{drag,Rocket Body}} - F_{\text{gravity}} = m \frac{dv}{dt} \quad (12)$$

$$\frac{1}{2} \rho_d (C_{D_d} A_{\text{drogue}} + C_{D_R} 2A_R) v(t)^2 - mg = m \frac{dv}{dt} \quad (13)$$

Where $\rho_d = 0.0022 \text{ slugs/ft}^3$ is the air density under drogue which is assumed to be constant as the average air density in the drogue regime between 550 ft and APOGEE above ground level. $C_{D_d} = 1.5$ and is the coefficient of drag for the Fruity Chutes 24" Elliptical parachute, A_{drogue} is 3.14 ft^2 , $C_{D_R} = 0.7$ is the estimated coefficient of drag of a tumbling upright cylinder and A_R is the cross sectional rocket area and is multiplied by 2 to account for the two bodies tumbling. Lastly, m is the dry mass of the vehicle. With the initial condition that $v(0) = 0$, we can solve this ODE such that:

$$t_{\text{drogue}} = \frac{v_{term}}{g} \text{ arccosh} \left(\exp \left(\frac{g \Delta z}{v_{term}^2} \right) \right) \quad (14)$$

Where Δz is the target apogee (4200 ft) minus the main deployment apogee (550 ft), v_{term} is the vehicles terminal velocity under drogue:

$$v_{term} = \sqrt{\frac{mg}{\frac{1}{2} \rho_d (C_{D_d} A_{\text{drogue}} + C_{D_R} 2A_R)}} = 92.1 \text{ ft/s} \quad (15)$$



Using $v_{term} = 92.1 \text{ ft/s}$, we calculate:

$$t_{drogue} = 41.6 \text{ s} \quad (16)$$

Descent time under main parachute:

First, assuming that in the regime $0 > z(t) > 550$, the rocket is traveling at its terminal velocity, we can calculate the descent time under main to be:

$$t_{main} = \frac{z_m}{v_{term,main}} = \frac{550}{12.6} = 43.6 \text{ s} \quad (17)$$

This calculation is conservative as there will be a transient state post main deployment in which the rocket has a velocity greater than its terminal velocity.

Total Descent Time

Returning to our total descent time:

$$t_{desc} = 41.6 + 43.6 = 85.2 \text{ s} \quad (18)$$

3.6.13 Drift Predictions

To calculate drift, we use the worst-case assumption that the vehicle drifts at the speed of the wind for the entire descent. We also make the worst-case assumption that apogee is reached directly over the launch pad (during ascent, the vehicle will typically travel into the direction of the wind). We also use the worst-case wind case of constant 20 mph winds. Winds higher than this value would result in NASA canceling flight. With these assumptions in mind, we can calculate the drift to be:

$$x_{drift} = t_{desc} * v_{wind} \quad (19)$$

$$x_{drift} = 85.2 \text{ s} * 20 \text{ mph} * \frac{1.46 \text{ ft/s}}{1 \text{ mph}} = 2488 \text{ ft} \quad (20)$$

This calculation falls very close to NASA Requirement 3.10 which necessitates that the recovery area shall be limited to a 2,500 ft radius from the launch pad. This requirement is extremely important for safety as it is important to ensure that the vehicle while descending remains within the recovery radius.

The team is confident in our drift remaining well under the 2500 ft radius based on the following rationale:

- i. The above calculation assumes that the rocket begins its descent immediately above the launch pad. This is an unrealistic assumption as weathercocking causes the rocket to turn into the wind during ascent.
- ii. The above calculation assumes that the rocket travels at the equivalent speed of the winds for the entirety of its descent.
- iii. The above calculation overestimates the descent time under main parachute.



Simulations were run in OpenRocket to verify the above. In Table 44, we show varying drift distances under varying constant wind conditions. In all simulations, the rocket was canted 5 degrees with the wind, the rocket contained 3 lbm ballast and there was no ACS deployment.

Table 44: Recovery drift as a function of wind speed based on OpenRocket simulations

Wind (mph)	Drift (ft)
20	2,015
15	1,711
10	1,487
5	1,215
0	981



4 Payload Design

4.1 Payload Mission Objectives

4.1.1 Payload Mission Sequence

After landing, the payload system starts the soil collection and analysis sequence. The payload bay begins with a 6 RPM rotation driven by a gearbox mechanism and DC brushed motor, causing an attached shovel to deploy outward from a separate gear train passively. As the payload bay completes successive rotations, the shovel scoops soil from the surrounding terrain and moves it into its containment and sampling chamber. The system is designed to perform 23 full payload bay rotations in accordance with VADL Requirement 3.2.3 and 3.5.13, with approximately half of the rotations digging into the ground.

As soil is collected, a small bladder filled with water, positioned next to the payload, passively unties and releases the water into the soil chamber. This water soaks the collected soil, allowing it to be accurately tested in place. Embedded sensors within the payload measure soil properties (pH, electrical conductivity, nitrate content) throughout this process. Data is logged on board with appropriate timestamps per NASA USLI Requirement 4.2.1. In this way, all mechanisms pertaining to soil collection, fluid release, and collection are controlled by a single actuator: the DC brushed motor.

4.1.2 Success Criteria

The payload mission success criteria are outlined in Table 45 below. These criteria define the conditions the payload mission must meet to be considered successful, including both pre-deployment and post-landing phases.

Table 45: *Payload Success Criteria*

Crit. Description	NASA Req. #	VADL Req. #
1 The payload survives landing within the prescribed kinetic-energy/impact limit of 75 ft-lbs.	Recovery System req. 3.2	N/A
2 The soil collection sequence autonomously begins after landing.	HAUS Mission req. 4.1	3.2.1
3 The shovel mechanism completes the intended 23-rotation collection cycle and successfully retracts without mechanical failure.	N/A	3.2.3
4 At least 100 mL of soil is collected and retained within the soil chamber.	HAUS Mission req. 4.1	3.2.1



Table 45 (continued): Payload Success Criteria

Crit. Description	NASA Req. #	VADL Req. #
5 Torque on the shovel face does not exceed 10 N m to safely prevent tipping of the tail section during soil collection.	N/A	3.2.5
6 The passive water-release mechanism functions as designed, providing soil moisture at a ratio of 1:1 (water:soil) for measurements.	N/A	3.4.3
7 Sensors collect and record accurate soil data, including pH, nitrate content, and/or conductivity.	HAUS Mission req. 4.2	3.5.14
8 The collected data are successfully transmitted to the team's ground station (or verified in onboard storage) without corruption and with time stamping.	HAUS Mission req. 4.2.1	3.5.14
9 All payload operations occur after vehicle apogee and landing and take less than 15 minutes to complete.	HAUS Mission req. 4.1.1	3.2.2
10 Payload integrates into the rocket within 30 minutes using standardized fasteners and the bulkplate interface.	N/A	3.1.3
11 Shovel extension is repeatable over 20+ trials without loss of motion, jamming, or gear tooth damage.	N/A	3.2.4
12 All rotating parts are lubricated or coated (e.g., PTFE-backed shovel, sealed gearbox) to prevent seizing under dust contamination.	N/A	3.2.6
13 The opening mechanism weighs no more than 0.6 lb and has an aft–fore length of no more than 2 inches.	N/A	3.2.7
14 All critical components (bulkplates, shovel arms, gearbox housing) have a minimum factor of safety of 2 under expected loads.	N/A	3.2.8

4.2 Alternative Payload Designs

4.2.1 Soil Extraction Methods — Feasibility Study

Early design concepts focused on an auger-based payload capable of collecting and ejecting soil into a catchment chamber, but these designs proved too complex because they necessitated multiple actuators. A horizontal linkage-based shovel scraper concept and a rotating belt with buckets design were also explored, though both suffered from mechanical complexity and reliability concerns. Simpler syringe-style samplers lacked a water-injection system necessary for accurate soil testing and did not have the necessary penetration force for compacted soil. A step-bit auger was also tested but had mechanical complexity and no simple way to reliably transfer soil for testing.



Ultimately, the team chose a rotating shovel design that uses a single motor to handle all operations—rotation, shovel extension/retraction, soil collection, and moisture addition. The shovel extends using a sandwiched gearbox which rotates with the payload bay around a stationary central rod, while rotation also loosens a rope to release a water-filled balloon for moisture. A soil sensor communicating with a VADL computer records measurements once the sample is collected and wetted.

Table 46 summarizes the trade study comparing soil excavation methods considered for the payload. Scores reflect team assessments of stability, actuation simplicity, sample-chamber compatibility, mechanical risk of failure, and innovation novelty. The highest composite score belonged to the rotating shovel payload and thus this influenced our selection.

Table 46: Payload Sampling Method Trade Study

Method	Stability	Actuation Simplicity	Sample Chamber Form Factor	Low Mechanical Failure Points	Innovation	Total Weighted Score
						100%
Rotating Shovel	9	10	8	8	9	8.85
Syringe Hole Punch	7	7	7	5	7	6.3
Step Bit Auger	7	4	8	6	7	6.15
Horizontal Scraper	6	6	8	4	8	5.7
Rotating Buckets	7	3	8	4	9	5.3
Auger — Non-Jettisoned Lander	9	4	6	5	3	5.3
Auger — Jettisoned Lander	2	5	5	4	6	4.2

The rotating shovel achieved the highest composite score due to its balance of stability, simple actuation, compatible geometry with the curved soil chamber, and relatively unlikely failure modes. Auger designs featured either high mechanical complexity with the jettisoned version or too many actuators with the horizontal lander version. The step-bit auger also featured mechanical complexity, whereas the syringe design lacked the puncture force needed to bore through varied soils. Bucket and scraper concepts offered promising innovation but introduced additional interfaces and potential jamming points relative to the shovel.

4.2.2 Shovel Extraction Designs

This section outlines the evolution of the shovel profile. Various designs were evaluated, and the conclusions drawn in the following trade study informed our final design choice.

**Table 47:** Shovel Extraction Design Trade Study

Design	Performance	Robustness	Weight	Soil Friction	Subsystem Adaptability	Total Weighted Score
						100%
Single Tooth with PTFE backed Sliding Surface (Current)	9	8	8	8	7	8.25
Excavatorstyle Teeth, Sharper Angle of Attack	8	8	8	5	7	7.45
Semicircular with Pointed Edge	6	6	9	5	7	6.4
Circular Profile (Conformal)	4	5	9	5	5	5.25

The first design considered was the circular profile shovel shown in Figure 72; however, it was quickly ruled out due to its extremely gentle angle of attack and large surface area, which proved unnecessary. This design was refined into another circular profile that came to a point for biting into the soil, shown in Figure 73. It was with this prototype that the team decided to redesign the curvature for a sharper angle of attack and bite into the ground. From this, both the excavator-toothed and single-tooth shovel designs were considered, with the excavator design shown in Figure 74. The single-tooth design was more effective overall, with fewer failure points, and PTFE was added to the back of the shovel to reduce soil friction. The single-tooth design is shown in Figure 75.

The existing design is made from PLA; however, we do not expect its structural rigidity to be sufficient to withstand parachute shock loads. As a result, we are investigating two alternatives: a fiberglass mold or an Onyx print with an external fiberglass shell for increased strength and stiffness.



Figure 72: Initial Payload CAD Exploded Assembly. (1) Rocket airframe, (2) non-rotating bulk plate, (3) preliminary shovel design, (4) rotating bulk plate.

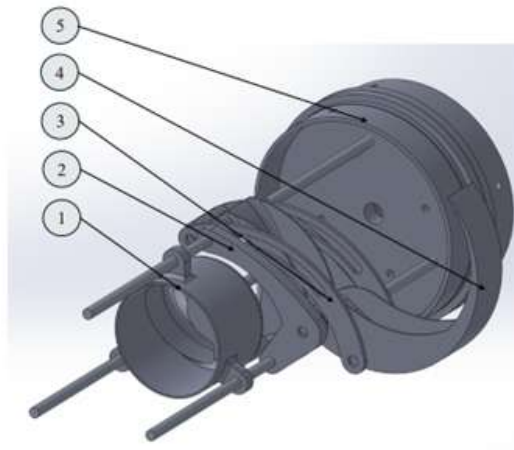


Figure 73: Second shovel design featuring a pointed tip with the same curvature as first prototype. (1) Soil containment chamber, (2) bearing mounts, (3) shovel arms, (4) redesigned shovel, and (5) RBS.

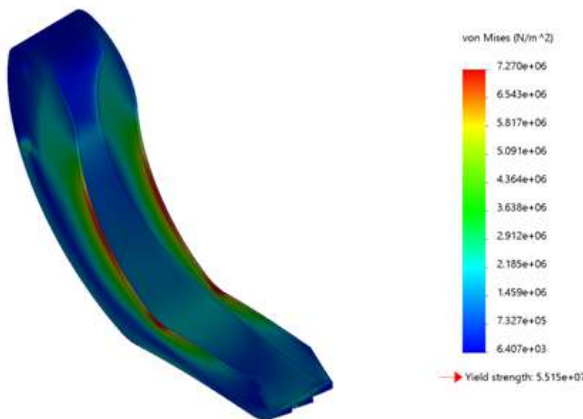


Figure 74: Second redesign of shovel face incorporating more aggressive angle of attack and excavator-inspired teeth. Shows preliminary FEA of the prototype.



Figure 75: Current shovel design including PTFE on back and one tooth to decrease failure points.



4.2.3 Soil Housing Designs

To fulfill NASA USLI Requirement 4.1 of collecting 50 mL of soil at the drop location, a properly sized soil housing chamber was developed. The design was guided by the rotating shovel collection method and the leading soil-extraction concept outlined in Table 46. The chamber dimensions were primarily constrained by the integrated sensors, outlined in section 4.3, which dictated the minimum chamber length needed for proper sensor placement. An FOS of at least 2 on chamber volume was required to ensure sufficient volume for soil collection, retention, and wetting. In accordance with NASA USLI Requirement 4.1, the collected soil needs to be fully contained and retained within a dedicated chamber, rather than remaining on the auger surface. Additionally, the chamber had to function as an independent containment unit, capable of passively filling with soil and securely retaining it throughout handling and testing. While not a strict requirement, it was considered advantageous for the system to avoid using additional actuators to transfer soil into the chamber, thereby simplifying the design, reducing power consumption, and minimizing potential failure points. Several concepts for soil entering the chamber were evaluated and compared in Table 48.

Soil Slide, Concept 1

The slide mechanism features an annular opening that allows soil to enter as the shovel rotates, without the need for any additional actuator, flap, or solenoid. Retention of the collected material depends on the geometry of the chamber, surface friction, and the vehicle's attitude during operation. This design minimizes potential failure points because the soil does not need to push through a physical barrier. However, there is a potential for backflow, where soil or water could escape if the orientation is unfavorable. There is a 3.52° tilt with the aft section of the vehicle, which prevents any soil or water backflow.

Spring-Loaded Trap Door, Concept 2

The spring-loaded trap door employs a hinged flap that opens inward under the force of the incoming soil and automatically closes to prevent outflow. This provides passive one-way retention without electrical actuation. The added mechanism, however, introduces complexity—springs and hinges are prone to fatigue, corrosion, and jamming from dust or small particulates. While more secure than the open slide, it carries higher manufacturing risk and may reduce long-term reliability under repeated use.

Actuated Door, Concept 3

The actuated door design uses a small rotary or linear solenoid (or micro-servo) to actively control a door or latch that seals the chamber after soil entry. During operation, the door opens to allow soil in as the shovel deposits material, then closes under electronic command to ensure complete retention during transport and testing. This approach provides the most precise control over soil containment and enables integration with sensor feedback systems (e.g., closing triggered by a soil-level reading). However, the additional actuator introduces higher power draw, wiring complexity, and potential single-point failures in extreme environments. Despite this, its controllability makes it advantageous for autonomous operations, ensuring reliable closure and retention is critical for mission success.



Table 48: Soil Entry Mechanism Trade Study

Design	Performance	Reliability	Soil Retention	Soil Friction	Total Weighted Score
	20%	25%	35%	20%	100%
Soil Slide	5	6	5	7	5.65
Spring-loaded Door	4	4	7	5	5.1
Actuated Door	6	4	7	3	5.2

4.2.4 Water Injection Justification

A requirement for water integration was established following experimental testing of the seven-in-one soil sensors (VADL requirement 3.4.3). Results showed that maintaining a consistent soil-to-water ratio was needed for accurate sensor readings and soil saturation. The addition of water allows ions to move within the soil, which is needed for reliable sensor response and pH measurement. All water used in testing was deionized to make sure that consistent conditions were used without changing the soil's natural composition.

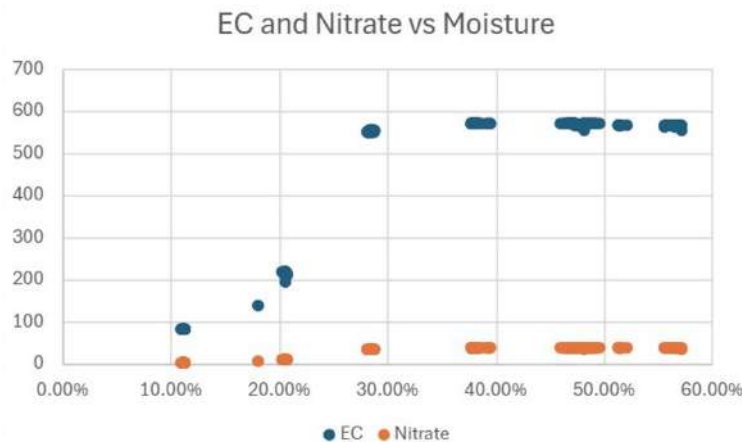


Figure 76: Graph of EC and Nitrate values vs. Moisture showing convergence of soil data after 30% moisture content reached.

Initial trials used a 3:1 soil-to-water ratio, as shown in Figure 76, in early prototypes to achieve stable sensor outputs. After consultation with a subject-matter expert and refinement of the sensor design, the VADL Requirement 3.4.3 was updated to a minimum of 1:1. This requirement has not been verified through testing with current sensors at this time, but it is supported by scientific literature [13], [12].

Assuming that the soil remains at 0% moisture content, simulating a Mars environment, the requirement is to provide the volume of water equal to the maximum soil collection. Realistically, the soil will contain more than 0% moisture, but because of the wide range of available water content (1:1 to 1:5 soil-to-water ratio), the soil sensors can operate up to 5



times their weight in water, providing a safety margin.

4.2.5 Water Injection Designs

Given VADL Requirement 3.4.3, a minimum 1:1 soil-to-water ratio is required to obtain valid sensor readings. To meet this, the following water integration concepts were evaluated.

Syringe-Driven Injection System, Concept 1

This water integration concept consists of a syringe with a plunger mechanically coupled to the non-rotating central shaft in the rotating shovel design. During operation, the rotation of the shovel assembly drives the plunger forward, using a carriage that converts rotational motion to linear motion, and injects a metered quantity of water into the soil chamber. This approach provides precise volumetric control and can be calibrated for specific water ratios. It also allows for a simple refill and maintenance procedure. However, it requires a robust mechanical coupling that does not deform in flight, as well as high-pressure seals. The design also has a limited water capacity per syringe (maximum 80 mL for the rotating shovel design), poses a risk of leakage under high-vibration loads, and adds weight.

Tether-Released Bladder System, Concept 2

In this configuration, a flexible latex water bladder is stored compactly and unraveled by a tether adhered to the non-rotating shaft. As the shaft rotates, the tether pulls the bladder open, passively releasing water into the soil chamber. This configuration is lightweight and low-power, making efficient use of the shaft's existing motion without requiring additional actuators. It is also adaptable to irregular payload geometries. Despite these benefits, the water release rate can be difficult to control, and there is a risk of incomplete discharge. However, with the rotating shovel design, the aft section's tilt encourages complete discharge throughout the payload bay's rotation.

Integrated Chamber Water Reservoir, Concept 3

The third concept is sealing the entire chamber with a water compartment directly within the soil chamber, separated by an actuated door connected to the non-rotating shaft. Once the shovel deposits soil, the door opens, allowing water to be mixed directly into the chamber's volume. This design is compact and self-contained, allowing for simultaneous soil collection and hydration while minimizing the need for separate plumbing or storage components. However, it depends on the actuated door mechanism described in Section 4.2.3, which increases system complexity and introduces potential sealing challenges. Furthermore, the available water volume is constrained by the chamber's geometry. Furthermore, there will be sloshing because the water chamber volume is larger than the maximum amount of water to be added.



Table 49: Water Integration Design Trade Study

Design	Reliability & Leak Risk	Mass Impact	Mechanical Complexity	Release & Timing Control	Total Weighted Score
	35%	15%	20%	30%	100%
Syringe Injection	5	3	4	9	5.7
Tether-Released Bladder	6	7	8	5	6.25
Integration Chamber-Water System	4	8	6	3	4.7

As shown in Table 49, the tether release bladder was chosen as the top design for the water integration due to its high ratings for being a simple yet reliable design.

4.2.6 Computing Unit

This section focuses on our selection of a central computing unit as outlined in VADL Requirements 3.5.12-14. All the boards considered had to be capable of PWM output, UART communication, Serial communication, and fit within a 6-inch diameter of the expected payload.

Table 50: Evaluation of final computing unit options

Component	Power Required	GPIO Ports	Data Rate	Size	Total Weighted Score
	50%	20%	10%	20%	100%
STM32F407VG	9	8	7	7	8.2
Teensy 4.1	9	10	9	10	9.4
Raspberry Pi 5	2	7	10	8	5.0

After weighing the criteria in Table 50, the Teensy 4.1 board is the best option. This also validates the use of a microcontroller rather than a microprocessor, such as the Raspberry Pi, given its power requirements.

4.2.7 Inertial Measurement Units

Our rocket uses an Inertial Measurement Unit (IMU) to trigger actions in the payload at critical points in flight, as outlined in VADL Requirement 3.5.2. All considered components must reliably collect the data outlined in VADL Requirements 3.5.3-10.



Table 51: IMU Trade Study

Component	Accuracy	Reliability	Integration	Size	Total Weighted Score
	30%	40%	20%	10%	100%
VN-100	10	10	9	9	9.7
3DM-GV7-AHRS	10	8	9	8	8.8
XSens MTi-610	10	7	9	8	8.4
STEMMA QT BN0085/BME280	2	2	10	10	4.4

After weighing the IMUs in Table 51, we selected the VectorNav VN-100, which is a combined IMU and Altitude Heading Measurement System (AHRS). Its versatility as a standalone ruggedized IMU with pressure measurement capabilities, leading performance in accurately sampling across wide environmental ranges, and reliable performance in previous years' competitions. Furthermore, the sensor offered plug-and-play integration with our microcontroller and peripheral electronics using the UART communication protocol.

4.2.8 Motor and Motor Controller

Multiple motor configurations were evaluated for the criteria outlined in Table 52. Overall, our motor needed to reach a minimum torque value while minimizing power, weight, and control complexity.

Table 52: Motor and Controller Trade Study

Component	Torque	Weight	Length	Power	Total Weighted Score
	30%	20%	20%	30%	100%
Tetrix MAX TorqueNADO + Sparkfun Driver	2	9	7	6	5.6
NEO Brushless + Spark MAX (100:1 Gearbox)	10	4	5	4	6.0
42GP-775 + BTS7960 Controller	8	6	8	10	8.2
Sito TA-70-10 + Harmonic Drive	9	5	10	7	7.8



The 42GP-775 Motor and BTS7960 Controller were the best choice for our payload actuation system due to their high torque output, low power consumption, and compact size. The BTS7960 is being used as a PWM motor actuator due to better max power handling compared to the Sparkfun, which can burn out at stall torque loads.

4.2.9 Power Delivery Trade Study

This section focuses on determining how to provide a steady 5-volt line for our electronics from the battery. These regulators must provide a steady, efficient power source for multiple components and were scored accordingly.

Table 53: Power Delivery Trade Study

Component	Output Ripple	Max Output Current	Efficiency	Line Regulation	Total Weighted Score
	30%	30%	10%	30%	100%
Pololu D36V50F5	9	10	8	4	7.7
TSR 1-2450	8	4	8	8	6.8
LM2596 Module	10	6	6	7	7.5

After weighing the criteria in Table 53, the Pololu D36V50F is the best option due to its high current supply and decent voltage regulation.

4.2.10 Sensor Selection Overview

Dedicated sensors will measure electrical conductivity, nitrate-nitrogen concentration, and pH. Sensors were first selected based on design constraints and then evaluated for accuracy and redundancy. Certain components considered measure all three characteristics, and they will be evaluated on each sampling parameter.

7-in-1 Nitrate, Phosphorus and Potassium Probe A widely available soil sensor is a 7-in-1 Nitrate, Phosphorus, and Potassium probe. They measure electrical conductivity, then interpolate the quantity of various ions given predetermined ratios and calibration curves [8]. These devices lack accuracy in measuring pH and, mainly, nitrate content because they rely on indirect methods. However, this component comes in a convenient form factor, as all necessary circuitry is housed in a waterproof package.

Ion Selective Electrode A more accurate, electrical-based ion sensor is an ion-selective electrode. They are constructed with glass or PVC membranes that allow specific ions to pass through; in this case, H⁺ for pH and nitrate. These ions generate an electric potential relative to that of a reference electrode. From this data and the Nernst equation, an estimate of ion concentration can be obtained. While this device is a far more accurate option, it presents its own unique implementation challenges. Typically, these devices are paired with a countertop console that does internal signal processing to display concentration values. To record these measurements within the payload, we will need to implement an amplifier circuit and an analog-to-digital converter into our hardware. We must also select



an electrode that does not contain a glass membrane, as it must withstand the forces of rocket flight.

Ion Selective Field Effect Transistor Finally, the other type of sensor considered is ion-selective field effect transistors. Similar to ion-selective electrodes, a membrane allows specific ions to pass into an area where a potential is generated. This area is the gate of the field-effect transistor, so the transistor's current or operating state changes depending on the ion concentration. This solution is highly durable and has been used in similar circumstances for aerospace applications. However, the technology is expensive, rare, and challenging to manufacture/purchase.

4.2.11 Sensor Selection: pH

Table 54: Soil pH Sensor Trade Study

Component	Reliability	Accuracy	Complexity	Durability	Total Weighted Score
	20%	40%	20%	20%	100%
Ion Selective Electrode (pH)	8	9	8	6	8.0
7-in-1 NPK Sensor	6	5	8	8	6.4
Ion Selective FET (pH)	8	9	6	7	7.8

After weighing the criteria in Table 54, the Ion Selective Electrode was concluded to be the ideal choice for measuring the pH of the extracted soil. The electrode will be sourced from NT Sensors and utilizes a PVC pH membrane. An electrode with a PVC membrane was chosen over a glass membrane because PVC is more likely to withstand the loads encountered during flight.

Table 55: Soil Nitrate Sensor Trade Study

Component	Reliability	Accuracy	Complexity	Durability	Total Weighted Score
	20%	40%	20%	20%	100%
Ion Selective Electrode (Nitrate)	8	9	8	6	8.0
7-in-1 NPK Sensor	6	3	6	8	5.2
Ion Selective Field Effect Transistor (Nitrate)	8	9	6	7	7.8

After weighing the criteria in Table 55, the Ion Selective Electrode was concluded to be the ideal choice for measuring Nitrate-Nitrogen of the extracted soil. The electrode will be



sourced from NT Sensors and utilizes a PVC Nitrogen-Nitrate membrane. An electrode with a PVC membrane was chosen for similar reasons to the pH electrode.

4.2.12 Sensor Selection: Electrical Conductivity

Unlike the previous two sensors, electrical conductivity does not rely on the same ion-selective principles. It is measured by applying an AC signal through the soil and measuring the voltage across the resistor, which allows conductivity to be calculated. Here, we consider the 7-in-1 sensor against a dedicated sensor, the Atlas Scientific Mini Conductivity Probe K 1.0.

Table 56: *Soil Electrical Conductivity Sensor Trade Study*

Component	Reliability	Accuracy	Complexity	Durability	Total Weighted Score
Mini Conductivity Probe K 1.0	8	9	8	6	8.0
7-in-1 NPK Sensor	6	7	6	8	6.8

According to analysis of the criteria in Table 56, the Atlas Scientific Mini Conductivity Probe proved to be the ideal choice for sampling the conductivity of the extracted soil. The probe has a similar mechanical profile to the ion selective electrodes chosen for other characteristics, making it easier to integrate mechanically whilst also being reliable and more accurate than the 7-in-1 NPK sensor.

4.2.13 Electronic Board and Housing

How our electronics are integrated is a key design factor. First, we consider a perf board, where components are mounted and connected with solder on an array of conductive holes. We also consider a PCB, where we design a board with the connections ordered and shipped for us to solder components onto. Finally, a breakout board can be purchased and attached to our microcontroller, so screw mount connections can be used to wire components.

Table 57: *Electronics Boards Trade Study*

Component	Size	Ease of Fabrication	Reliability	Parasitics / EMI Protection	Total Weighted Score
Perf Board	7	4	5	2	4.7
PCB	10	6	10	8	9.2
Breakout Board	4	10	8	4	6.6



According to the trade study in Table 57, perf boards and breakout boards are ideal during prototyping stages for quick testing and iterating circuit designs. Although these boards are readily available, wired connections on breakout boards and soldered connections on perf boards lead to signal noise, parasitics, and poor reliability at high frequencies. A breakout board also increases wiring complexity, and a perf board is time-consuming to produce or debug. The design should be transitioned to a custom PCB upon verifying the functionality of a breakout board/perf board prototype. PCB offers higher reliability, cleaner routing, improved signal integrity, and greater mechanical durability for actual rocket deployments, especially during subscale and full-scale launches.

4.3 Leading Payload Design

4.3.1 Mechanical Subsystem Overview

The leading mechanical subsystems are chosen, designed, and tested based on the criteria derived from the previous section. Therefore, all designs and their characteristics are the most optimal to meet both the external NASA requirements most effectively, and the internal VADL requirements. The overarching payload subsystem overview covers all direct payload subsystems such as soil collection, electronics, STEMnaut HAUS, and shovel extension. Other relevant subsystems such as the Rotating Bulkplate System (RBS), Leg Deployment System (LDS), and Parachute Detachment System (PDS) have been covered in the vehicle section of the report, as they pertain more to the overall functionality of the rocket structure rather than its role as a soil collection system. This organizational choice was made primarily to focus on safety and structural analysis rather than soil collection functionality. The secondary payload, the Apogee Control System (ACS), will be discussed in a subsequent section.

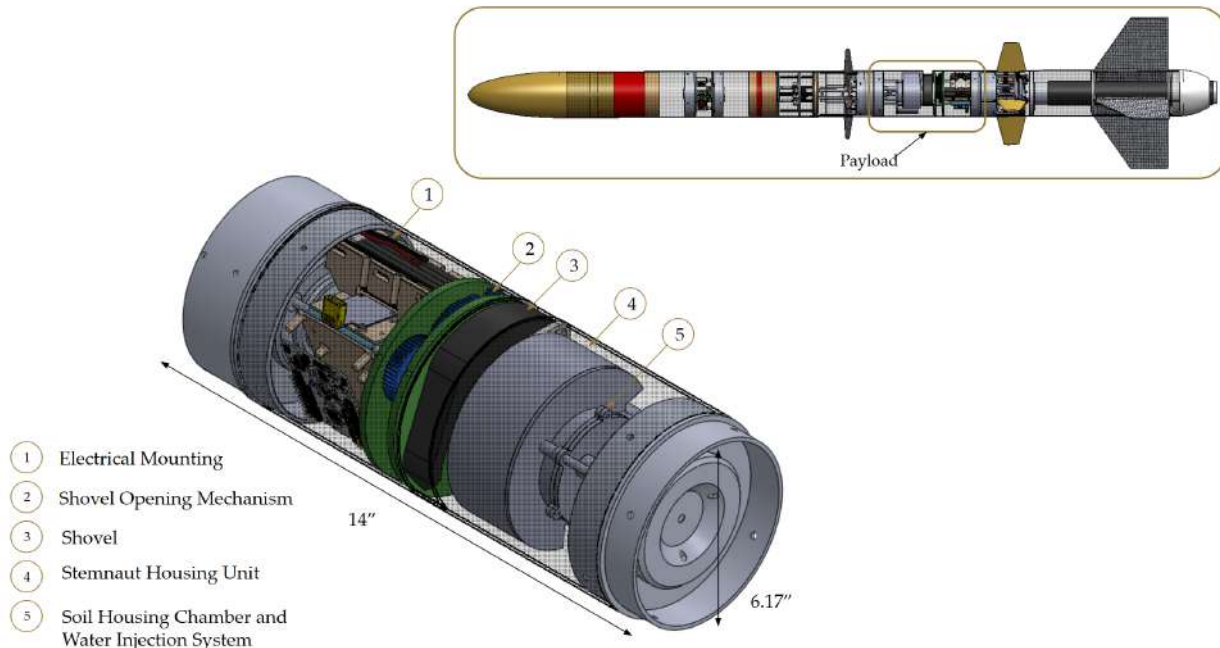


Figure 77: Proposed payload bay and ballooned list of subassemblies.



The goal of the payload is to meet NASA USLI Requirements 4.1–4.7.2 while also meeting VADL Requirements 3.1.1–3.4.3. Once landed on the passively actuated landing legs (as described in Section 3.3.10), the software will initiate the digging procedure. This involves detaching the parachute via the Parachute Detachment System (PDS, described in Section 3.3.9), and actuating the electric DC brushed motor.

The motor spins the payload around the non-rotating shaft, which is attached to the Leg Deployment Mechanism (LDS) via a flange coupler. This rotation causes the system to spin relative to a stationary gear set-screwed to the shaft, driving the gears in the Payload Shovel Actuation System (PSAS) while simultaneously unwinding the knot in the Fluid Delivery System (FDS). Once the motor has spun 23 times, the shovel will dig into the soil and, as it continues rotating outward, begin collecting the surrounding material.

4.3.2 Rotating Shovel Opening Mechanism

This section describes the shovel actuation mechanism responsible for translating payload rotation into shovel deployment and soil collection. A series of gears arranged in a sandwiched gearbox assembly facilitate this motion. The gears are precisely 3D-printed in Onyx on the Markforged printer, with concentric gears integrated into single parts to ensure torque is transmitted properly. The input and output gears use D-shafts to prevent slippage.

The gearbox provides a total 1:47.41 input-to-output rotation ratio, as shown in Equation 21, although the shovel hinge itself does not perform a full 360° rotation. The gearbox assembly is sandwiched between two ABS structural bulkplates, which are secured to the airframe using three #10-32 bolts along the bulkplate edges. As the payload motor rotates the payload bay 23 times, the shovel opens outward at a rate of approximately 0.21 inches per rotation and collects soil in successive passes that increase in volume each rotation. The CAD of the Shovel Extension gearbox can be viewed in Figure 78.

$$\frac{\omega_{\text{out}}}{\omega_{\text{in}}} = \left(\frac{15}{20}\right) \left(\frac{15}{40}\right) \left(\frac{15}{50}\right) \left(\frac{15}{60}\right) \left(\frac{15}{30}\right) \left(\frac{30}{30}\right) \left(\frac{30}{15}\right) = 47.41 : 1 \quad (21)$$



Figure 78: Shovel Extension Gearbox CAD.



Shovel Extension Calculation

After 23 rotations, the shovel will have extended 4.79 inches from the shovel tip to the exterior of the 6.17-inch airframe. Equations 22, 23, and 24 were used to determine the distance from the shovel to the ground upon landing. The calculations reference Figure 79, which contains measurements from the SolidWorks assembly.

$$\text{Difference in height} = 4.63 \text{ in} - 2.16 \text{ in} = 2.47 \text{ in} \quad (22)$$

$$\text{Slope} = \frac{2.47 \text{ in}}{40.22 \text{ in}} = 0.0614 \quad (23)$$

$$h(x) = 2.16 \text{ in} + 0.0614(9.79 \text{ in}) = 2.76 \text{ in} \quad (24)$$

Once this value was obtained, Equations 25, 26, and 27 were performed to solve for the number of shovel rotations needed for the shovel tip to reach the soil:

$$\text{Rotations per inch} = \frac{23 \text{ rotations}}{4.79 \text{ in}} = 4.80 \frac{\text{rotations}}{\text{in}} \quad (25)$$

$$2.76 \text{ in} \times 4.80 \frac{\text{rotations}}{\text{in}} = 13.26 \text{ rotations} \quad (26)$$

$$23 \text{ total rotations} - 13.26 \text{ rotations} \approx 9 \text{ soil-pass rotations} \quad (27)$$

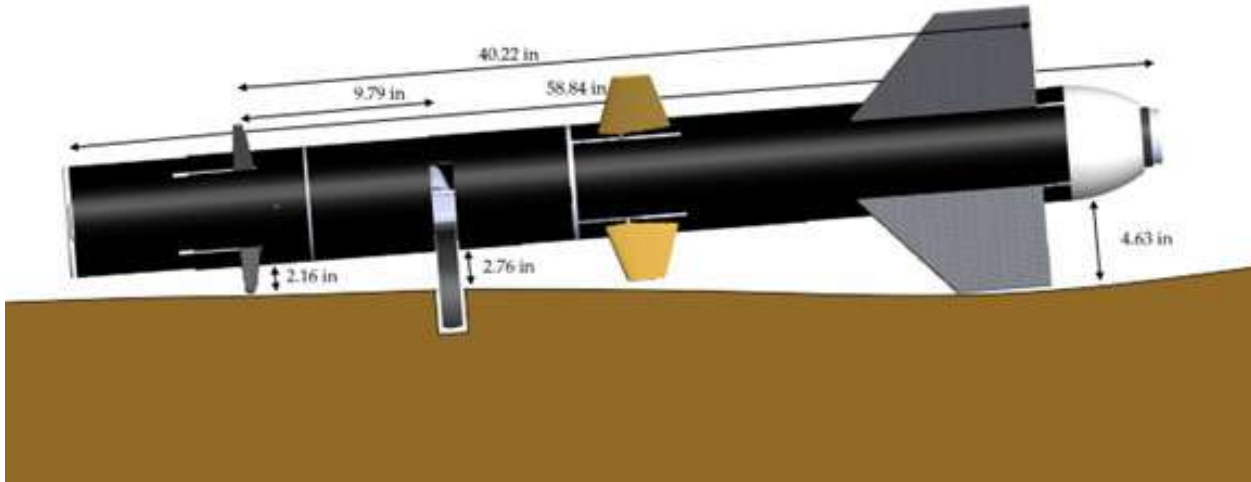


Figure 79: Shovel Extension Calculation Diagram.



Shovel Load Calculation

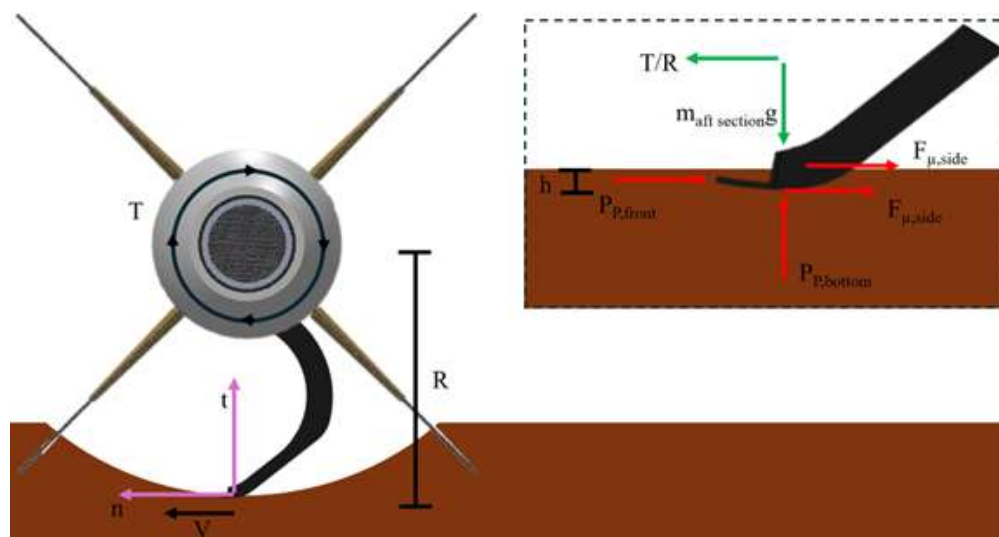


Figure 80: Forces on shovel during digging and extension. Red arrows indicate external forces, green arrows indicate payload reaction forces, and pink arrows represent the normal–tangential coordinate systems.

The following hand calculations referencing the dimensions in Figure 80 and values in Table 58 were made to determine the torque and tail section mass required to drive the shovel deployment and digging. Beginning with the work done from *Calculation of Excavation Force for ISRU on Lunar Surface*, a normal–tangential coordinate frame is employed due to the payload’s axial actuation [7]. The forces that act on the shovel are the passive earth pressure on the front and bottom of the shovel and the kinetic soil friction on the sides and bottom of the shovel.

Passive earth pressure represents the resistance of the soil mass to being displaced, as expressed in Equation 28. For the normal force used in the friction equations, the dynamic earth pressure (additional normal pressure) is calculated using Equation 29. Equations 31 through 35 apply Newton’s Second Law in the normal and tangential directions.

In the tangential direction, since the payload rotates at a constant rate, the tangential acceleration is zero. Thus, in Equation 32, the left-hand side is zero, while the right-hand side consists of the friction forces and passive earth pressure on the front face. In the normal direction, acceleration is a function of velocity and radius; the maximum value is used to calculate the highest load case. In Equation 36, the left-hand side represents the force of the shovel, while the right-hand side corresponds to the weight required to hold the shovel in place and the passive earth pressure. Solving Equation 29 for torque and



Equation 36 for mass yields Equations 33 and 37, respectively.

$$P_P = K_0 \rho g h \quad (28)$$

$$F_N = P_{PE} = \frac{1}{2} \rho g h^2 W K_{PE} \quad (29)$$

$$K_{PE} = \frac{\cos^2(\Phi + \alpha + \phi)}{\cos(\phi) \alpha \cos^2(\delta - \alpha - \phi) \left(1 - \sqrt{\frac{\sin(\delta+\Phi) \sin(\Phi+\phi)}{\cos(\delta-\alpha-\phi) \cos(\alpha)}}\right)^2} \approx 0.625 \quad (30)$$

$$\sum F_t = m_s a_t \quad (31)$$

$$0 = \frac{T}{R} - F_{\mu, \text{side}} - F_{\mu, \text{bottom}} - P_{P, \text{front}} \quad (32)$$

$$T = \rho g h R (\mu h K_{PE} + K_0) \quad (33)$$

Substituting representative values:

$$\begin{aligned} T &= (1600 \text{ kg/m}^3)(9.81 \text{ m/s}^2)(0.005 \text{ m})(0.198 \text{ m}) \\ &\quad \times [0.5(0.005 \text{ m})(0.0254 \text{ m})(0.625) + (0.573)] \\ &= 8.90 \text{ N}\cdot\text{m} \end{aligned} \quad (34)$$

$$\sum F_n = m_s a_n \quad (35)$$

$$m_s v^2 / R = P_{P, \text{bottom}} - m_{\text{aft}} g \quad (36)$$

$$m_{\text{aft}} = \frac{\rho g h K_0 - m_s R \omega^2}{g} \quad (37)$$

Substituting known parameters:

$$\begin{aligned} m_{\text{aft}} &= \frac{(1600)(9.81)(0.005)(0.573) - (0.1)(0.198)(0.628)^2}{9.81} \\ &= 4.58 \text{ kg (10.1 lbm)} \end{aligned} \quad (38)$$

Table 58: Variables used to solve shovel torque and mass requirement calculations.

Name	Variable	Value / Description
Roll axis to shovel tip	R	0.198 m (7.79 in)
Coefficient of friction [3]	μ	0.5
Inclination angle of blade	α	90°
Internal friction angle	Φ	0°
Inclination angle of acceleration	ϕ	0°
Friction angle between soil and dirt	δ	0°
Soil density [11]	ρ	1600 kg/m ³
Acceleration of gravity	g	9.81 m/s ²
Shovel digging depth	h	0.005 m
Passive earth pressure coefficient	K_0	0.573
Dynamic earth pressure coefficient	K_{PE}	0.625
Width of shovel	W	0.0254 m (1 in)
Angular velocity	ω	0.628 rad/s (6 RPM)
Estimated mass of shovel	m_s	0.1 kg

Dividing by the gearbox ratio, the expected input torque required from the central gear on the non-rotating shaft is:

$$T_{\text{non-rotating}} = \frac{8.90 \text{ N}\cdot\text{m}}{47.41} = 0.187 \text{ N}\cdot\text{m}$$

With a 23.8 N·m maximum torque motor, VADL Requirement 3.2.4 is met. To estimate total soil collected, the following relationships were used along with Figure 81.

$$A_{\text{soil}} = R^2 \cos^{-1}\left(\frac{r}{R}\right) - r\sqrt{R^2 - r^2} \quad (39)$$

$$V_{\text{soil}} = A_{\text{soil}} W_{\text{shovel}} \times 1000 \text{ mL/m}^3$$

Substituting representative values:

$$A_{\text{soil}} = (0.2)^2 \cos^{-1}\left(\frac{0.11}{0.2}\right) - 0.11\sqrt{0.2^2 - 0.11^2} = 0.021 \text{ m}^2$$



$$V_{\text{soil}} = 0.021 \text{ m}^2(0.00635 \text{ m})(1000) = 135.97 \text{ mL}$$

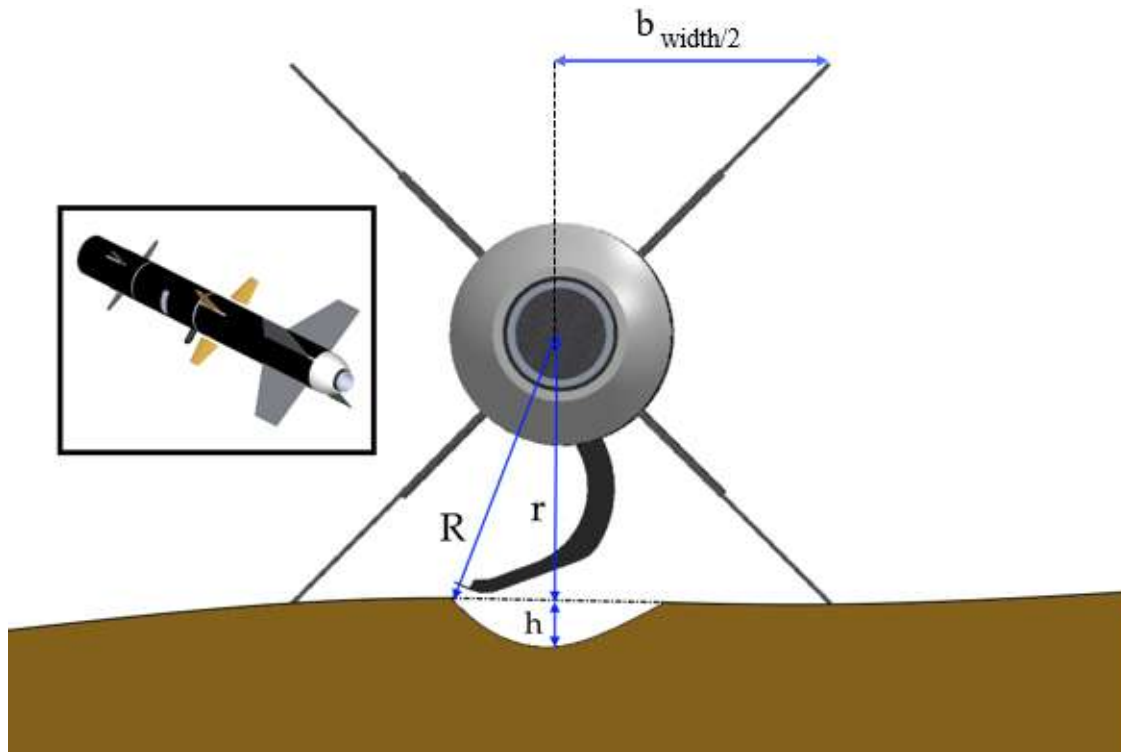


Figure 81: Shovel Excavation Diagram.

4.3.3 Tipping Calculation

To evaluate the potential for tipping of the payload section under load, the tail-section weight was taken as 28.1 lbm (125 N) based on the *Vehicle Massing* data presented in Section 3.3.2. The tipping model considers the moment balance between the soil reaction acting on the shovel and the restoring moment from the weight of the tail section acting through the landing-leg contact points.

The geometry used for this analysis is shown in Figure 81 with values from Table 58 from the *Shovel Load Calculation* subsection (Section 4.3.2). The shovel acts at a radius of

$$R = 0.198 \text{ m},$$

while the supporting fins/legs provide a half-base width of

$$b_{\text{width}/2} = 0.135 \text{ m}.$$

From the *Shovel Load Calculation*, the maximum torque produced during soil collection (T) is 8.9 N·m, which corresponds to a maximum soil reaction force of The maximum



soil reaction force at the shovel edge can be expressed as shown in Equation 40:

$$F_{\max} = \frac{T}{R} = \frac{8.9 \text{ N}\cdot\text{m}}{0.198 \text{ m}} \approx 44.9 \text{ N.} \quad (40)$$

For the payload not to tip, the restoring moment due to the payload's weight must exceed the overturning moment produced by the soil reaction force, as defined by the tipping criterion in Equation 41:

$$F_{\max} h_{cg} < W b_{width/2}, \quad (41)$$

where h_{cg} is the vertical distance from the ground to the payload's center of gravity.

Using $h_{cg} = R = 0.198 \text{ m}$ and $W = 125 \text{ N}$, the overturning moment from the shovel load is calculated in Equation 42:

$$F_{\max} h_{cg} = (44.9 \text{ N})(0.198 \text{ m}) \approx 8.9 \text{ N}\cdot\text{m}, \quad (42)$$

and the restoring moment from the payload weight is given in Equation 43:

$$W b_{width/2} = (125 \text{ N})(0.135 \text{ m}) = 16.9 \text{ N}\cdot\text{m}. \quad (43)$$

Comparing the two moments in Equation 44 confirms that the restoring moment exceeds the overturning moment:

$$8.9 \text{ N}\cdot\text{m} < 16.9 \text{ N}\cdot\text{m}, \quad (44)$$

thus satisfying the tipping criterion established in Equation 41.

Finally, the factor of safety (F.S.) against tipping is calculated in Equation 45:

$$\text{F.S.} = \frac{W b_{width/2}}{F_{\max} h_{cg}} = \frac{16.9}{8.9} \approx 1.90. \quad (45)$$

Thus, even under the maximum estimated digging load, the payload section will not tip. This provides a comfortable margin of stability, which can be further increased by either reducing the shovel pass depth or increasing the fin/leg span in future iterations.

Shovel Opening Mechanism Analysis

The following trade study, featured in Table 59, informed our selection of the gearbox sandwich opening mechanism. While other mechanisms were designed and tested, the gearbox stood out primarily because it was designed with manufacturability in mind and had the greatest chance of resisting deflection under parachute shock loads while remaining retractable.

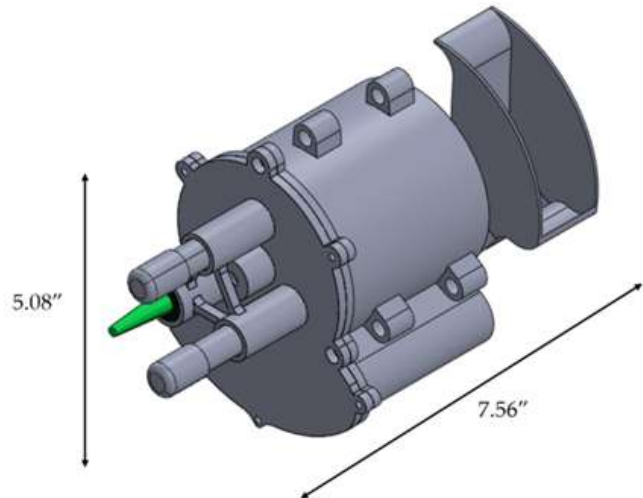
The tradeoff in weight was deemed acceptable given that the gearbox is robust, supports the shovel's torque requirements, and ensures reliable gear meshing throughout the digging process.

**Table 59:** Shovel Opening Mechanism Trade Study

Mechanism	Practicality /Robustness	Manufacturability	Simplicity	Retractability	Weight	Total Weighted Score
	20%	25%	5%	35%	15%	100%
Gearbox Sandwich	9	10	5	10	6	8.15
Threaded Rope	7	9	8	0	9	7.45
Rack and Pinion	7	5	8	10	8	6.95
Miter Gear Design	3	5	9	10	9	6.5
4-Gear Gearbox	7	5	7	10	7	6.6

4.3.4 Soil Housing Chamber

The soil housing chamber is required to contain 50 mL of soil, satisfying the NASA USLI Requirement 4.1. As shown in Figure 82, the chamber geometry follows the shovel profile and aligns with the soil slide so that collected soil naturally enters the chamber. The calculated internal usable volume is ~250 mL, which allows for 150 mL of water to mix with 100 mL of soil (FOS of 2) and minimizes the excess free space that could allow soil to shift during motion. The aft section of the payload is tilted 3.52° due to the landing leg and fin geometry, so that gravity will drive the soil to enter the chamber, and soil backflow will be prevented.

**Figure 82:** Standalone Soil Housing Chamber with Sensors Integrated. Maximum dimensions are shown.

After soil collection, water is injected into the chamber, explained in section 4.3.4, deploying after 6 rotations, while soil collection occurs after 14 rotations (see Equation 7). The payload continues rotating for an additional 17 rotations over a total of 4 minutes, ensuring mixing of soil and water into a slurry. Sensor probes are mounted through ports



in the chamber wall, seen in Figure 83, with $\frac{1}{2}$ inch of clearance beyond the probe tips to maintain unobstructed soil flow.

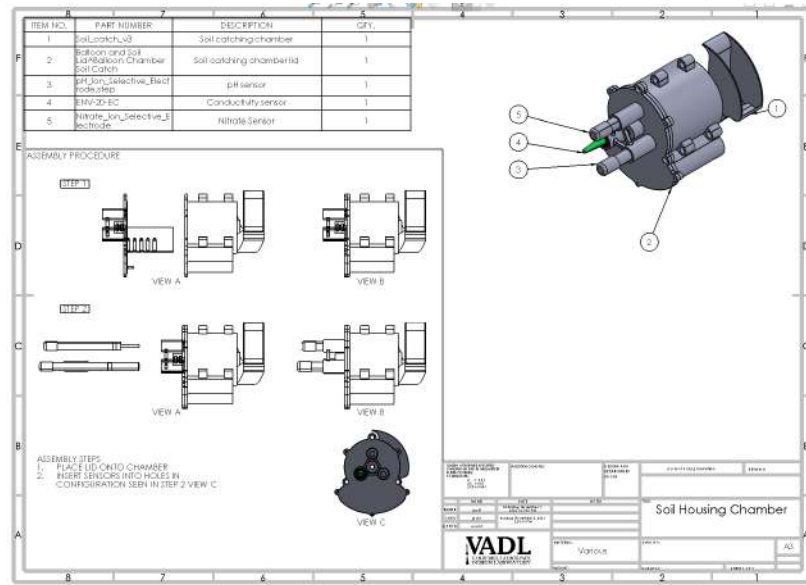


Figure 83: Drawing with exploded view with 1. Soil collection chamber, entry slide, and bladder chamber, 2. Soil chamber lid, 3. pH sensor 4. EC sensor, 5. Nitrate Sensor .

The chamber material must withstand repeated contact with soil, water, and foreign particulates while remaining fully watertight. Due to its complex geometry, the chamber was 3D printed, and multiple materials and print processes available to the team were evaluated (seen in Table 60). Based on the trade study, ABS was selected for its durability, thermal stability, and ability to be vapor-smoothed for leak prevention. Additional waterproofing measures include gaskets and dual O-rings at all penetrations into the chamber, as well as sealed interfaces around the sensors.

Table 60: Soil Chamber Material Trade Study

Material	Sealing Ability	Environment Durability	Toughness & Bibration	Density	Thermal Tolerance	Total Weighted Score
	30%	20%	20%			
ASA	7	8	7	8	8	7.5
ABS	8	7	7	8	8	7.60
PLA	5	5	5	6	3	4.70
Nylon PA12 SLS	6	5	9	9	7	6.90
Onyx	6	6	9	8	7	7.00

4.3.5 Water Injection System

The selected water integration concept is the tether-released bladder system shown in Figure 84. A flexible bladder is stored in a separate compartment and secured closed



with a total of three (two redundant, one main) highwayman hitch knots tied to a tether attached to the non-rotating shaft. As the payload rotates, the tether unwinds after six rotations and releases the knot, opening the bladder and discharging 150 mL of water into the soil chamber over 17 rotations, which saturates the soil to a soil-to-water ratio of 1:1. The tether includes slack corresponding to six shaft rotations to delay the water release.

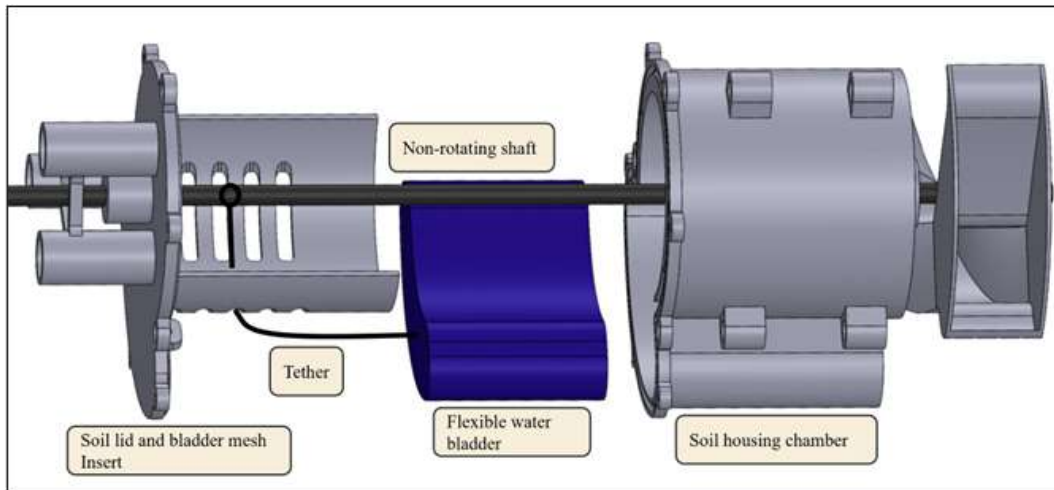


Figure 84: Exploded view of the tether-released bladder water integration system

Since the bladder is contained in a separate chamber, the water passes into the soil chamber through a nylon mesh layer, adhered to the soil lid, so that the bladder does not obstruct the soil or the sensors. As a worst-case under compression, the bladder could compress up to a maximum of 2 in within the chamber while maintaining a factor of safety (FOS) of 2.35, as shown in Equations 46 and 47, without the tether releasing the knot.

$$L_s = N_{\text{trd}}\pi d = 6\pi(0.25 \text{ in}) = 4.71 \text{ in} \quad (46)$$

$$FOS = \frac{L_s}{\Delta L_{\max}} = \frac{4.71 \text{ in}}{2.00 \text{ in}} = 2.35 \quad (47)$$

Laboratory testing was conducted on the tethered latex bladder to verify that mechanical failure would not occur at the knot. Testing consisted of two configurations: (1) drop testing, and (2) static compression within a rigid containment chamber. Drop testing involved releasing the filled bladder from heights of 10 ft, 15 ft, 20 ft, and 25 ft, at which point the bladder wall ruptured. At failure, the landing velocity of the bladder was 40.1 ft/s in Equation 48, yielding a 3.2 FOS relative to the expected landing velocity of 12.6 ft/s, as shown in Equation 49.

$$v = \sqrt{2gh} = \sqrt{2(32.174 \frac{\text{ft}}{\text{s}^2})(25 \text{ ft})} = 40.1 \frac{\text{ft}}{\text{s}} \quad (48)$$

$$N = \frac{v}{v_{\text{fall}}} = \frac{40.1 \frac{\text{ft}}{\text{s}}}{12.6 \frac{\text{ft}}{\text{s}}} = 3.18 \approx 3.2 \quad (49)$$



Assuming a 26 g peak deceleration on impact, the transient pressure rise (P) was evaluated hydrostatically in Equation 50:

$$P = \rho ah \quad (50)$$

where ρ is the density of water (1000 kg/m^3), a is the maximum shock acceleration ($26g = 26 \times 9.81 \text{ m/s}^2$), and h is the height of the water column, 3 in = 0.0762 m .

The bladder wall thickness was measured as $t = 0.35 \text{ mm}$. When modeled as a thin-walled cylinder with internal pressure $P = 1.94 \times 10^4 \text{ Pa}$ and radius $r = 0.03296 \text{ m}$, the hoop stress can be solved for with Equation 51:

$$\sigma_{\text{cyl}} = \frac{Pr}{t} = \frac{(1.94 \times 10^4 \text{ Pa})(0.03296 \text{ m})}{3.5 \times 10^{-4} \text{ m}} = 1.83 \times 10^6 \text{ Pa} = 1.83 \text{ MPa} \quad (51)$$

Given that the nominal tensile strength of natural latex is $\sigma_{\text{ult}} = 22.5 \text{ MPa}$ [10], the resulting factor of safety can be calculated in Equation 52:

$$N = \frac{\sigma_{\text{ult}}}{\sigma_{\text{cyl}}} = \frac{22.5 \text{ MPa}}{1.83 \text{ MPa}} = 12.3 \quad (52)$$

These results indicate that the bladder wall maintains a sufficient safety margin under impact and compression conditions representative of descent and landing.

4.3.6 STEMNaut Selection and Housing

The STEMNaut housing and scale selection are important for accurately showing the design and functionality of the USLI payload. To represent human and system interactions that relate to a crewed extra-terrestrial mission, consideration was given to human proportions of the shrunken astronaut figurines (“STEMNauts”). Since the HAUS is meant to model a compact two-crew deep-space habitat, the volume of the HAUS (40 in^3) corresponds to a linearly shrunken housing unit by a factor of 1:40–1:50 relative to an human-sized habitat. The STEMNauts human figures, scaled to approximately 0.5 inches in height, which shows a realistic scaling of human dimensions inside this proportional volume model. The CAD of the STEMNaut housing bay can be viewed in Figures 85 and 86.

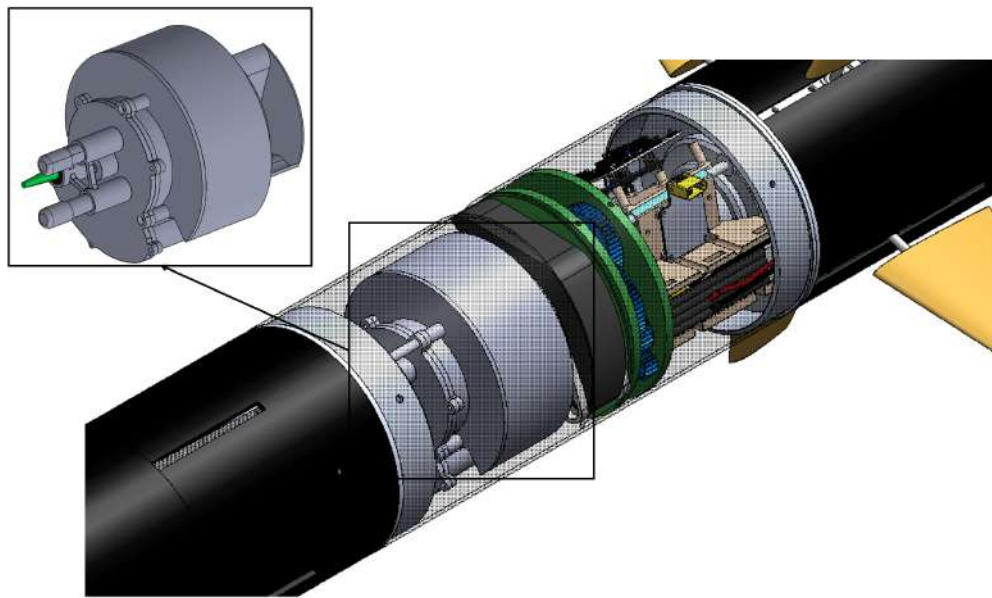


Figure 85: STEMNaut housing integrated into the payload bay. STEMNauts chambers will exist in this centrifugal habitat, with discrete separation from the payload atmosphere, and soil housing chamber. It is 2.38 inches long axially, with an internal volume of approximately 40 cubic inches.

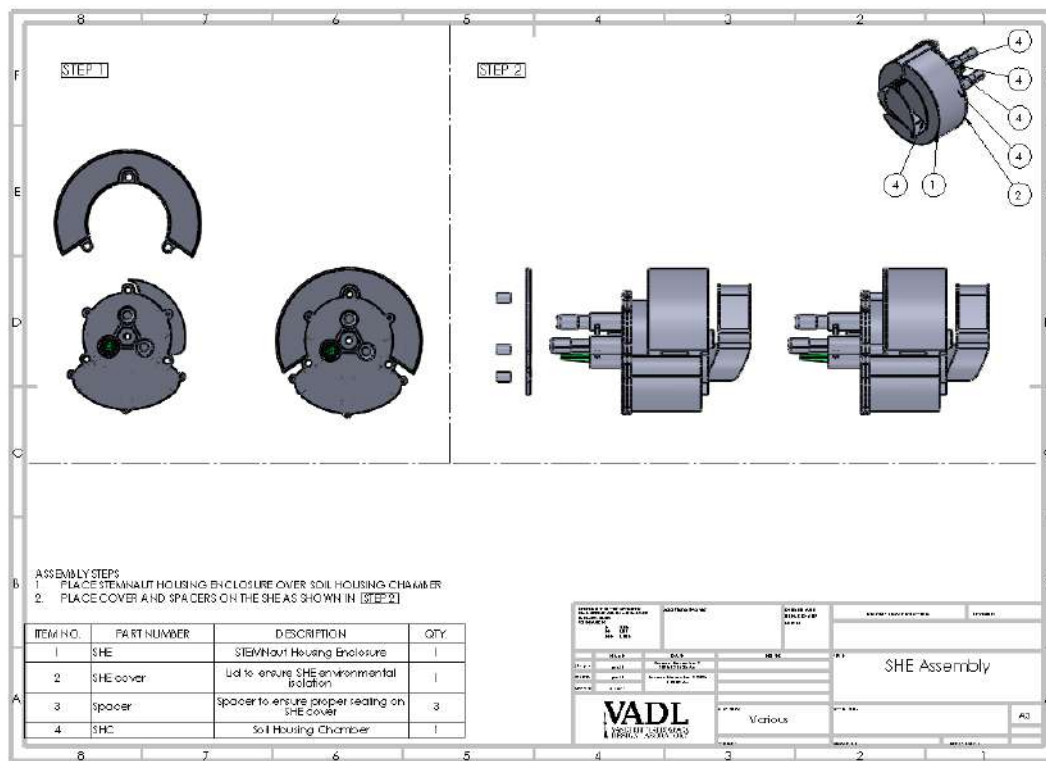


Figure 86: STEMNaut housing assembly engineering drawing. This gives greater context of the components in the assembly, and their context within the HAUS.



4.3.7 Electrical Systems Overview

The Payload Electrical System (PES) will have three primary functions: flight state detection, motor actuation, and soil sensing, as described in VADL Requirements 3.5.1, 3.5.13, and 3.5.14. These systems will work in tandem to properly sample and record soil data through a central microcontroller, the Teensy 4.1.

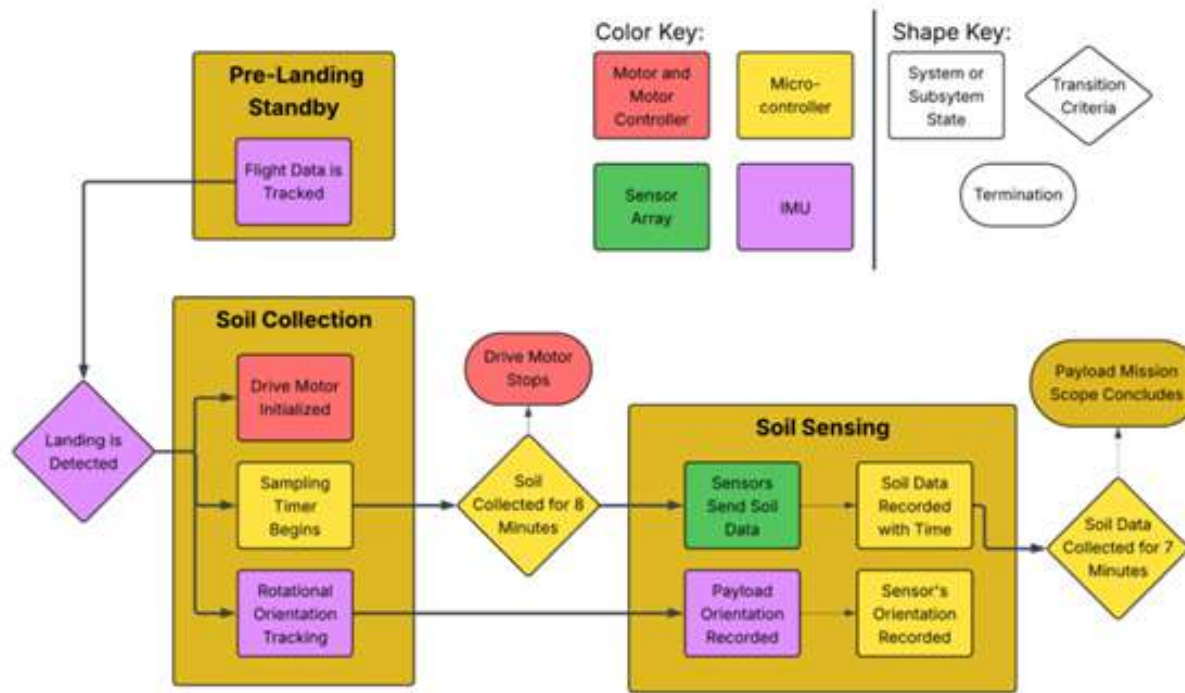


Figure 87: Flowchart of payload states and primary component operations

Figure 87 shows the actions of our payload electrical system. Our software will act as a state machine that switches component operations when the criteria displayed are met.



4.3.8 Electrical Schematic

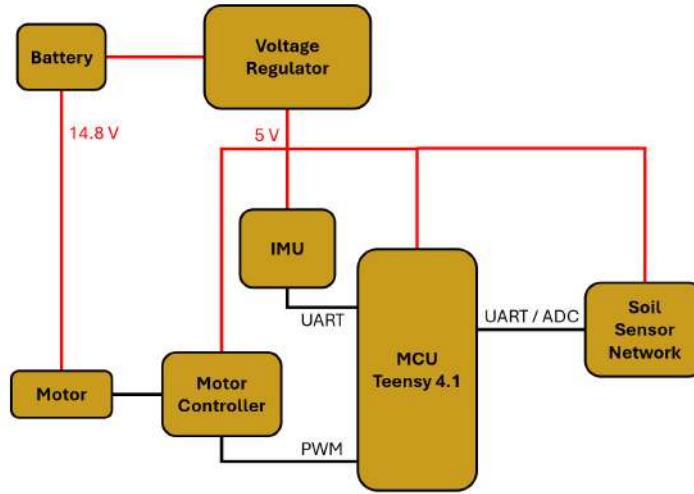


Figure 88: High level electrical schematic with power connections indicated in RED and communication connections indicated in BLACK

Figure 88 represents the schematic of payload electronics. The Teensy 4.1 microcontroller acts as the main processing unit, and it interfaces the IMU with UART, motor controller with PWM, and the soil sensor network with UART and ADC. The 14.8 V battery is converted to 5 V by the voltage regulator to power all components except for the motor, which will be powered directly by the battery.

4.3.9 Chosen Electrical Components

The final payload electronics were selected based on the trade studies presented in Sections 4.2.8–4.2.15. The system includes the following components:

- Teensy 4.1 Microcontroller
- VectorNav VN-100 Inertial Measurement Unit (IMU)
- HW-039 Motor Driver
- 42GP-775 Permanent Magnet DC Planetary Reduction Motor
- Pololu 5V, 5.5A Step-Down Voltage Regulator (D36V50F5)
- NTsensor pH Ion-Selective Electrode Sensor
- NTsensor Nitrate Ion-Selective Electrode Sensor
- NTsensor Reference Electrode
- Atlas Scientific Mini Conductivity Probe (K 1.0)
- Atlas Scientific EZO™ Conductivity Circuit Interface

4.3.10 Payload Battery Sizing and Life Calculations

To determine the power capacity of the payload battery and satisfy VADL Requirement 3.5.15, the following calculations were performed based on component datasheets.



The payload will be powered by a 14.8 V LiPo battery sufficient to properly power our motor.

- **Teensy 4.1 Microcontroller:** Current draw = 100 mA (600 MHz @ Nominal 5 V input)

$$BEC \rightarrow 90\% \text{ efficiency}, P_{\text{mcu}} = 5 \text{ V} \times 0.1 \text{ A} = 0.5 \text{ W}$$

$$P_{\text{bat}} = \frac{0.5 \text{ W}}{0.9} = 0.556 \text{ W}$$

$$I_{\text{bat}} = \frac{0.556 \text{ W}}{14.8 \text{ V}} = 37.6 \text{ mA}$$

- **VectorNav VN-100 IMU:** Current draw = 40 mA (@ Nominal 5 V input)

$$BEC \rightarrow 90\% \text{ efficiency}, P_{\text{imu}} = 5 \text{ V} \times 0.04 \text{ A} = 0.2 \text{ W}$$

$$P_{\text{bat}} = \frac{0.2 \text{ W}}{0.9} = 0.222 \text{ W}$$

$$I_{\text{bat}} = \frac{0.222 \text{ W}}{14.8 \text{ V}} = 15 \text{ mA}$$

- **Motor:** 1.33 A (16 W at 6 rpm with load)

$$BEC \rightarrow 90\% \text{ efficiency}, P_e = 12 \text{ V} \times 1.33 \text{ A} = 15.96 \text{ W}$$

$$P_{\text{bat}} = \frac{15.96 \text{ W}}{0.9} = 17.73 \text{ W}$$

$$I_{\text{bat}} = \frac{17.73 \text{ W}}{14.8 \text{ V}} = 1.198 \text{ A}$$

- **Sensor (EC probe @ 5 V nominal):** Current draw = 50 mA

$$BEC \rightarrow 90\% \text{ efficiency}, P_e = 5 \text{ V} \times 0.05 \text{ A} = 0.25 \text{ W}$$

$$P_{\text{bat}} = \frac{0.25 \text{ W}}{0.9} = 0.278 \text{ W}$$

$$I_{\text{bat}} = \frac{0.278 \text{ W}}{14.8 \text{ V}} = 18.8 \text{ mA}$$

Pre-Launch/Launch Current Draw:

$$I_{\text{pre}} = 37.6 \text{ mA} + 15 \text{ mA} = 52.6 \text{ mA}$$

Post-Landing Current Draw:

$$I_{\text{post}} = 37.6 \text{ mA} + 15 \text{ mA} + 18.8 \text{ mA} + 1.198 \text{ A} = 1.2694 \text{ A}$$

Battery Specification:

Battery = 14.8 V, 2200 mAh LiPo

Energy Consumption:

$$\begin{aligned}\text{Pre-Launch/Launch (5 hours): } & 52.6 \text{ mA} \times 5 \text{ h} = 0.253 \text{ Ah} \\ \text{Post-Landing (0.333 hours): } & 1.2694 \text{ A} \times 0.333 \text{ h} = 0.423 \text{ Ah} \\ \text{Total Consumption: } & 0.253 \text{ Ah} + 0.423 \text{ Ah} = 0.676 \text{ Ah}\end{aligned}$$

Battery Utilization:

$$\text{Consumption} = \frac{0.676 \text{ Ah}}{2.2 \text{ Ah}} \times 100 = 30.7\% \text{ of total capacity}$$

Based on these calculations, the mission will consume 676 mAh of power from the 14.8 V LiPo battery. This makes the 2200 mAh battery a safe choice to satisfy our payload requirements, and it is a standard component that is easy to source.

4.3.11 Chosen Soil Sensors and Integration

NTSensor pH and Nitrate Ion Selective Electrodes and the Atlas Scientific Electrical Conductivity Probe will be the sensor array, satisfying VADL Requirements 3.5.17-19. This sensor combination was selected for its smaller size and greater accuracy. These sensors will be interfaced with a microcontroller for data acquisition and logging. The electrical conductivity probe has a UART interface to talk directly with the microcontroller [1], and the ion selective electrodes will have an amplifier circuit connected to an analog-to-digital converter. The microcontroller will handle data logging and store the data on an SD card, timestamped to the time when the sample took place, satisfying VADL Requirement 3.5.14.

4.3.12 Electrical Mounting

Electrical systems are mounted in the payload surrounding the actuator that spins the payload. The proximity of all components to each other reduces the possibility of wire disconnections and breakages under the high-g environment of rocket launch and parachute deployment as covered by VADL Requirement 3.5.21. The mounting is primarily 3D-printed and modular, using heat-set inserts, enabling quick swaps. The LiPo Battery is well protected and encased in 3D-printed plastic, with zip ties to hold it in place. All PCB-based components are mounted using M3 through-holes and heat-set inserts for consistent reliability, regardless of how many times the system is taken apart.

4.3.13 PCB Manufacturing

The PCB will integrate a Teensy 4.1 breakout board along with other embedded components and will include connectors to ensure reliable off-board interfacing. The PCB layout will be done in Altium Designer, and the boards will be manufactured by JLCPCB, which produces high-quality boards and offers an integrated pick-and-place assembly service at a low cost.



4.3.14 Payload Mass Breakdown

This section contains a mass distribution of the payload and its subsystems, shown in Table 61. The total weight of the payload section has been measured to be 9.2 lbm.¹

Table 61: *Payload Mass Breakdown*

Component	Material	Percent of Payload	Est. Mass (lbm)
Shovel and Mounting Arms	Onyx	1.5%	0.14
Gearbox Assembly	Onyx	3.0%	0.27
Electronics & Sensors	PCB, Wiring, PLA	43.0%	3.96
Water Bladder & Chamber	Latex + PLA + Water	5.2%	0.48
Bulkplates & Supports	Aluminum	21.5%	1.98
Airframe	Fiberglass	25.8%	2.38
Total		100%	9.2

4.3.15 Payload Verification Plan

This section outlines the procedure for verifying that all payload systems function correctly and integrate properly, as shown in Table 62. Validation will involve a series of controlled physical tests to confirm the operation of the following:

- **Water Integration System** — bladder releases water concurrently with payload rotation.
- **Shovel Opening Mechanism** — opens over 23 payload-bay rotations (VADL Requirement 3.2.3) to 4.97 in from tip to airframe and resists digging torque.
- **Sensor Functionality** — pH, nitrate, and conductivity data are captured and transmitted.
- **Mechanical Support** — legs and fins stabilize the system during digging.

¹Table mass totals (9.2 lbm) reflect current CAD + estimates and will be reconciled after hardware weigh-in.

**Table 62:** Payload Verification Plan

Component / System	Test Objective	Verification Method	Success Criteria	Responsible
Shovel Mechanism	Confirm actuation and retraction	Run the motor for 23 payload-bay rotations, then reverse direction	Opens fully and retracts without binding	Evan T.
Water Integration System	Verify water release with payload rotation and chamber watertightness	Rotate payload; visually inspect soil chamber for water and electronics for dryness	Water released; chamber watertight; electronics dry	Catherine
Soil Sensors	Validate measurement accuracy and logging	Bench test, then integrated test with wetted soil sample	Readings logged to computer; values within expected range	Ashley
Bulkplates & Legs	Ensure structural support during landing and digging	Drop / impact test of payload module; rotate RBS after test	No visible deformation; RBS rotates freely; no interference	Jack L.

4.3.16 Mock Tail Section Design and Manufacturing

Creating a 1:1 replica of our rocket aft landed section allows for the payload verification methods described in Table 62. It also serves the dual purpose of allowing the team building the launch vehicle to practice fabrication techniques that will transfer well to both the subscale and full-scale vehicles. The following test platform, shown in Figures 89 and 91, was constructed using fiberglass instead of carbon fiber to reduce cost, and BlueTube instead of fiberglass to reduce weight and accommodate the max load capacity of the Aurelia X6 drone that will be used for drop-testing the payload. As shown in Figure 90, the manufacturing process included (1) reinforcing the BlueTube bolt-hole surfaces with fiberglass sheet layups, (2) cutting fin slots, and (3) assembling the fins using half-lap joints with fiberglass fillets. The assembly replicates the double-reinforced rigid motor retention system of the full-scale launch vehicle, increasing the fins' flexural strength. Threaded rods bonded with epoxy centering rings form the primary load path, carrying tension during parachute deployment and compression upon landing.

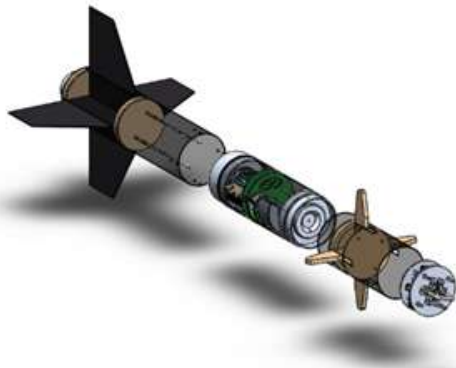


Figure 89: Drop-Test Assembly of the Rocket Aft Section — Simplified, Lightweight Version Used for Preliminary Landing Tests.

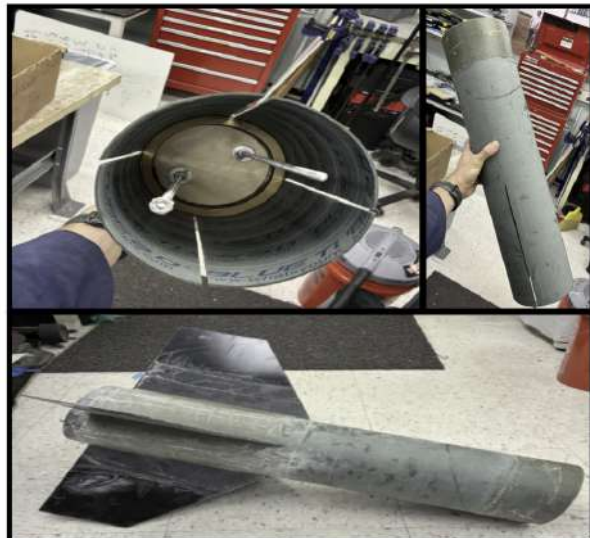


Figure 90: Manufacturing Process of the Payload Test Platform — Sequential Snapshots Showing Fabrication and Assembly Steps.



Figure 91: Fully Assembled Tail Section — Final Integrated Configuration of the Rocket's Aft Module.



Figure 92: Subassembly Drop Test of the Payload Platform.



Figure 93: Fully Assembled Payload



Sub-section drop tests were conducted both with and without the payload components and Leg Deployment Bay, as shown in Figure 92, matching the expected landing kinetic energies of each section to ensure structural stability during impact. The maximum drop height was approximately 3.5 ft, corresponding to a 20 lb assembly mass. This configuration replicates the expected full-scale landing kinetic energy of 69 ft-lbs.

$$mgh = 69 \text{ [ft-lbs]}$$

$$20 \text{ lbs} \cdot h = 69$$

$$h = 3.5 \text{ ft}$$

4.3.17 Tip-Over Test

The Tip-Over Test simulates post-landing deployment in a static scenario without parachute shock forces. The rocket will be held upright and tipped over, allowing the payload to begin its opening, digging, and soil testing sequence once the airframe hits the ground.

This test replicates all functional payload behaviors of the Drop Test except for impact energy validation, which will be tested separately. The goal is to confirm soil penetration capability, shovel motion, and system stability under controlled conditions. A preliminary Tip-Over Test was conducted in which a failure in the Rotating Bulkplate System (RBS) was observed. The complete test will be repeated and analyzed before CDR. The expected results from the next Tip-Over Test are shown in Table 63.

Table 63: Tip-Over Test — Expected Results

Test Parameter	Description	Expected Outcome
Orientation	Rocket tipped from 90° to 0° during static deployment simulation.	Stable ground contact achieved without structural displacement.
Soil Collection	Observe shovel rotation and deposition into the soil chamber during actuation sequence.	50–136 mL of soil successfully collected and retained within the chamber.
Structural Behavior	Visual inspection of airframe and payload during shovel deployment and extension.	No visible deflection, cracking, or delamination of any structural components.

4.3.18 Drop Test

The Drop Test validates payload functionality under realistic landing conditions, assessing whether all mechanisms withstand impact (substantially lessened by parachute deployment) and perform sequentially post-landing. The test will involve dropping the



full vehicle — excluding the nosecone, main, avionics, and drogue bays — from a controlled height representative of a maximum landing impact energy of 75 ft-lbs per NASA USLI Requirement 3.2. The drop height is expected to be 300–400 ft, using a drone to carry and release the vehicle. Once the IMU determines that the rocket has landed, the payload will autonomously initiate soil collection, water integration, and data logging. The expected results are shown in Table 64.

Objectives:

- Validate shovel actuation under impact-induced stress.
- Confirm payload structural survivability.
- Verify sensor calibration post-impact.
- Assess recovery and data-transmission reliability.

Table 64: Drop Test — Expected Results

Subsystem	Test Goal	Verification Method
Shovel	Structure does not fail under impact and shovel still performs soil collection sequence.	Post-test visual inspection for deformation; confirm soil is collected and retained.
Gearbox	Maintains integrity and properly actuates upon landing with all gears still meshing.	Visual inspection of gearbox housing; rotate payload bay to confirm smooth actuation.
Water Integration System	Releases water into the soil collection chamber without leaking into electronics or wiring bays.	Open chamber and visually confirm water present in chamber; inspect electronics compartment for moisture.
Sensors	Transfer soil-testing data (pH, nitrate, conductivity) to VADL computers after impact.	Download logged data; compare values to control sample / bench test to confirm reasonable accuracy.
Structure	Bulkplates and supports remain intact with no shearing, tensile, or torsional failure.	Detailed structural inspection of bulkplates, fasteners, and RBS interface for cracking, yielding, or delamination.

4.4 Apogee Control System (ACS)



4.4.1 ACS Objective

As per NASA USLI Requirement 4.MISC, teams are allowed to fly an additional experimental payload. The secondary payload VADL is launching the Apogee Control System (ACS) to adjust the trajectory to achieve the target apogee. Implementing a system to control the drag of the rocket midflight is optimal for performing well in the target apogee category. Note that when the drag coefficient (C_D) is mentioned, it is in reference to the frontal area or just the rocket unless stated otherwise. A CAD of the ACS and its exploded view can be viewed in Figure 94.

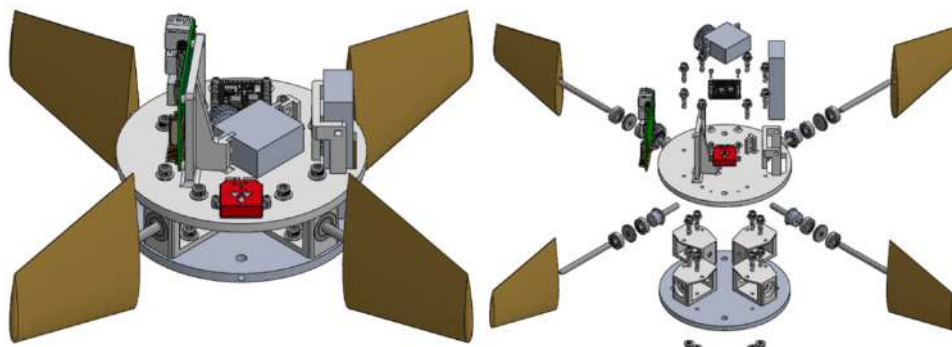


Figure 94: Collapsed (left) and exploded (right) view of preliminary ACS CAD.

4.4.2 Success Criteria

Success criteria for the ACS can be viewed in Table 65.

Table 65: Flight Control System Verification Criteria

Criterion #	Description	Relevant Requirements
1	Detect stages of flight using redundant acceleration and altitude data. ACS deployment occurs after MECO and 3,500 ft AGL.	VADL 2.4.3
2	Increase the drag coefficient (C_D) to at least 2 in reference to the cross-sectional area of the rocket.	VADL 3.6.1
3	Achieves target apogee within 5% error.	VADL 3.6.2
4	Maintains a static stability margin greater than 2 when fins are deployed.	VADL 2.4.1
5	ACS has minimum effect on ascent prior to deployment.	VADL 2.4.1 VADL 2.4.2 VADL 2.4.6

4.4.3 ACS Alternative Designs Overview

Fundamentally, the ACS needs to have a minimal impact on the rocket's performance during motor burnout and then needs to increase the drag of the rocket to achieve the target apogee. The system shall only induce drag as per VADL Requirement 2.2.4. Table 66 is a trade study of the general ACS design based on common industry and amateur rocket solutions.

Table 66: Apogee Control System (ACS) General Design Trade Study

Design	Performance	Manufactur-	Mass	Structural Rigidity	Design Flexibility	Total Weighted Score
	10%	30%	20%	30%	10%	100%
Drag Plate	9	8	7	5	2	6.2
Clamshell	5	4	3	2	2	2.9
Fins	7	7	7	9	8	6.9

From the trade study, the fins were chosen due to their high structural rigidity and consistency. This gives additional design flexibility in how the drag is induced via the fin type and actuation.

4.4.4 Fin Design

The constraining requirement that guides the size of the ACS fins is VADL Requirement 2.2.3, to have a deploy floor of 3500 ft. This is because the fins must be large enough to induce enough drag to reach the target apogee. At 3500 ft altitude, the vehicle's velocity is fairly low, and drag is proportional to the square of velocity. Thus, the higher up in altitude the fins are deployed, the larger they need to be to reach the same goal apogee.

Preliminary CD calculations were run using flight data from a prior full-scale vehicle launch. These simulations were run to determine what CD is necessary to reach a target apogee of 4200 ft with an ACS deployment at or above 3500 ft. A predictive apogee model – further discussed in Section 4.4.8 – was utilized in this simulation to predict a theoretical apogee with an increased CD at every timestep during the flight. The predicted apogee vs. time can be viewed in Figure 95.

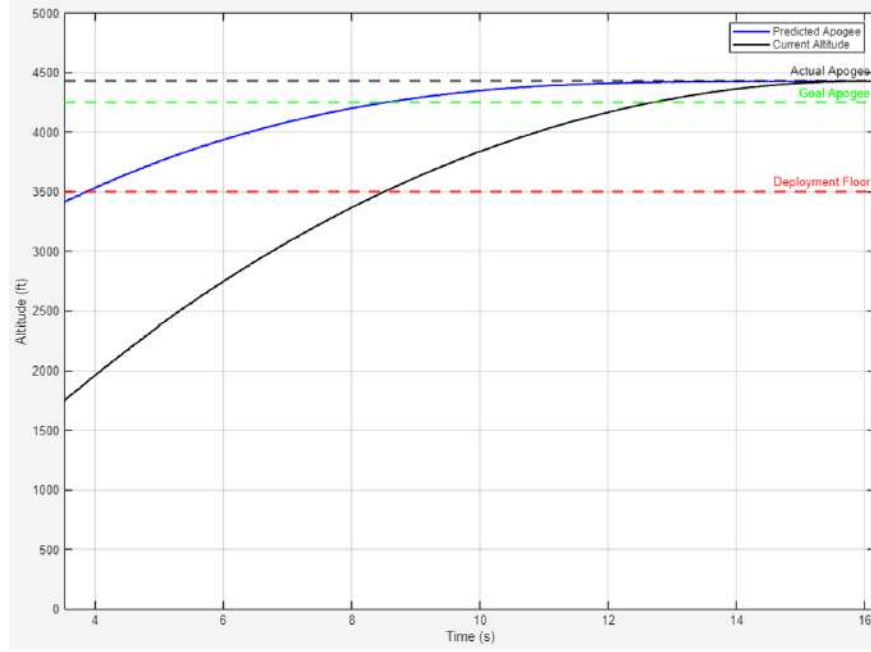


Figure 95: Predicted apogee vs. time for prior full-scale flight data. The ACS has a deployed CD of 2.

The vehicle that provided the flight data in this simulation was 6.17 in diameter and a dry mass of 41 lbm. As can be seen above, a deployed ACS CD of 2 achieves an apogee of 4200 ft at a deployment altitude of 3500 ft. To determine what fins would achieve a CD of about 2, the fins are assumed to act as flat plates with a CD of 1.28, and the baseline rocket is assumed to have a CD of 0.4 and diameter of 6.17 in. The derivation for fin area can be seen in Equations 53 and 54:

$$\frac{1}{2}\rho v^2 (C_{D_o} A_r) = \frac{1}{2}\rho v^2 (C_{D_F} A_F) + \frac{1}{2}\rho v^2 (C_{D_r} A_r) \quad (53)$$

$$C_{D_o} A_r = C_{D_F} A_F + C_{D_r} A_r \quad (54)$$

Where CD_o is the overall CD, CD_F is the fin CD, CD_r is the baseline rocket CD, AF is the fin area, and Ar is the rocket cross-sectional area. The equation can be solved as shown in Equation 55:

$$A_F = A_r \frac{C_{D_o} - C_{D_r}}{C_{D_F}} = \frac{\pi(6.17 \text{ in})^2}{4} \cdot \frac{2 - 0.42}{1.28} = 37 \text{ in}^2 \quad (55)$$

To maintain symmetry with the tail section, 4 fins are used. Thus, each fin needs to have an area of at least 9.2 in² of frontal area. With the area needed established, the geometry of the fin is investigated in Table 67.



Table 67: Fin Design Trade Study

Design	Aerodynamics	Manufacturability	Mass	Structural Rigidity	Total Weighted Score
	20%	50%	10%	20%	100%
Airfoils	8	7	7	8	7.4
Grid Fins	6	2	5	5	3.7
Flat Plates	5	8	7	7	7.1

Airfoils are the optimal design for ACS, as they provide minimal drag during the initial ascent (VADL Requirement 2.2.2). The team decided to size up area the fins to 12 in² to provide for greater flexibility in apogee control. The CD of the deployed fins at 90 deg was determined to be on average 2.14 from CFD simulations using the k- ω model as outlined in Section 4.4.8. This was achieved by designing fins as a trapezoid with a height and base of 4 in, and top of 2 in. This decreases the bending moment on the ¼" rod that supports the fin, as calculated below using the force on a single fin at full deployment (Equations 56, 57, and 58):

$$F_D = \frac{1}{2} \rho v_{\max}^2 C_D A \quad (56)$$

$$F_D = \frac{1}{2} \left(2.38 \times 10^{-3} \frac{\text{slugs}}{\text{ft}^3} \cdot \frac{(\text{lbf} \cdot \text{s})^2}{\text{slugs} \cdot \text{ft}} \right) (549 \text{ ft/s})^2 \left(1.28 \cdot 12 \text{ in}^2 \cdot \frac{1 \text{ ft}^2}{144 \text{ in}^2} \right) = 38.26 \text{ lbf} \quad (57)$$

$$\sigma = \frac{My}{I} = \frac{\left(\frac{38.26 \text{ lbf}}{2} \cdot \frac{4 \text{ in}}{3} + \frac{38.26 \text{ lbf}}{2} \cdot \frac{4 \text{ in}}{2} \right) \cdot \frac{0.25 \text{ in}}{2}}{\frac{\pi(0.25 \text{ in})^4}{32}} = 20785 \text{ psi} \rightarrow 20.8 \text{ ksi} \quad (58)$$

Given the expected max stress on the rod supporting the fin is 20.8 ksi and VADL Requirement 2.1.1, the rod is made of M2 Tool steel ($\sigma_{yield} = 133.4$ ksi) giving a FOS of 6.4. With the side dimensions of the airfoil and the rod dimensions decided, these values are then applied to find an appropriate NACA airfoil for this application. From VADL Requirement 3.6.2, a symmetric airfoil is needed to simplify the aerodynamics effects on the rocket. The thickness-to-chord ratio is determined using the length of the base airfoil (4 in) and the combined diameter of the rod with additional support (0.25 in + 0.2 in = 0.45 in), as shown in Equation 59:

$$\frac{T}{C} = \frac{0.45 \text{ in}}{4 \text{ in}} = 0.125 \quad (59)$$

From these values, the NACA 0012 and 16-012 are found to be the options that fit the design requirements the best as seen in Table 68.

**Table 68:** NACA Fin Design Trade Study

Design	CD	Thickness at CP	Aerodynamics Center	Total Weighted Score
				30%
NACA 0012	6	9	7	7.5
NACA 16-012	8	5	7	6.5

The center of aerodynamic pressure for thin symmetric airfoils lies 25% down the chord. Due to the trapezoidal shape of the airfoil, the aerodynamic center moves towards the geometric center as the height of the fin increases. By integrating across the entire fin, it was found that the overall aerodynamic center of the fin is 0.74 in from the geometric center give a trapezoid fin of 4 in wide and 4 in tall with a chord length of 2 in. The center of pressure along each axis was found in MATLAB using the equations shown in Equations 60 and 61:

$$x_{cp} = \frac{\int_A x dA}{\int_A dA} \quad (60)$$

$$y_{cp} = \frac{\int_A y dA}{\int_A dA} \quad (61)$$

Ideally, the fin is mounted on the center of pressure as this allows for if the gearbox fails the fins will simply align with the airstream (VADL Requirement 2.2.6). Thus, the NACA 0012 is determined to be the best airfoil for the ACS.

4.4.5 Fin Deployment Mechanism

To satisfy VADL Requirement 2.2.4, the deployment from inline with the streamline to maximum drag (90 degree deployment) shall not induce a roll or lift on the rocket. Figure 96 indicates various fin transition positions and the induced effect on the rocket.

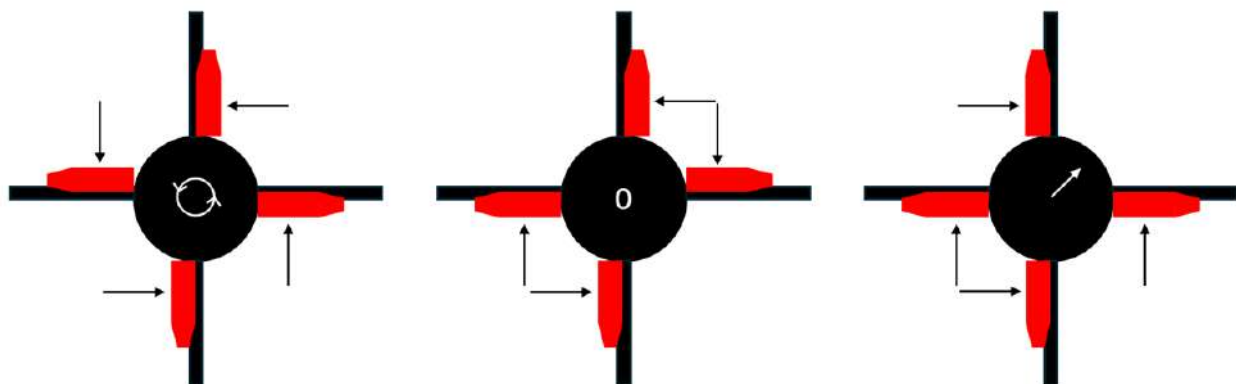


Figure 96: Shows the 3 different fin transition orientations (red) and their induced effect. (Left) roll. (Middle) drag. (Right) lift.

For the ACS, it will move the fins as the middle configuration does as to only induce drag on the rocket. This means the fins need to be driven in the opposite direction as the adjacent fins. Additionally, to increase the reliability of the system, it shall be driven by a single actuator. To get this motion a miter and spur gear train seen in Figure 97 is used with the spur gear where the input from the servo and the miter gears are the output to the fins.

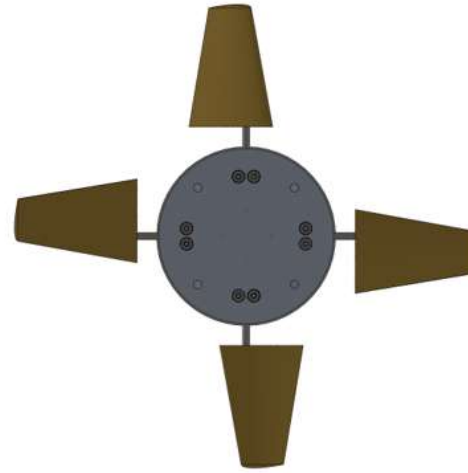
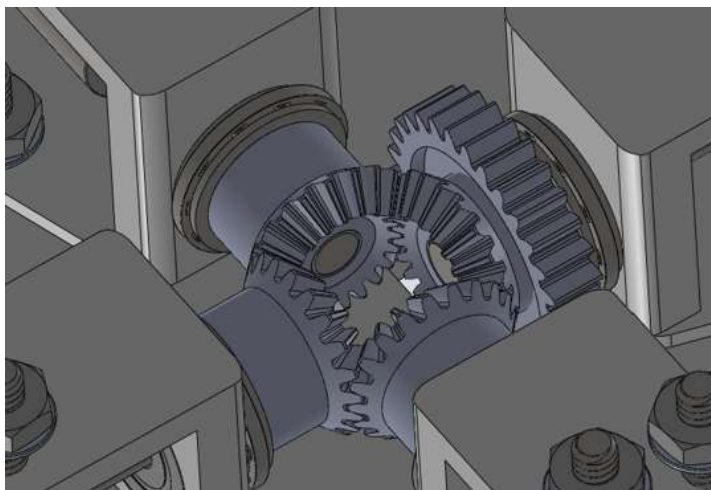


Figure 97: (left) Miter and spur gear train for the ACS and (right) fin deployment demo.

The fin connects to the first rod via a key and epoxy. This then transfers to the gear that is only attached via epoxy. With the fins off 50% of the cord length, a torque is applied from the air pressure. The maximum torque exerted by each fin occurs post deflection to



90 deg. The equations for calculating the torque are shown in Equations 62–64:

$$F = \frac{1}{2} \rho V^2 (C_D A) \quad (62)$$

$$F = \frac{1}{2} \left(2.38 \times 10^{-3} \frac{\text{slugs}}{\text{ft}^3} \cdot \frac{(\text{lbf} \cdot \text{s})^2}{\text{slugs} \cdot \text{ft}} \right) (245 \text{ ft/s})^2 \left(1.28 \times 12 \text{ in}^2 \cdot \frac{1 \text{ ft}^2}{144 \text{ in}^2} \right) = 7.62 \text{ lbf} \quad (63)$$

$$T = F \times r = 7.62 \text{ lbf} \times 0.74 \text{ in} \times \frac{1 \text{ ft}}{12 \text{ in}} = 0.47 \text{ lbf} \cdot \text{ft} \quad (64)$$

To transfer the torque from the fins to the gear, it is transmitted through the 2-ton epoxy layer. The maximum shear stress is used to calculate the corresponding failure torque, as shown in Equations 65 and 66. This results in a factor of safety of 91 for the gears.

$$F_{\text{shear}} = \tau A = 2250 \text{ psi} \times \pi (0.25 \text{ in} \times 0.39 \text{ in}) = 697.5 \text{ lbf} \quad (65)$$

$$T = 697.5 \text{ lbf} \times 0.74 \text{ in} \times \frac{1 \text{ ft}}{12 \text{ in}} = 43.01 \text{ lbf} \cdot \text{ft} \quad (66)$$

4.4.6 Electronics Design

ACS electronics are designed to be simple and reliable. For a general breakdown of electrical components, trade studies are found in Section 4.2. The ACS runs on a Raspberry Pi 4b microprocessor over the Teensy microcontroller used for the payload. This was chosen due to its ease of integration and the plethora of online resources, trading efficiency of the microcontroller. The SinceCam 60 kg (4.4 lbf-ft) brushless servo motor was chosen due to its high torque rating (FOS = 2.34) and availability reducing prototype time and cost. For the onboard simulation, altitude and velocity are used to predict the apogee of the rocket if the ACS deploys. As seen in the trade study found in Section 4.2.7, the VectorNav VN-100 was selected for its versatility and integrate altimeter. A LiPo 7.4 V 2200 mAh battery is utilized to ensure enough current is ran to maintain an average IMU logging frequency of 100 Hz.



4.4.7 Software and State Machine (CONOPS)

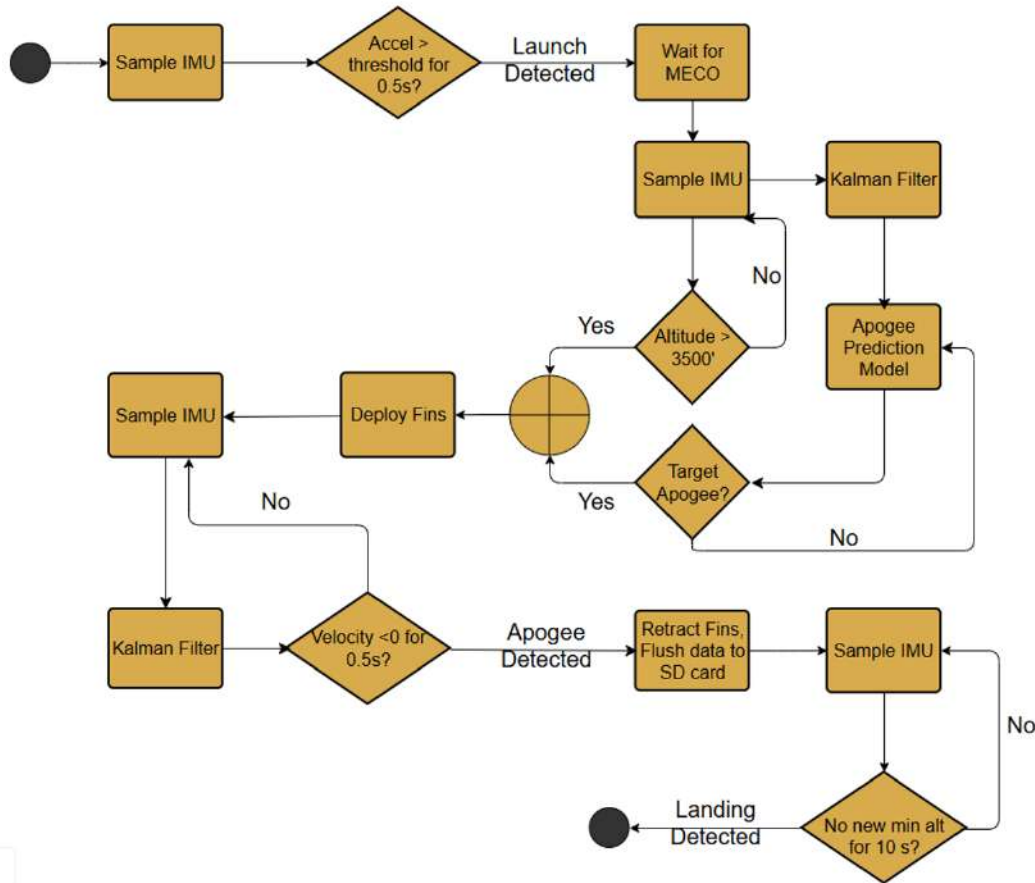


Figure 98: ACS software flow diagram.

As seen in Figure 98, the ACS utilizes both altimeter and accelerometer data to determine states of flight (launch, MECO, apogee, landing). The accelerometer is used to detect launch once a certain threshold is met for at least 0.5 s. Then, once launch is detected a timer runs for a hardcoded input based on the motor specifications to lock ACS decisions until MECO. This is done because the apogee prediction model utilizes a Kalman filter which may spike under high acceleration and cause a premature apogee prediction. Following the MECO timer, the apogee prediction model continuously calculates for apogee at 100 Hz until that criterion is met, and the vehicle has risen above 3500 ft. The 3500 ft floor is added to ensure compliance with NASA USLI Requirement 2.1 which states that no altitude points will be given to teams flying below 3,500 ft.

Following ACS deployment, the flight computer waits to see a negative velocity for 0.5 s before retracting the fins and flushing data to the SD card. Fin retraction is done to prevent any entanglement issues with recovery shock cords, and flushing to the SD card is done at this point to ensure all data during the ascent is saved if an off-nominal event causes the flight computer to fail during descent or landing. Landing is determined when no new minimum altitude is detected for 10 s.



4.4.8 Apogee Prediction Model

The ACS utilizes a simplified 1-Dimensional rocket flight simulation based on the same simulation framework outlined in Section 3.6.9. Given a known dry mass, rocket diameter, and current altitude and velocity data from the IMU, the ACS flight computer calculates the predicted apogee if the fins were deployed at that specific moment in time. Once the apogee prediction reaches the target apogee threshold, the fins deploy. This model uses the Runge-Kutta 4th order method to retain numerical convergence with a relatively large step size of 0.1 s. For the sake of reducing computational complexity in a real-time system, air density is modeled as a function of altitude, as shown in Equation 67. The rocket is assumed to be moving vertically upward, with no angular deviation or wind effects considered at apogee.

$$\rho(h) = \rho_0 e^{-h/8500} \text{ (kg/m}^3\text{)}, \quad \rho_0 = 1.225 \text{ (kg/m}^3\text{)} \quad (67)$$

4.4.9 Manufacturing Methods and Estimated Massing

The ACS uses a variety of manufacturing methods based on the material and tolerancing of the components. The bulk plate the hardware is secured to is machined using CNC; The brackets and fins are printed out of Markforged Onyx filament; And most other components are off the shelf. With the complete assembly achieving a total mass of 3 kg.

4.4.10 System Verification

VADL's design methodology aims to focus on reducing points of failure to achieve mission success. To this end, the team has and will continue to analyze failure modes in the ACS that affect flight performance. Mechanical failure of the gearbox is mitigated by holding the fins at their aerodynamic center, causing them to naturally center along the vehicle axis due to the freestream of air. Electronic failure is mitigated through careful stress testing of wiring and other components.

4.4.11 ACS Fin Design

Multiple methods of verification shall be conducted prior to full-scale vehicle integration. Wind tunnel testing shall verify CFD analysis, and hardware in the loop testing shall verify ACS flight code and logic. The latter shall use JSBSim – an open-source flight software – to feed flight data into the ACS flight computer to check performance for a variety of launch conditions. The subscale flight planned for November 22 shall prove the actual ACS performance in flight.

5 Safety

5.1 Safety Overview and Processes

Safety of our members is the top priority guiding all policies and operations at VADL. Because of this unwavering commitment, the safety precautions and standards outlined in the Safety Matrices and Hazard Analyses in Section 5 are primarily focused on protecting the wellbeing of our personnel. Any risks that could compromise the health or safety of a team member or bystander are rated with the highest severity and addressed with the utmost urgency.

The team upholds a Written Safety Agreement established during the proposal period, and every member is expected to hold both themselves and one another accountable to its standards. This includes the SSO's responsibility to enforce all fabrication and ground-test-related safety protocols, as well as each team member's duty not only to follow these guidelines but also to question them if they appear misaligned with either VADL's established practices or fundamental common sense. It also outlines the authority of the licensed RSO in all launch-related activities and the basic safety rules of such activities.

5.1.1 Project Components

To succeed in the 2025-26 mission of collecting and testing a soil sample after safe rocket launch and recovery, each subsystem must work safely in tandem. These subsystems include vehicle structures, payload mechanisms, and electrical/controls architecture. Each poses its own unique risks which must be 1) Identified, 2) Categorized by severity and likelihood, and 3) Prepared for and mitigated. As important as it is to act in the event of an emergency (preparedness), it is equally important to take measures to prevent its occurrence in the first place (mitigation). This entire process is documented in the Hazard Analysis Matrices in report Sections 5.2-5.5.

5.1.2 Safety Personnel

VADL maintains strong safety practices through collective responsibility and designated safety personnel. Every member upholds the Written Safety Statement, while several experienced individuals ensure consistent implementation and oversight of safety policies.

Jamie Danis, senior mechanical engineer, serves as Student Safety Officer (SSO). By NASA USLI Rules 5.1–5.2, Jamie collaborates with Chris Dondanville (RSO) to adapt and enforce the VADL Launch and Safety Checklist, monitor safety throughout design, construction, testing, and launches, and maintain hazard analyses, failure mode analyses, and Safety Data Sheet information in accordance with VADL Requirements 2.1.1-5. In addition, the SSO is responsible for enforcing all safety guidelines and procedures during ground-test and fabrication processes, and assists the RSO during launches. The SSO also consults with subject matter experts—Chris (RSO) for launch safety, and Jonathan Zak (former SSO and current master's student) for lab safety and legacy procedures.



Jamie conducts regular team safety meetings and will conduct safety checks before all safety-critical activities, including ground, flight, and drop tests.

Mark Thelen, mechanical engineer and laboratory manager, serves as Staff Safety Officer. He supports safe operations by procuring equipment, conducting training, and overseeing the storage of energetic materials.

Chris Dondanville, VADL's Range Safety Officer, holds a NAR Level 3 certification and extensive experience in high-powered rocketry and Student Launch. He supervises launch sites, motor and charge handling, and approves any vehicle or component changes following a successful full-scale flight (USLI Rule 2.6.7).

5.1.3 Safety Practices Overview

Following the Lab Safety Audit described in the VADL Proposal, a number of new processes and hardware-related safety practices have been implemented within VADL, and are listed below.

Legacy Safety Practices

As VADL has operated as a safe USLI team for years, a number of legacy safety practices have ensured the health and safety of the team members and all personnel as well as the launch vehicle itself during rigorous development and testing cycles. The most critical of these practices (as determined by the risk level in the following safety matrices) are outlined below:

Power Tool Qualification and Scrap Management

Mitigates major lacerations from untrained use of mills, saws, grinders, or disorganized scrap storage.

Launch Safety Oversight and NAR Safe Distances

Mitigates major trauma from unsafe launch site setup, vehicle prep, or improper distances.

Mental Health and Fatigue Policy

Mitigates tool misuse and accidents caused by exhaustion or high-stress work conditions.

Respiratory & PPE Enforcement (Composites, Epoxy, Fumes)

Mitigates respiratory, skin, and eye hazards from dust, resin, and soldering fumes.

Electrical Wire Strain Relief & Routing

Mitigates pulled/damaged wires and short circuits. Procedure: Use cable strain relief clips, route wires through fixed/tensioned channels, and avoid crossing connections to prevent mechanical or electrical failure as per VADL Requirement 3.5.21.

Parachute Deployment Redundancy

Mitigates recovery failure. Procedure: Keep main parachute separate from drogue, use back-up charges, and test deployments at multiple sites to ensure reliable recovery; this supports VADL Requirement 4.1.3-6.

Energetic Material Safety & Handling

Mitigates premature or non-secure charges. Procedure: Mount charges properly, use insulated terminals, verify amounts on a scale, and restrict handling to trained personnel.

Structural Load Safety & Factor-of-Safety Parts

Mitigates bolt tear-out, cup/bulkplate failure. Procedure: Use redundancy and high factor-of-safety designs, mark torque stripes on fasteners, inspect and replace stressed parts after each test/flight (supports VADL Requirements 2.1.1-2, and 4.1.7).



Updated Safety Practices

Following the Lab Safety Audit described in the VADL Proposal, a number of new processes and hardware-related safety practices have been implemented within VADL, the most crucial of which are listed below.

More Compartmentalized Motor Storage

To ensure the fewest number of rocket motors removed from a blast-proof environment, VADL has purchased 2 new steel Magloc blast-proof motor storage boxes to store motors by rated impulse and therefore decrease the total number of motors in each box. This decreases the total number of exposed motors for each motor retrieval.

Expansion of LiPo Battery Storage and Transportation Protocols

While the storage of LiPo batteries (within fireproof bags in metal cabinets) met safety specifications, the transportation of LiPo batteries required more oversight. Therefore, VADL has implemented LiPo transport cans, which are decommissioned US Army munition cans with small ventilation holes. These will be used to transport batteries to and from launch, and will serve both as a safe transport chamber and a centralized batte

Ground-Test Safety Kit

To ensure safe practices during ground tests (deployment test, wind pull test, tip-over test, etc.), a Ground-Test Safety Kit has been created and is stored in lab for convenient use. It has already been used by the team.

5.1.4 Compliance with Laws and Regulations

To ensure rocket flight safety for all VADL members and our launch vehicle, relevant National Association of Rocketry (NAR), Federal Aviation Administration (FAA), and Tennessee state laws are compiled below and referenced in the Written Safety Statement signed by all members before Proposal submission, complying with VADL Requirement 5.3.

National Association of Rocketry (NAR)

All members must review and follow the NAR High Power Rocket Safety Code (HPRSC). Printed and digital copies are available in the VADL office and shared folder. The Launch Minimum Distance Table will be posted and enforced at every launch. Key points include: 1) Members only fly motors within certification scope. 2) Launches require a 5-second countdown, with pad access limited to safety personnel. 3) All flights must meet the posted Minimum Distance Table and stability requirements.

Federal Aviation Administration (FAA)

VADL follows FAA 14 CFR Part 101, Subpart C. Launches are prohibited with over 50% cloud cover, under 5 miles visibility, at night, near airports, or in controlled airspace without authorization. Operations must stay at least 457 m (1,500 ft) or one-quarter of max altitude from nonparticipants, with fire precautions in place.

Tennessee and Local Laws

VADL complies with NFPA-based Tennessee fire codes and avoids launching or collecting materials from state parks, eliminating permit requirements. Tools are cleaned after launches to prevent soil or biological transfer.



Energetic Materials

VADL uses only certified Ammonium Perchlorate Composite Propellant (APCP) motors per NASA USLI Requirement 2.7. Motors are purchased by an L3 Certified Mentor, stored in MAGloc Explosives Magazines, and removed only by the Staff Safety Officer. All handling and loading are supervised by safety officers or RSO Chris Dondanville, following strict PPE and checklist procedures.

Team Compliance

All members were briefed on these regulations as well as all internal Vanderbilt safety standards and procedures at the first Team Safety Briefing and will be reminded before each launch. Jamie Danis, Student Safety Officer, ensures education and compliance in lab and field environments.

5.1.5 Documentation Processes

In addition to the following hazard analysis matrices, VADL employs extensive safety documentation to ensure safe operations both in-lab and in-field, (helping to support VADL requirement 4.1.7). This includes 1) General launch and safety checklists, 2) Checklists tailored for specific launches and field tests, 3) documented safety briefings, 3) Tool qualification documents (as described in Section 5.1.3), and 4) Design review/fabrication quality documentation (to ensure sufficient communication between all team members, avoiding premature fabrication procedures locking in a design before sufficient review).

For reference, first drafts of the Drop Test Safety Briefing and Subscale Manufacturing Go/No-GO Document are included below:

Subscale Go/No-GO and Build Procedure (VADL 2025-26)

VADL
VANDERBILT AEROSPACE
DESIGN LABORATORY

Pre-Drop Test Safety Briefing (One Week Prior)

Date: –
Delivered by: Jamie Danis – Student Safety Officer
Audience: All team leads and test participants

Purpose
This 18 lb tail-section drop test from 400 ft verifies landing kinematics, electronics survivability, and landing actuation. Safety is the top priority for 1) Personnel, 2) Hardware, and 3) Environment.

Personnel Risks

- Risks:** Impact injury, rotor hazards, burns/pinches.
- Controls:** 150 ft exclusion zone (only pilot and safety officer inside), PPE (hard hats, glasses, gloves, closed-toe shoes), spotters on all sides, constant comms, and pilot abort authority.

Vehicle / Payload Risks

- Risks:** Chute failure, hard landing, data loss.
- Controls:** Verify each subsystem by Test Day - 7, drop over grass. Verify with integrated tests by Test Day - 4.

Environmental Risks

- Risks:** Soil disturbance, contamination, temp/humidity effects on body tube or payload component fit-up.
- Controls:** Fiberglass wraps on BugTubes joints, calm weather (<10 mph), landowner-approved test area, complete clamp, covered transport.

Project Management

Risks: Missed deadlines, poor coordination.

- Controls:** Subsystem tests 10/22–10/23, drop test 10/25, checklists due 48 hrs prior, weather backup 11/1, designated recorder.

Section 1

Certify the design.

All Tasks are dependent on a completed subscale design, as validated by the following relevant leaders:

Jamie Danis (Vehicle), _____
Ben Racapé (Simulations), _____
Caleb Strout (Avionics), _____
Thor Hammer (Electronics), _____
Jack Leidel (President), _____
Evan Ticknor (Payload), _____

Section 2

Build the rocket.

Tasks are ordered by timeline priority. Task streams are labeled by numbers, and each task in a stream is labeled by letters. For example, Task 1A must be completed before task 1B, but task streams 1 and 2 can be completed in parallel.

Each task stream is dependent on some necessary “Off The Shelf” parts. The Responsible Engineer for each task stream certifies that their necessary materials are either in-hand or are currently on-order with a timely lead time.

Figure 99: Left: Drop Test Safety Briefing. Right: Sub-Scale Manufacturing Go/No-Go Document.



5.1.6 Safety Matrices

All safety matrices in Sections 5.2-5.5 follow a general format in which the risk level is identified, recorded and the preparedness/mitigation strategies are identified, documented, and implemented. The risk level is then updated, and future responsibilities are documented and tracked in future reports. Thus, PDR is a continuation and extension of the risks identified in the VADL Proposal, with added categories for Failure Mode, Environmental, and Project Management Risks, as well as recently identified Personnel risks.

Preparedness: Preparedness is the process of preparing to respond to an emergent situation with necessary procedures, equipment, and training. When properly prepared for, the severity of an emergency is decreased.

Mitigation: Mitigation is the process of taking preliminary steps to prevent a situation from happening. While it does not lessen the severity of an emergent situation like preparedness does, it decreases the likelihood of one occurring in the first place.

Risks are categorized by severity and likelihood in the following risk matrix. For reference, a Catastrophic event in the context of Personnel and Environmental Hazards involves death, serious injury, or serious property damage such as an uncontrolled building fire. In the context of FMEA and Project Management Hazards, a Catastrophic failure means complete mission failure, loss of entire launch vehicle with all subsystems, or total failure to complete the required project by the NASA USLI launch date. A Critical failure jeopardizes a portion of launch vehicle or poses a moderate safety risk to personnel. A Marginal risk jeopardizes a component that can be replaced or remade quickly or in-field. A Negligible event involves small injury, property damage, or failure that can be healed or fixed within a day, such as a paper cut.

Risk Assessment Scoring				
	Catastrophic (1)	Critical (2)	Marginal (3)	Negligible (4)
Frequent (A) [61-100% Chance]	1A	2A	3A	4A
Probable (B) [41-60% Chance]	1B	2B	3B	4B
Occasional (C) [16-40% Chance]	1C	2C	3C	4C
Remote (D) [4-15% Chance]	1D	2D	3D	4D
Improbable (E) [1-3% Chance]	1E	2E	3E	4E

Figure 100: Risk assessment scoring matrix

Risk Key	
	High
	Moderate
	Low
	Negligible

Figure 101: Risk Key

By the above logic, preparing for a risk can decrease its severity when it happens, and mitigating a risk decreases its likelihood of occurring in the first place.

5.2 Personnel Hazard Analysis

The most pressing issue for VADL is the safety of our members. Therefore, great care was taken in identifying, preparing for, and mitigating these risks. At this point in the design process, many field and lab-related risks have been identified through common sense and by interviewing past and current team members about their experiences. Many of these risks were identified in the Proposal document but more have become apparent since then. Most of these recently identified risks are fabrication-related, as they've surfaced during prototype creation and testing. As the team moves into the stages of subscale launch and integrated payload-vehicle testing, additional field-related hazards will be identified, prepared for, and mitigated.



Hazard for People (Setting)	Causes	Risk Level Before Treatment	Preparedness Strategy	Mitigation Strategy	Risk Level At PDR	Future Responsibility
Identified Before Proposal (Updated Up to PDR)						
Minor Lacerations/Burns (In-Lab)	1. Hand tool misuse 2. Soldering iron routine use	2B	* Two wall-mounted lab first aid kits	1. Common hand tool training during initial Safety Briefing 2. Soldering iron training and cleanup held by electrical team lead	3C	* Check and restock first aid kit bimonthly [Jamie Danis] * Remain in lab during high-traffic times [Jamie Danis]
Major Lacerations (In-Lab)	1. Power tool misuse (Reciprocating Saw, Miter Saw, Angle Grinder, Mill, Lathe) 2. Disorganized hazardous scrap metal bin	1D	* Severe-injury first aid kit mounted and visible * 7 min walk / 2 min drive to VU Emergency Dept.	1. Instituted and enforced Tool Qualification Listing 2. Completely cleaned, reorganized, and dehazardized scrap metal racking	2D	* Continue power tool qualification trainings and enforcement [Jamie Danis] * Work with Mark Thelen to expand them [Jamie Danis]
Uncontrolled Fire (In-Lab)	1. Haphazard power cable management 2. Improper LiPo Battery storage 3. Improper energetic material storage	1D	* 2 wall-mounted fire extinguishers in-date and visible	1. Organize and execute lab cleanup 2. Keep LiPo batteries in fire-resistant, pressure-relieved, damage-resistant steel containers 3. Energetic materials stored in explosion-rated containers, and only handled and stored by Staff Safety Officer, Mark Thelen	1E	* Continue energetic material personnel restriction [Mark Thelen] * Enforce continuous use of new LiPo battery storage procedure (2 modified ammo cans with LiPo bags) [Jamie Danis]
Trips/Falls (In-Lab)	1. Disorganized scrap material area 2. Overcluttered lab floor	3B	* First aid kits * Vanderbilt Health Services	1. Complete cleanup of scrap material area 2. Lab-wide cleanup and relocation of clutter to dumpster or storage	3D	* Hold future cleanups as needed (3 so far) [Jamie Danis]



Hazardous Dust Inhalation (In-Lab)	1. Fabrication (Composites, wood) 2. In-Lab composite grinding	2B	* Respirators and replacement filters acquired and located throughout lab in visible and accessible locations * Sawhorses built and available for outdoor composite grinding	1. Portable HEPA filtration unit tested and located at Indoor Composite Fabrication Workstation 2. All composite grinding and sanding done strictly outdoors (policy enforced, and outdoor alternative made available)	2D	* Continue enforcing outdoor composite workstation (built and stored in loading-dock closet) [Jamie Danis]
Skin/Eye Irritation (In-Lab)	1. Haphazard composite sheet storage 2. Insufficient PPE availability/visibility 3. Fabrication (Composites)	3B	* Topical analgesic available in lab first aid kits * Handwash and eyewash sink available in lab	1. Dedicated, closed containers for composite materials 2. PPE acquired and distributed visibly 3. Dedicated composite fabrication workstation with posted PPE and mitigation policies	4D	* Continue enforcing outdoor composite workstation (built and stored in loading-dock closet) [Jamie Danis]
Electrical Shock (In-Lab)	1. Misuse of corded power tools 2. Insufficient experience when preparing payload electrical system	2D	* First aid kits * Vanderbilt Health Services	1. Use of cordless powertools 2. Electrical work over 12V restricted to dedicated, trained electrical team	3D	* Continue to enforce electrical safety [Ashley Fu, Jamie Danis]
Soldering Fume Inhalation (In-Lab)	1. Unhelpful Helping Hands setup 2. Lack of proper fume-filtering fan setup	3B	* Organic Vapor respirators available and visible	1. High-quality helping-hands acquired 2. Fume fan acquired	4C	* Continue to enforce soldering safety [Ashley Fu, Jamie Danis]
Energetic Material Combustion (In-Lab)	1. Improper /irresponsible energetic material storage 2. Accident while preparing ejection charges	2C	* Dedicated energetic material location in storage room, and in lab when actively working on them	1. Strictly enforced policy of motors only handled by Staff Safety Officer 2. Ejection charges only prepared by trained personnel	2E	* Continue to enforce energetic material restrictions [Mark Thelen, Jamie Danis]
Exhaustion/Fatigue/Mental Anguish (In-Lab)	1. Demanding work hours 2. Pressure to perform while tired	3A	* Policies regarding mental well-being prioritization posted and enforced	1. Zero tolerance policy for operating tools while significantly tired or altered in any way 2. Everyone in the team commits to respect the mental well-being prioritization of others	3E	* Continue to implement mental health prioritization throughout the year, especially during high-stress periods. (Already successfully implemented in high-stress time before drop test) [All Team Members]
Minor Lacerations/Burns (Ground Test)	1. Insufficient Safe Distance observed during ground test	3D	*Ground Test Safety Kit assembled, labeled and posted at lab exit	1. Ground Test Safety Kit used to cordon off a Safe Zone for drop and ejection tests and provide ample PPE on-site	3E	* Ground Test Safety Kit successfully built and implemented on all ground tests to date (x3) [Jamie Danis]



Fire (Ground Test)	1. Ground test conducted in dry/grassy area	2D	*Ground Test Safety Kit assembled, labeled and posted at lab exit	1. Ground Test Safety Kit includes fire extinguisher and water for onsite dousing	2E	* Ground Test Safety Kit successfully built to include Fire Response Implements and implemented on all ground tests to date (x3) [Jamie Danis]
Minor Laceration/Burn (Launch)	1. Mistake when preparing vehicle/payload 2. Fall risks inherent to outdoor work	3C	* Field first-aid kit inspected and prepared	1. All field tasks strictly overseen by RSO, acknowledged with complete authority over launch 2. Proper shoes and outerwear will be worn	3E	* Obey all safety procedures and instructions upon first launch, troubleshoot if necessary [All Team Members, Jamie Danis]
Major Laceration (Launch)	1. Improper Safe distance observed during launch 2. Improper launch site clearance observed	1D	* Field first-aid kit inspected and prepared * Multiple present team members trained in life-saving measures	1. NAR High Power Rocket Safety Code Minimum Safe Distance strictly followed 2. All field tasks strictly overseen by RSO, acknowledged with complete authority over launch	2E	* Obey all safety procedures and instructions upon first launch, troubleshoot if necessary [All Team Members, Jamie Danis]
Fire/Major Burn (Launch)	1. Improper launchsite choice and ground preparation 2. Motor CATO	1D	* Launch Go-Bag includes fire extinguisher and water for onsite dousing	1. Launchsite chosen to comply with NAR High Power Rocket Safety Code 2. All energetic material transported in explosive-rated steel containers exclusively by Mark Thelen	2E	* Obey all safety procedures and instructions upon first launch, troubleshoot if necessary [All Team Members, Jamie Danis]
Hazard for People (Setting)	Causes	Risk Level Before Treatment	Preparedness Strategy	Mitigation Strategy	Risk Level At PDR	Future Responsibility
Identified After Proposal						
Fiberglass dust and fumes during laser cutting	Indoor laser cutting (due to inability to bring outside), weak ventilation, inconsistent respirator use	2B	Respirators and fans available. Policy to leave sequestered laser cutting room when cutting for extended periods, still with respirator on	Primary: Outsource waterjetting of fiberglass to SendCutSend; Secondary: HEPA vacuum cleanup, change out respirator and air purifier filters, post signage	2C	* Monitor all fiberglass lasercutting and builds personally, and ensure early BOMs for all projects to enable the lead times associated with outsourcing, the primary option [Jamie Danis]
Epoxy skin or eye irritation	Gloves out of stock (large team and many epoxy layups already) / sleeves, poor ventilation, resin contact	3C	PPE and MSDS posted	Barrier sleeves, fume-hood/outdoor curing, sealed epoxy waste bin	3E	* Ensure sufficient supply of disposable PPE in lab [Jamie Danis]



Thermal burns from curing and exotherm	Large resin batches, heat gun misuse, unsupervised hot-box	2D	Heat gloves, IR thermometer	Limit batch size, monitor temps, supervise hot-box	3E	* Oversees All Epoxy Layups as both Vehicle Lead and Safety Officer [Jamie Danis]
Pinch/crush injury (payload arm/auger)	Accidental motion during test, unsecured payload, injury during assembly	2C	First aid kit, gloves during powered assembly or testing	Leather gloves during powered assembly or testing. Pre-test safety briefing	3D	* Stringent testing (lab and field) procedures, complimented with tight testing safety procedures [Sean Conroy], [Jamie Danis]
Overexertion lifting fiberglass sections	Lifting 15–25 lb sections overhead	3C	Work gloves, wheeled cart	Two-person lift rule, step stool for rail loading	3D	* Emphasize safe lifting practices and police others' lifting practices [All Members], [Safety Officer]
Drone prop or battery fire (drop test)	Damaged LiPo, unsafe landing, rotor strike, overmassaged payload	2C	Batteries stored in ventilated metal cans	Preflight prop check, safe zone setup, extinguisher on site	2D	* Keep a thorough understanding of drone battery limitations, and ensure drop test mass is tested on drone with equivalent ballast before risking payload [Jamie Danis]
Noise exposure (tools, motor firings)	Extended saw/grinder use, no hearing PPE	4C	Ear protection available	Enforce earplug use, include in briefings. Enforce "fair warning" period before operating loud machinery with others present.	4C	* Oversees all mill, lathe, and miter saw usage as both Vehicle lead and Safety Officer [Jamie Danis]

Figure 102: Personnel hazard analysis matrix

5.3 Failure Modes and Effect Analysis

Secondary only to risks to the health and safety of people (our VADL personnel and to other people who may be affected by our launch vehicle and related activities), VADL holds the safety of our launch vehicle and integrated subsystems in incredibly high importance. Recoverability and safe landing is at the heart of every design decision made on the Vehicle Design Team, and stable/reliable payload actuation at the heart of every electrical/payload design decision. Therefore, it remains vital to identify hazards to our launch vehicle, payload, and related subsystems. This is done through a Failure Modes and Effect Analysis, where system or component failure modes are identified with their associated causes, along with our planned mitigation and preparedness strategies.



Failure Mode	Causes	Previous Risk Level (Before Mitigation)	Preparedness Strategy	Mitigation Strategy	Current Risk Level (After Mitigation)	Future Responsibility
Vehicle Subsystems						
Pulled or damaged wires in electrical systems (ACS, PDM, Avionics)	1. High load at launch, recovery deployment, or landing	2D	1. ACS doesn't deploy without proper signal from altimeter 2. Back-up charges for PDM	1. Use cable strain relief clips 2. Route wires through fixed channels to prevent movement during vibration or ejection	3E	1. Continue to utilize cable strain relief clips 2. Utilize tensioned holes around wires
Cross-wiring or shorting between soldered connections in electronics	1. Unsafe soldering 2. Exposed wires	2D	1. Bring comprehensive electrical equipment in a dedicated tool box to launches	1. Insulate solder joints using discrete hot glue pools, allowing for later rework if needed 2. Run full continuity and insulation resistance check before launch	2E	1. Re-solder connections that are potential risks 2. Keep track of wiring diagrams to prevent cross-wiring
Altimeter misconfiguration or malfunction	1. Improper use of altimeter 2. Misinterpretation of altimeter data and specifications	1D	1. Launch in a sufficiently large launch site 2. Employ a loud communication signal in case of catastrophe	1. Follow all manufacturer-recommended setup and testing procedures for the EasyMini altimeter 2. Perform ground pressure test with dual altimeters to verify separation logic and trigger thresholds	1E	1. Retain altimeter data sheet for future reference
Catastrophic motor failure	1. Improper staging 2. Combustion instability	1D	1. Take all appropriate safety precautions before approaching/handling CATO	1. Multiple motors will be brought to launch site 2. Bolted, not epoxied, tail section joints allow for quick replacement or rebuild 3. Ensure safe handling procedures and an emergency response protocol are reviewed before motor installation	2E	1. Continue taking safety measures when handling damage from CATO 2. Reflect on causes of motor failure



Dud or failed ignition	1. Poor contact between ignitor and motor 2. Wet conditions	3C	1. Waiting 60 seconds to check and re-set ignition 2. Take all safety precautions when setting up an ignitor	1. Redundancy ensured by carrying multiple motors to the launch sight 2. Verify igniter resistance and continuity immediately prior to flight	3D	1. Verify ignitor resistance and continuity 2. Keep multiple motors
Inability to source motors	1. Lack of time management 2. Outside delays in shipping/delivery	2D	1. Three primary motors secured in lab 2. Four back-ups ordered and tracked	1. Utilize back-up motors, checking with all data sheets and specifications to ensure mission fit	3E	1. Replenish back-up motors supplies 2. Replenish primary motors
Insufficient blast pressure to overcome leg friction	1. Improper measuring of black powder 2. Miscalculation of strength needed to deploy drogue	2C	1. Back-up charges 2. Main parachute deployment system separate to ensure safe recovery, even failing drogue	1. Controlled secondary blast (via OTS EasyMini) ensures redundancy 2. Test deployment at multiple field sites with varying temperatures and pressures	3D	1. Retain data for future testing and black powder loading
Cord tangling from drogue blast	1. Improper packing of recovery systems	3B	1. Main parachute deployment system separate to ensure safe recovery without drogue deployment	1. Lightweight blast plate included 2. Separation testing performed and configuration documented after each test	4D	1. Packing recovery system is handled meticulously 2. Eliminating unnecessary material to prevent tangling
Sliding of PDM wrap to the side of U-bolt	1. Side-loaded main parachute deployment 2. Failure of blast plate pre-tensioning mechanism	2C	1. PDM latch capable of withstanding a significant portion of main shock load, so as long as the capstan effect is not lost entirely, the parachute should not detach in the air	1. Square U-bolt prevents slippage 2. Include a quick-reference diagram in the launch checklist to verify proper wrap placement	3C	1. Complete comprehensive testing on the PDM at different angles
Electrical systems fail to detect vehicle landing	1. Wiring error upon impact of landing 2. Misinterpretation of altimeter data	2D	1. Default state of payload is under a locked latch	1. Intensive testing during drop tests to set rigid landing conditions	2D	1. Analyze data after each flight to record what went right and wrong
Premature electrical detection of landing	1. Excessive vibration during flight	3C	1. Parachute detachment delay of 10 seconds	1. Add filtered logic (like time-delay confirmation) to prevent false triggering from vibration or ejection shocks 2. Rigid landed-state criteria	3D	1. Update electronics to measure data properly 2. Update landed-state criteria from flight to flight
Pitching of vehicle	1. Wings of ACS deploy unevenly 2. ACS deploys during motor burnout 3. ACS deploys during high velocity	3C	1. ACS deploys at a minimum apogee requirement 2. Motor burn-time is hard coded into the program depending on the motor utilized, setting a minimum period of time before ACS deployment	1. ACS located aft of the center of gravity, only inducing drag 2. ACS is mechanically locked through miter gears to prevent uneven deployment of the fins	3D	1. Redundancy check locking system to ensure function after each flight



Premature blast charge (before vehicle hits apogee)	1. Mishandling altimeters 2. Improper pressure hole ports	2C	1. Drogue deploys early 2. Main parachute still deploys if vehicle doesn't hit target apogee	1. Add delays in deployment to delay after apogee 2. Proper port sizing, installation, handling so altimeters get proper readings 3. Proper mounting of charges	2D	1. Resetting all blast charges in between tests and flights 2. Continual testing of altimeters to ensure proper readings
Non-secure blast charge	1. Blast charge ports improperly mounted	2C	1. Insulation around terminal to prevent damage to electronics 2. Utilize proper safety measures when working with black powder	1. Utilizing a screw terminal 2. Performing overview and redundancy check from team mentors 3. Tension-checking wires	3D	1. Clearing workspaces after handling black powder 2. Replacing insulation
Blast charge leakage	1. Black powder handled improperly	2C	1. Insulation around terminal to prevent damage to electronics 2. Use scale to measure appropriate amount of black powder	1. Utilizing magnetic putty in the hole of bulk-plate where the blast charge wiring goes through	4D	1. Clearing workspaces after handling black powder 2. Reset scale after each measure to ensure absolute zero
Short-circuiting in avionics electronics	1. Cross-wiring 2. Improper wiring connections	1C	1. Have in-field repair strategies for any wiring faults	1. Single-strand wiring for all electronics	1E	1. Continue to single-strand wire all connections 2. Utilize tensioned holes around wires
Load-bearing on wires	1. Load during flight 2. Load impact upon landing	3C	1. Have in-field repair strategies for any wiring faults	1. Using tensioned holes around wiring to transfer load from wires	3D	1. Replace wires that have experienced significant wear
Drogue deployment failure	1. Hole in parachute 2. Neglecting proper blast chamber preparation	2C	1. Main parachute deployment system separate to ensure safe recovery without drogue deployment 2. Back-up charges in case of electronic failure	1. Perform calculations to allocate appropriate blast charges for deployment 2. Design systems simply and reliably 3. Extensive testing before flight	2D	1. Replace parachute after any tears or overuse
Main deployment failure	1. Hole in parachute 2. Neglecting proper blast chamber preparation	1C	1. Ensure proper launch safety communications and safe distances observed 2. Back-up charges in case of electronic failure	1. Perform calculations to allocate appropriate blast charges for deployment 2. Design systems simply and reliably 3. Extensive testing before flight	1E	1. Replace parachute after any tears or overuse



Structural failure, bolt tear-out, cracking, or delamination	1. Extreme weather conditions 2. Over-loading joints	2D	1. Manufacture duplicates of highest-risk and highest-criticality parts	1. Avoid unnecessary adhesives (no thread-locker) so bolted joints remain serviceable for rapid field repair 2. Apply torque stripe markings to visually verify no fastener backout during testing or flight	3E	1. Repair any cracks or failures after every flight 2. Replace any fasteners that have experienced significant wear
Payload Subsystems						
Deployment of water in-flight (mechanical fault)	1. Water chamber becomes dislodged 2. Water chamber opens	3D	1. Payload is designed to still accomplish mission, through with less accuracy 2. Electrical components are completely sealed in final design	1. Use redundant securing mechanisms and vibration-tested containers 2. Testing balloon material under higher-than-anticipated loads to incorporate safety factor	3E	1. Replacing latex balloon after each test 2. Sanding down all possible snag points for balloon
Water fails to deploy before soil sensing (mechanical)	1. Water chamber is damaged upon landing, doesn't release	2D	1. Collection still occurs without water deployment 2. Soil sensing still occurs without addition of water	1. Simplify moving components 2. Conduct cycle-lift testing to ensure mechanical actuation reliability	3D	1. Replace any parts related to mechanical that may experience repeated stress
Water fails to deploy before soil sensing (electrical)	1. Electronics don't properly detect landing	2D	1. Collection still occurs without water deployment 2. Soil sensing still occurs without addition of water	1. Include pre-launch verification test for electrical continuity and logic confirmation through OTS	3D	1. Replacing any damaged parts after all flights and testing
Electronic failure due to water leakage	1. Water leaks into electronics bay	1D	1. Plastic layer to waterproof electronics 2. Utilizing silicon, o-rings, silicon-grease, and torquing all bolts to compress gasket	1. Two layers of waterproofing for water chamber 2. Water located aft and physically below electronics bay to require upstream flow for water to leak into electronics bay	2E	1. Repeating waterproofing techniques with each flight 2. Replacing any plastic waterproofing that may have punctured during testing or flight
Rotating Bulkplate System unlocks while in flight	1. Excessive vibration during flight, launch, or landing 2. Excessive rotation during flight, launch, or landing	1D	1. Bulk-plate has to rotate many times before being too far extended to dig at landing. Therefore, the mission can still be completed even with multiple rotations in-flight	1. Design includes mechanical lock or latch that remains engaged until ground contact or deployment command	2D	1. Fully reset RBS after each test and flight 2. Ensure mechanical lock is set prior to each flight



Rotating Bulkplate System locks under bending moment upon landing	1. Material deformation	1C	1. Software safeguard to rotate the system in the reverse direction, clearing the chamber or fixing deformation 2. Motor stores enough power to drive through any interruptions in the event of rotational resistance	1. Reinforce shaft supports 2. Tighten clearance tolerance to prevent binding under load 3. Increase bending rigidity through more bearing contact surface area	2D	1. Fully reset RBS after each test and flight 2. Thoroughly inspect for any plastic deformation after each flight
Cup holding bulkplate together breaks during flight	1. Load applied during parachute deployment 2. Bolt tear-out due to shock load	1D	1. Redundancy and factor of safety implementation 2. Safe field test and launch procedures in remote case of failure.	1. Extensive analysis on the cup-bulkplate interface for active and passive sides 2. Ensure a safety factor of at least 3.5 for all predictable load conditions 3. Analyze for conditions at initial launch shock	1E	1. Replace bulkplate after plastic deformation is observed 2. Continue to analyze structural effectiveness of design
Airframe bolt tear-out	1. Excessive torque between active side of rotating system and airframe	1D	1. Redundancy and factor of safety implemented in fasteners 2. Fabrication of duplicate critical parts	1. Sample airframe component tensile tested with same bolt configuration to ensure bolt pattern doesn't affect strength of the airframe beyond designated safety factor	2E	1. Replacing fasteners that experience significant stress after each test and flight
Structural deflection or deformation of shovel deployment mechanism	1. Impact upon landing	1D	1. Motor retains enough power to smooth out deformations through rotation	1. Upgrade from 6061 aluminum to 316 stainless steel rotating threaded rods	2E	1. Monitor continued stress on threaded rods and replace when plastic deformation occurs
Asymmetric or unbalanced loading of the payload deployment mechanism	1. Damage to leg system upon landing	3C	1. Shovel extension includes factor of safety to reach ground in event of uneven landing	1. Add symmetric supports 2. Dual-sided mounts to distribute forces evenly and prevent twisting or fatigue failure	3E	1. Ensuring leg system is continually symmetric after each test and flight 2. Performing any repairs after damage to leg system
Shock and impact sensitivity during landing or flight	1. Excessive vibration during flight 2. Impact upon landing	3C	1. Threshold for withstanding vibration and impact during flight to prevent any premature action from electronics	1. Anticipate impacts with ANSYS structural simulation 2. Reinforce critical joints and select materials capable of absorbing or damping shock loads	3D	1. Replacing joints and materials that experience continual stress 2. Update simulations frequently



Misalignment of gears, cords, or linkages due to deflection or shock	1. Parachute deployment 2. Excessive load during launch, breaking shear pins	3C	1. Safety factor implemented to ensure sensors will still function with less soil collected than estimated	1. Add alignment features (bushings, guides, or rigid springs) to maintain proper gear engagement	3E	1. Minimizing unnecessary cords or linkages to prevent damage 2. Replacing alignment features as they experience stress
Excessive torque on shovel during soil contact	1. Unexpectedly firm ground at collection point 2. Lever arm excessively long	1C	1. Safety factor implemented to ensure sensors will still function with less soil collected than estimated	1. Shorten landing legs to reduce clearance between shovel and soil	2D	1. Replace any joints on shovel that may become points of failure 2. Analyze ground conditions and make adjustments to power
Failure to collect soil or need to retract shovel (failure of cable design)	1. Level of torque damages shovel 2. Shovel doesn't deploy	1D	1. Safety factor implemented to ensure sensors will still function with less soil collected than estimated	1. Integrate a simple, reliable shovel retraction mechanism	2E	1. Replace any joints on shovel that may become points of failure 2. Analyze ground conditions and make adjustments to power
Drained or insufficient battery power across electrical systems	1. Improper charging of battery 2. Incorrect measurement of power needed to complete full mission	1D	1. Include backup batteries in Avionics, ACS, PDM, and payload subsystems 2. All electronics will have at least 4 hours of power at time of launch	1. Perform detailed power calculations and tests to ensure capacity and discharge rate for mission duration	2E	1. Replacing all batteries after extensive use and testing 2. Charging all batteries before flight
Broken or damaged electrical connections	1. High load at launch, recovery deployment, or landing 2. Cross-wiring or shorting of connections	1D	1. ACS doesn't deploy without proper signal from avionics 2. Back-up charges for PDM	1. Use cable strain relief clips 2. Route wires through fixed channels to prevent movement during vibration or ejection	2E	1. Continue to utilize cable strain relief clips 2. Utilize tensioned holes around wires
Data corruption or overwriting	1. Data collection at a higher frequency than electronics can process 2. Power loss	2D	1. Embedded SD card reader 2. Enable easy switch to lower sampling rates to reduce processor load 3. Key data backs up onto microcontroller and SD card	1. Implement watchdog timer resets and fault-tolerant communication protocols to preserve data integrity 2. Housing that mechanically secures SD card	3E	1. Access microcontroller to collect key data points
Software crashes or lockups	1. Power interruption	3D	1. EEPROM saves data in case of power loss 2. After reboot, microcontroller can access most recent data saved	1. Use lower sampling rates to reduce processor load 2. Perform repeated software drop tests to confirm stability	3E	1. De-bugging power loss and adjusting design for future flights



Misinterpretation or loss of IMU/sensor data	1. Improper integration of IMU 2. Power loss	2D	1. In case of data loss, redundant data collected via backup sensor assembly	1. Apply periodic calibration routines 2. Use duplicate sensor assemblies for redundancy	3E	1. Re-calibrate electronics with IMU periodically
Noisy or lost sensor signals / physical sensor damage	1. Extreme weather conditions 2. Avionics experience intense vibration	3C	1. Spare avionics components in the case of damage before flight	1. Perform impact and temperature testing 2. Shield or isolate sensors from high-vibration environments	3E	1. Calibrate all electronics in any environmental conditions faced

Figure 103: Failure modes and effect analysis matrix

5.4 Environmental Concerns

When conducting any tests or launches outdoors (or even in-lab), it becomes vital to acknowledge, prepare for, and mitigate effects between the launch vehicle and the surrounding environment (VADL requirement 5.2). This includes effects on the vehicle by the environment (eg. airframe dimensional instability with outdoor temperature variations) and effects on the environment by the vehicle (eg. improper hazardous fabrication chemical disposal). The following hazard analysis matrix identifies these risks and their preparedness and mitigation strategies.



Environmental Hazard	Causes	Previous Risk Level (Before Mitigation)	Preparedness Strategy	Mitigation Strategy	Current Risk Level (After Mitigation)	Future Responsibility
Wrong state detection/Inaccurate reading of the altitude	1. Wind gusts 2. Thermal pockets	1D	1. Robust physical construction to withstand the impact	Using conditional statements for determining the states: 1. Stable non-decreasing altitude 2. Current altitude within 20 feet of the ground altitude	1E	* Rigorously test the IMU detection and motor/latch actuation both independently and integrated with their controlled subsystems
False soil conductivity reading data	1. Rain before launch	3C	1. Understanding of water content upper limit, and the effect proper mixing has on this	1. The soil retention chamber autonomously mixes the soil-water slurry, and therefore generates a mixed sample even at higher than-expected water rates	4C	* Ensure integrated payload testing in environments with a variety of moisture content
Effect in amount of soil collected	1. Landing in rocky area	2C	1. Motor has enough torque to flip until the mechanism can collect soil	1. Choose launch sites with less rocky areas	2D	* Establish go-to launch sites with limited rocky areas
Electrical component overheating from motor casing	1. High environmental temperature	1C	1. Carbon fiber plate as a heat shield from motor	1. ACS doesn't deploy, rocket still completes safe flight	3C	* Complete design and thermal testing of insulating motor plate
Vehicle lands in water	1. Rain before launch	3C	1. Shovel extension to collect water 2. Team members wearing proper shoes to retrieve vehicle	1. Design shovel to extend to accommodate for puddles 2. Plan launch in a flat area with low risk of large accumulation of water	3C	* Consider use of hot glue on soldered joints for pseudo-waterproofing
Microcontroller timing and clock issue	1. Extreme cold temperature	1D	1. Elevated internal temperature within the air frame/body tube due to the fiber glass's insulative property	1. Scrub all launches below 32F degrees outside.	2E	* Continue to employ a disciplined launch or field test go/no-go procedure



Battery fail to function	1. Extreme cold 2. Wind turbulence	2D	1. ACS doesn't deploy, rocket still completes safe flight 2. Back-up systems to autosave data in the event of a power disconnect 3. Backup batteries for critical systems	1. Check batteries function before flight 2. Fully charge LiPo batteries before traveling to launch site 3. Bring extra batteries to launch	3D	*Replacing batteries *Recharging batteries after use
Material left at launchsite	1. Disorganization 2. Rushing to leave site	4C	1. Comprehensive launch site checklist adherence	1. Checklist to ensure all materials brought were collected	4E	* Rigorous launchday checklists, including packing beforehand, operations during launch day, and cleanup after launch
Air traffic at time of launch	1. Lack of communication with NAR 2. Lack of planning	1D	1. Backup launch date coordinated	1. All subscale launches are held on private property, following NAR protocols 2. All full-scale launches are held at sanctioned NAR locations, where the NAR provides airspace waivers	1E	* Continue to monitor legality of launching/testing at a site with our specific test setup
Poor visibility	1. Intense fog 2. Cloudy, overcast weather	3C	1. No launch, reschedule for back-up date 2. Delay launch	1. Monitor weather conditions in the days leading up to planned launch 2. Have a back-up launch date set in case of no-fly conditions	1C	* Monitor weather conditions in the days leading up to planned launch * Have a back-up launch date set in case of no-fly conditions
Distortion of components	1. Extreme cold weather 2. Extreme heat	2D	1. Peer reviewing designs before beginning manufacturing	1. Tolerancing parts properly in design 2. Ensuring minimal perfectly fitting components 3. Choosing low thermal expansion coefficient materials "IE fiber glass instead of blue tube"	2E	* Peer reviewing designs before beginning manufacturing
Vehicle drifts into possibly unrecoverable area	1. Excessive drift due to exceptional wind conditions 2. Insufficiently sized launchsite selection	1D	1. Tracking weather conditions 2. In the event of a lost vehicle, employ vehicles GPS in PDM bay 3. Failing this, divide into groups and grid search surrounding areas	1. Considering drift of varying flight simulations to estimate max launch site requirements 2. Always angle launch rail into wind direction	1E	* Ensure GPS functionality on launch day. *Prepare for lengthy and logistically difficult recovery operations if necessary
Vehicle lands in tree	1. Improper rail angle 2. Excessive winds	2D	1. Saw branches 2. Follow relevant safety procedures to use saw 3. PPE 4. Recieve permission from land owner to modify trees if necessary	1. Avoid launching in the direction of trees 2. Analyze wind conditions 3. Adjust launch rail angle and direction accordingly	2E	* Contact a local professional who is available for tree removal or scaling to recover vehicle if necessary
Wildlife	1. Insects 2. Snakes 3. Mammals	3E	1. Bring bug spray 2. Close toed shoes and PPE at launch. 3. Universal enforced buddy system at launch	1. Limit food at launch	4E	* Continue to limit food at the launchsite

Figure 104: Environmental concerns analysis matrix



5.5 Project Management Risks

As mentioned in Section 5.3, the safety of our NASA USLI project is of vital importance to every team member. Therefore, an organized and forward-looking team considers not only mechanical, electrical, and launch-related failure points, but also logistical and operational failures throughout the 9-month-long integrated team effort to accomplish the stated mission. Project management hazards are listed below, with their severity graded based on how likely they are to derail or invalidate the performance and viability of our mission-forward launch vehicle and HAUS payload, as described in Section 5.1.6.

Project Hazard	Causes	Previous Risk Level	Preparedness Strategy (Before Mitigation)	Mitigation Strategy	Current Risk Level (After Mitigation)	Future Responsibility
Missing deadline to submit NASA documentation	1. Poor scheduling 2. External delay 3. Miscommunication	1D	1. Internal VADL report deadlines (At least one week in advance)	1. Keep updated spreadsheet with delegated tasks and deadlines 2. 3x weekly stand-ups to encourage accountability	1E	1. Start drafting documentation at a minimum of 3 weeks in advance 2. Communicate any issues with meeting responsibilities
Funding runs out	1. Poor budgeting 2. Emergency	2C	1. Plan to reach out to VU School of Engineering to inquire about emergency funding if necessary	1. Utilizing order sheets to track spending 2. Implementing a safety factor for budget	2E	1. Avoid excessive and unnecessary spending 2. Allocate funding according to highest needs
Conflict within subteam	1. Disagreement in design 2. Personality disagreements	3D	1. Policy of a dedicated third party mediate a discussion between team leads	1. Encourage team bonding outside of working 2. Communicate clearly and effectively	3E	1. Have a respectful attitude when team members communicate
Conflict within team leads	1. Someone misses deadline 2. Personality disagreements	1C	1. Policy of a dedicated third party mediate a discussion between team leads	1. All team leads attend stand-ups 3x weekly	3C	1. Have a respectful attitude when team leads communicate
Design conflict with Team Mentor	1. Disagreement in design 2. Conflicting experience	2C	1. Plan to consult other team mentors, adn establish healthy streams of communication with multiple mentors	1. Weekly meetings with team mentor to keep everyone on the same page 2. Clearly stating plans design criteria/decisions well ahead of manufacturing 3. Follow-up meeting to present alternative designs	3C	1. Keep Team Mentor connected with team 2. Use past experiences to prevent conflicts
Launch scheduling conflict	1. Poor planning	2D	1. Enforce policy of "skill redundancy" where at least two people know how to operate each system or assemble each component in-field	1. Schedule launches 6 weeks in advance 2. Communicate during team meetings with increasing frequency as we get closer to launch	2D	1. Plan launches in advance 2. Communicate all dates with team in advance



Loss of documentation	1. Computer crash	2C	1. Backing up versions of the document sharing system 2. Having team leads re-record important design plans	1. Utilizing cloud software to auto-save and back-up all documentation 2. Using USB drives to store information	2D	1. Save CAD files frequently 2. Keep auto-save on for all Microsoft documentation
Failing to meet outreach goals	1. Poor planning 2. Poor turnout for events	3D	1. Use VADL network to plan last-minute events 2. Expand to virtual events to reach more students	1. Reach out to 80 schools 2. Following up via email 3. Making connections in person and through vanderbilt professors	3E	1. Send thank-you's to points of contact for outreach events 2. Stay connected for future VADL events 3. Expand network of school connections

Figure 105: Project management risks matrix

6 Project Plan

6.1 VADL Internal Requirements Derivation and Verification

Table 69: VADL General Requirements

Req #	Description	Design Requirements	NASA Requirement	Method	Verification Details
General Requirements					
Program Management					
1.1.1	VADL team standups shall be conducted three times a week, informed of and participate in provided school is in session.	All VADL team members will be informed of and participate in three standup sessions a week.	N/A	I	VADL President will initiate standups on designated dates and times. All VADL team members will either be in attendance or inform Team Lead of absence with an update on work done.
1.1.2	Adult Mentor presentation meetings shall be conducted once a week, provided school is in session.	Necessary VADL team members will be informed of and help present a weekly presentation with Advisor.	N/A	I	VADL President and Adult Mentor will initiate weekly meetings on a designated date and time. VADL team members with items to present will be in attendance.
1.1.3	A Gantt chart with deadlines on deliverables and test dates will be followed throughout the project.	A Gantt chart discussing VADL milestones will be published for team members to reference.	N/A	I	VADL President and Team Leads will sign off on deliverables and tests according to Gantt chart milestones. Gantt chart will be updated based on schedule changes.
1.1.4	VADL Team Leads will be responsible for delegating tasks related to their team's deliverables, and meeting regularly to evaluate progress and next steps.	All VADL Team Leads will provide tasks with their teams regularly to ensure deliverables are on time.	N/A	I	VADL President will assess team progress at standups. Team members will communicate with team leads if their tasks do not suite them or if deadlines will not be met.

Req #	Description	Design Requirements	NASA Requirement	Method	Verification Details
Financials					
1.2.1	The VADL team shall maintain a centralized budget and track expenses on a centralized sheet that will track all purchases made by the team.	VADL team members will budget and order sheet.	N/A	I	All VADL orders will be conducted weekly through the centralized budget and order sheet.
1.2.2	A 15% contingency fund shall be maintained for emergency expenses only, as deemed by the VADL President and an Adult Mentor.	VADL President will set aside requested contingency funds and inform team members what situations constitute an emergency that could access said funds.	N/A	I	VADL President will have awareness of amount of money remaining within the contingency fund.
Outreach and Engagement					
1.3.1	VADL team members shall provide instructional STEM lessons to K-12 students within the Nashville community.	VADL members will conduct outreach to K-12 schools in the Nashville area, providing person STEM presentations and learning activities.	1.1	I	The outreach team leader will keep track of scheduled events and look for opportunities to engage with the communities with the help of all VADL members
1.3.2	VADL-hosted outreach events shall be designed to be engaging and accessible, ensuring meaningful participation for audience of all ages.	Events will incorporate videos, audience interaction, creative assignments, and hands-on activities to engage the targeted audience.	1.1	I	VADL team members will assess students' engagement with quizzes and hands-on activities at the end of the lessons.
1.3.3	The VADL team shall use social media to share its work and progress with the public.	The VADL team will run social media platforms, including Instagram, X, YouTube, LinkedIn, and the team's official webpage.	1.2	I	Ongoing evaluation and monitoring of VADL social media accounts shall be conducted to ensure effective engagement.
1.3.4	VADL shall reach a total of at least 2000 participants in all outreach and engagement events throughout this project cycle.	Attendance will be recorded in all outreach and engagement events throughout this project cycle.	N/A	I	The outreach team leader will confirm attendance with educational institutions and document participation at all outreach and engagement activities.

Req #	Description	Design Requirements	NASA Requirement	Method	Verification Details
Vehicle Requirements					
Launch Vehicle Construction					
2.1.1	Each structural tension member within the load path of the vehicle shall be designed with a UTS safety factor of at least 2.5.	Each structural component (in-members within the load path of the vehicle) shall be designed with a UTS safety factor of at least 2.5.	N/A	A	Hand calculations, ANSYS Mechanical, manufacturer's website.
2.1.2	Each structural compression member within the load path of the vehicle shall be designed with a UTS safety factor of at least 2.5.	Each structural component (in-members within the load path of the vehicle) shall be designed with a UTS safety factor of at least 2.5.	N/A	A	Hand calculations, ANSYS Mechanical, manufacturer's website.
2.1.3	All composite layups performed by VADL shall have an off-45 degree offset pattern to set pattern. maximize its multi-directional strength.	All composites will be designed formed by VADL to be fabricated with such an off-45 degree offset pattern to set pattern.	N/A	I	Enforcement during fabrication, examination of cut composite edge for desired pattern.
2.1.4	All brittle-failure materials and welds shall be directly load tested them separate from load tested above their maximum expected load.	Qualify brittle components by and welds shall be directly load testing them separate from load tested above their maximum expected load.	N/A	T	Direct load testing and material inspection.
2.1.5	Load bearing and Aerodynamic structures are designed with manufacturing in mind, weighed against time, cost, and feasibility.	Apply DFMA principles during the design process.	N/A	A	Manufacturing processes are well documented, easily executed, and repeatable.
2.1.6	Minimize drag force on vehicle through implementation of aerodynamic geometries.	Minimize drag force of vehicle.	N/A	A	Utilizing literature and CFD, the drag on the rocket shall be analyzed and minimized.
2.1.7	Vehicle shall be designed to accommodate both primary and backup motors.	Vehicle design will not be impacted based on a change of motor.	N/A	A, D	Simulations will indicate that vehicle can perform with backup motor. Backup motor will physically be able to fit within the vehicle

Req #	Description	Design Requirements	NASA Requirement	Method	Verification Details
Apogee Control System					
2.2.1	Vehicle maintains a static stability margin of greater than 2 when ACS fins are deployed.	The vehicle SSM will be greater than 2.	2.11	A	CFD analysis verifies that vehicle SSM is above 2 when fins are fully deployed.
2.2.2	ACS fins have minimal effect on vehicle CD when not deployed.	CD of rocket is not drastically increased compared to rocket without ACS.	N/A	A	CFD analysis has yielded an average CD of 0.42 across 50-600 fps.
2.2.3	ACS fins may not deploy below 3500 ft AGL.	ACS fins may only deploy above 3500 ft AGL.	2.1	T	ACS flight computer has been tested using a pressure cooker to simulate flight and confirmed that fins will not be actuated below 3500 ft AGL.
2.2.4	ACS shall not induce a roll or lift effect on the rocket, only inducing drag.	ACS will only induce a drag on the rocket.	N/A	I	Symmetrical design that has all induced roll and lift moments have opposing reactions.
2.2.5	ACS shall be located aft of CG.	ACS located aft of CG.	N/A	I	Fulscale rocket CG will be measured to ensure ACS fins are aft of it.
2.2.6	Failure of gearbox will not destabilize vehicle.	Airfoils held at aerodynamic center to not destabilize flight should gear box fail.	N/A	A, D	Subscale flights and wind tunnel tests.
Parachute Detachment System (PDS)					
2.3.1	Shall not yield under main parachute shock and shall be repeatable.	PDS shall not yield under repeated usage.	2.4	A, T	Capstan Calculations and load tests shall be conducted to verify repeatability.
2.3.2	Shall separate the shock cord link from the tail section with 100% reliability.	PDS shall detach shock cord reliably.	N/A	D	Test parachute detachment under field conditions 20+ times.
2.3.3	Maintain tension in the shock cord during rocket ascent to engage shockcord friction.	PDS will maintain friction in the cord during rocket ascent to shock cord during ascent.	N/A	A	Design PDS with tensioned blast plate to maintain tension.
2.3.4	Electrical system supplies appropriate voltage off-the-shelf to EM latch.	PDS supplies appropriate voltage to EM latch.	N/A	A, I	PDS supplies appropriate voltage to EM latch

Req #	Description	Design Requirements	NASA Requirement	Method	Verification Details
2.3.5	The PDS electronics shall be able to run continuously for at least 5 hours.	Payload electronics will be able to run for 5 hours.	2.2	T	This will be tested through a runtime test where the system will be on standby for 4 hours and 45 minutes and then run through detachment operations.
Leg Deployment Mechanism (LDM)					
2.4.1	Legs deploy at drogue with 100% reliability.	Legs always deploy.	N/A	T	Test LDM through 5+ parachute deployment tests and 20+ in lab decoupling tests.
2.4.2	Passive system that doesn't require any electrical components.	System passively actuates.	N/A	A, I	LDM is designed to actuate using potential energy from springs.
2.4.3	LDM shall stand Payload a diagonal distance from the ground to collect soil.	LDM holds up Payload for digging.	N/A	A	LDM leg length shall be designed to hold payload above the ground at a distance the shovel can dig.
2.4.4	Transfer parachute shock load between RBS and PDS.	LDM shall have proper load paths through different sections.	N/A	A	LDM has designated load paths for shock to go through.
2.4.5	Before deployment legs are stored full inside the airframe.	Legs are stored in airframe.	N/A	A	LDM legs shall be designed to be stored in the airframe.
Payload Requirements					
Orientation-Independent					
3.1.1	Landing Orientations shall not impact on payload success.	Payload mission requirements shall be satisfied via any landing orientation.	N/A	D	Soil collection mechanism either is able to reorient itself or does not depend on the orientation.
3.1.2	In the event the payload displaces itself during collection, the payload shall be able to continue soil collection.	Soil collection is able to continue places itself after payload is displaced.	N/A	T	Soil collection shall begin and it will continue collection soil at which it will be displaced.
3.1.3	Payload shall integrate into the rocket within ≤ 30 minutes using standardized fasteners.	Mounting points match bulkplate interface pattern.	N/A	I, T	Timed integration trial with flight team.

Req #	Description	Design Requirements	NASA Requirement	Method	Verification Details
Soil Extraction					
3.2.1	The shovel shall autonomously collect at least 100 mL of soil.	The shovel has to have the necessary dimensions to collect 100 mL soil safely over 23 rotations where it is taking larger volumetric passes.	4.1	A, D	This is referencing our soil collection calculation and can be measured physically by pouring out collected soil.
3.2.2	Soil collection shall not take more than 10 minutes to complete from landing not including analysis.	The rpm of the payload bay must be sufficient to complete the 23 rotations in under 10 mins.	4.1.1	A	This will be verified by dividing payload rotations by rpm of the payload bay to solve for minutes.
3.2.3	Shovel extension shall be completed in less than 24 payload bay rotations	the gear ratio of the sandwiched gearbox should be at least 47:1 output to input	N/A	A, D	this will be verified by integration testing of the electronics to ensure they rotate the payload 23 times and that the shovel is extended fully by the last rotation.
3.2.4	Shovel extension shall be repeatable over 20+ trials.	The gear teeth must remain in spec at all times during flight and shocks.	N/A	T	This will be verified through repeated testing of the efficacy of the opening mechanism.
3.2.5	The torque on the shovel face shall not exceed 10 Nm.	The shovel has to dig at such an angle that it bites through soil effectively so that excess torque is not induced. additionally the geometry must be designed to reduce frictional losses between the shovel and dirt.	N/A	A	This is referencing our shovel torque calculation with added torque for safety and can be verified by reading the power supplied by the motor.
3.2.6	All rotating parts shall be lubricated or coated to prevent seizing under dust contamination.	Use PTFE-backed shovel and sealed gearbox.	N/A	I	Inspect after soil tests for smooth operation.
3.2.7	The opening mechanism shall have an aft-fore length of no more than 2 inches	Choose lightweight materials weigh no more than 0.6 lbs and (like Onyx) for gear and bulk have an aft-fore length of no plate manufacturing more than 2 inches	N/A	I	Weight and measure the length of the opening mechanism physically
3.2.8	All critical components shall have a failure factor of safety of at least 2	choose robust materials for all structurally significant parts	N/A	A	verify the factor of safety is met for all parts based on hand calc analysis and FEA
Soil Containment					

Req #	Description	Design Requirements	NASA Requirement	Method	Verification Details
3.3.1	Soil containment chamber	The inner volume of the chamber shall house at least 250mL must equal or exceed 250mL combined soil and water.	4.1	A	This will be verified by measuring the volume of the chamber physically to deduce the amount of material it can house.
3.3.2	Soil containment chamber	Sealant must be used to trap moisture in the chamber. shall be waterproof.	N/A	D	This will be verified by filling it with water and testing for leakages.
3.3.3	Soil collected shall not fall out of chamber when orientation changes.	Chamber geometry or door mechanism shall keep soil in chamber during reorientation.	N/A	D	With soil in the chamber.
3.3.4	Containment chamber shall have the ability for soil to be extracted and for the system to be reset between trials.	Adequate space, and integration have the ability for soil to be ease to disassemble and reassembled payload in < 2 hours.	N/A	D	2 consecutive payload tests with soil extraction and system reset between
3.3.5	Soil shall interface with all 3 sensor membranes regardless of orientation	Chamber sizing and sensor orientation ensures proper interface with soil water slurry.	N/A	D	full payload integration demonstration with sensor testing.
3.3.6	Soil chamber shall be capable of securing all sensors and pre-venting in flight disassembly	Proper securing of sensors and protection under flight loads.	N/A	D	Demonstrate safe sensor securement during drop test.

Req #	Description	Design Requirements	NASA Requirement	Method	Verification Details
Electrical and Sensing					
3.5.1	The payload electronics shall have water-tight isolation from the collection bay.	Payload electronics shall be isolated from collection bay.	4.1	D	This will be demonstrated by filling the collection bay with water and observing any leakage.
3.5.2	The payload shall track when the rocket is in pre-flight, launched, and landed state using an IMU.	Computing unit will have constant values to reference and determine flight states from IMU values.	4.1	T	This will be tested through examining IMU state records during drop tests.
3.5.3	The payload shall sample IMU acceleration, yaw, pitch, roll, and pressure at least 100 Hz with deterministic timing.	Payload IMU will be capable of determining acceleration, yaw, pitch, roll, and pressure at least 100 Hz with deterministic timing.	4.1	D	This will be verified by sampling from IMU with printed timestamps, and measuring the average rate of sampling.
3.5.4	The payload electronics shall log IMU data to non-volatile memory.	IMU acceleration, orientation, and altitude will be logged to on-board SD card.	4.1	D	Payload electronics and IMU will be powered on before, removing SD card, and verifying stored flight data file contains requisite IMU data.
3.5.5	The payload shall derive altitude from IMU pressure data.	Altitude will be calculated from pressure data using ground level pressure value.	4.1	D	Ground pressure will be sampled using the IMU and compared to external barometer.
3.5.6	The payload shall detect launch based on altitude and acceleration threshold.	Launch will be detected from consecutive increasing altitude data points.	4.1	D	This will be verified by passing mock IMU data to payload program to trigger "LAUNCHED" state.
3.5.7	The payload shall detect descent based on continuously decreasing altitude.	Descent will be detected from consecutive decreasing altitude data points.	4.1	D	This will be verified by performing pressure cooker test on payload electronics to trigger "DESCENT" state.
3.5.8	The payload shall detect landing based on low-motion thresholds.	Landing will be detected from consecutive non-changing altitude data point.	4.1	D	This will be verified by letting payload electronics remain motionless in pressure cooker to trigger "LANDED" state.
3.5.9	The payload shall calibrate initial altitude using IMU.	Initial altitude will be recorded at payload startup and used as a reference point.	4.1	D	Pressure sampled during test will be fed to altitude calculation, which will be verified with GPS altitude reading.

Req #	Description	Design Requirements	NASA Requirement	Method	Verification Details
3.5.10	The payload shall maintain flight-logic accuracy > 16g acceleration.	The acceleration thresholds for launch and descent will be set to reasonable values lower than IMU saturation point.	4.1	T	This will be tested by passing mock IMU data and verifying flight state triggering despite IMU saturation.
3.5.11	The payload shall track the time in milliseconds after landing.	Computing unit will have a designated timer to track time after IMU detects landing.	4.1.1	D	This will be demonstrated by the computing unit displaying/recording accurate timing when a landed state is indicated.
3.5.12	Payload operations will halt after 15 minutes from landing.	Computing unit will halt all operations after internal timer reads 15 minutes from landing.	4.1.1	D	This will be demonstrated by the computing unit halting sensor recording after 15 minutes from landed state indication.
3.5.13	The payload shall drive the collection motor for 23 rotations after landing.	Computing unit will drive the motor and stop after 23 rotations as determined by the IMU orientation.	4.1.1	D	This will be demonstrated by the computing unit rotating the motor 23 rotations from landed state indication.
3.5.14	The payload shall repeatedly record soil nitrate content, pH level, electrical conductivity and time after landing to a file on a SD card after landing.	Computing unit will calculate record soil nitrate content, pH level, electrical conductivity and time after landing onto an SD card after landing.	4.2.1	D	This will be demonstrated by the computing unit writing all four data points onto an SD card from landed state indication.
3.5.15	The payload electronics shall be able to run continuously for at least 5 hours.	Payload electronics will be able to run for 5 hours.	2.2	T	This will be tested through a runtime test where the system will be on standby for 4 hours and 45 minutes and then run through soil collection operations.
3.5.16	The payload shall validate sensor health at boot.	Computing unit will indicate if reading is being generated by sensor.	4.2	D	This will be demonstrated through examining an indicator that is true to sensor operation.
3.5.17	The payload sensors shall accurately sample the soil's pH.	Payload will be able to sense pH accurately.	4.2	T	This will be tested by having calibrated sensor test a sample with a known pH and seeing the variance in its reading.
3.5.18	The payload sensors shall accurately sample the soil's Electrical Conductivity.	Payload will be able to sense electrical conductivity accurately.	4.2	T	This will be tested by having calibrated sensor test a sample with a known electrical conductivity and seeing the variance in its reading.

Req #	Description	Design Requirements	NASA Requirement	Method	Verification Details
3.5.19	The payload sensors shall accurately sample the soil's Nitrogen-Nitrate.	Payload will be able to sense nitrate accurately.	4.2	T	This will be tested by having calibrated sensor test a sample with a known nitrate content and seeing the variance in its reading.
3.5.20	The payload electronics shall be able to automatically conduct its mission scope after descent.	Payload electronics will conduct operations when IMU detects a landed state.	4.1, 4.2	T	This will be tested by feeding artificial data to the IMU that indicate landing, and by conducting a full drop test.
3.5.21	The payload electronics shall be physically secured and electrically wired such that forces of launch, ascent, descent and landing do not damage the assembly.	Payload electronics shall have an enclosure and circuitry that does not allow for disconnects or damage to occur < 30 g.	4.1, 4.2	T	This will be tested by conducting a full drop test.
ACS					
3.6.1	ACS shall increase the CD of the rocket to at least 2.0 relative to the rocket body frontal area.	Deployed ACS CD is above 2.0.	N/A	A	CFD analysis has verified that CD is above 2.0 when fins are fully deployed.
3.6.2	The ACS shall modulate the final competition apogee to be within 5% of the target.	Apogee is within 5% of 4200 ft	2.1, 2.3	T	Simulations shall be verified using full-scale vehicle flight.
3.6.3	The ACS electronics shall be able to run continuously for at least 5 hours.	ACS electronics will be able to run for 5 hours.	2.2	T	Run full electrical system until it takes for LiPo cell voltage drops to 3 V.

Req #	Description	Design Requirements	NASA Requirement	Method	Verification Details
Recovery Requirements					
Hardware					
4.1.1	Each shock cord shall have a total length of at least 3x the length of the vehicle section it joins.	Size shock cords based on lengths	N/A	I	Verification of section lengths after manufacturing. Measurement of shock cord lengths.
4.1.2	When shock cords are taut, each section must maintain at least 10 feet of separation between sections during descent.	Size shock cords to ensure at least 10 feet of separation	N/A	I	Measurement of shock cord lengths. Layout of independent sections under taut shock cord lengths and measurement of clearance.
4.1.3	The recovery system shall be designed to ensure that the tail section of the rocket lands first.	Design recovery system to ensure that the tail section lands first. Deploy main parachute from nose cone.	N/A	I	Layout of independent sections under taut shock cord lengths and ensure that the tail section is furthest from main parachute.
4.1.4	All shock cords shall maintain a factor of safety of at least 4.0 during peak accelerations experienced during flight (main deployment).	Size drogue and main parachutes to minimize snatch force at main deployment. Select shock cord material with a high ultimate strength.	N/A	A	Calculate predicted snatch force at main deployment using terminal velocity under drogue parachute.
4.1.5	Each shock cord must be ≥ 5 ft to reduce deployment forces.	Ensure that each shock cord is at least 5 feet long.	N/A	I	Measurement of shock cord lengths after they are cut.
4.1.6	The parachute shall be detached within 2 seconds of controller and payload electronics detecting criteria for "Landed" state of rocket.	Electrically independent microcontroller and IMU will command an EM latch to detach the parachute upon landing detection.	N/A	D	Perform short drop test to trigger landed state and verify EM latch actuation.
4.1.7	Bulkplates shall be attached to the airframe using radial bolts to allow for rapid assembly and repair.	Bulkplate lips shall be designed with 1.5x extra bolt diameter thickness in order to allow safe radial bolt-in.	N/A	I	All bulkplates will be designed to use radial bolts.

Req #	Description	Design Requirements	NASA Requirement	Method	Verification Details
Avionics					
4.2.1	The chosen avionics system shall sample at a rate of at least 50 Hz during ascent.	Select altimeter with a sampling rate of at least 50 Hz and ensure it has sufficient storage to store data points.	N/A	A	Review of chosen altimeter's data sheet. Testing within pressure chamber and review of logged data.
4.2.2	The chosen avionics system and battery shall be capable of running for 4 hours before battery drainage.	Select altimeter with efficient power usage. Select altimeter battery with sufficient capacity.	3.4	T	Battery drainage test of altimeter system.
4.2.3	An electrically independent RF/EM shielded compartment GPS tracking device shall separate from other electronic transmit the launch vehicle's systems. location continuously for the flight and recovery process to a ground receiver for up to 4 hours.		3.12, 3.13	T	Perform drain test of GPS system, transceiving to ground station using flight designated hardware and mounting solution.
Energetics					
4.3.1	Energetics shall be sized to give a safety factor of 4.	Calculate black powder masses with a safety factor of 4.	N/A	I	Calculate black power sizing. Weigh final amounts and ensure a factor of safety of 4.
4.3.2	Backup energetics charges shall be 20% greater than the main charge.	Calculate backup black powder masses to have 20% more mass than the main charge.	N/A	I	Calculate backup black powder sizing. Weigh final amounts and ensure that the backup charges weigh 20% more.
Safety Requirements					
5.1	All safety protocols and PPE will be enforced as a team, documentation used by the VADL team shall list out safety protocols within the Safety necessary Personal Protective Binder. PPE will be readily available within the lab. checks, and procedures of use.		5.1	I	Inspection of PPE prior to work done, and Safety Binder safety protocol steps followed while work is done.
5.2	VADL shall create, maintain and enforce safety protocols and an approval hierarchy based on process risk levels. A documented approval hierarchy will be produced to delegate and an approval responsible team member on proving tasks.		5.2	I	Hierarchy of approval published for the team. Signed safety statement by each member. Frequent consultation and consideration of safety procedures.

Req #	Description	Design Requirements	NASA Requirement	Method	Verification Details
5.3	VADL team members shall adhere to all FAA, NAR, Tennessee State, Davidson County, and Nashville City regulations when approving tasks on the team. VADL team members will research and understand relevant regulations when assembling and testing components.	Responsible team members will here to all FAA, NAR, Tennessee State, Davidson County, and Nashville City regulations when approving tasks on the team. VADL team members will research and understand relevant regulations when assembling and testing components.	N/A	I	Procedures checked against relevant regulations by responsible team member.
5.4	VADL team leads shall complete an Incident Report Form findings related to an incident following any incident that threatened the safety of team members or team environment. VADL team leads shall compile the Student Safety Officer to explain the incident and its lessons learned.	VADL team leads shall compile an Incident Report Form findings related to an incident following any incident that threatened the safety of team members or team environment. VADL team leads shall compile the Student Safety Officer to explain the incident and its lessons learned.	5.2	I	Incident Report Form will be signed by responsible team lead and Student Safety Officer within designated time from incident.

6.2 Testing Plan

The NASA USLI competition culminates in the competition launch in late April. VADL is determined to verify every aspect of the rocket individually and fully assembled to ensure the team's success.

6.2.1 Vehicle

Materials

Table 70: Airframe (Spiral Wound Epoxy Glass Tubing (Fiber Glass)) Load Testing

Load Test	Flight Application	Impact	Requirement(s)	Team Member(s)	Status
Bolt tear out	Parachute shock	Determine failure load on airframe through bolt-airframe interface.	VADL 1.1	JD, RN, JR	IP
Compression	Motor burn	Determine failure load on airframe under axial compression.	VADL 1.1	JD, RN, JR	IP
Hoop	Landing shock	Determine failure load on airframe under hoop compression.	VADL 1.1	JD, RN, JR	IP

Table 71: 3D Printed Filaments (PLA, PETG, ONYX) Load Testing

Load Test	Flight Application	Impact	Requirement(s)	Team Member(s)	Status
Tension	All	Determine failure load of material in tension	VADL 1.1	JD, RN, JR	NV
Compression	All	Determine failure load of material in compression	VADL 1.1	JD, RN, JR	NV
Bolt Shear	All	Determine failure load of material in retaining bolts	VADL 1.1	JD, RN, JR	NV

Avionics

Table 72: Avionics (EasyMini V2) Pressure Tests

Pressure Test	Flight Application	Impact	Requirement(s)	Team Member(s)	Status
Pressure Cooker	Rocket ascent	Verify altimeters and avionics	NASA 3.1 NASA 3.3	CS, BR	IP
Shock Tube	Rocket ascent	Verify altimeters and avionics	NASA 3.1 NASA 3.3	CS, BR	NV

6.3 Budgeting

Projected Funding

Our fundraising initiative has been successful thus far, and we have raised sufficient funds to cover our current expenses. We have been given \$5,000 from the Dalton VADL Fund, \$5,000 from the Vanderbilt Dean's Fund, \$4,000 from past alumni, and have \$1,800 in excess funds. See the figure below for an updated figure of our fundraising.

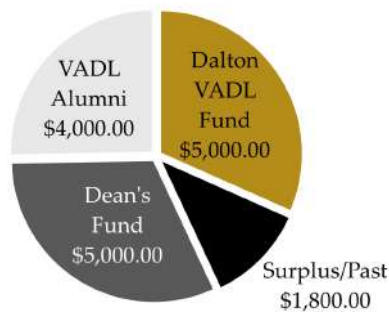


Figure 106: Breakdown of current funds raised

Expense Breakdown

Our current expenses to date are \$4,167 and are all displayed in the chart and table below. All of our expenses are tracked by our treasurer, team leaders, and faculty mentor. Before any item is purchased, our mentor and a team leader must approve the expenditure to ensure it is necessary and that we don't already have the item in stock. So far, about 25% of our expenses have gone to electrical costs, 25% to vehicle costs, 42% to payload, 5% to safety, and the remaining 3% to general expenses.

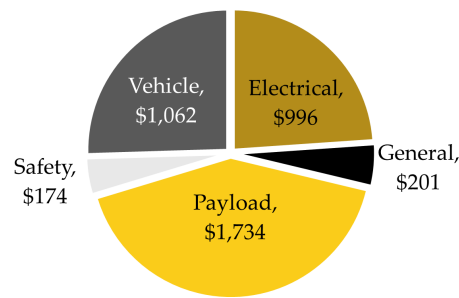


Figure 107: Breakdown of current expenses

Table 73: VADL Expenses Breakdown



Project Segment	Date Ordered	Team Member	Expense Catagory	Vendor	Quantity	Cost	Total Cost	Description
Electrical Expenses								
\$ 996.34								
Fall	6-Oct	Joel Berinstein	Electrical	NTsensors	1	263.98	263.98	Mini Reference ISE Electrode
Fall	6-Oct	Joel Berinstein	Electrical	NTsensors	1	422.37	422.37	pH Ion Selective Electrode
Fall	6-Oct	Sadie Pullen	PDS	DigiKey	1	1.6	1.6	electrical connector
Fall	9-Oct	Joel Berinstein	Electrical	DigiKey	2	3.5	7	BNC female to SMA Male Connector
Fall	9-Oct	Joel Berinstein	Electrical	Newark Electronics	2	5.8	11.6	MA40S4S Ultrasonic Transmitter
Fall	9-Oct	Sadie Pullen	Electrical	DigiKey	25	3.76	3.76	Rectangular Connectors
Fall	9-Oct	Joel Berinstein	Electrical	AtlasScientific	3	7.99	23.97	SMA Breakout Board
Fall	14-Oct	Thor Hammer	Electrical	Amazon	1	15.99	15.99	Automotive connectors
Fall	14-Oct	Thor Hammer	Electrical	Amazon	1	24.42	24.42	Dev Board
Fall	14-Oct	Thor Hammer	Electrical	Amazon	1	36.99	36.99	Digital Soldering Iron
Fall	14-Oct	Joel Berinstein	Electrical	AtlasScientific	1	67.99	67.99	EZO™ Conductivity Circuit
Fall	14-Oct	Thor Hammer	Electrical	Amazon	1	45.99	45.99	LiPo (2 pack)
Fall	14-Oct	Thor Hammer	Electrical	Amazon	2	16.92	33.84	LiPo Battery
Fall	14-Oct	Thor Hammer	Electrical	Amazon	1	12.49	12.49	PCB Pack (7x9, 10 ct)
Fall	14-Oct	Thor Hammer	Electrical	Amazon	1	4.19	4.19	Soldering Flux
Fall	14-Oct	Thor Hammer	Electrical	Amazon	1	15.17	15.17	Soldering Iron Handle
Fall	14-Oct	Thor Hammer	Electrical	Amazon	1	4.99	4.99	Soldering Mat
General Expenses								
\$ 200.77								
Fall	14-Oct	Jamie Danis	General	McMaster	10	5.62	56.2	1/4" - 20 Al Rods (3')
Fall	14-Oct	Jamie Danis	General	McMaster	3	9.79	29.37	1/4"-20 Al Nuts (100 pack)
Fall	14-Oct	Jamie Danis	General	McMaster	2	12.6	25.2	1/4"-20 Al Washers (100 pack)
Fall	14-Oct	Jamie Danis	General	Amazon	1	33.28	33.28	8" Calipers
Fall	14-Oct	Ben Racape	General	Amazon	1	16.96	16.96	Multi-Adapter
Fall	14-Oct	Jamie Danis	General	McMaster	1	23.12	23.12	T-Slotted Extruded Al Framing (4 ft, double slot)
Fall	14-Oct	Jamie Danis	General	McMaster	1	16.64	16.64	T-Slotted Extruded Al Framing (4 ft, single slot)
Payload Expenses								
\$ 1,733.56								
Fall	14-Aug	Evan Ticknor	Payload	Amazon	1	9.99	9.99	1.6" x 16.5" auger



Fall	14-Aug	Jamie Danis	Payload	McMaster	1	3.63	3.63 1/4" round bar
Fall	14-Aug	Jamie Danis	Payload	McMaster	1	4.59	4.59 1/4-20 threaded rod
Fall	14-Aug	Jamie Danis	Payload	McMaster	1	5.36	5.36 3/8" round bar
Fall	14-Aug	Rais Nurhidajat	Payload	Amazon	1	97.42	97.42 RS485 Modbus Soil Sensor 7 in 1
Fall	26-Aug	Evan Ticknor	Payload	Amazon	3	\$79.72	\$239.16 7-in-1 soil sensor
Fall	26-Aug	Evan Ticknor	Payload	Amazon	1	\$9.99	\$9.99 Encoder
Fall	26-Aug	Evan Ticknor	Payload	Amazon	1	\$90.00	\$90.00 Motor Controller
Fall	26-Aug	Evan Ticknor	Payload	Amazon	1	\$15.39	\$15.39 Motor Driver
Fall	28-Aug	Evan Ticknor	Payload	Amazon	1	\$14.99	\$14.99 Kevlar String
Fall	1-Sep	Evan Ticknor	Payload	Amazon	1	\$32.61	\$32.61 soil test kit
Fall	1-Sep	Evan Ticknor	Payload	Amazon	1	\$9.99	\$9.99 TTL converter
Fall	8-Sep	Evan Ticknor	Payload	Amazon	1	24.84	24.84 MDF board 8 pack
Fall	8-Sep	Evan Ticknor	Payload	Amazon	1	39.99	39.99 Motor with gearbox
Fall	8-Sep	Evan Ticknor	Payload	Amazon	2	11.96	23.92 Power distribution board
Fall	8-Sep	Evan Ticknor	Payload	getfpv	1	24.99	24.99 Power distribution board
Fall	8-Sep	Evan Ticknor	Payload	Amazon	1	34.99	34.99 Soil
Fall	15-Sep	Evan Ticknor	Payload	Digikey	1	4.01	4.01 electrical Connector
Fall	15-Sep	Catherine Knox	Payload	Mcmaster	1	26.54	26.54 lead screw rod , 1/4 - 20
Fall	15-Sep	Catherine Knox	Payload	Mcmaster	1	6.45	6.45 lead screw, 1/4 -16
Fall	15-Sep	Evan Ticknor	Payload	Amazon	2	80.23	160.46 soil sensor
Fall	15-Sep	Evan Ticknor	Payload	Amazon	2	29.4	58.8 STM32 Nucleo
Fall	22-Sep	Evan Ticknor	Payload	McMaster	2	8.2	16.4 Ball Bearing
Fall	6-Oct	Evan Ticknor	Payload	McMaster	2	7.45	14.9 1/4" roller bearing
Fall	6-Oct	Evan Ticknor	Payload	McMaster	1	9.24	9.24 10 thou shims
Fall	6-Oct	Evan Ticknor	Payload	McMaster	8	19.13	153.04 15 tooth nylon gear
Fall	6-Oct	Evan Ticknor	Payload	McMaster	1	20.5	20.5 20 tooth nylon gear
Fall	6-Oct	Evan Ticknor	Payload	McMaster	1	36.83	36.83 40 tooth nylon gear
Fall	6-Oct	Evan Ticknor	Payload	McMaster	1	39.75	39.75 50 tooth nylon gear
Fall	6-Oct	Evan Ticknor	Payload	McMaster	1	47.5	47.5 60 tooth nylon gear
Fall	6-Oct	Evan Ticknor	Payload	McMaster	10	11.66	116.6 6mm flanged roller bearing
Fall	6-Oct	Sean Confoy	Payload	McMaster	2	8.2	16.4 Ball Bearing
Fall	6-Oct	Sean Confoy	Payload	McMaster	1	9.74	9.74 Ball Bearing
Fall	6-Oct	Catherine Knox	Payload	Amazon	1	9.95	9.95 cheesecloth
Fall	6-Oct	Catherine Knox	Payload	McMaster	1	2.87	2.87 O-rings
Fall	6-Oct	Catherine Knox	Payload	Amazon	2	10.92	21.84 Rubber gasket sheet - cutting



Fall	6-Oct Catherine Knox	Payload	Amazon	2	11.54	23.08 Rubber gasket sheet -laser cutting
Fall	6-Oct Sean Confoy	Payload	McMaster	2	3.54	7.08 Shaft Collar
Fall	9-Oct Evan Ticknor	Payload	McMaster-Carr	1	28.76	28.76 30 tooth gear
Fall	9-Oct Evan Ticknor	Payload	McMaster-Carr	6	11.66	69.96 6mm flanged roller bearing
Fall	15-Sep Catherine Knox	Payload	Mcmaster	1	35.97	35.97 flange for nut
Fall	15-Sep Catherine Knox	Payload	Mcmaster	1	12.86	12.86 linear rod - 3 feet
Fall	15-Sep Catherine Knox	Payload	Mcmaster	1	34.8	34.8 nut for lead screw
Fall	15-Sep Catherine Knox	Payload	Mcmaster	2	17.11	34.22 o rings
Fall	15-Sep Catherine Knox	Payload	Mcmaster	1	6.92	6.92 o rings
Fall	15-Sep Catherine Knox	Payload	Mcmaster	1	6.64	6.64 o rings
Fall	15-Sep Catherine Knox	Payload	Mcmaster	1	3.39	6.78 shaft seal o ring
Fall	9-Oct Catherine Knox	Payload	Amazon	1	9.95	9.95 Nylon cloth for mesh to in containment chamber
Fall	9-Oct Catherine Knox	Payload	McMaster-Carr	1	2.87	2.87 O-rings to seal non-rotating shaft (1 pack)
Safety Expenses					\$	174.17
Fall	1-Sep Jamie Danis	Safety	Amazon	1	\$9.79	\$9.79 Danger Tape
Fall	1-Sep Jamie Danis	Safety	Amazon	1	\$24.47	\$24.47 Field First Aid Kit
Fall	1-Sep Jamie Danis	Safety	Amazon	1	\$11.99	\$11.99 Fire Extinguisher Wall Mounts
Fall	1-Sep Jamie Danis	Safety	Amazon	3	\$9.99	\$29.97 LiPO Fire Retardant Bags
Fall	1-Sep Jamie Danis	Safety	Amazon	1	\$32.98	\$32.98 Portable Steel Cans
Fall	5-Sep Jamie Danis	Safety	Amazon	1	\$27.99	\$27.99 Small fume extractor
Fall	5-Sep Jamie Danis	Safety	Amazon	1	\$23.99	\$23.99 Soldering Helping Hands
Fall	14-Oct Jamie Danis	Safety	McMaster	1	12.99	12.99 Loto Plug Cages (Pack of 4)
Vehicle Expenses					\$	1,062.16
Fall	5-Sep Jamie Danis	Vehicle	Amazon	1	\$21.79	\$21.79 Wood Glue
Fall	22-Sep Jamie Danis	Vehicle	McMaster	1	13.04	13.04 3/8" Squared U-Bolt
Fall	22-Sep Jamie Danis	Vehicle	McMaster	2	4.8	9.6 3/8" Squared U-Bolt
Fall	22-Sep Jamie Danis	Vehicle	McMaster	1	8.26	8.26 8-32 7/8" Bolts
Fall	22-Sep Rais Nurhidajat	Vehicle	Aerotech	2	303.99	AeroTech L1940X-PS RMS-75/3840 Reload Kit (1 607.98 Pack) - 12194P
Fall	22-Sep Jamie Danis	Vehicle	McMaster	5	9.37	46.85 Al 1/4-20 Rod
Fall	22-Sep Jamie Danis	Vehicle	McMaster	1	10.03	10.03 AL Nuts
Fall	22-Sep Jamie Danis	Vehicle	McMaster	1	3.37	3.37 Al washers



Fall	22-Sep Jamie Danis	Vehicle	McMaster	1	10	10 M4 bolts
Fall	22-Sep Jamie Danis	Vehicle	McMaster	1	46.2	46.2 Marine Grade 1/4" Plywood
Fall	22-Sep Jamie Danis	Vehicle	McMaster	1	10.25	10.25 Oversize AL Washers
Fall	22-Sep Jamie Danis	Vehicle	McMaster	1	2.55	2.55 St Nuts
Fall	22-Sep Jamie Danis	Vehicle	McMaster	1	9.5	9.5 St washers
Fall	9-Oct Jamie Danis	Vehicle	Fibreglast	1	51.45	51.45 4 oz Fiberglass fabric, Part 262-C (50 Yard Paclage)
Fall	9-Oct Jamie Danis	Vehicle	Amazon	1	21.99	21.99 Cotton Release Cloth
Fall	9-Oct Jamie Danis	Vehicle	SouthCo	1	113.09	113.09 EM Door Latch
Fall	9-Oct Jamie Danis	Vehicle	Amazon	2	4.47	4.47 Plastic Wrap
Fall	14-Oct Jamie Danis	Vehicle	Amazon	1	9.99	9.99 Cutoff Wheels for dremel
Fall	14-Oct Jamie Danis	Vehicle	Fibreglast	1	61.75	61.75 Product number (Bottom of page): 2160-B
				<i>Total</i>		
				Costs	\$	4,167.00



Remaining Expenses

Based on predictions made by our team leaders, we have about \$9,500 in expenses remaining. Team leaders compiled their remaining expenses, and we compiled them below to ensure we stay within our budget. We also added a 15% contingency fund in case any unexpected costs arise. Based on our current and projected expenses, our total spending for the year will come to nearly \$13,600. We were able to save money by recycling past materials and leftover stock from previous years. We will continue to track and monitor all expenses to ensure we stay under budget.

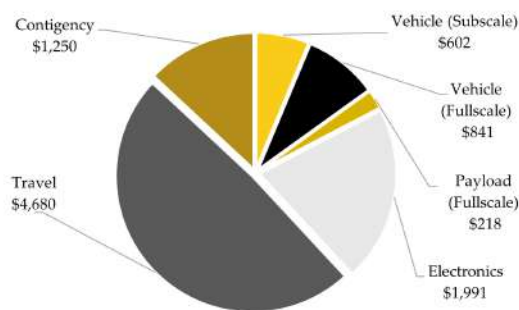


Figure 108: Breakdown of remaining expenses

Table 74: VADL Remaining Expenses Budget



Category	Item	Quantity	Unit Price	Total Price
Vehicle (Subscale)				602.02
	<i>4" G12 Fiberglass Body tube stock</i>	2	141.27	282.54
	<i>4" 6061-T6 Al Round Bar</i>	4	27.53	110.12
	<i>1/8" DragonPlate carbon fiber fin plate</i>	4	17.84	71.36
	<i>Motor hardware</i>	1	138	138
Vehicle (Fullscale)				841.17
	<i>6" G12 Fiberglass Body tube stock</i>	1	279.81	279.81
	<i>6" 6061-T6 Al Round Bar</i>	4	43.76	175.04
	<i>1/8" DragonPlate carbon fiber fin plate</i>	4	96.58	386.32
Payload (Fullscale)				217.6
	<i>6mm aluminum d shaft rod 40mm long</i>	3	3	9
	<i>1/4-20 ID Ball Bearing</i>	4	7.3	29.2
	<i>6mm ID ball bearing</i>	12	14.95	179.4
Electronics				1991.19
	<i>Pololu 5V Step-Down Voltage Regulator D36V5</i>	4	34.95	139.8
	<i>Teensy 4.1 Microcontroller</i>	4	53.2	212.8
	<i>Teensy 4.1 Breakout Board</i>	4	23.9	95.6
	<i>JST-XH Connector Kit (assorted sizes)</i>	1	17.99	17.99
	<i>VectorNav VN-100</i>	1	1,525	1525
Travel				4680
	<i>Transportation</i>	4	70	280
	<i>Lodging</i>	8	400	3200
	<i>Food</i>	8	150	1200
	<i>Net Cost</i>			8331.98
	<i>15% Contingency</i>			1249.797
	<i>Total Cost</i>			9581.777

6.4 Project Timelines

Overview

This year, VADL chose to include two separate, essential timelines, each in the Gantt chart format. The first timeline includes all NASA-specific milestones, such as deadlines for report submissions and official flight dates. The second timeline is a VADL-specific timeline outlining a multi-phase framework VADL will follow throughout the life cycle of the project as outlined below.

Phase 0: Review all NASA guidelines and mission requirements, with an emphasis on getting new members acquainted with the process of competing in NASA's Student Launch Initiative. This phase was completed just after the release of the 2025-2026 handbook.

Phase 1: Solidify concepts and develop initial design ideas for various components of the rocket, specifically the soil collection and sensing mechanism. Discussions of material selection also begin. This process occurred over 3 weeks after the conclusion of phase 0.

Phase 2: Transform initial design drawings into CAD. Research on which sensors and electrical components we would use for soil collection and sensing on the payload. Trade studies and stress tests on the materials to be used for both the payload and vehicle. Form fully detailed assemblies of both the payload and vehicle, and eventually the subscale rocket. All aspects lead to proposal development.

Phase 3: Prototype designs for the payload, specifically the shovel mechanism, using 3D printed materials. We iterated through multiple shovel designs and tested them with different types of soil. Simulations of the basic vehicle structure, along with vehicle design and fiberglass fabrication. Soil-sensing devices are tested to inform decisions about which sensor to use. Subscale rocket manufacturing begins. All aspects lead to PDR.

Phases 4 and 5: Focus on design finalization and testing of full-scale and subscale rockets. Payload integration in the full scale and the successful combination of both the ACS and the PDS in the subscale. Full-scale drop and tip tests, our subscale flight, and vehicle demonstration flight will be performed. Towards the end of phase 5, we will complete CDR.

Phase 6: Revisions to our designs and sub-systems after collecting data from test launches and the drop and tip tests. Evaluate whether a second vehicle demonstration flight will be necessary. All aspects lead to FRR and final launch preparations.

Phase 7: Final launch preparations before heading to Huntsville and competing.

Phase 8: Evaluate and reflect on the performance of our rocket. Determine successes, failures, and what could be conducted differently. All aspects lead to PLAR.

A preliminary timeline of the 2025-2026 season is shown below. These activities and events are outlined in the two separate Gantt charts, each with dates spanning across the entire project duration.

NASA Milestones

- RFP released — Aug 8, 2025.
- Submission: Proposal — Sep 22, 2025 (8:00 a.m. CT).



- Awarded proposals announced — Oct 7, 2025.
- Q&A: Kickoff and PDR — Oct 9, 2025.
- Submission: PDR report/slides/flysheet — Nov 3, 2025 (8:00 a.m. CT).
- Teleconference: PDR — Nov 3–25, 2025.
- Q&A: CDR — Dec 3, 2025.
- Deadline: Subscale flight — Jan 7, 2026.
- Submission: CDR report/slides/flysheet/datasheet — Jan 7, 2026 (8:00 a.m. CT).
- Teleconference: CDR — Jan 14–Feb 5, 2026.
- Q&A: FRR — Feb 11, 2026.
- Deadline: Vehicle Demo Flight (VDF) — Mar 9, 2026.
- Submission: FRR report/slides/flysheet — Mar 9, 2026 (8:00 a.m. CT).
- Teleconference: FRR — Mar 16–Apr 3, 2026.
- Deadline: PDF and VDF re-flight — Apr 6, 2026.
- Submission: FRR Addendum (if applicable) — Apr 6, 2026.
- Q&A: Launch Week — Apr 15, 2026.
- Teams arrive (HSV) — Apr 22, 2026. Launch Week events Apr 23–24
- Launch Day and Backup Launch Day - Apr 25 and Apr 26.
- Submission: PLAR (HSV teams) — May 11, 2026.

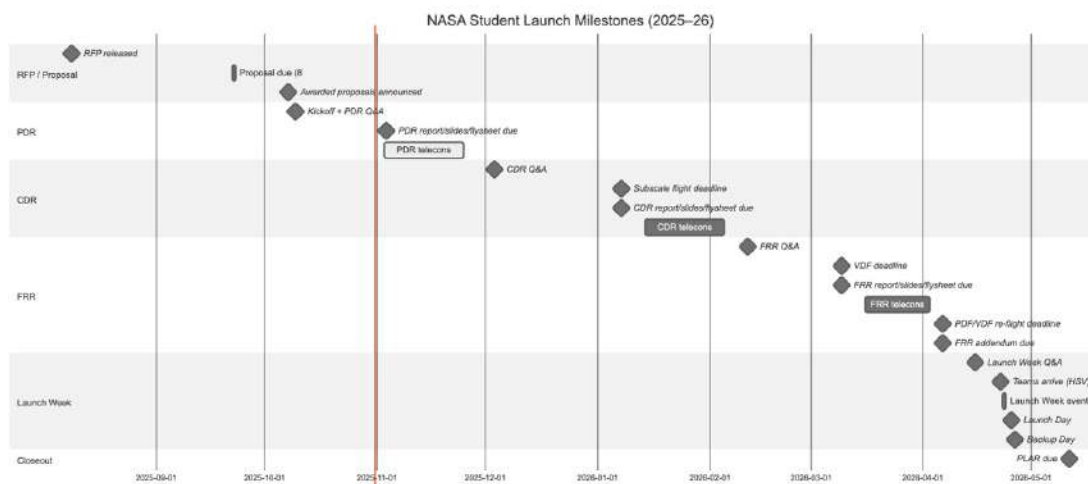


Figure 109: NASA milestones gantt chart

VADL Milestones

- Phase 0: Review NASA documents: Aug 8-Aug 15
- Phase 1: Project Planning and Brainstorming: Aug 8-Aug 29
- Phase 2: Preliminary Design and Testing: Aug 22-Sep 26

- 2.1. Initial Payload Prototyping and Testing: Aug 22-Sep 26
- 2.2. Initial Electronics Trade Studies and Testing: Aug 22-Sep 26
- 2.3. Material procurement and Testing: Sep 5-Sep 26
- 2.4. Proposal: Sep 12-Sep 22

Phase 3: Prototyping and Validating: Sep 19-Nov 7

- 3.1. Prototyping shovel designs (CAD and 3D printing): Sep 19-Oct 20
- 3.2. Advancing soil sensor selection: Sep 19-Oct 13
- 3.3. Developing Vehicle Design (OpenRocket, MATLAB, CAD): Sep 19-Oct 3
- 3.4. Vehicle Manufacturing Prototyping (fiberglass cutting and squaring): Sep 26-Oct 13
- 3.5. Subscale Manufacturing: Oct 17-Nov 7

Phase 4: Subscale Final Design and Testing: Nov 7-Nov 22

- 4.1. Apogee Control System (ACS) design finalization: Nov 7-Nov 12
- 4.2. Parachute Detachment system (PDS) Design finalization: Nov 7-Nov 12
- 4.3. Integration of ACS and PDS in subscale design: Nov 12-Nov 20
- 4.4. Testing of ACS and PDS in test environments: Nov 18-Nov 22
- 4.5. Flight of Subscale: Nov 22

Phase 5: Full-scale Final Design and Testing: Oct 1-Feb 20

- 5.1. Iterating through subsystem designs: Oct 1-Jan 23
- 5.2. Conducting subsystem tests: Nov 1-Feb 20
- 5.3. Full-Scale Vehicle Manufacturing: Jan 23-Feb 13
- 5.4. Testing Payload Integration (Drop and Tip Tests): Feb 13-Feb 20
- 5.5. Vehicle Demonstration Flight: Feb 20

Phase 6: Revisions and Reworking: Feb 20-Apr 15

- 6.1. Improving our design and integration strategies: Feb 20-Apr 15
- 6.2. Potential for second vehicle demonstration flight: Mar 13-Apr 15
- 6.3. Final launch prep and testing: Apr 6-Apr 15

Phase 7: Launch Week: Apr 15-Apr 24

- 7.1. Performing final launch preparations: Apr 15-Apr 22
- 7.2. NASA USLI Competition: Apr 22-Apr 24



Phase 8: Closeout: Apr 24- May 11

8.1. PLAR and project reflection: Apr 24- May 11

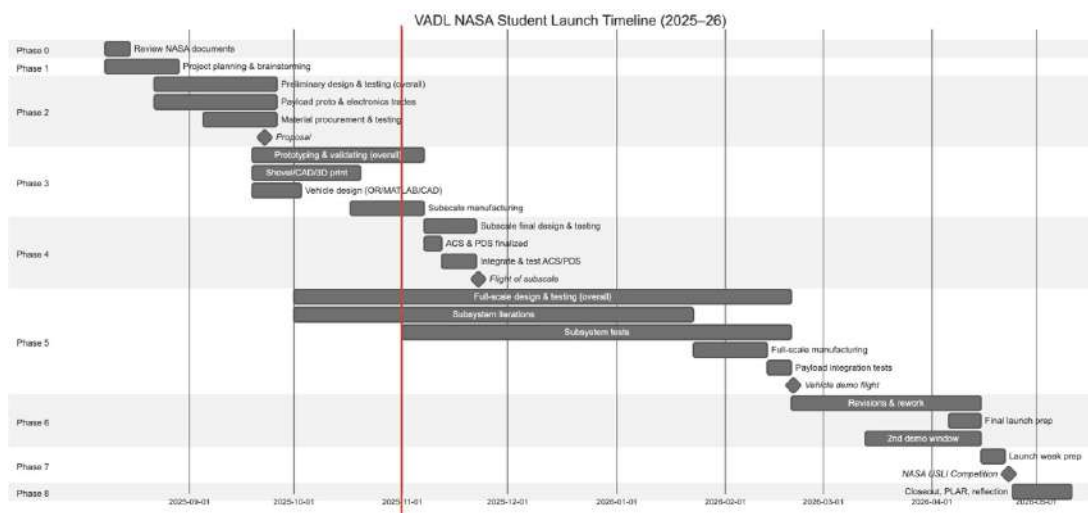


Figure 110: VADL milestones gantt chart

6.5 Program Management

VADL's competition team is divided into four teams: Payload, Vehicle, Simulations, and Electrical. These teams are all led by a member of our engineering senior design team, who delegates goals, tasks, direction, and communication with other sub-teams. Our project teams are Payload and Vehicle, who are responsible for creating the deliverable competition products. Our functional teams, Simulations and Electrical, work alongside the project teams to inform design decisions with simulations and design electronics for mission functionality, respectively.

Our work breakdown structure is derived from our VADL requirements and Gantt chart milestones and dictated by sub-team heads. We have standup meetings three times a week and a weekly presentation meeting with advisors to ensure proper communication between sub-teams and to provide progress updates on upcoming deadlines. We have continued from the proposal to have team members track daily hours on a shared spreadsheet. From proposal to PDR, our team has contributed a collective 1,693 hours.

6.6 Outreach Overview and Update

Our STEM engagement plan has been off to a great start and has been executed as outlined in the proposal. So far, we have presented at two schools, Franklin High School and Merrol Hyde Magnet School. We have also been a part of two Nashville community events: the TN Maker Fest and STEAM Day at the Nashville Zoo. We presented to nearly 300 students between the two schools and interacted with approximately 400 students between the two community events. We have educated them on our rocket, what



engineering means, past and current NASA projects, and the future of space exploration, while also conducting hands-on activities. Students have been very receptive to our lessons, asked many questions, and shown a significant increase in their excitement about rocketry and STEM as a result of our participation.

In the future, we plan to continue to spread more excitement about rocketry and STEM. We have three more events booked for the next month and a half. We are also still in contact with other schools to book more outreach events. We have been leveraging connections from schools we have been to and Vanderbilt's connections to contact teachers. We are also looking for more community events in the Nashville Area. We will continue to spread excitement about rocketry and STEM and are eager to surpass the milestone of engaging with more than 1,000 students.

A References

- [1] EZO TM *Conductivity Circuit Wiring diagram*. Tech. rep. Accessed November 2, 2025. Atlas Scientific, Nov. 2017. URL: https://files.atlas-scientific.com/EC_EZO_Datasheet.pdf.
- [2] Tanmay B. Gholap et al. "Computational Study on Base Drag Reduction for a Boat-tailed Axisymmetric Jet Nozzle Through Base Geometry Modifications". In: 2021 IEEE Pune Section International Conference (PuneCon). IEEE. Pune, India: IEEE, 16-19 Dec. 2022.
- [3] M. Huang et al. "Soil compaction and its impacts on soil structure and function: a review". In: *Soil and Tillage Research* 163 (2016), pp. 1–15. DOI: [10.1016/j.still.2016.05.003](https://doi.org/10.1016/j.still.2016.05.003). URL: <https://www.sciencedirect.com/science/article/pii/S0038080616301196>.
- [4] Theo W. Knacke. *Parachute Recovery Systems Design Manual*. Santa Barbara, CA: Para Publishing, 1992.
- [5] F. R. Menter. "Two-Equation Eddy-Viscosity Turbulence Models for Engineering Applications". In: *AIAA Journal* 32.8 (Aug. 1994), pp. 1598–1605. DOI: [10.2514/3.12149](https://doi.org/10.2514/3.12149).
- [6] Richard Nakka. *A Simple Method for Estimating the Flight Performance of a Hobby Rocket*. Accessed: 2025-11-01. n.d. URL: <https://www.nakka-rocketry.net/>.
- [7] NASA. *NASA Systems Engineering Handbook*. Tech. rep. NASA/SP-2007-6105 Rev1. Accessed November 2025. Washington, D.C.: National Aeronautics and Space Administration, 2007. URL: <https://ntrs.nasa.gov/api/citations/20070018151/downloads/20070018151.pdf>.
- [8] NBL-S-TMC-7/7-in-1 *Soil Integrated Sensor*. Tech. rep. Accessed November 2, 2025. Changsha Zoko Link Technology Co., Ltd. URL: <https://www.scribd.com/document/747666798/7-in-1-Soil-Composite-Sensor-Manual>.
- [9] W. G. Pflanz. *Recovery Systems Design Guide*. Technical Report AFFDL-TR-78-151. Finite-mass opening-load ("Pflanz") method. Wright-Patterson Air Force Base, OH: Air Force Flight Dynamics Laboratory, 1978.
- [10] M. L. Rahman et al. "Tensile properties of pre-vulcanised natural rubber latex films via hybrid radiation and peroxide vulcanisations". In: *ResearchGate* (2018). URL: https://www.researchgate.net/publication/328694993_Tensile_properties_of_pre-vulcanised_natural_rubber_latex_films_via_hybrid_radiation_and_peroxide_vulcanisations.
- [11] ScienceDirect Topics. *Soil Density*. <https://www.sciencedirect.com/topics/agricultural-and-biological-sciences/soil-density>. Accessed November 2025. n.d.
- [12] United States Environmental Protection Agency. *SW-846 Test Method 9045D: Soil and Waste pH*. Revision 4; November 2004. 2004. URL: <https://www.epa.gov/sites/default/files/2015-12/documents/9045d.pdf> (visited on 11/01/2025).



- [13] USDA Natural Resources Conservation Service. *Soil pH: A Key Soil Health Indicator*. Soil Health Technical Note. 2022. URL: https://www.nrcs.usda.gov/sites/default/files/2022-11/pH%20-%20Soil%20Health%20Guide_0.pdf (visited on 02/09/2025).

B Federal Aviation Regulations

B.1 Subpart C—Amateur Rockets

B.1.1 § 101.21 Applicability

- (a) This subpart applies to operating unmanned rockets. However, a person operating an unmanned rocket within a restricted area must comply with § 101.25(g)(2) and with any additional limitations imposed by the using or controlling agency.
- (b) A person operating an unmanned rocket other than an amateur rocket as defined in § 1.1 of this chapter must comply with 14 CFR Chapter III.

[Docket FAA-2007-27390, 73 FR 73781, Dec. 4, 2008, as amended by Docket FAA-2022-1355, Amdt. 101-11, 87 FR 75846, Dec. 9, 2022]

B.1.2 § 101.22 Definitions

The following definitions apply to this subpart:

- (a) **Class 1—Model Rocket** means an amateur rocket that:
 - (1) Uses no more than 125 grams (4.4 ounces) of propellant;
 - (2) Uses a slow-burning propellant;
 - (3) Is made of paper, wood, or breakable plastic;
 - (4) Contains no substantial metal parts; and
 - (5) Weighs no more than 1,500 grams (53 ounces), including the propellant.
- (b) **Class 2—High-Power Rocket** means an amateur rocket other than a model rocket that is propelled by a motor or motors having a combined total impulse of 40,960 Newton-seconds (9,208 pound-seconds) or less.
- (c) **Class 3—Advanced High-Power Rocket** means an amateur rocket other than a model rocket or high-power rocket.

[Docket FAA-2007-27390, 73 FR 73781, Dec. 4, 2008]

B.1.3 § 101.23 General Operating Limitations

- (a) You must operate an amateur rocket in such a manner that it:
 - (1) Is launched on a suborbital trajectory;
 - (2) When launched, does not cross into the territory of a foreign country unless an agreement is in place between the United States and the country of concern;
 - (3) Is unmanned; and
 - (4) Does not create a hazard to persons, property, or other aircraft.
- (b) The FAA may specify additional operating limitations necessary to ensure that air traffic is not adversely affected, and public safety is not jeopardized.

[Docket FAA-2007-27390, 73 FR 73781, Dec. 4, 2008]

B.1.4 § 101.25 Operating Limitations for Class 2—High-Power Rockets and Class 3—Advanced High-Power Rockets

When operating Class 2—High-Power Rockets or Class 3—Advanced High-Power Rockets, you must comply with the General Operating Limitations of § 101.23. In addition, you must not operate Class 2—High-Power Rockets or Class 3—Advanced High-Power Rockets:

- (a) At any altitude where clouds or obscuring phenomena of more than five-tenths coverage prevail;
- (b) At any altitude where the horizontal visibility is less than five miles;
- (c) Into any cloud;
- (d) Between sunset and sunrise without prior authorization from the FAA;
- (e) Within 9.26 kilometers (5 nautical miles) of any airport boundary without prior authorization from the FAA;
- (f) In controlled airspace without prior authorization from the FAA;
- (g) Unless you observe the greater of the following separation distances from any person or property that is not associated with the operations:
 - (1) Not less than one-quarter the maximum expected altitude; or
 - (2) 457 meters (1,500 ft).
- (h) Unless a person at least eighteen years old is present, is charged with ensuring the safety of the operation, and has final approval authority for initiating high-power rocket flight; and
- (i) Unless reasonable precautions are provided to report and control a fire caused by rocket activities.

[74 FR 38092, July 31, 2009, as amended by Amdt. 101-8, 74 FR 47435, Sept. 16, 2009]

B.1.5 § 101.27 ATC Notification for All Launches

No person may operate an unmanned rocket other than a Class 1—Model Rocket unless that person gives the following information to the FAA ATC facility nearest to the place

of intended operation no less than 24 hours before and no more than three days before beginning the operation:

- (a) The name and address of the operator; except when there are multiple participants at a single event, the name and address of the person so designated as the event launch coordinator, whose duties include coordination of the required launch data estimates and coordinating the launch event;
- (b) Date and time the activity will begin;
- (c) Radius of the affected area on the ground in nautical miles;
- (d) Location of the center of the affected area in latitude and longitude coordinates;
- (e) Highest affected altitude;
- (f) Duration of the activity; and
- (g) Any other pertinent information requested by the ATC facility.

[Docket FAA-2007-27390, 73 FR 73781, Dec. 4, 2008, as amended by Docket FAA-2007-27390, 74 FR 31843, July 6, 2009]

B.1.6 § 101.29 Information Requirements

- (a) **Class 2—High-Power Rockets.** When a Class 2—High-Power Rocket requires a certificate of waiver or authorization, the person planning the operation must provide the information below on each type of rocket to the FAA at least 45 days before the proposed operation. The FAA may request additional information if necessary to ensure the proposed operations can be safely conducted. The information shall include for each type of Class 2 rocket expected to be flown:
 - (1) Estimated number of rockets;
 - (2) Type of propulsion (liquid or solid), fuel(s), and oxidizer(s);
 - (3) Description of the launcher(s) planned to be used, including any airborne platform(s);
 - (4) Description of recovery system;
 - (5) Highest altitude, above ground level, expected to be reached;
 - (6) Launch site latitude, longitude, and elevation; and
 - (7) Any additional safety procedures that will be followed.
- (b) **Class 3—Advanced High-Power Rockets.** When a Class 3—Advanced High-Power Rocket requires a certificate of waiver or authorization, the person planning the operation must provide the information below for each type of rocket to the FAA at least 45 days before the proposed operation. The FAA may request additional information if necessary to ensure the proposed operations can be safely conducted. The information shall include for each type of Class 3 rocket expected to be flown:
 - (1) The information requirements of paragraph (a) of this section;
 - (2) Maximum possible range;
 - (3) The dynamic stability characteristics for the entire flight profile;
 - (4) A description of all major rocket systems, including structural, pneumatic, propellant, propulsion, ignition, electrical, avionics, recovery, wind-weighting, flight control, and tracking;
 - (5) A description of other support equipment necessary for a safe operation;
 - (6) The planned flight profile and sequence of events;



- (7) All nominal impact areas, including those for any spent motors and other discarded hardware, within three standard deviations of the mean impact point;
- (8) Launch commit criteria;
- (9) Countdown procedures; and
- (10) Mishap procedures.

[Docket FAA-2007-27390, 73 FR 73781, Dec. 4, 2008, as amended by Docket FAA-2007-27390, 74 FR 31843, July 6, 2009]



C NAR High Power Rocket Safety Code



NAR High Power Rocket Safety Code

Approved March 2006

1. **Certification.** I will only fly high power rockets or possess high power rocket motors that are within the scope of my user certification and required licensing.
2. **Materials.** I will use only lightweight materials such as paper, wood, rubber, plastic, fiberglass, or when necessary ductile metal, for the construction of my rocket.
3. **Motors.** I will use only certified, commercially made rocket motors, and will not tamper with these motors or use them for any purposes except those recommended by the manufacturer. I will keep smoking, open flames, and heat sources at least 25 feet away from these motors.
4. **Ignition System.** I will launch my rockets with an electrical launch system, and with electrical motor igniters that are installed in the motor only after my rocket is at the launching or prepping area. My launch system will have a safety interlock that is in series with the launch switch that is not installed until my rocket is ready for launch, and will use a launch switch that returns to the "off" position when released. If my rocket has onboard ignition systems for motors or recovery devices, these will have safety interlocks that interrupt the current path until the rocket is at the launch pad.
5. **Misfires.** If my rocket does not launch when I press the button of my electrical launch system, I will remove the launcher's safety interlock or disconnect its battery, and will wait 60 seconds after the last launch attempt before allowing anyone to approach the rocket.
6. **Launch Safety.** I will use a 5-second countdown before launch, and will ensure that everyone in the launch site is paying attention and that no person is closer to the launch pad than allowed by the accompanying Minimum Distance Table. I will check the stability of my rocket before flight and will not fly it if it cannot be determined to be stable.
7. **Launcher.** I will launch my rocket from a stable device that provides rigid guidance until the rocket has attained a speed that ensures a stable flight, and that is pointed to within 20 degrees of the vertical. If the wind speed exceeds 5 miles per hour I will use a launcher length that permits the rocket to attain a safe velocity before separation from the launcher. I will use a blast deflector to prevent the motor's exhaust from hitting the ground. I will ensure that there is no dry grass within a clear distance of each launch pad determined by the accompanying Minimum Distance table, and will increase this distance by a factor of 1.5 if the rocket motor being launched uses titanium sponge in the propellant.
8. **Size.** My rocket will not contain any combination of motors that total more than 40,960 N-sec (9208 pound-seconds) of total impulse. My rocket will not weigh more at liftoff than one-third of the certified average thrust of the high power rocket motor(s) intended to be ignited at launch.



9. **Flight Safety.** I will not launch my rocket at targets, into clouds, near airplanes, or on trajectories that take it directly over the heads of spectators or beyond the boundaries of the launch site, and will not put any flammable or explosive payload in my rocket. I will not launch my rockets if wind speeds exceed 20 miles per hour. I will comply with Federal Aviation Administration airspace regulations when flying, and will ensure that my rocket will not exceed any applicable altitude limit in effect at that launch site.
10. **Launch Site.** I will launch my rocket outdoors, in an open area where trees, power lines, buildings, and persons not involved in the launch do not present a hazard, and that is at least as large on its smallest dimension as one-half of the maximum altitude to which rockets are allowed to be flown at that site or 1500 feet, whichever is greater.
11. **Launcher Location.** My launcher will be at least one half the minimum launch site dimension, or 1500 feet (whichever is greater) from any inhabited building, or from any public highway on which traffic flow exceeds 10 vehicles per hour, not including traffic flow related to the launch. It will also be no closer than the appropriate Minimum Personnel Distance from the accompanying table from any boundary of the launch site.
12. **Recovery System.** I will use a recovery system such as a parachute in my rocket so that all parts of my rocket return safely and undamaged and can be flown again, and I will use only flame-resistant or fireproof recovery system wadding in my rocket.
13. **Recovery Safety.** I will not attempt to recover my rocket from power lines, tall trees, or other dangerous places, fly it under conditions where it may recover in spectator areas or outside the launch site, or attempt to catch it as it approaches the ground.

MINIMUM DISTANCE TABLE				
Installed Total Impulse (N-sec)	Equivalent Motor Type	Minimum Clear Distance (ft.)	Minimum Personnel Distance (ft.)	Minimum Personnel Distance (Complex Rocket) (ft.)
0 - 320.00	H or smaller	50	100	200
320.01 - 640.00	I	50	100	200
640.01 - 1280.00	J	50	100	200
1280.01 - 2560.00	K	75	200	300
2560.01 - 5120.00	L	100	300	500
5120.01 - 10,240.00	M	125	500	1000
10,240.01 - 20,480.00	N	125	1000	1500
20,480.01 - 40,960.00	O	125	1500	2000

Note: A complex rocket is one that is multi-staged or that is propelled by two or more rocket motors

Figure 111: National Association of Rocketry - High Power Rocket Safety Code



D Written Safety Statement

Vanderbilt Aerospace Design Laboratory - Written Safety Agreement

As a member of the Vanderbilt Aerospace Design Laboratory, I agree to abide by all posted (physically and digitally) safety procedures as well as all verbal safety-related instructions given in lab and in the field by the Student Safety Officer (Jamie Danis), Range Safety Officer (Chris Dondanville), or Staff Safety Officer (Mark Thelen). This includes, but is not limited to, PPE usage, power tool qualification, and personal relocation.

Before each rocket launch, range safety inspections will be conducted by the Range Safety Officer. The Range Safety Officer holds authority to inspect the design and construction of the vehicle and payload, and has the final authority to scrub launches based on any concerns related to the safety of all personnel and the launch vehicle. Failure to comply with the determination of the Range Safety Officer may lead to the disqualification of our team from the NASA University Student Launch program.

I also agree to familiarize myself with, and to abide by:

1. All NASA USLI safety rules [2025-2026 NASA Student Launch Handbook, Rules, Sect. 5]
2. All NAR (National Association of Rocketry) safety standards and requirements [NAR High Power Rocket Safety Code]
3. All applicable FAA (Federal Aviation Administration) regulations and policies [FAA 14 CFR, Subchapter F, Part 101, Subpart C]
4. All pertinent Tennessee State Laws regarding high-powered model rocketry flight [NFPA 1127 Code for High Power Rocket Motors]
5. All guidelines and warnings set out in the compiled Safety Data Sheets for all hazardous material in lab (found in the shared Safety folder and under the fume hood in the laboratory).

My signature below indicates that I fully understand, acknowledge, and accept all of the above. I acknowledge that failure to abide by the above may lead to my exclusion from certain tasks in the laboratory, a revocation of my permission to attend launches, or the revocation of VADL's permission to launch our rocket in the NASA USLI Competition. I acknowledge that my failure to sign and agree to abide by the above rules will result in my removal from the VADL program.

Signed:

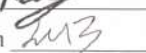
- Neal Bagai 
- Joel Berinstein 

Figure 112: Written Safety Agreement



- Jamie Danis Jamie Danis
- Kalyn Day Kalyn Day
- Sean Confoy Sean Confoy
- Ashley Fu Ashley Fu
- Sean Gentry Sean Gentry
- Samantha Gordon Samantha Gordon
- Thor Hammer Thor Hammer
- Catherine Knox Catherine Knox
- Jack Laddel Jack Laddel
- Evan Levine Evan Levine
- Samir Menon Samir Menon
- Caleb Oblepias Caleb Oblepias
- Xavier Onwu Xavier Onwu
- Patrick Purev Patrick Purev
- Sadie Pullen Sadie Pullen
- Jack Radochia Jack Radochia
- Ben Racape Ben Racape
- Sanampreet Singh Sanampreet Singh
- Colin Strout Colin Strout
- Caleb Strout Caleb Strout
- Evan Ticknor Evan Ticknor
- Abbott Van Heerden Abbott Van Heerden
- Parker Violand Parker Violand